Photodecomposition Pathways for

Photoactivatable Platinum(IV) Diazido

Anticancer Complexes
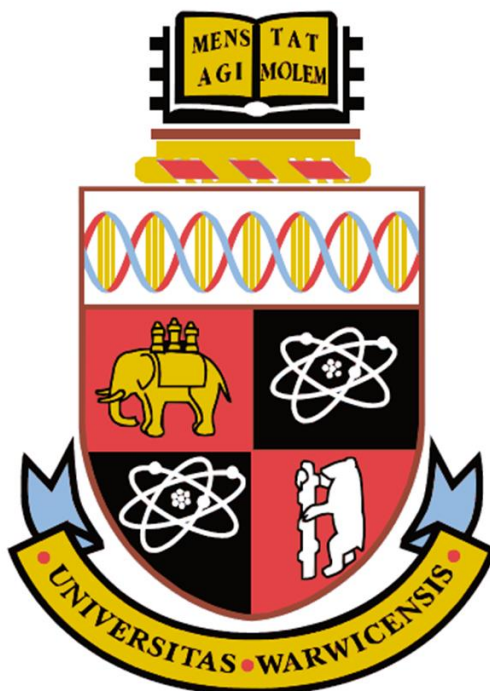
A Thesis Submitted for the Degree of

Doctor of Philosophy

Jennifer S. Butler, B.Sc

Supervisor: Prof. Peter J. Sadler, FRS

University of Warwick, Department of Chemistry

November 2014

Table of Contents

Acknowledgments

Also this could not have been done without the PJS group. I enjoyed all the years spent in the group, especially hearing all the random topics that I never thought were possible, Evyenia, Khatija, Nichola, Joan and Adam you all truly made the group very enjoyable!! Also special thanks to Maria for her friendship and chats in the office over the years. I would also like to thank all the friends I have over the years in Warwick including Rene, Oat and Kara who made my first year very enjoyable! Also thanks to Anne-Marie, Zoe, Blossom, Massimo, Luca and Hussein for their friendship and support during the last year of my PhD.

None of this would have been possible without financial support, I sincerely thank the European Research Council (ERC) for this opportunity.

Finally, a special thank you to my family back home, without their support and encouragement over the years would have made this period in my life very difficult. I also thank my mother and father who encouraged me throughout my PhD, especially when I faced difficult times, thanks mammy and daddy. Thanks also to my older bro, Tommy for his advice...despite not really understanding what I'm doing, nevertheless I truly appreciated it!! Last but not least, a special thank you to my sister Anne-Marie, despite being a whole country away, it never seemed like that given all the phone calls. Thanks for your encouragement and support over the years especially when I loosing hope, without you this would not have been possible.

Declaration

I hereby declare that the work contained in this thesis is the original work of the author, except where specific reference is made to other sources, with the nature and extent of the author's contribution indicated (as appropriate) where work was based on collaborative research. The work was undertaken at the Department of Chemistry, University of Warwick between October 2010 and June 2014 and has not been submitted, in whole or in part, for any other degree, diploma or other qualification. A list of research papers published or in preparation from this work is given below.

Jennifer Butler

June 2014

Abstract

Photo-activatable platinum(IV) diazido complexes with the general formula of *trans,trans,trans*-[Pt(N$_3$)$_2$(OH)(X)(py)(am$_1$)] (X is a hydroxide or carboxylate and am$_1$ is an aliphatic/aromatic amine) show dark-stability under physiological conditions but can induce a photo-cytotoxic effect in cancer cells after irradiation with UVA, blue and/or green light. These platinum(IV) diazido complexes can platinate DNA and induce different lesions that are distinctly different from those generated by the anticancer drug *cis*-platin. Through the use of EPR, multinuclear NMR, and UV-visible absorption spectroscopy, as well as mass spectrometry and some cell studies, this thesis aims to investigate the pathways of photochemical decomposition and in particular the release of azidyl ligands and their subsequent involvement in photo-cytotoxicity.

Firstly, the irradiation of *trans,trans,trans*-[Pt(N$_3$)$_2$(OH)$_2$(py)$_2$] (**40**, py = pyridine) with blue light in the presence of the spin trap 5,5-dimethyl-1-pyrroline-N-oxide (DMPO) led to the detection of a characteristic quartet-of-triplets EPR spectrum, assigned to the azidyl radical adduct, DMPO-^{14}N$_3$. Irradiation of ^{15}N-**40**, led to the detection of a quartet-of-doublets EPR spectrum as assigned to the DMPO-^{15}N$_3$ spin adduct. This confirmed that the $^{\bullet}$N$_3$ radicals arose from the platinum(IV)-bound azide. The DMPO-N$_3$ spin adduct was also detected from the photo-irradiation of *trans,trans,trans*-[Pt(N$_3$)$_2$(OH)$_2$(MA)(py)] (**44**, MA = methylamine) with blue light.

A greater yield in the DMPO-N$_3$ spin adduct was formed in PBS/D$_2$O. This effect was attributed to the Brownian motion of the $^{\bullet}$N$_3$ radicals. Interestingly, photo-irradiation in the cell culture medium-, RPMI-1640 led to a reduction in the DMPO-N$_3$ spin adduct. This reduction was accredited to the variety of components present in the cell culture medium which could behave as radical quenchers. Alternative nitrone spin traps, α-4-pyridyl-1-oxide-*N-tert*-butylnitrone (4-POBN) and 5-diethoxyphosphoryl-5-methyl-1-pyrroline-*N*-oxide (DEPMPO) also led to the trapping of the azidyl radicals from irradiated **40**, forming the 4-POBN-N$_3$ (triplet-of-quartets) and DEPMPO-N$_3$ (octet-of-triplets) spin adducts EPR spectra, respectively. DEPMPO was the most efficient azidyl radical trap; with the DEPMPO-N$_3$ spin adduct possessing the longest lifetime in aqueous media.

Extending the wavelength of activation to green light (517 nm), also led to the detection of DMPO-N$_3$ from the photo-irradiation of **40** in RPMI-1640, *trans,trans,trans*-[Pt(N$_3$)$_2$(OH)(SAD)(py)$_2$] (**56**,SAD=succinate), *trans,trans,trans*-[Pt(N$_3$)$_2$(OH)(ethyl-methyl-SAD)(py)$_2$] (**57**) and *trans,trans,trans*-[Pt(N$_3$)$_2$(OH)(N-MI)(py)$_2$] (**58**, N-MI = N-methylisatoate) in H$_2$O/DMF. The DEPMPO-N$_3$ was also detected from the gamma-ray irradiation of **40**, which appears to be the first report of the activation of a platinum(IV) diazido anticancer complex with gamma-rays, a procedure which might be useful of clinical use.

The azidyl radicals generated from irradiated **40** were unreactive towards both glycine and L-tyrosine. However, in the presence of L-tryptophan the azidyl

radicals were quenched. Detection of free azide by ^{14}N NMR spectroscopy confirmed that this quenching mechanism proceeded through a one-electron transfer pathway. The photo-cytotoxicity of **40** was supressed in the presence of low doses of L-tryptophan in A2780 ovarian cancer cells. From this study, it was deduced that the photo-cytotoxicity of **40** is comprised of both an acute (radical) and chronic (DNA platination) based mechanisms. Additionally, certain cancers have reported on the depleted serum levels of L-tryptophan, in particular ovarian cancer cells. This suggests the extent of the photo-cytotoxicity of **40** can be controlled in the presence of L-tryptophan.

Photo-irradiation of **40** in the presence of melatonin, an analogue of L-tryptophan was also performed. Despite, the structural similarity between L-tryptophan and melatonin, the presence of the 5-methoxy substituent present in melatonin induced an alternative photo-decomposition pathway of **40**. Photo-irradiation of **40** in the presence of melatonin with blue light also led to the detection of the quartet EPR spectrum assigned to the hydroxyl radical adduct, DMPO-OH. Through multinuclear NMR and mass spectrometry the quenching of both the azidyl and hydroxyl radicals by melatonin was determined. Additionally, mass spectrometry also detected a mass adduct attributed to a platinum(II)-melatonin complex. This dual antioxidant and metal-binding ability of melatonin was attributed to the observed photo-protective effect in A2780 ovarian cancer cells. Melatonin regulates circadian rhythms with a maximum concentration during dark hours. Consequently, treatment of antineoplastic tissue with **40** during the hours of melatonin production may be ineffective.

Platinum accumulation and absorption has been suggested to be mediated by organic cation transporters (OCTs), in particular OCT2. Irradiation of **40** was monitored in the presence of cimetidine, an OCT2 inhibitor. A new strong absorption band at ca. 354 nm was assigned to an S→Pt^{II} LMCT band. High resolution mass spectroscopy identified a mass adduct assigned to a novel platinum(II)-cimetidine species. The loss of coordinated pyridine from irradiated **40** as detected by ^{1}H NMR spectroscopy and the quenching of the azidyl radical by cimetidine were correlated with the observed photo-protective effect in HaCaT keratinocytes cells.

Abbreviations

γ-PGA	γ-polyglutamic acid
4-POBN	α-4-pyridyl-1-oxide-*N-tert*-butylnitrone
5'-GMP	5'-guanosine monophosphate
8-oxodG	8-hydroxydeoxyguanosine
AdCSV	Adsorptive cathodic stripping voltammetry
ALA	Aminolevulinic acid
a.m.u	Atomic mass units
AR	Androgen receptor
ATP	Adenosine triphosphate
AuNRs	Gold nanorods
Bec-1	Beclin-1
CA	Citric acid
CDDP	*Cis*-platin
Cim	Cimetidine
CNTs	Carbon nanotubes
CORMs	Carbon monoxide releasing molecules
CPPS	Cell penetrating peptides
CTPs	Copper transporter proteins
CTTS	Charge-transfer-to-solvent
CTX	Chlorotoxin
CW-EPR	Continuous wave electron paramagnetic resonance
DEPMPO	5-diethoxyphosphoryl-5-methyl-1-pyrroline-*N*-oxide
DEPT	Distorsionless enhancement by polarization transfer
DFT	Density functional theory
DMPO	5,5-dimethyl-pyrroline-*N*-oxide
DMS	Dimethyl-sulfide
DMSO	Dimethylsulfoxide
DNA	Deoxyribonucleic acid
EC_{50}	50% growth effective concentration
EGF	Epidermal growth factor
ENDOR	Electron-nuclear double resonance
EPR	Enhanced permeability and retention
EPR	Electron paramagnetic resonance
ET	Electron transfer
EtOH	Ethanol
FDA	Food and Drug Administration
h	hour
*h*Ctr1	Human copper transporter 1
HMDSO	Hexamethyl-disiloxane
HOMO	Highest occupied molecular orbital
HPLC	High performance liquid chromatography
HRMS	High resolution mass spectrometry
HSPs	Heat shock proteins
HYSCORE	Hyperfine sublevel correlation
IC_{50}	50% growth inhibition concentration
IC	Internal conversion
ICP-MS	Inductively coupled plasma mass spectrometry

ILCT	Intraligand-charge-transfer
ISC	Intersystem crossing
IVCT	Intravalent-charge-transfer
LC3	Light chain-3
LED	Light emitting diode
LF	Ligand-field
LMCT	Ligand-to-metal-charge-transfer
LUMO	Lowest unoccupied molecular orbital
MAP	Microtubule-associate protein
MLCT	Metal-to-ligand-charge-transfer
MLT	Melatonin
MMP2	Metalloproteinase-2
MMP^+	Methyl-4-phenylpyridinium
MMR	Mismatch repair
MNP	Methyl-2-nitrosopropane
Mol equiv	Molar equivalents
NAC	N-acetyl-cysteine
NAD^+	Nicotinamide adenosine dinucleotide
NC	Negative control
NER	Nucleotide excision repair
NMR	Nuclear magnetic resonance
NP	Nanoparticle
OCT	Organic cation transporter
PACT	Photoactivation of a chemotherapeutic
PDT	Photodynamic therapy
PEG	Polyethylene glycol
pH*	pH in deuterated solvent
PpIX	Photoporhyrin
ppm	Part per million
PS	Photosensitiser
Py	Pyridine
RFQ	Rapid freeze quench
ROS	Reactive oxygen species
RNR	Ribonucleotide reductase
RNS	Reactive nitrogen species
RT	Room temperature
s	Second
SAR	Stucture activity relationship
SOD	Superoxide dismutase
SOMO	Singly occupied molecular orbital
SRIXE	Synchroton-radiation induced X-ray emission
SWCNTs	Single-walled carbon nanotubes
TEA	Tetraethyl ammonium
TfR	Transferrin
TSPOs	Translocator proteins
UBQ	Ubiquitin
UVA	Ultra-violet light
WHO	World Health Organistion
XANES	X-ray absorption near-edge structure
XFS	X-ray fluorescence

Publications

1. Zhao, Y.; Farrer, N.J.; Li, H.; Butler, J.S.; McQuitty, R.J.; Habtemariam, A.; Wang, F.; Sadler, P.J.

   De Novo Generation of Singlet Oxygen and Ammine Ligands by Photoactivation of a Platinum Anticancer Complex.

   Angew. Chem. Int. Ed. 2013, 52, 13633

2. Liu, Z.; Deeth, R. J.; Butler, J. S.; Habtemariam, A.; Newton, M. E.; Sadler, P.J.

   Reduction of Quinones by NADH Catalyzed by Organoiridium Complexes

   Angew. Chem. Int. Ed. 2013, 52, 4194-4197

3. Butler, J. S.; Sadler, P. J.

   Targeted delivery of platinum-based anticancer complexes

   ***Curr. Opin. Chem. Biol.* 2013, 17, 175-188**

4. Butler, J. S.; Woods, J. A.; Farrer, N. J.; Newton, M. E.; Sadler, P. J.

   Tryptophan Switch for a Photoactivated Platinum Anticancer Complex

   J. Am. Chem. Soc. 2012, 134, 16508-16511

Conferences Attended

1. Analysis of free radicals, radical modifications and redox signaling, Birmingham, UK. April 2011.

2. Warwick University Chemistry Postgraduate Symposium, Coventry, UK. May 2011

3. Bruker EPR and NMR Users Meeting, Coventry, UK. Nov 2011

4. RSC Dalton Conference. Coventry, UK. April 2012

5. Warwick University Chemistry Postgraduate Symposium, Coventry, UK. May 2012. Poster Presentation

6. Photoactivatable metal complexes: from theory to therapy, London, UK. June 2012.

7. Photoactivatable metal complexes: exciting potential in biotechnology and medicine, Buckinghamshire, UK. June 2012.

8. XI International Symposium on Platinum Coordination Compounds in Cancer Chemotherapy, Stem Cells, DNA repair mechanisms, DNA-damaging agents, Verona, Italy. October 2012. Poster Presenation

9. Warwick University Chemistry Postgraduate Symposium, Coventry, UK. May 2012. Oral Presentation

Courses

1. Academic Writing, Oct – Dec 2011.

2. Project Management, May 2012.

3. Decision Making and Leadership, April 2013.

4. Transferable Skills I (Oct – Jun 2011)

5. Transferable Skills II (Oct – Jun 2012)

6. Transferable Skills III (Oct – Jun 2013)

Chapter I

Introduction

This thesis is concerned with the identification and reactivity of photo-products generated from the photo-decomposition of novel photo-activatable platinum(IV) diazido anticancer complexes. Current platinum anticancer agents are losing their potency due to acquired or intrinsic resistance mechanisms. Novel platinum anticancer agents with unique mechanisms of action appear to be essential for future chemotherapy. Therefore, in this Chapter a summary on the history of developed platinum anticancer complexes is given, followed by an introduction to the concept of targeted delivery of platinum anticancer complexes. Finally, attention is focused on new phototherapy-based methods.

1.1 Cancer

Cancer remains a main contribution of deaths worldwide (Figure 1.1). The World Health Organistion (WHO) estimates approximately 13.1 million related cancer deaths to rise to 22 million by 2030.[1] Cancer initation is a multistep process, however numerous studies have correlated free radicals and reactive species in the formation of pathophysiological diseases including cancer.[2] Freidmann reported ca. 80% of the oxgyen consumed is converted to adenosine triphopshate (ATP) by the mitochondria, the remaining 20% is partially reduced to reactive oxygen species (ROS).[3] Additionally, oxidation of the amino acid L-arginine leads to the formation of nitric oxide ($NO^{\bullet}$), a reactive nitrogen species (RNS). Moreover, exposure to UV-light, X-rays or gamma radiation can also lead to ROS/RNS generation.[4]
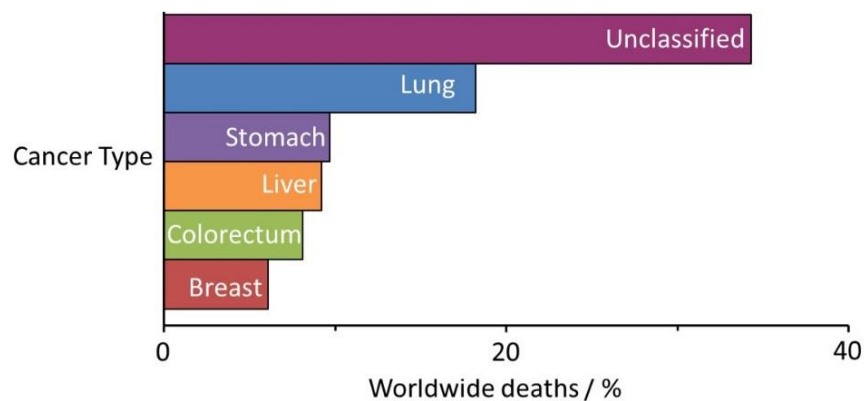
Figure 1.1 Percentage of cancer types contributing to worldwide deaths by 2030 (data obtained from the WHO).

The term ROS/RNS is used to encompass an arrary of reactive oxygen/nitrogen species, some posssessing an unpaired electron referred to as radical species (Table 1.1). Both ROS and RNS are typically short-lived species (ca. $t_½$ of 10^{-9} s) and can induce damage to DNA, lipids, membranes, proteins and peptides. Valko reported that one human cell is exposed to ca. 1×10^5 oxidative hits/day.[5] Consequently, the cell has developed various resistance mechanisms to prevent daily damage induced from either ROS or RNS present at low concentrations. Resistance mechanisms include nucleotide excision repair (NER), mismatch repair (MMR) processes and the presence of antioxidants. Intracellular antioxidants such as vitamin C and E, glutathione and superoxide dismutase (SOD), amoung others, possess the ability to scavenge ROS and RNS preventing cell damage.[6] As reported by Sies, the imbalance between oxidants and antioxidants favouring the oxidant is defined as oxidative stress.[7]

Table 1.1 Classification of both reactive oxgyen species (ROS) and reactive nitrogen species (RNS).

ROS	RNS
$^\bullet$OH (hydroxyl radical)	$^\bullet$N$_3$ (azidyl radical)
$^{\bullet-}$O$_2$ (superoxide)	NO$^\bullet$
$^\bullet$O$_2$R (peroxyl)	$^\bullet$O$_2$N (nitrogen dioxide)
$^\bullet$OR (alkoxyl)	HNO$_2$ (nitrous acid)
HOCl (hypochlorous acid)	N$_2$O$_3$
O$_3$ (ozone)	NO$_2^-$
ONOO- (peroxynitrite)	NO$_3^-$
^{1}O$_2$ (singlet oxgyen)	
H$_2$O$_2$ (hydrogen peroxide)	

Where $^\bullet$ refers to a paramagnetic species

ROS include the hydroxyl ($^\bullet$OH) radical, singlet oxygen (^{1}O$_2$) and hydrogen peroxide (H$_2$O$_2$). The $^\bullet$OH radical has been identified as the most reactive and damaging ROS.[8] It has the ability to react with all DNA nucleobases, resulting in numerous products. In contrast, ^{1}O$_2$ has been reported to react specifically with the guanine nucleobase of DNA.[5] Products of biological damage are termed "biomarkers", a common biomarker, 8-hydroxydeoxyguanosine (8-OH-G), has been identified by various spectroscopic techniques.[9,10] Interestingly, H$_2$O$_2$ toxicity arises in the presence of metal ions, typically iron(II) or copper(I) which reduce H$_2$O$_2$ and generate the reactive $^\bullet$OH radical, either through the Haber-Weiss or Fenton process.[11] Additionally, the majority of RNS are derived from NO$^\bullet$, formed from the oxidation of L-arginine. NO$^\bullet$ has the ability to readily diffuse through the

cytoplasm and plasma membrane $NO^{\bullet}$ reacts with other ROS such as H_2O_2 and HOCl producing a variety of reactive nitrogen derivates. Similar to ROS, RNS induce equivalent DNA damage.[12]

Excessive generation of ROS/RNS in non-maligant tissue(s)/organ(s) is unfavourable. However, generation of these reactive species specificially in neoplastic tissue offers the potential of DNA damage and thereby inducing cell death of tumour tissue. Banerjee *et al.* recently reported the induction of apoptosis in leukemia cells through the formation of both ROS and RNS generated from a dibasic hydroxamic acid complex.[13] Moreover, the generation of $^1O_2$ has also been attributed to cell death and is currently used in Photodynamic Therapy (see section **1.7.1**). Therefore, ROS/RNS can act as potential "tumourgenetic" agents.[6] However, due to their transient nature, detection of these reactive radical species is not facile. Currently, the most commonly used technique for radical detection is electron paramagnetic resonance (EPR) spectroscopy. This technique is used throughout this thesis, therefore a brief description to the theory and data characterisation is provided.

1.2 Electron Paramagnetic Resonance

Electron paramagnetic resonance is the study of unpaired electrons, commonly referred to as a radical species. A wide variety of radicals exist ranging from organic molecules to inorganic metals. Many divisions of EPR spectroscopy have been developed including, electron-nuclear double resonance (ENDOR),[14] hyperfine sublevel correlation (HYSCORE)[15] and spin trapping (ST) EPR spectroscopy.

Consequently, EPR has been exploited in numerous research fields ranging from archeology[16,17] to medicine.[18,19]

1.2.1 Theory

EPR possesses the same physical principles as nuclear magnetic resonance (NMR) spectroscopy. However the former is concerned with electron spin compared to the nuclei spin as with NMR. An EPR spectrum can be acquired in either continuous-wave (CW) or pulsed mode.[20] In CW-EPR, a low power microwave signal ca. 200 mW is continuously sent to the sample. In this thesis, CW-EPR spectroscopy was used. Therefore, subsequent descriptions and discussions are based on CW-EPR, unless otherwise stated.

In the absence of a magnetic field ($B_0 = 0$) the two electron spin states α (+ ½, aligned opposite the magnetic field) and β (- ½, aligned with the magnetic field) are degenerate. However, once a magnetic field is applied ($B_0 \neq 0$) these spin states are no longer equivalent and are energetically separated (ΔE ($E_\alpha - E_\beta$)) as shown in Figure 1.2.[21] The separation of the two electron spin states in the presence of a magnetic field is referred to as the electron Zeeman effect,[20] and is defined by Equation 1.1, where g is the g value (defined on p 8) and μ_B is the Bohr Magneton (-9.274×10^{-24} J T^{-1}).

$$\Delta E = h\nu = \pm \frac{1}{2} g |\mu_B| B_0 \qquad \text{Eq 1.1}$$
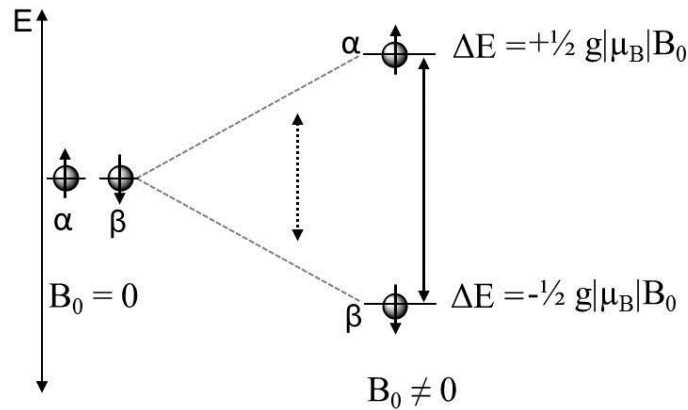
Figure 1.2 Energy separation of the α and β spin states in the absence ($B_0 = 0$) and presence ($B_0 \neq 0$) of a magnetic field (B_0), where the resonance condition is fulfilled (solid arrow) and not fulfilled (dashed arrow) (figure adapted from ref 20).

Most EPR spectrometers operate at a constant microwave frequency and scan the magnetic field.[22] The most common microwave frequency used in EPR is ca. 9-10 GHz, also known as the X-band.[23] EPR spectrometers are classified into different bands, dependent on their operating microwave frequency. EPR spectrometers lower than X-band are commonly used for *in vivo* detection, whereas higher than X-band e.g. W-band (94 GHz) are used to determine biological distances typically in proteins.[24] Throughout this thesis, X-band EPR spectroscopy was used.

EPR spectra are presented in the first-derivative, despite the absorption curve being recorded. In CW-EPR mode a field modulation with phase-sensitive detection is commonly used. This is primarily utilised to enhance the resultant EPR signal and allows the EPR spectrometer to differentiate a true EPR signal from noise and/or interference. The result is that the slope of the absorption curve is measured due to the EPR signal being a function of the external applied field (Figure 1.3).[25]
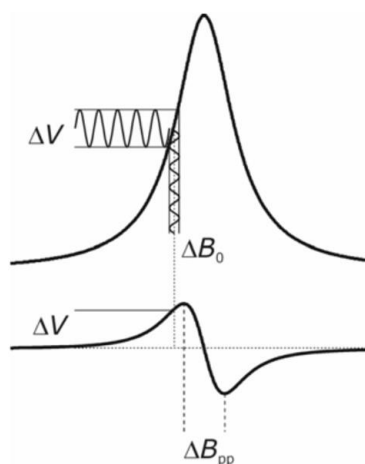
Figure 1.3 Illustration of an EPR spectrum recorded with field modulation (ΔB_0) in phase-sensitive detection. Resultant EPR spectrum is the slope of the absorption curve (figure adopted from ref 25).

1.2.2 Characterisation of EPR spectra

1.2.2.1 Hyperfine coupling

EPR spectra are characterised *via* two main parameters. Firstly, hyperfine splitting (equivalent to the *J* coupling in NMR) arises from the coupling of an unpaired electron with a magnetically active nucleus with spin (I) greater than zero. Hyperfine splitting constants are denoted by the symbol "a^Y", where y signifies the magnetically active nucleus the electron is coupling with and is measured in millitesla (mT) or Gauss (G). The number of expected lines in an EPR spectrum can be deduced from 2nI+1, where n refers to the number of equivalent magnetically active nuclei with a spin (I) greater than zero.[26] The standard free radical 4-hydroxy-2,2,6,6-tetramethyl-piperidine-1-oxyl (Tempol) generates a triplet EPR spectrum. This is produced from the coupling of the unpaired electron with the nitroxidic nitrogen possessing a spin (I) of 1 (Figure 1.4).
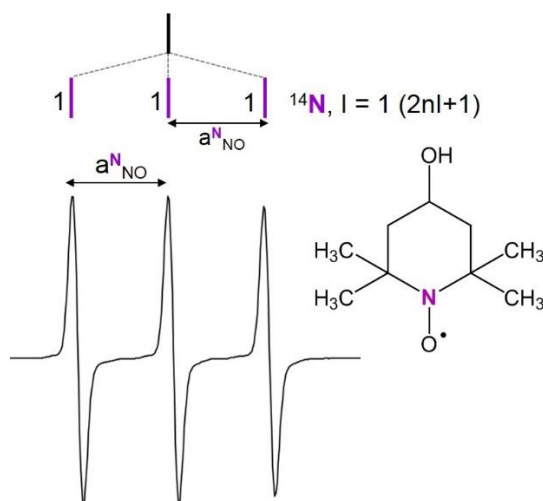
Figure 1.4 Triplet EPR spectrum of the standard free radical Tempol produced from the coupling of the unpaired electron with the nitrogen nucleus with I =1 and a^N_{NO} refers to hyperfine coupling constant of the nitroxide nitrogen measured in Gauss units.

The nitroxide (a^{NO}) and β-proton (a^H) hyperfine coupling constants have been reported to be dependent on the dielectric constant of the solvent.[27] The hyperfine coupling value is dependent on the solvent and EPR parameter settings, in particular the microwave power and modulation amplitude can alter the resultant hyperfine splitting value.[28] Therefore, unless EPR spectra are recorded under the identical EPR parameters, differences in the hyperfine splitting values are possible. Additionally, the hyperfine coupling constant(s) can determine the spin density of the unpaired electron on each atom present in the spin adduct. This can be calculated from the McConnell equation,[29] which will be discussed in more detail in **Chapter III**.

1.2.2.2 g value

The second parameter commonly used to characterise EPR spectra is the Landé

Factor or more commonly known as the g value. This parameter is equivalent to the

chemical shift (δ) parameter in NMR spectroscopy. It is independent of the

microwave frequency and is determined from the resonance condition below

(Equation 1.2), where h is Plank's constant 6.626×10^{-34} J.s, ν is the frequency

(MHz), β is the Bohr Magneton constant (9.274×10^{-24} J.T^{-1}) and B_0 is the magnetic

field (G).

$$g = \frac{h\nu}{\mu_B B_0} \qquad \text{Eq. 1.2}$$

The g value is the centre of the EPR spectrum and values of g are usually close to

the value of the free electron, $g_E = 2.0023$. The g-value varies for each radical

detected and is commonly regarded as a radical "fingerprint".[30]

An application of EPR referred to as EPR spin trapping is ulitilsed in this work for

the detection of ROS/RNS generated from photo-activatable platinum(IV) diazido

anticancer complexes. EPR spin trapping is used to detect short-lived radicals, those

possessing short life-times, ca. $< 10^{-9}$ s.[31] EPR spin trapping is described in more

detail in **Chapter III**. Next, a chronological background into the development of

these novel Pt^{IV} chemotherapeutic agents is provided.

1.3 Metals in medicine

Today, a variety of metal complexes with potential anticancer activity are being

discovered in research laboratories. Translation of these complexes from "bench to

clinic" is becoming increasingly difficult, especially since there is a lack of public

acceptance of the use of "metals in medicine" as recently reported by Mjos.[32] This

negative attitude towards metal-based therapeutics may be explained by the Bertand diagram[33] which describes even essential metals become "toxic" at certain levels. However, the use of metals for therapeutic treatment can be dated back to ca. 1912, involving the use of salvarsan. Developed by Ehrlich, this arsenic-based antimicrobial agent was effective in the treatment of syphillis.[34] Metals have also been successfully incorporated into diagnostic agents for imaging of abnormal tissues.[35] Additionally, clinical trials investigating the use of metal complexes in both therapy and diagnosis are significantly increasing.[36] Currently, ca. 50% of anticancer treatments involve the use of a platinum-based chemotherapeutic agent.[37]

1.4 Platinum

1.4.1 Pt^{II} complexes

Platinum has a range of oxidation states from 0 to +6. However, the most common oxidation states are +2 and +4. A square-planar structural geometry is exhibited by Pt^{II} (d^8) complexes. This is due to the splitting of the d orbitals, completely filling the lower orbitals, leaving the upper most orbitals (d$_x{}^2$- $_y{}^2$) empty (Figure 1.5). Various isotopes of platinum exist, however ^{195}Pt (33.8% natural abundance)[38] is the only nuclear magnetically active isotope with a spin (I) of ½.
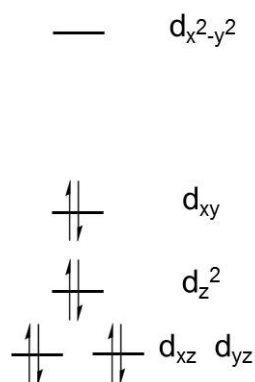
Figure 1.5 Splitting of the d-orbitals of a square-planar Pt^{II} (d^8) complex possessing strong donor ligands.

The arrangement of the ligands coordinated to the platinum centre can give rise to *cis* or *trans* isomers. To date, *cis*-diamminedichloroplatinum(II) is the most successful metallodrug, accidentally discovered in 1965 by Rosenberg, commonly referred to as *cis*-platin (**1**, Figure 1.6).[39] This complex can also exist as its inactive geometrical isomer, *trans*-platin (**2**, Figure 1.6).
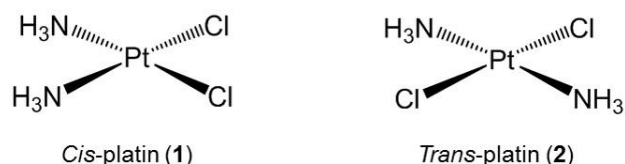
Figure 1.6 Structures of *cis*-platin (CDDP, **1**) and *trans*-platin (TDDP, **2**).

1.4.2 *Cis*-platin and its mechanism of action

Cis-platin (CDDP, **1**) was reported to exhibit anticancer activity towards a number of cancers including testicular, ovarian and bladder cancers.[40] After administration of CDDP via infusion or intravenous injection into the blood plasma, it remains stable due to the high chloride concentration (ca. 100 mM).[41] Under these conditions, hydrolysis of CDDP is supressed, as the relatively inactive CDDP is readily distributed throughout the entire body.[42] Early studies reported that CDDP

11

enters the cell through passive diffusion[43] or by active uptake.[44] Recently the influx of CDDP into the cell has been reported to be mediated via copper transporters, in particular the *hCtr1*.[45] Platinum accumulation has also been reported to be mediated by organic cation transporters (OCTs),[46,47] this will be discussed in more detail in **Chapter VI**.

The intracellular concentration of chloride in the cytoplasm has been reported by Jennerwein and Anderson in a variety of human carcinoma cells to range from ca. $20 - 55$ mM.[48,49] Consequently, once inside the cytoplasm, CDDP is subject to hydrolysis due a reduced chloride concentration. An active postively-charged chloroaqua Pt^{II} species, $[Pt(Cl)(NH_3)_2(OH_2)]^+$ is formed. This species is thought to induce the observed cytotoxic effect (Figure 1.7).
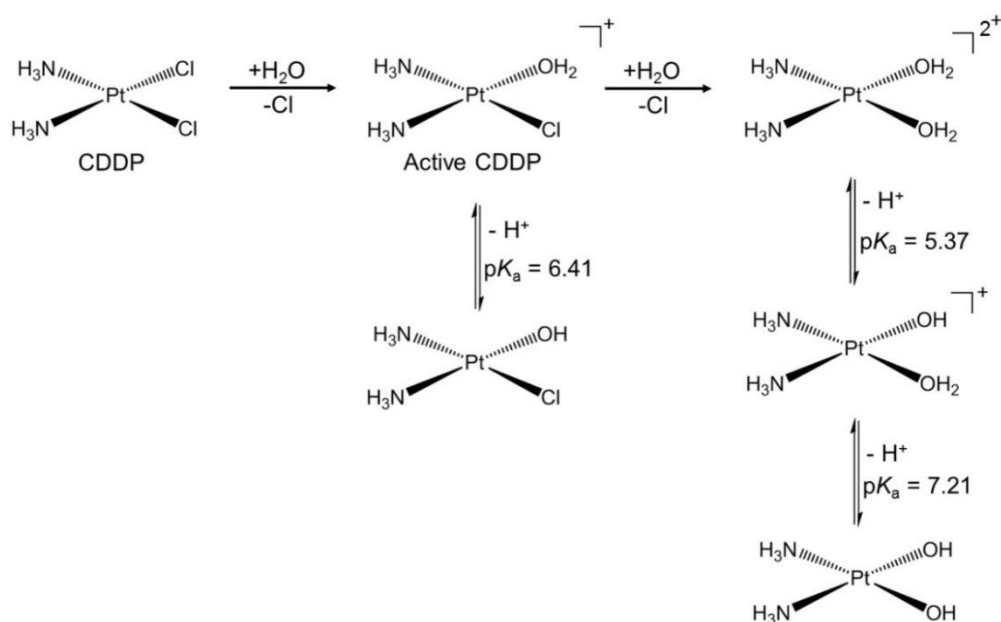
Figure 1.7 Stepwise hydrolysis of *cis*-platin occurring in the cytoplasm of the cell and the subsequent deprotonation to the hydroxido complexes with respective pK_a values at 300 K.[50]

It has been reported that under physiological conditions, the majority of heteroatoms present in the purine and pyrimindine nucleobases (Figure 1.8) of DNA possess the ability to bind to Pt^{II}. Numerous reports have identified binding of Pt^{II} occurs preferentially at the N^7 atom of the purine nucleobase guanine (G),[51-56] forming the major 1,2-d(GpG) intrastrand cross links (ca. 60-65%) between two adjacent guanines[57] (Figure 1.9**A**). Minor 1,2(ApG) intrastrand crosslinks (20-25%) also occur with the nucleobase adenine. Additonally, 1,3-(GpXG) crosslinks (ca. 2%), which possess an extra base between the guanine resides have been identified. Moreover, interstrand crosslinks between two guanine residues on opposite strands of the DNA molecule (Figure 1.9**B**) have also be reported to form.[58]
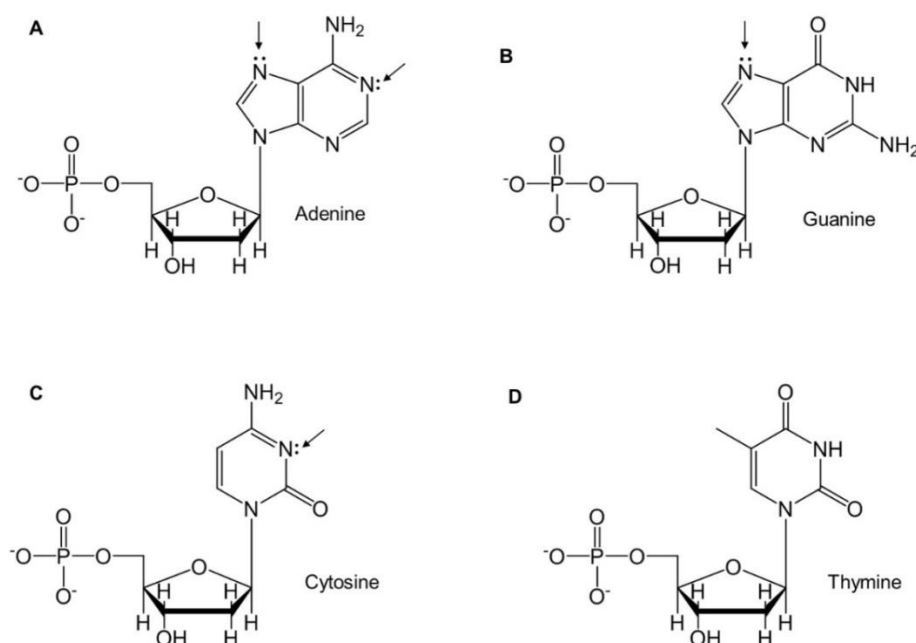
Figure 1.8 Structures of purine and pyrimidine DNA nucleobases showing (↓) possible coordination site(s) to Pt in each nucleobase.
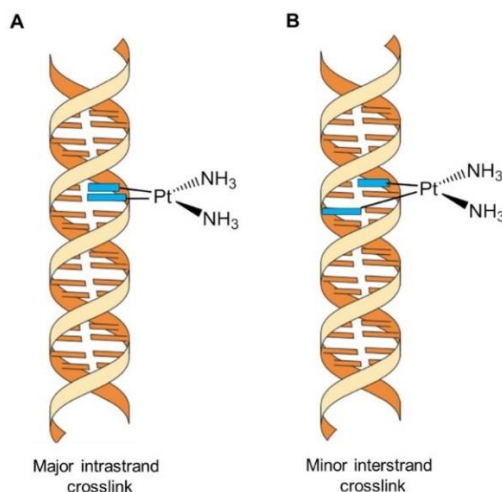
Figure 1.9 CDDP-DNA crosslinks showing (**A**) major 1,2-(GpG) and (**B**) minor G-G interstrand crosslinks, where ■ refers to the guanine nucleobase (figure adapted from ref 58).

The formation of the 1,2-(GpG) crosslinks have been determined by both X-ray crystallography and nuclear magnetic resonance (NMR) methods.[59-61] These CDDP-DNA crosslinks distort the DNA molecule resulting in unwinding and bending (Figure 1.10),[62] altering the structure of the DNA significantly. The generation of these CDDP-DNA adducts disrupt cellular replication, and lead to apoptosis, a programmed mechanistic cell death pathway.[63] To date *cis*-platin remains the most potent anticancer agent for the treatment of a variety of cancers with high cure rates. The potency of *cis*-platin is not without its associated side-effects. As mentioned above, once CDDP enters the cytoplasm it is subject to hydrolysis forming active Pt^{II}-species (Figure 1.6). Pt^{II}-species exhibit a high affinity towards sulfur-containing molecules.[64]
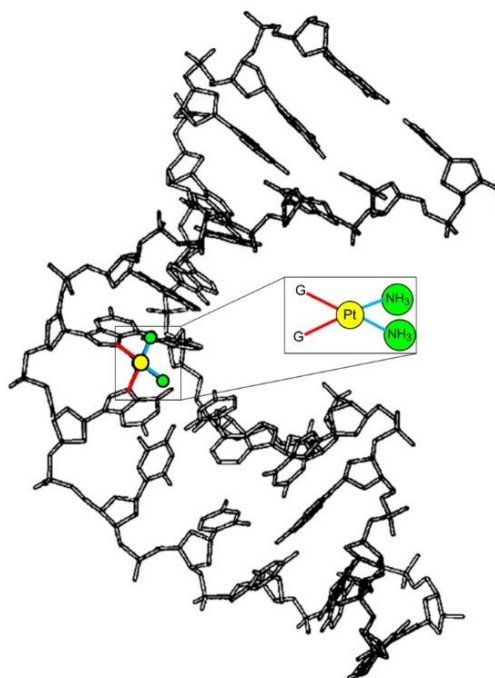
Figure 1.10 Bending of the DNA molecule from a solution structure of DNA platinated DNA by cis-platin (figure adapted from ref 62).

In the intracellular milieu an array of sulfur-based molecules exist in amino acids, proteins and peptides (Figure 1.11). Glutathione (GSH), a thiol-based tripeptide consisting of glutamate (Glu), cysteine (Cys) and glycine (Gly) is one of the most abundant peptides in the cell, with concentrations ranging from $0.5 - 10$ mM and has been shown to interact with *cis*-platin, forming Pt-S(GS) adducts.[65,66] L-methionine (Met) and L-cysteine (cys) amino acids are present in a wide variety of proteins and peptides.[67] Formation of these Pt^{II}-S based species has been attributed to the observed toxic side effects and resistance mechanisms,[68] consequently reducing the active form of CDDP reaching the designated target, DNA.[69] The nucleus was reported to possess $< 1\%$ of the total platinum dose administered. These side-effects have been limiting factors in the continuation of *cis*-platin therapy in

the clinic, in some instances.[70] For these reasons, second generation platinum anticancer complexes have been developed.
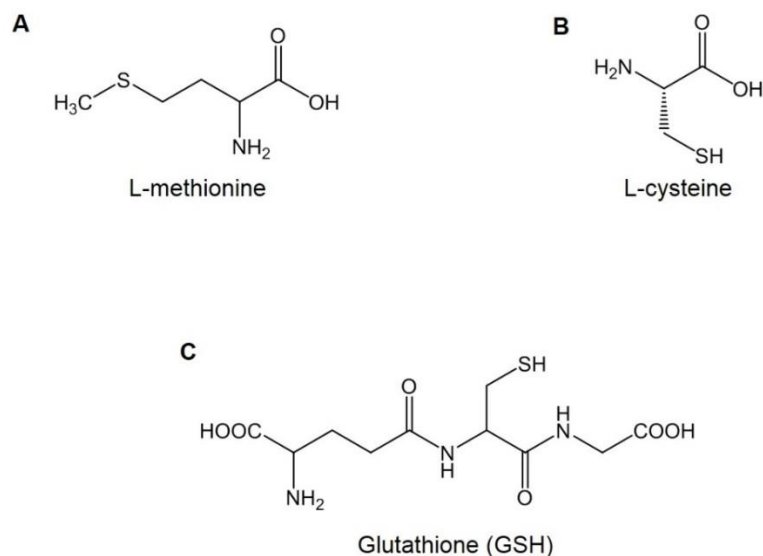
Figure 1.11 Structures of abundant intracellular sulfur-containing molecules.

1.4.3 Second generation Pt^{II} anticancer complexes

In an attempt to overcome the associated side-effects of CDDP, new platinum anticancer complexes where labile ligands were replaced for more stable ligands, those not readily substituted by water, were developed. Numerous publications of new platinum complexes with potential antitumour activity have appeared,[71] however only a few complexes have reached clinical trials.[58,72,73] Carboplatin (**3**, Figure 1.12), a second generation Pt^{II}-anticancer drug has the two chlorido ligands (in *cis*-platin) replaced by a chelated 1,1-cyclobutanedicarboxylate. This substitution rendered carboplatin more stable than CDDP. A consequence of this stability is the reduced reactivity and cytotoxicity of carboplatin resulting in higher doses (300 – 450 mg m^{-2}) needing to be administered to achieve an equivalent potency as CDDP.[74] Hydrolysis of carboplatin generates identical active Pt^{II}-species previously observed from the aquation of CDDP, such that both CDDP and

16

carboplatin are used for the treatment of similar types of cancer. Carboplatin has been approved world-wide for the treatment of cancer and has recently been the drug of choice in the treatment of ovarian cancer over CDDP. It is currently in clinical trials to assess its efficiency in the treatment of salivary gland cancer.[75,76]

Oxaliplatin (**4**, Figure 1.12), marketed as Eloxatin is another world-wide approved Pt^{II}-anticancer complex. The first drug reported to overcome *cis*-platin resistance through the extension of the bulky dach (cyclohexane-1,2-diamine) group into the DNA major groove,[77] preventing the binding of DNA repair proteins. Additional, bi-functional adducts between the N^1 of adenine and the N^7 of guanine DNA nucleobases were formed by oxaliplatin.[78] These adducts were another possible parameter to contribute to overcoming *cis*-platin resistance. Related complexes include nedaplatin (**5**, Figure 1.12), lobaplatin (**6**, Figure 1.12) and heptaplatin (**7**, Figure 1.12) currently unapproved by the Food and Drug Administration (FDA), but in clinical use in Japan, China and South Korea.[79]
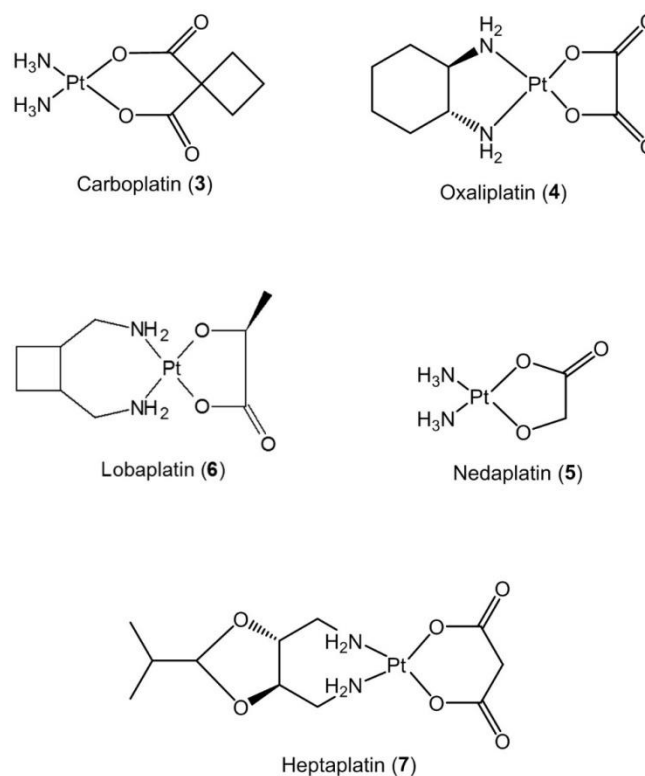
Figure 1.12 Structures of second generation Pt^{II} anticancer complexes.

1.4.4 *Trans* complexes

1.4.4.1 *Trans*-platin

Trans-platin (**2**) the structural isomer of *cis*-platin, was shown to be inactive towards tumour cells. This was thought to be due to its inability to form 1,2-(GpG) intrastrand crosslinks,[80] the major platinated crosslinks inducing cell death. Similar to *cis*-platin, hydrolysis of *trans*-platin generates both mono and bis-aqua species (Figure 1.13), where hydrolysis of *trans*-platin to its mono-aqua form occurs faster than *cis*-platin. The formation of the bis-aqua species for *trans*-platin does not readily occur due to the *trans*-effect. This is the effect of the *trans* ligand on the rate of substitution, independent on the nature of the nucleophile. Monofunctional-DNA adducts have been reported to be formed from the interaction of *trans*-platin with

DNA. However, facile displacement of these monofunctional-DNA adducts by a variety of nucleophiles such as thiourea and GSH may explain its inactivity.[81]
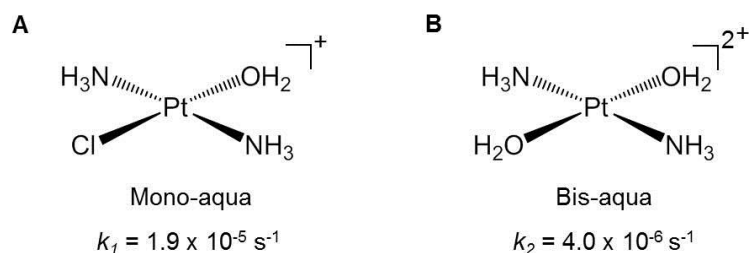
Figure 1.13 Hydrolysis products of *trans*-platin showing (**A**) mono-aqua and (**B**) bis-aqua species with respective rate constants at 298 K.

1.4.4.2 Varying carrier ligands

Farrell has argued that the rapid displacement of the monofunctional-DNA adducts observed for *trans*-platin can be prevented by replacement of the ammine (NH_3) groups with more bulky substituents. Complexes of the type *trans*-$[PtCl_2L_2]$, where L = pyridine or picoline were synthesised (Figure 1.14) and shown to be more cytotoxic in the L1210 leukaemia cell line than their corresponding *cis*-isomers.[82] This led to additional substitutions of the NH_3 groups in *trans*-platin for methyl-imidazole, quinoline, sulfoxides and iminoether-based ligands. All resultant complexes exhibited equivalent or greater cytotoxic profiles than their corresponding *cis*-isomers in both *cis*-platin sensitive and resistant cell lines.[83-88]
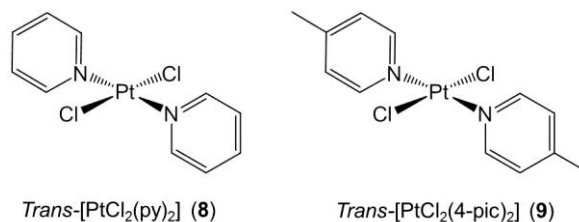
Figure 1.14 Structures of *trans*-$[PtCl_2L_2]$ anticancer complexes where L is (**A**) pyridine and (**B**) 4-picoline synthesised by Farrell.[82]

A comprehensive review by Kalinowska-Lis describes the numerous *trans*-platinum complexes synthesised and their cytotoxic activities.[89] The activity of these *trans*-configured complexes in *cis*-platin resistant cell lines, suggested that these geometrical isomers induce their cytotoxic effect through a different mechanism of action compared to *cis*-platin. Consequently, these reports rebutted the studies performed by Rosenberg and Cleare, in which they suggested a *cis*-configuration a necessary requirement for a chemotherapeutic effect.[90-92] New mechanisms of action offer potential in overcoming conventional resistance mechanisms.[93] However, the reactivity of Pt^{II} complexes with intracellular based nucleophiles (Figure 1.11) still remained, reducing the amount of active Pt^{II} reaching the target molecule, DNA. Efficient delivery of the Pt^{II} active species has been investigated through the use of platinum complexes in the +4 oxidation state.

1.4.5 Pt^{IV} complexes

Pt^{IV} complexes with six strong field ligands are typically octahedral, low spin, $5d^6$ (Figure 1.15). In the +4 oxidation state, platinum complexes are mostly substitution inert and thermally stable. Reduction of Pt^{IV} is required to generate the active Pt^{II} species. Reduction can proceed via intracellular reduction with biological reducing agents (Figure 1.11). Until reduction occurs, the platinum complex remains inactive in the Pt^{+4} oxidation state, referred to as a "prodrug" form. This kinetic inertness prevents unwanted side reactions occurring and has the potential to deliver more platinum to the tumour cell.

$$\underline{\quad} \quad \underline{\quad} \quad d_z{}^2 \; d_{x^2-y^2}$$

$$\underline{\uparrow\downarrow} \quad \underline{\uparrow\downarrow} \quad \underline{\uparrow\downarrow} \quad d_{xy} \; d_{xz} \; d_{yz}$$
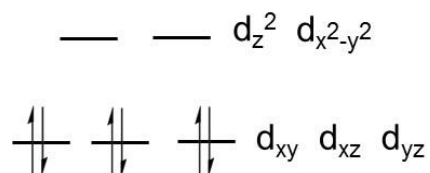
Figure 1.15 Splitting of the d-orbitals of an octrahedral Pt^{IV} complex (d^6) possessing strong donor ligands.

This Pt^{IV} prodrug strategy was exploited during the development of tetraplatin (**10**), iproplatin (**11**), satraplatin (**12**) as shown in Figure 1.16. Both tetraplatin and iproplatin were investigated in phase I clinical trials for their anticancer activity. The facile reduction of **10** to its Pt^{II} active form led to unwanted side-effects *in vivo*. This was attributed to its high reduction potential ($E^{°}$) of ca. -90 mV ($\pm$ 20 mV vs Ag/AgCl). On the contrary, the slow reduction of **11** with a reported $E^{°}$ value ca.-730 mV ($\pm$ 100 mV vs Ag/AgCl) rendered it an inactive anticancer complex.[94] The break-through came from the development of satraplatin (**12**) possessing a reduction potential of ca. -250 mV, which appeared to be in a suitable range. Satraplatin is reduced by intracellular metal-containing redox proteins to its active Pt^{II} form (**13**) at a slower rate than tetraplatin and yet faster than iproplatin. Satraplatin has yet to be approved by the FDA but has been involved in numerous clinical trials.[58,79] It has been reported to be an efficient anticancer agent for the treatment of prostate cancer[95] and is currently being investigated in combination therapy.[96]
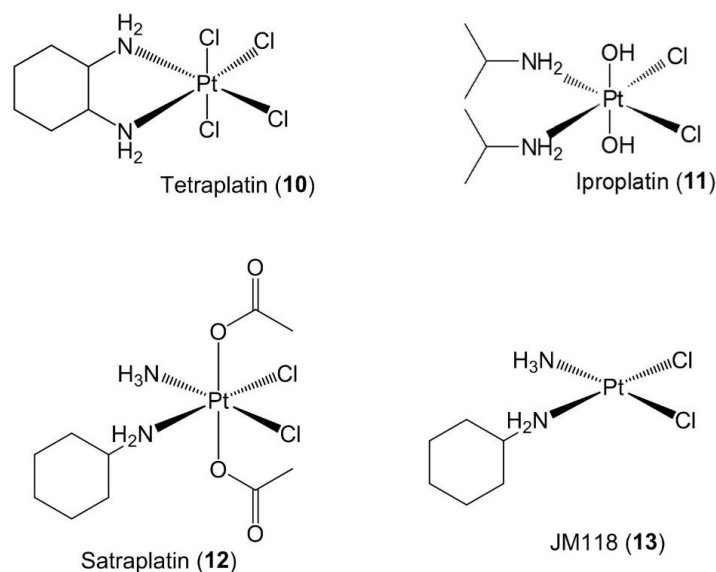
Figure 1.16 Structures of tetraplatin, (**10**); iproplatin, (**11**); satraplatin, (**12**) and JM118 reduced form of satraplatin (**13**).

The equivalent or greater cytotoxic profiles of *trans*-based complexes led to the development of numerous *trans*-Pt^{IV}-anticancer complexes. The complex, *trans*-[PtCl$_2$(dma)(ipa)(OH)$_2$] (**14**) was compared to its corresponding Pt^{II} analogue, *trans*-[PtCl$_2$(dma)(ipa)] (**15**), where (dma= dimethylamine, ipa= isopropanamine). Only **14** demonstrated *in vivo* cytotoxicity in human ovarian carcinoma xenografts in mice, whereas **15** only exhibited *in vitro* activity.[97] Similar comparison studies were performed with *trans*-[PtCl$_4$(NH$_3$)(4-py-MeOH)] (**16**) and *trans*-[PtCl$_2$(NH$_3$)(4-py-MeOH)] (**17**). Interestingly, **17** was determined to be ca. four-fold more active than **16**.[98] The lower activity of **16** was attributed to its slow reduction from the inactive Pt^{IV} to the active Pt^{II} form.

Trans-[PtCl$_2$(dma)(ipa)(OH)$_2$] (**14**)

Trans-[PtCl$_2$(dma)(ipa)] (**15**)

Trans-[PtCl$_4$(NH$_3$)(4-py-MeOH)] (**16**)

Trans-[PtCl$_2$(NH$_3$)(4-py-MeOH)] (**17**)
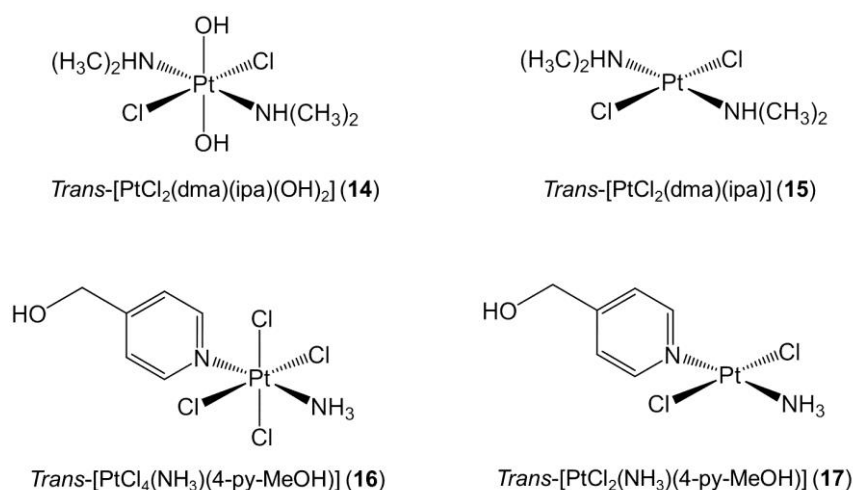
Figure 1.17 Structures of *trans*-platinum(IV) complexes (**14** and **16**) and their corresponding *trans*-platinum(II) analogues (**15** and **17**).

Despite the reduced side-effects of these novel Pt^{IV}-anticancer complexes relative to *cis*-platin (**1**), the active Pt^{II}-species are still generated through intracellular reduction. Chemical reductions can occur throughout the body given the array of biological reducing agents present in all cells. Therefore, intracellular reductions are not specific to tumour cancer cells resulting in non-malignant tissue being damaged. Recent research on the efficient delivery of platinum anticancer complexes has focused on the concept of targeted delivery.

1.5 Targeted delivery

Targeted delivery has the potential to reduce unwanted side-effects whilst simultaneously improving the efficiency of the chemotherapeutic agent. Targeted delivery exploits the use of a variety of scaffolds such as carbon nanotubes (CNTs), liposomes and biodegradable peptides for efficient delivery of the platinum anticancer complex to its biological target, typically DNA. Incorporation of the platinum formulation into these scaffolds serves to protect the platinum anticancer

complex from premature hydrolysis or intracellular reduction. These processes are achieved either through passive or active targeted delivery.

1.5.1 Passive drug delivery

Innovative designs of nano-vectors to achieve efficient drug delivery and their complexity are emerging. Min *et al.* have conjugated a Pt[IV] prodrug (**18**) to amine-functionalized PEGylated gold nanorods (AuNRs), reduced to Pt[II] by cellular reductants. The Pt[IV]-PEG-AuNRs were most active in the MCF-7 breast cancer cells exhibiting an IC$_{50}$ of 0.18 μM, significantly more potent than free *cis*-platin, with an IC$_{50}$ of 11.8 μM.[99]
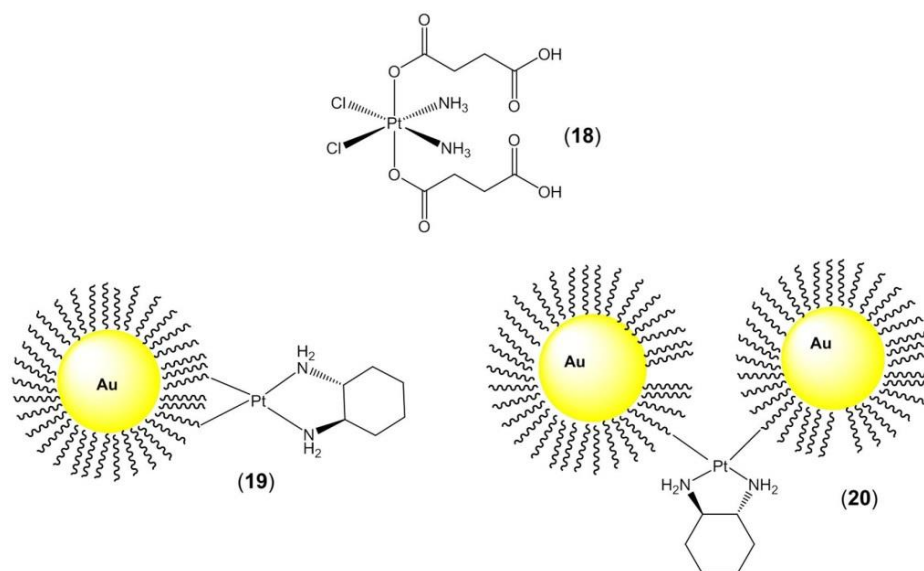
Figure 1.18 Pt[IV] prodrug complex, (**18**); Active component of oxaliplatin tethered to AuNP functionalised with PEG linker, (**19**, **20**).

In similar work, Brown *et al.* functionalised AuNPs with thiolated PEG tethered to the active fragment of oxaliplatin, {Pt(*R,R*-dach)}$^{2+}$, (**19** and **20**). Similarly, these Pt-AuNPs were almost six-fold more active towards A549 lung cancer cells than free oxaliplatin but ca. five-fold more active, or as active, as free oxaliplatin in

various colon cancer cell lines.[100] These results demonstrated increased potency of platinum complexes conjugated to gold nanoparticles/rods.

1.5.2 Active drug delivery

Delivery of anticancer agents *via* nanocarrier scaffolds is efficient for reaching the tumour site through the enhanced permeability and retention (EPR) effect.[101] Although the attachment of receptor-binding molecules (particularly for receptors over-expressed in cancer tissues) on the surface of NPs can also enhance the uptake of the nanocarrier into the tumour cell through receptor-mediated internalisation. The most common receptors targeted in nanotechnology include the folate (FR), epidermal growth factor (EGF) and the transferrin (TfR) receptors.

1.5.2.1 Epidermal growth factor (EGF)

The overexpression of the EGF receptor in human tumours, in particular NSCLC (non-small cell lung cancer), renders it another potential target. Bhirde *et al*. attached *cis*-platin (dissolved in DMSO) and EGF to oxidised singled-walled carbon nanotubes (SWCNTs) to target squamous cancer. *In vivo* studies revealed SWCNTs-CDDP-EGF (**21**) to be selective towards HNSCC (head and neck squamous cell carcinoma). Tumour growth regression was significant in mice treated with SWCNT-CDDP-EGF bearing HNSCC xenografts in contrast to mice treated with SWCNT-CDDP.[102]
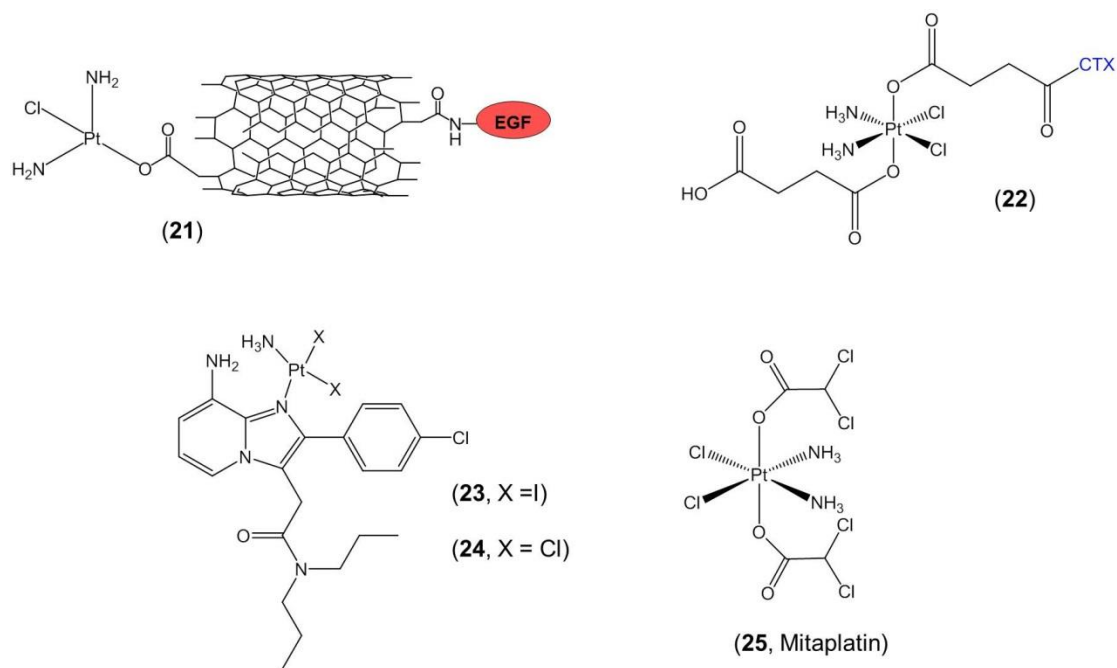
Figure 1.19 SWCNT bio-conjugated with *ci*s-platin and epidermal growth factor (**21**); Pt[IV]-chlorotoxin conjugate (**22**); Platinum translocator protein (TSPO) binding ligand conjugates with various X groups (**23**, **24**); Mitaplatin (**25**).

1.5.2.2 Proteins/peptides

Various peptide sequences can bind preferentially to tumour cells and so can act as cancer targeting ligands. For example, chlorotoxin (CTX), a 36-amino acid peptide which blocks small-conductance chloride channels, binds to functional proteins such as matrix metalloproteinase-2 (MMP2) (overexpressed in glioma and related cancers) and chloride ion channels overexpressed in different types of cancers. CTX was conjugated to a Pt[IV]-succinato complex (**22**) for delivery of *cis*-platin. The cytotoxicity of **22** towards MCF-7 breast, A549 lung and HeLa cervical cancer cells was less potent than CDDP but more active than both the Pt[IV] precursor and CTX alone. The reduced activity of the Pt[IV] complex was attributed to its kinetic inertness.[103]

Translocator proteins (TSPOs) are peripheral benzodiazepine receptors (PBRs) overexpressed in both human and rat glioma cells. Margiotta *et al*. conjugated *cis*-{Pt^{II}(NH$_3$)(X)$_2$} to TSPO-binding ligands (**23** and **24**). Such conjugates showed potency equivalent to that of *cis*-platin through apoptosis. Both complexes were equally active towards sensitive A2780 and resistant A2780cis breast cancer cells.[104]

The Warburg effect, the ability of cancer cells to produce energy through a high rate of glycolysis, helps tumour cells survive. The FDA-approved anticancer agent dichloroacetate (DCA) can reverse the Warburg effect. The Pt^{IV} prodrug Mitaplatin (**25**) contains two DCA units, and once internalised is reduced to *cis*-platin (**1**) which can attack nuclear DNA, while the DCA can attack mitochondria selectively. Mitaplatin alters the mitochondrial membrane potential of cancer cells, promoting apoptosis by releasing cytochrome c and translocating apoptosis-inducing factor from mitochondria to the nucleus. The cytotoxicity of **25** is equivalent or exceeds most well-known Pt^{IV} complexes and is comparable to CDDP.[105]

Cell penetrating peptides (CPPs) are another well-known class of drug carriers due to their ability to pass through cell membranes. The TAT peptide is a widely studied CPP. Conjugates of the TAT peptide (YGRKKRRQRRR) with a Pt^{IV} analogue of oxaliplatin generated complexes (**26** and **27**) were ca. four-fold more potent in ovarian, colon and lung cancer cells lines than the free Pt^{IV} analogues of oxaliplatin. The diconjugate **27** displayed slightly lower cytotoxicity, indicating that an extra TAT peptide did not enhance the cytotoxicity.[106]
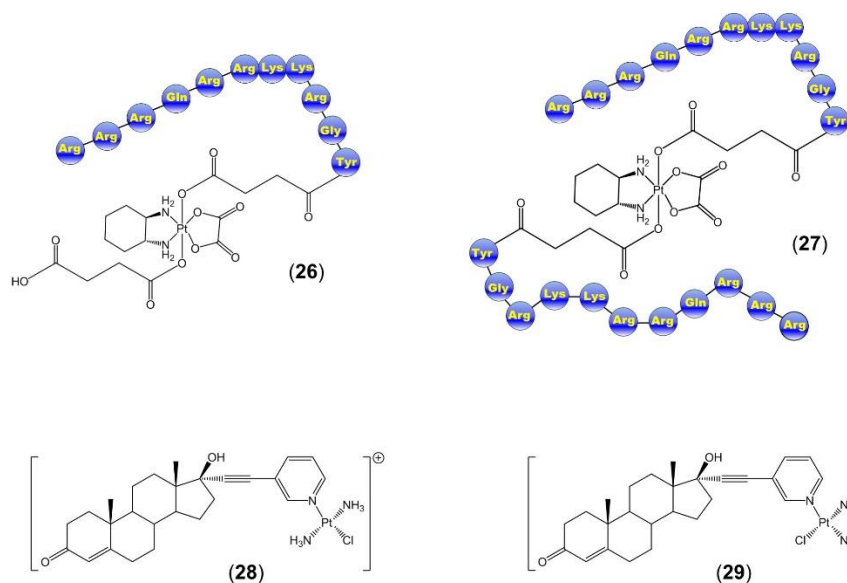
Figure 1.20 Oxaliplatin-TAT mono- (**26**) and di- (**27**) peptide conjugates; Example of *cis* (**28**) and *trans* (**29**) steroidal platinum(II) complexes.

Since the androgen receptor (AR) is up-regulated in breast, ovarian and prostate tumour cells, Huxley *et al.* designed multiple androgenic steroidal ligands with various nitrogen-containing heterocyclic rings conjugated to either *cis*-platin *or* *trans*-platin (**28** and **29**) as platinum drug delivery vectors. These [$Pt^{II}(NH_3)_2Cl$(steroid)] conjugates were two- to twelve-fold more cytotoxic than the non-steroidal complexes, but in similar activity range as CDDP.[107]

Despite these many advances in both passive and active delivery of chemotherapeutic agents, the development of intrinsic or acquired resistance remains a major drawback of platinum anticancer complexes. Zamble *et al.* reported the development of resistance as a main factor contributing to the discontinuation of platinum drugs in the clinic.[54] The onset of resistance has been attributed to a variety of factors including genetic instability, heterogeneity and mutation rate of tumour cells. Cellular DNA is protected *via* five repair pathways, including

nucleotide excision repair (NER), mismatch repair (MMR), double strand break, base excision repair and direct repair, recently reviewed by Martin *et al.*.[6] To overcome resistance mechanisms alternative therapeutic therapies such as phototherapy have been developed.

1.6 Photochemistry

The section describes the various processes which occur in coordination complexes during a photo-chemical reaction. A photo-chemical reaction commonly involves a chemical effect induced in the molecule after the absorption of ultra-violet, visible or infrared radiation. Interaction of a molecule in the ground state (A) with radiation (*hυ*) leads to the formation of an excited state (A*). This process is commonly referred to as photo-excitation. Photo-excitation occurs only if the energy difference between the ground (A) and excited (A*) states is equal to the energy of the photon (*hυ*) absorbed by the molecule:

$$E_{A*} - E_A = hυ$$

The oscillator strength *f* defines the probability of light absorption for a certain transition and is defined by equation 1.3, where: m_e is the mass of the electron, $μ$ is the transition dipole moment, e is the charge of the electron, Ĥ is the dipole moment operator and Ψ_A and Ψ_{A*} are the wave-functions of the ground (A) and excited (A*) states, respectively.[108]

$$f = \frac{8\pi^2 m_e \nu |\mu|^2}{3he^2} \quad \text{Eqn 1.3} \qquad \mu = \int \Psi_A \hat{H} \Psi_{A*} d\tau \quad \text{Eqn 1.4}$$

For certain transitions, the transition dipole moment ($μ$) can be zero which results in an oscillator strength *f* of zero, and so the transition is forbidden. Selection rules

govern whether transitions are allowed ($\mu \neq 0$) or forbidden ($\mu = 0$). Forbidden transitions are usually observed when:

- $\Delta S \neq 0$, transitions between spin states of different multiplicity.

- $\Delta l \neq \pm 1$

- Laporte Rule transitions between states of equal parity (g ↔ g, u ↔ u) are forbidden.

The Beer-Lambert law describes the absorbance (A) of radiation by a homogenous solution and is proportional to the path-length (l, cm) and concentration (c, M):

$$A = \varepsilon c l$$

where ε is the extinction coefficient (M^{-1} cm^{-1}) and its value is used to determine the strength of the transition. Various transitions can occur with the promotion of an electron from the highest occupied molecular orbital (HOMO) to the lowest unoccupied molecular orbital (LUMO). Transitions are termed according to the localisation of the electron density transfer. For octahedral complexes, both the metal and ligand orbitals can be involved in various transitions, depicted in Figure 1.21. A variety of electronic transitions can occur namely ligand-field (LF) and charge-transfer transitions typically ligand-to-metal charge transfer (LMCT), metal-to-ligand charge transfer (MLCT), charge-transfer-to-solvent (CTTS), intraligand-charge transfer (ILCT). The selection rules (p 30) determine which transitions are allowed.
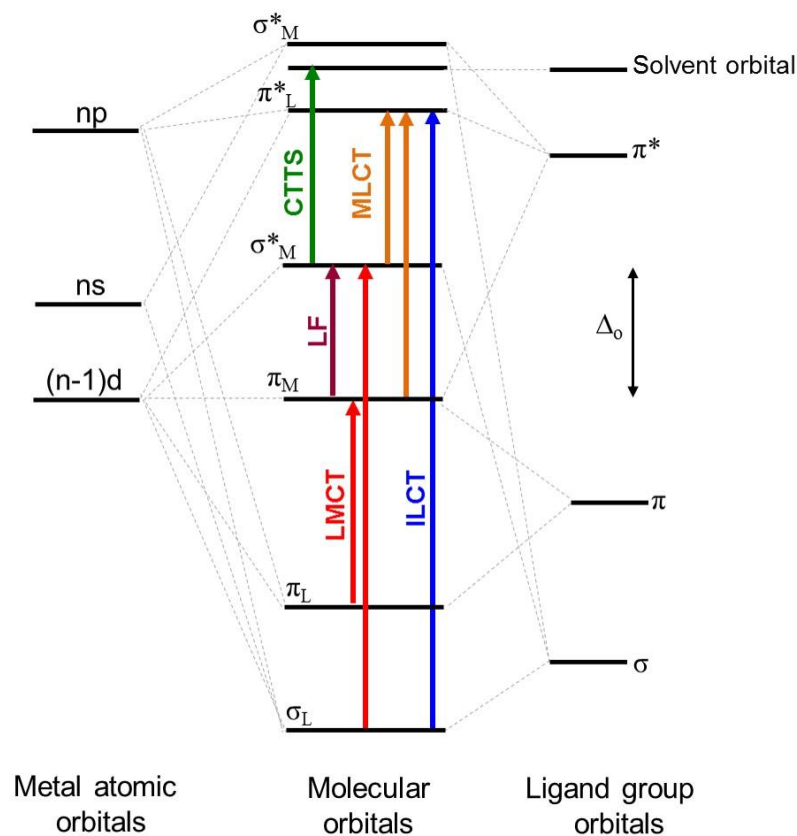
Figure 1.21 Molecular orbital diagram for an octahedral complex and the variety of electronic transitions that can be induced.

1.6.1 Electronic Transitions

1.6.1.1 Ligand-Field (LF)

The redistribution of electrons within partially filled d-orbitals is commonly referred to as ligand-field (LF) or d ↔ d transitions. As shown in Figure 1.15, in an octahedral complex the five d-orbitals are split into two higher energy (e_g) orbitals (d_z^2, $d_{x^2-y^2}$) and three lower energy (t_{2g}) orbitals (d_{xy}, d_{yz} and d_{xz}). Theoretically, the absorption of a photon equal to the energy difference between the higher and lower orbitals (Δ_o, Figure 1.21) can result in the promotion of an electron from the lower orbitals (t_{2g}) to the higher (e_g) orbitals.

In theory, the Laporte rule states transitions between states of equal parity, d ↔ d transitions are forbidden. However, experimentally the Laporte rule can be relaxed either due to the (**a**) centre of symmetry being temporarily destroyed due to the vibration of metal-to-ligand bonds in an octahedral complex possessing six identical ligands, or (**b**) the octahedral complex is not completely symmetric due to the presence of different ligands. However, these transitions are generally weak ($\varepsilon \sim$ 500 M^{-1} cm^{-1}) and often masked by stronger transitions.

1.6.2.2 Charge-transfer (CT) Transitions

Charge-transfer transitions are allowed by both ΔS and the Laporte selection rules. Being both orbital- and spin-allowed, results in intense charge-transfer transitions with high extinction coefficients ($\varepsilon = 10^3 - 10^6$ M^{-1} cm^{-1}). If the ligand orbitals are filled and the metal-d orbitals are empty, charge transfer from the ligand to the metal (LMCT) can occur. Similarly, a metal in a low oxidation state (i.e. electron rich) with low lying ligand molecular orbitals can result in charge-transfer from the metal to the ligand (MLCT).

1.6.2.3 Intraligand (IL) and Charge-Transfer to Solvent Transitions

Transitions between ligands generally occur in complexes possessing ligands with multiple bond(s) such as pyridine. These transitions only involve the ligands and the central metal atom does not impose much effect on the transition. Intraligand charge-transfers (ILCT) are both orbital- and spin-allowed and possess high extinction coefficients ($\varepsilon = 10^3 - 10^5$ M^{-1} cm^{-1}), similar to LMCT and MLCT transitions.

Charge-transfer to solvent (CTTS) transitions occur in complexes with either (**a**) low oxidation number or where (**b**) an increase in oxidation number without a change in the coordination sphere occurs. These transitions are allowed ($\varepsilon = 10 - 10^3$ M^{-1} cm^{-1}) but are dependent on the solvent reduction potential.

Excited states are intermediate states and their energy can be dissipated through a variety of both radiative and non-radiative processes. These are referred to as deactivation pathways.

1.6.2 Deactivation pathways of excited states

The decay of excited states can occur through either photo-physical or photo-chemical pathways. The Jablonski diagram accurately depicts the various photo-physical deactivation pathways (Figure 1.22).[109] The process of absorption occurs almost instantaneously on a time-scale of ca. 10^{-15} s. Both fluorescence and phosphorescence are emissive pathways. Fluorescence readily occurs between states of the same multiplicity (Sn→S0, where n is equal to an integer). However, phosphorescence occurs between two states of different multiplicity (e.g. T1→S0), therefore $\Delta S \neq 0$ and possess longer life-times. Both internal conversion (IC) and intersystem crossing (ISC) are non-radiative type processes. ISC involves the molecule moving between levels with a change in multiplicity ($\Delta S \neq 0$), contrary to IC.
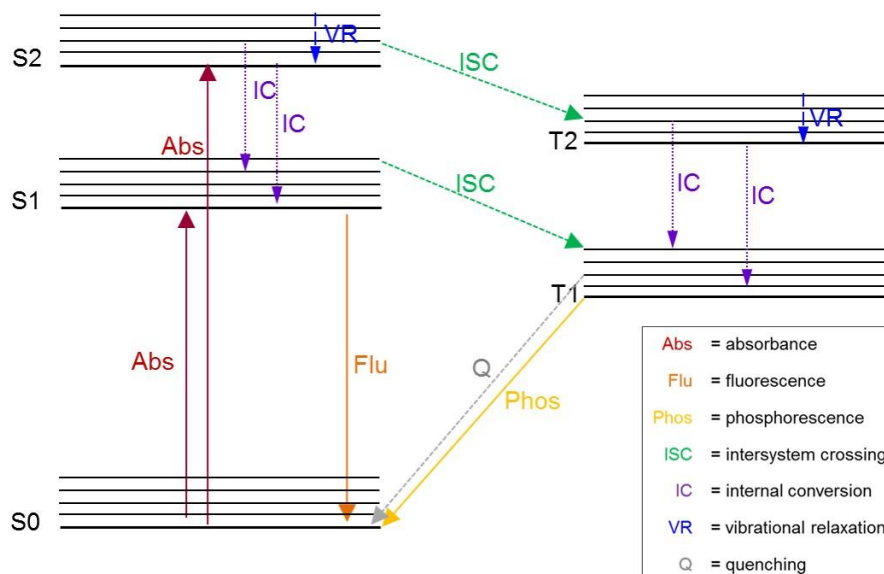
Figure 1.22 Jablonski diagram showing various deactivation pathways where S0 refers to ground singlet state; Sn (n ≠ 0) refers to singlet excited state and Tn (n ≠ 0) refers to triplet excited state (figure adapted from ref 109).

Generally, processes whereby $\Delta S = 0$ are faster and those with $\Delta S \neq 0$ are slower, i.e. lead to longer lived states (Table 1.2).

Table 1.2 Time-scale of deactivation processes

Process	Time Scale (s)
Absorption	~ 10^{-15}
Fluorescence	~ 10^{-9}
Phosphorescence	~ 10^{-3} to seconds
ISC	~ 10^{-7} - 10^{-4}
IC (to lower excited state)	~ 10^{-12}
IC (to ground state)	~ 10^{-6}

34

Additional, photo-chemical deactivation pathways exist, which compete with photo-physical pathways. Photo-chemical reactions are initiated at the excited state. The promotion of an electron to an excited state has potential to weaken certain bonds within the molecule. In general, photo-chemical reactions can be deduced from the electronic transitions present in the complex. Complexes possessing LF transitions typically undergo photo-isomerisation, photo-racemisation and photo-solvation. In contrast, complexes exhibiting LMCT transitions photo-decompose through a photo-reduction process. Reduction of the metal centre and loss of ligand(s) are commonly observed during photo-reductions. In this thesis, photo-redox pathways are observed and will be discussed in section **1.8.2.**

1.7 Phototherapy

The use of light in the treatment of various diseases can be dated back to about three thousand years ago, used by both Egyptians and Chinese civilisations.[110] Phototherapy involves the use of light in combination with a chemical agent to induce a cytotoxic effect in the biological region of interest. The concept of phototherapy can be dated back to ca. 1900 from reports by Oscar Raab, effectively reporting on the cytotoxic effect of acridine in combination with light on infusoria.[111]

1.7.1 Photodynamic therapy

Studies performed by Dougherty led to the development of photodynamic therapy, PDT.[112,113] PDT involves the administration of a non-toxic complex, a photo-sensitiser (PS), into a patient's bloodstream. After an incubation period (to allow sufficient accumulation of the PS into the target tissue) the PS is subject to

irradiation at a specific wavelength. Longer wavelengths of light (>600 nm) are used in PDT owing to its ability to penetrate into deeper tissues (Figure 1.23).[114] PDT is often used in cancer treatment[115] but extends into treatment of both infectious diseases and disorders.[116]
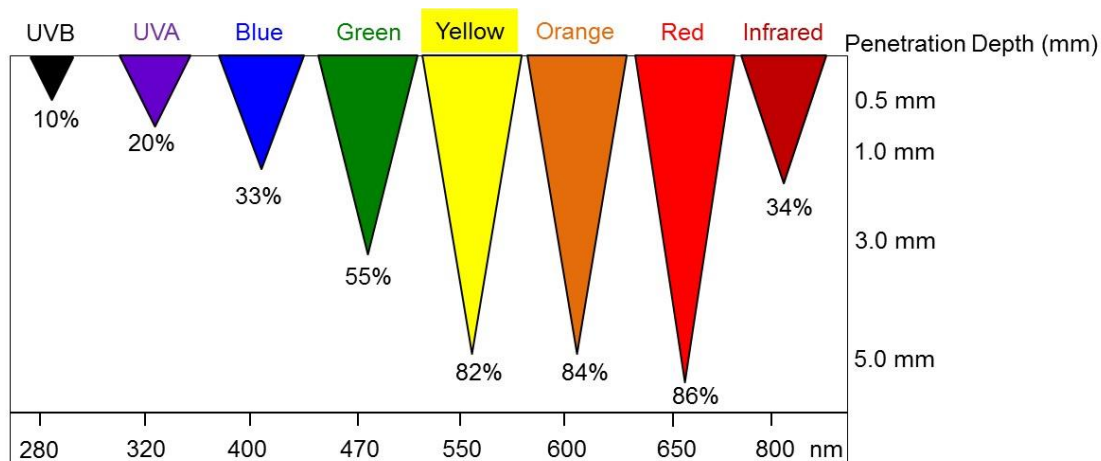
Figure 1.23 Percentage and depth penetration by various wavelengths of light (figure adapted from ref 114).

Often, PS are porphyins consisting of four pyrrole rings fused together by methine bridges and possess an absorption in the region of 600-800 nm.[117] The first generation photo-sensitiser synthesised by Dougherty, Photofrin® (Figure 1.24**A**), was approved clinically for the treatment of lung, esophageal and bladder cancer.[118] In contrast, Foscan® (Figure 1.24**B**), a second generation PS compound, has been clinically approved for head and neck cancer. Interestingly, this compound accumulates more specifically in the cancerous tissue and is irradiated with a slightly longer wavelength of light (652 nm) compared to Photofrin at 630 nm.[119]

36
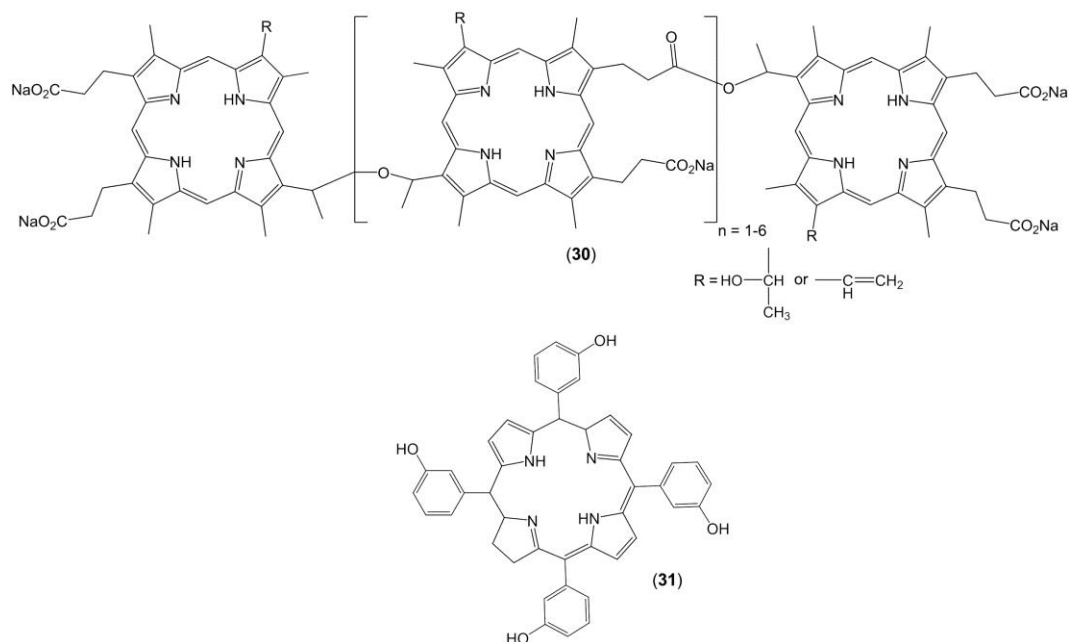
Figure 1.24 Structures of the clinically approved photo-sensitisers Photofrin (**30**) and Foscan (**31**).

1.7.1.1 Mechanism of PDT

PDT has three essential requirements: (a) a photo-sensitiser, (b) light and (c) molecular oxygen (O_2) necessary to induce a PDT effect in the cancerous tissue. The PS should have minimal dark toxicity in both human and animal models.[115] The process involves the irradiation of the PS in the ground (S0) state with a specific wavelength of light (generally matched to the absorption of the administered compound). Photon excitation promotes the PS into a single excited (S1) state. Once absorption occurs, the excited state can dissipate its energy through photo-physical pathways, as previously described (Figure 1.25).[113,117] The longer lifetime (ca. μs – ms) of the triplet excited (T1) state compared to the singlet excited (S1) state suggests that the T1 excited state is involved in the photodynamic effect. The energy of the T1 state can be dissipated through phosphorescence (T1→S0).
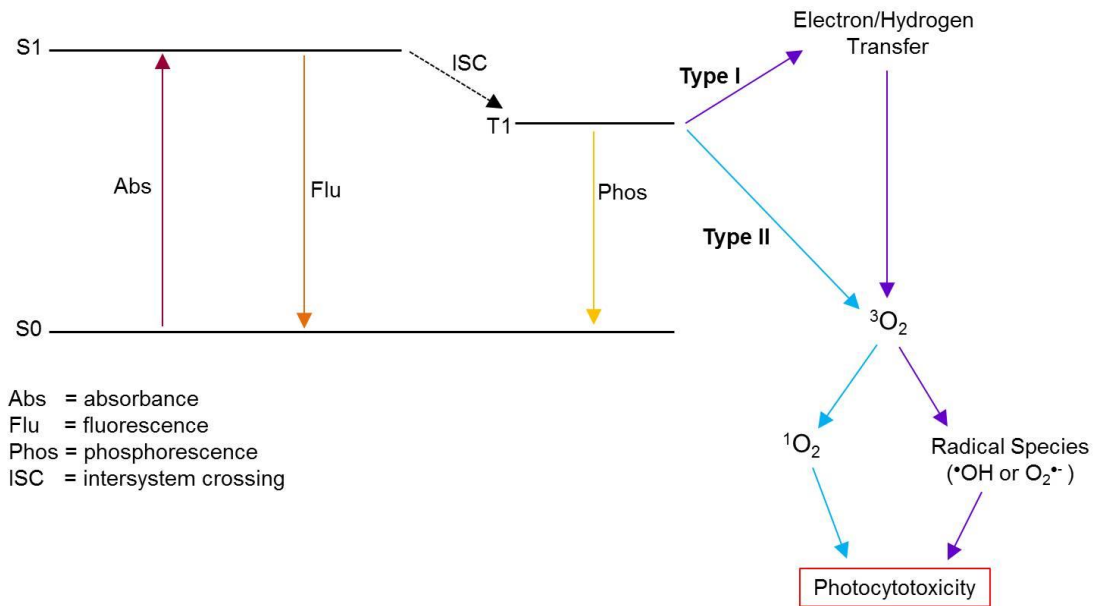
Figure 1.25 Absorption of light by the singlet ground state (S0), generating a singlet excited (S1) and the triplet excited (T1) states, the latter formed through intersystem crossing (ISC). Quenching of the T1 state by molecular oxygen ($^3O_2$) *via* type I (→) or type II (→) processes induces the PDT effect through the formation of various reactive oxygen species (figure adapted from ref 117).

Quenching mechanisms for the T1 excited state have been reported to induce the observed PDT effect.[120] Two quenching processes exist, type I and type II. The type I process involves either an electron or hydrogen transfer between the T1 state and a molecular substrate i.e. cell membrane, generating free radical species. These formed radical-based species interact with molecular oxygen ($^3O_2$) present in the cell leading to the formation of ROS. In contrast, a direct interaction between the T1 excited state and $^3O_2$ occurs during type II. Through an energy transfer mechanism, singlet oxygen ($^1O_2$, $^1\Delta_g$) is generated from this interaction (Figure 1.25). As mentioned earlier, $^1O_2$ is a well-known cytotoxic species and is believed to be the main contributor to cell death from treatment *via* PDT. Both processes are

reported to proceed during PDT. The ratio of type I over type II is dependent on the concentration of the substrate, molecular oxygen and the administered photosensitiser.[121]

PDT remains a highly used cancer therapy treatment as opposed to surgery due to its non-invasive nature. Additionally, the formation of $^1O_2$ has been attributed as the main cytotoxic species inducing the PDT effect. Formed at the site of irradiation, $^1O_2$ has a short life-time and more importantly possesses a very short diffusion distance of ca. 0.02 µm.[122] Thereby, healthy nearby cells remain undamaged.

However, numerous disadvantages are associated with current PDT therapy. Firstly, the requirement of molecular oxygen inside the cell is a limiting factor of PDT treatment, due to the common hypoxic ($^3O_2$-deficient) environment of cancerous tissue.[123] Secondly, despite the reported non-invasive nature, the long clearance times (4-8 weeks) of the PS from the patient's body limit the patient's exposure to daylight up to periods of a couple of months.[117] Finally, resistance mechanisms similar to those previously reported for conventional chemotherapy and radiotherapy treatments have emerged.[124] PDT resistance has been reported to be dependent on both the concentration of the PS and the light dose administered.[125] Antioxidant enzymes have been reported to inactivate the toxic reactive oxygen species ($^{\bullet}OH$, $O_2^{\bullet-}$ and $^1O_2$) during first stage PDT treatment.[125] Another mode of resistance has been noted through heat shock proteins (HSPs) which possess the ability to prevent unwanted protein aggregation and stabilise unfolded proteins, resulting in the repair of the damage induced by PDT.[126] Therefore, another mode of cancer therapy is needed to overcome current resistance mechanisms.

1.8 Photo-chemotherapy

Photo-activation of a chemotherapeutic (PACT) differs from conventional PDT as the administered complex remains non-toxic until photo-activation with visible light without the requirement of molecular oxygen (type III mechanism). As mentioned, Pt^{IV} complexes are kinetically inert making them ideal candidates as photo-activatable platinum prodrugs.

1.8.1 Photo-activatable Pt^{IV} diiodo complexes

Similar to PDT, longer wavelengths of light (> 600 nm) are preferred for PACT, for deep penetration into the cancerous tissue. The wavelength of activation for inorganic complexes can be determined from the exhibited electronic transitions. The first photo-activatable Pt^{IV}-diiodo complexes were synthesised in the Bednarski laboratory. All these Pt^{IV} complexes possessed an ethylene-diammine ligand as the non-leaving group, opposed to the ammine ligands present in *cis*-platin. This was specifically chosen to avoid photo-isomerisation and render the resultant complex more stable. Kratochwil investigated the absorption bands of *cis,trans*-$[Pt(en)(Cl)_2(X)_2]$ complexes, (where en = ethylenediammine and X = Cl, Br, I). The complex *cis,trans*-$[Pt(en)(Cl)_2(I)_2]$ (**32**, Figure 1.26) with the least electronegative atom absorbed energy at the longest wavelength.[127] Therefore, the choice of ligands coordinated to the Pt^{IV} centre can directly promote activation at longer wavelengths.[128] Despite activation at longer wavelengths, complex **32** exhibited an equivalent dark and light cytotoxicity, attributed to its high reduction potential of ca. 75 E/mV. This large reduction potential rationalised its facile reduction by biological reducing agents (e.g. GSH) to the active Pt^{II} species.[129]

To increase the dark stability, the chlorido ligands where substituted by hydroxido-based ligands. The resultant complexes (**33**-**35**, Figure 1.26) exhibited lower reduction potentials and possessed a LMCT band at ca. 400 nm.
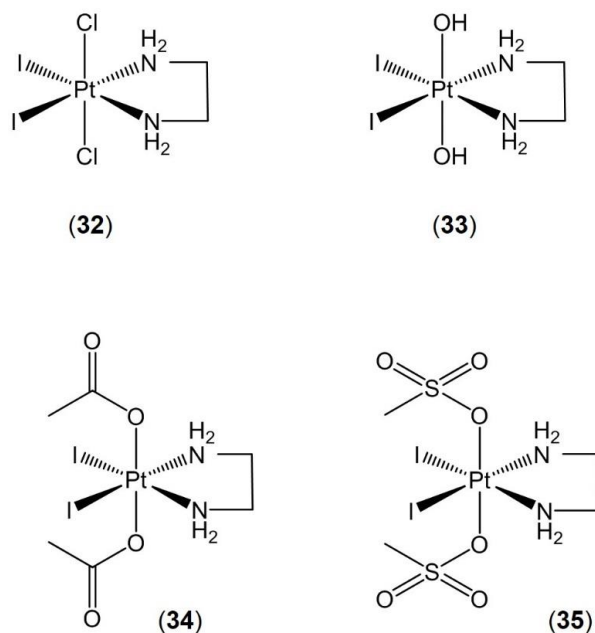
Figure 1.26 Structures of early photo-activatable Pt^{IV}-diiodo complexes.

Nuclear magnetic resonance (NMR) studies revealed the reduction of the Pt^{IV}-diiodo complexes (**32**, **33** and **35**) by both glutathione (GSH) and N-acetyl-cysteine (NAC).[130] Complex **34**, the most potent complex, displayed ca. 65% DNA platination after 6 h, in contrast to *cis*-platin, which induced ca. 90% DNA platination after an equivalent time period.

The abundance of biological reducing agents throughout the body (refer to Figure 1.11), suggested reduction of Pt^{IV} to Pt^{II} was not specific to tumour cells. Therefore, effective Pt^{IV} photo-activatable prodrugs should exhibit dark-stability in the presence of biological reducing agents. Consequently, alternative ligands to iodides were investigated.

1.8.2 Photo-activatable Pt^{IV} diazido complexes

Transition metal complexes possessing azido ligands have been reported to be light sensitive, regardless of the transition metal centre. Vogler was the first to report on the photo-chemical nature of platinum diazido complexes. Photo-irradiation of *trans*-$[Pt(CN)_4(N_3)_2]^{2-}$ at 300 nm UVA gave rise to the loss of two azide ligands, in the form of azidyl ($^{\bullet}N_3$) radicals. This proceeded through a simultaneous two one-electron reduction of the Pt^{IV} centre without formation of a Pt^{III} intermediate species,[131] as shown below.

$$[Pt(CN)_4(N_3)_2]^{2-} \xrightarrow{h\nu} [Pt(CN)_4]^{2-} + 2(^{\bullet}N_3)$$

The formation of the $^{\bullet}N_3$ radicals were confirmed by electron paramagnetic resonance (EPR). This technique is specific for the characterisation of paramagnetic species and will be discussed in more detail in **Chapter III**. Moreover, irradiation of *cis*-$[Pt(PPh_3)_2(N_3)_2]$ led to the formation of hexazabenzene (N_6) and $[Pt(PPh_3)_2]_2$. Bubbles were observed in the irradiated solution, attributed to the decomposition of N_6 into nitrogen gas.[132] Interestingly, $[Pt(N_3)_6]^{2-}$, initially synthesised and characterised by Beck *et al.* was photo-irradiated by Volger *et al.* with ca. 314 nm UVA and reported to undergo a two photon (four-electron) reduction *via* a Pt^{II} intermediate generating Pt^0, as shown below. The formation of a black precipitate upon additional irradiation confirmed the generation of Pt^0.[133]

$$[Pt(N_3)_6]^{2-} \xrightarrow{h\nu} [Pt(N_3)_4]^{2-} + 3(N_2)$$
$$\downarrow h\nu$$
$$Pt + 3(N_2) + 2(N_3)^-$$
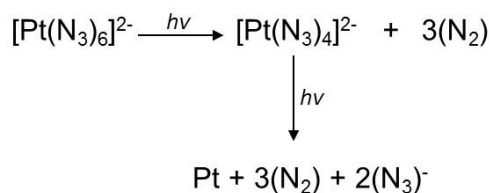
The development of second-generation photo-activatable platinum(IV) complexes was paved by the work performed by Bednarski and Vogler and the concept of PDT.

Both *cis* (**36**) and *trans* (**37**) – photo-activatable diammine platinum(IV) complexes were investigated (Figure 1.27).[134,135] Complexes **36** and **37** exhibited dark stability in the presence of intracellular reducing agents, as monitored by NMR spectroscopy.[136,137] Irradiation of complexes **36** and **37** at 365 nm UVA led to the observation of gas bubbles, presumed to be nitrogen gas.[138] Both complexes displayed IC$_{50}$ values (50% inhibitory concentration) similar to both *cis* and *trans*-platin. Interestingly, photo-irradiation of **37** in the presence of dimethyl-sulfide (DMS) led to the formation of a new carbon-to-carbon bond.[139] Furthermore, in a separate study performed by Farrer *et al.*, *trans*-diam(m)ine diazido Pt^{IV} complexes were determined to possess a greater photo-cytotoxic activity than their *cis*-isomers. The difference in activity was proposed to be due to the *trans*-based complexes targeting different cellular components or inducing different DNA lesions.[140] Despite the dark stability of **36** and **37** and their ability to induce a photo-cytotoxic effect in HaCaT human keratinocytes cells, these complexes were limited to photo-activation at 365 nm UVA.
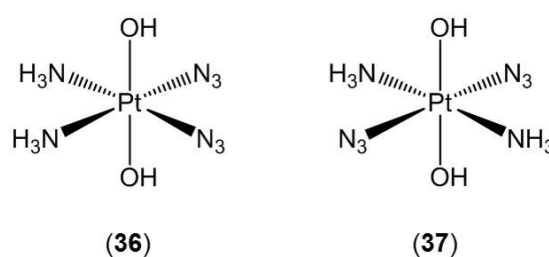
Figure 1.27 Structures of platinum(IV) diammine diazido complexes synthesised in the Sadler group.

Ways to lower the energy of the LMCT band of the Pt^{IV} diazido complexes involved the initial replacement of the ammine (NH$_3$) group by a π-acceptor pyridine ligand.

Unfortunately, **38** (Figure 1.28) did not exhibit a LMCT band at lower energy (ca. 289 nm). Nevertheless, substitution of the pyridine ligand (**38**) for the ammine (NH$_3$, **37**) ligand decreased the IC$_{50}$ value from ca. 99.2 μM to 1.9 μM in A2780 ovarian cancer cells. The stark difference in the photo-cytotoxicity values was attributed to the formation of alternative Pt^{II}-DNA adducts by **38**.
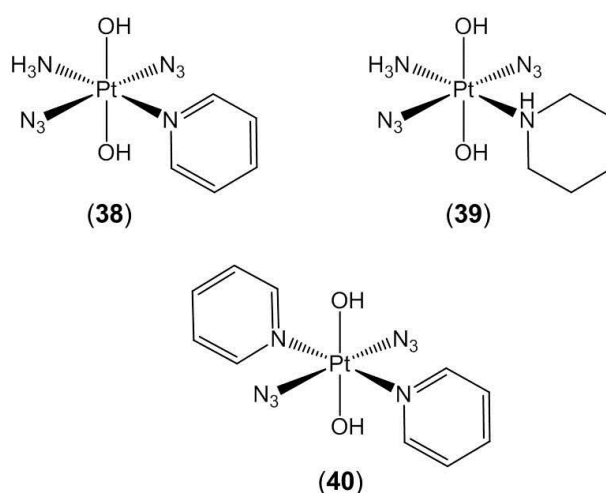
Figure 1.28 Structures of mono-pyridine (**38**); mono-piperidine (**39**) and bis-pyridine (**40**) platinum(IV) diazido complexes.

Photo-irradiation of **38** at 365 nm UVA in the presence of 5′-guanosine monophosphate (5′-GMP, model for nucleobase guanine) identified binding to the N^7 of 5′-GMP and generated both *trans* mono-[Pt(N$_3$)(NH$_3$)(py)(GMP)]$^+$ and bis-[Pt(NH$_3$)(py)(GMP)$_2$]$^{2+}$ adducts[141] (Figure 1.29). The formation of these different platinated-DNA adducts suggested that **38** induced its photo-cytotoxic effect through a novel mechanism of action. The formation of such a complex suggested a method of overcoming current resistance mechanisms of platinum anticancer complexes.
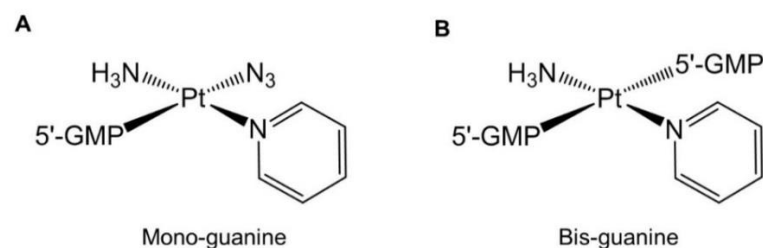
Figure 1.29 Structures of (**A**) mono- and (**B**) bis-guanine species formed from the photo-activation of complex **38** in the presence of 5'guanosine monophosphate (5'-GMP) (figures from ref 141)

Recently, Westendorf reported on **38** photo-irradiated *in vivo*. Photo-irradiation of **38** with UVA in mice bearing xenografted OE19 esophageal carcinoma gave rise to anti-tumour activity. The induction of the observed photo-cytotoxic effect was reported not to proceed through an apoptosis pathway (similar to *cis*-platin), but through an autophagic pathway.[142] Autophagy is an additional cell death mechanism, extensively reviewed by He *et al.*.[143]

Moreover, the pharmacological activity of **38** was compared with an analogue possessing a piperidine ligand (**39**, Figure 1.28). Despite the piperidine being more basic and more lipophilic, both complexes displayed similar photo-cytotoxic profiles with minor differences in selectivity.[144]

This work led to the replacement of the second ammine ligand to a pyridine ligand, generating the complex *trans,trans,trans*-[Pt(OH)$_2$(N$_3$)$_2$(py)$_2$] (complex **40**, Figure 1.28). This was the first photo-activatable platinum(IV) diazido anticancer complex to be activated with UVA, blue and green light. Complex **40** exhibited a LMCT

band at ca. 294 nm, which decreased upon irradiation, attributed to the loss of the coordinated azide ligands.[145]

Complex **40** has demonstrated its photo-cytotoxic activity in a number of cancer cell lines. It was an order of magnitude more potent than *cis*-platin in HaCaT human keratinocyte cell line. Photo-irradiation of complex **40** in the presence of 5′-GMP led to the observation of both gas bubbles attributed to nitrogen gas and various photo-products. These photo-products were characterised by ^{195}Pt NMR spectroscopy. An initial minor species, $[Pt(N_3)(py)_2(GMP)]^+$ (**41**) was detected at -2212 ppm. An additional species at -2288 ppm was detected and assigned as the bis-guanine species, $[Pt(py)_2(GMP)_2]^{2+}$ (**42**). A third species at ca. 874 ppm was assigned to $[Pt(OH)_2(py)_2(GMP)]$ (**43**), the oxidised form of species **41**.[145]
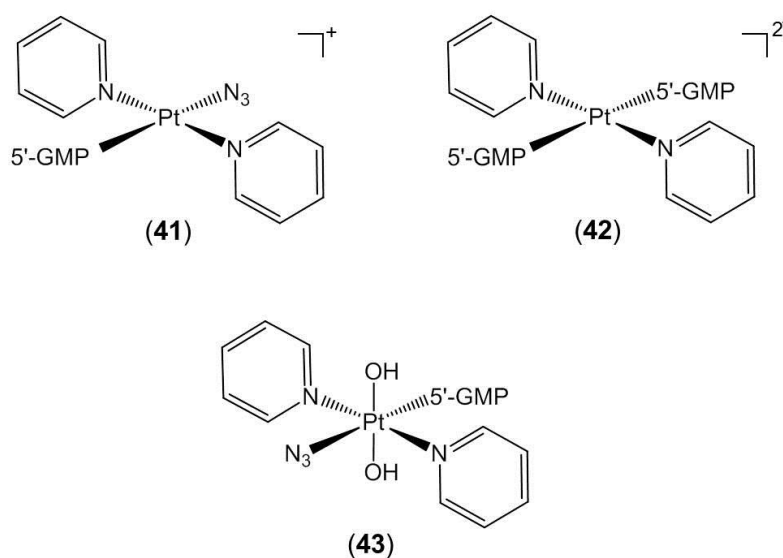
Figure 1.30 Structures of platinated DNA adducts formed from the photo-irradiation of complex **40** (figures adapted from ref 145).

Recently, Pracharova *et al*. demonstrated that photo-irradiated **40** efficiently stalled RNA polymerase II to a greater extent than *cis*-platin. They deduced that

transcription inhibition has potential to initiate various downstream cellular effects, which may contribute to the photo-cytotoxic effect of **40**.[146]

To date, complex **40** is the most potent platinum(IV) diazido photo-activatable anticancer complex. However, questions remain regarding its photo-decomposition pathways and the nature of additional photo-products. As mentioned above, gas bubbles were observed from the photo-irradiation of **40**. These were suggested to be due to N_2 gas from the dimerisation of two azidyl ($^\bullet N_3$) radicals (Figure 1.31**A**). However, potential formation of hydrogen peroxide (H_2O_2) and singlet oxygen *via* hydroxyl radicals ($^\bullet OH$) could also account for the observed gas (Figure 1.31**B**). Formation of RNS and/or ROS have potential to contribute to the photo-cytotoxicity of **40** (Figure 1.31**C**).

As can be seen from Figure 1.31, all potential radical species are either ROS/RNS related species. These species are notoriously known for their oxidative damage ability as mentioned in **section 1.1**. Moreover, due their short life-times of ca. $< 10^{-9}$ s direct detection by EPR spectroscopy is not feasible. Consequently, EPR spin trapping is commonly used for their detection and characterisation. The concept of spin trapping EPR will be described in detail in **Chapter III**.
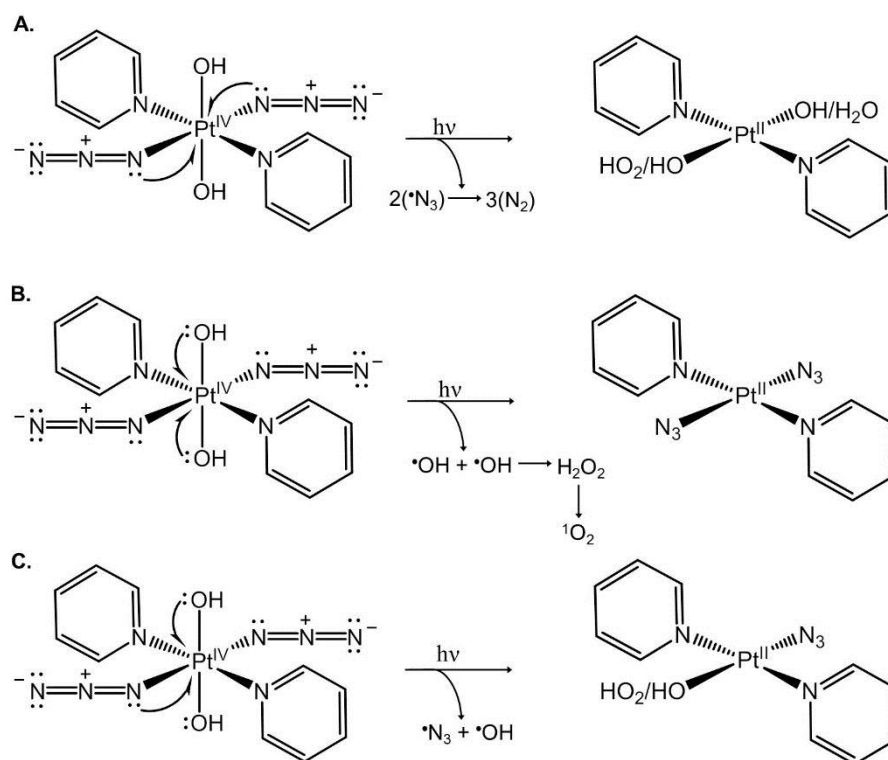
Figure 1.31 Photo-irradiation of complex **40** leading to the reduction of Pt^{IV} to Pt^{II} *via* two one-electron donations from (**A**) two azide; (**B**) two hydroxyl; (**C**) one azide and one hydroxyl ligands.

Recently, photo-activation of *trans,trans,trans*-$[Pt(N_3)_2(OH)_2(py)(MA)]$ (**44**, MA = methylamine) identified the formation of singlet oxygen ($^1O_2$) in additional to Pt-N nitrene intermediates.[147,148] Therefore, the photo-chemical reactions of Pt^{IV} diazido complexes have potential to generate numerous photo-products which can contribute the overall photo-cytotoxic effect.

(**44**)
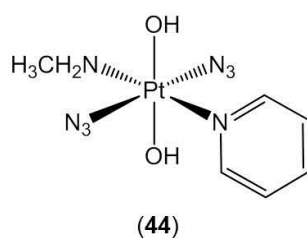
Figure 1.32 Structure of *trans,trans,trans*-$[Pt(N_3)_2(OH)_2(py)(MA)]$.

1.8.3 Photo-activatable anti-tumour transition metal complexes

FDA-approved carboplatin was recently photo-irradiated at 365 nm and reported to be ca. ten-fold more active in A2780 ovarian cancer cells than non-irradiated carboplatin.[149] Mitra *et al*. reported on two distorted square-planar ferrocenyl Pt[II] complexes with dark stability ($IC_{50} = 60$ μM) which upon photo-irradiation with visible light (400-700 nm) induced a photo-cytotoxic effect with IC_{50} values of ca. 9.8 μM (**45**) and 12.0 μM (**46**) in HaCaT immortalised human skin keratinocytes cells. These ferrocenyl Pt[II] complexes induced their photo-cytotoxicity *via* the PDT effect.[150]

The concept of light-activated anticancer complexes has also been extended to other transition metals. In the Chakravarty group, glucose-appended photo-cytotoxic iron(III) complexes with phenolate ligands (**47**) demonstrated anticancer activity in HeLa cervical cancer cells with IC_{50} values of ca. 10 μM and 20 μM upon photo-activation with visible (400-700 nm) and red light (600-720 nm), respectively. Furthermore, selective uptake of an iron(III) tetradentate phenolate complex with a biotin functional group selectively accumulated in HepG2 hepatocellular cancer cells inducing a photo-cytotoxic effect *via* ROS production.[151] The Chakravarty group have also synthesised photo-activatable copper(II)[152] and vanadium(IV)[153] anti-tumour complexes. Additionally, the Sadler group noted the photo-cytotoxicity for a family of ruthenium(II) arene-based anticancer complexes (**48**) irradiated with both UVA and white light.[154]
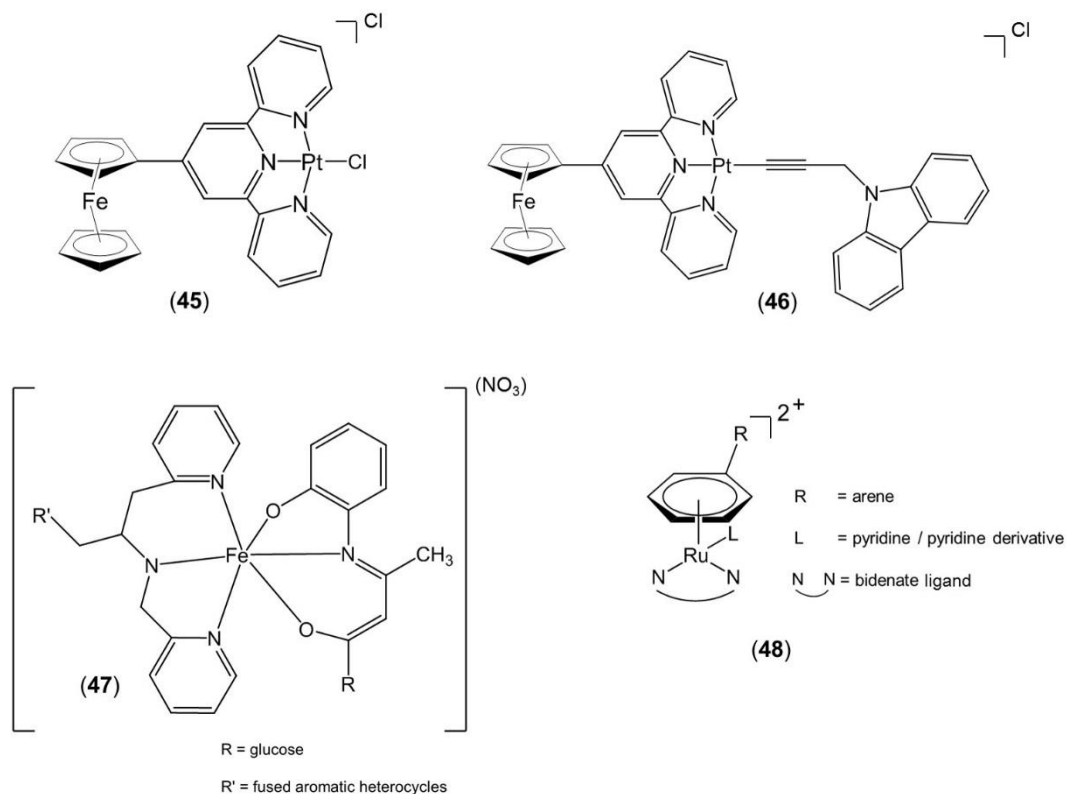
Figure 1.33 Structures of alternative photo-activatable complexes synthesised in the Chakravarty (**45**-**47**) and Sadler (**48**) groups (structures adapted from ref 150, 151 and 154).

Additionally, Kastl *et al*. reported on the photo-cytotoxicity of a rhenium(I) indolato complex (**49**), inactive in the dark with an EC_{50} value of ca. 100 µM. However, irradiation at 505 nm resulted in an EC_{50} value of ca. 0.1 µM, in HeLa cervical cancer cells.[155] Structure activity relationships (SARs) identified the most potent complex possessed an σ-accepting fluorine ligand on the pyridine moiety (**50**) with an EC_{50} value of ca. 0.3 µM upon irradiation with red light.[156]
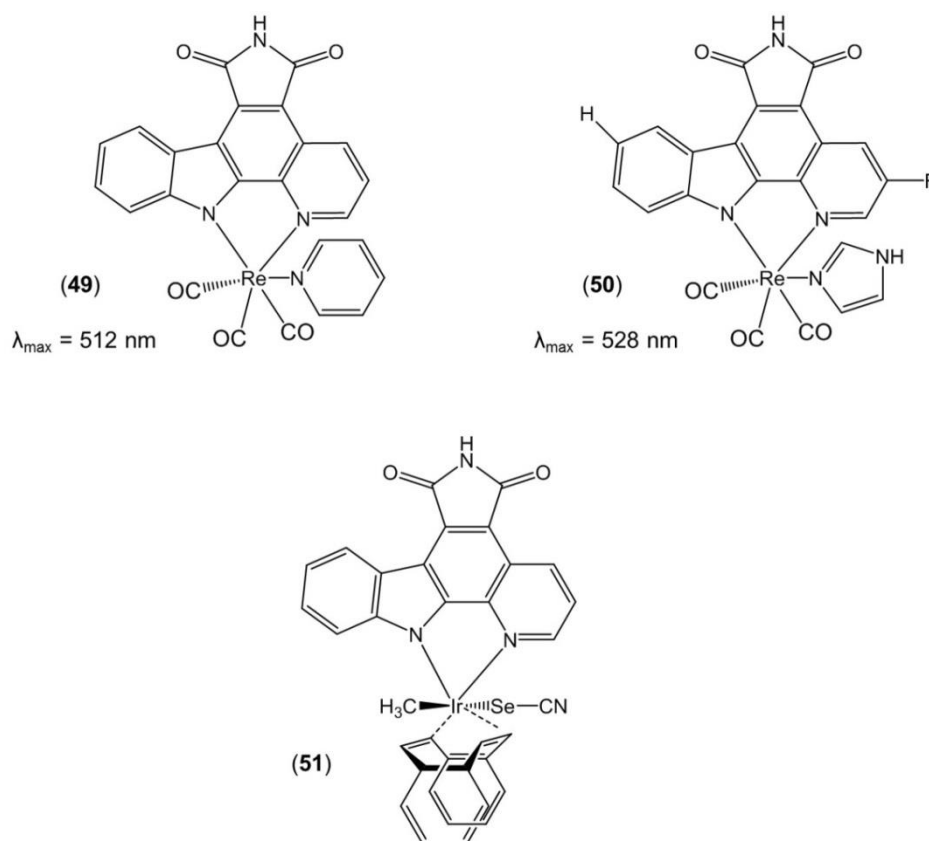
Figure 1.34 Structures of photo-activatable rhenium(I) pyrido-carbazole (**49** and **50**) and iridium (III) complex (**51**) with a dual mechanism of action synthesised in the Meggers group.

Interestingly, both Chakravarty and Meggers groups devised anti-tumour complexes possessing dual mechanisms of action. Prasad *et al.* reported on a oxidovanadium(IV) complex possessing a anthracenyl fluorophore and dipeptide (Gly-Gly-OMe) moiety.[157] This oxidovanadium(IV) complex is photo-cytotoxic upon irradiation and has the ability to specifically target the mitochondria of cancer cells and induce apoptosis *via* ROS. In a similar manner, Kastl *et al.* reported on the first photo-activatable iridium complex (**51**) with visible (λ = 450 nm) light inducing apoptosis in HeLa cervical cancer cells. Simultaneously, **51** exerted a

light-independent anti-angiogenicity through inhibition of the protein kinases, VEGFR3.[158]

Finally, photo-activation of transition metal complexes has also been pursued for the release of carbon monoxide (CO). Similar to nitric oxide (NO) and hydrogen disulphide (H₂S), carbon monoxide (CO) plays an important role in numerous physiological processes. [159]The ability of CO to induce a cyto-protective effect particularly against oxidative stress has rendered it a possible therapeutic. In recent years, a more targeted approach for delivery of CO to the target site has been explored through the carbon monoxide releasing molecules (CORMs) *via* photo-irradiation. Motterlini first reported on the concept of a photo-irradiated CORM from a manganese decacarbonyl based complex (**52**).[160] Release of CO upon irradiation allows both spatial and temporal control on the release of CO. Numerous [M(CO)y] based complexes have been synthesised (**53**-**55**, Figure 1.35).[161-163]

Recently, Pfeiffer *et al*. reported on the synthesis of various [Mn(CO)₃(tpm)]⁺ (where tpm = tris(pyrazlyl)methane) with a conjugated peptide. These complexes were stable in the dark and only illustrated CO release upon photo-irradiation at 365 nm (UVA).[164] They are currently being investigated for the selectively in cancerous cells. Moreover, [Mn(CO)₃(tpm)]⁺ loaded in a nano-diamond, a new form of nano-carbon, has been shown to be stable in the dark causing no change in the myoglobin assay, and offers a more targeted delivery approach for the release of CO.[165]
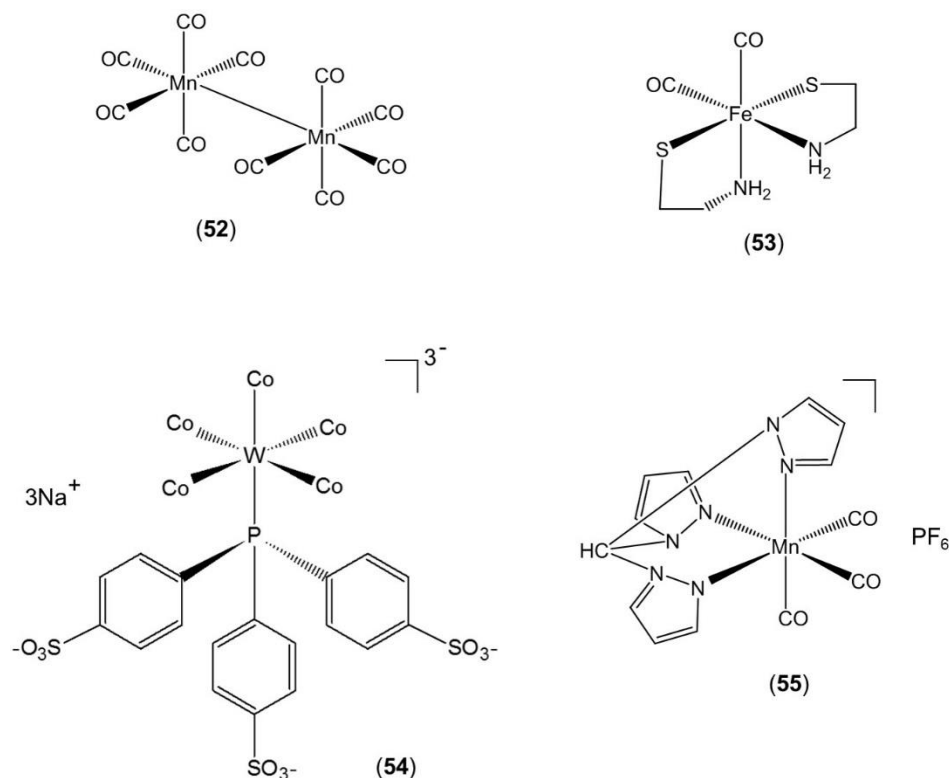
Figure 1.35 Structures of various PhotoCORMs including first photo-irradiated manganese decacarbonyl molecule synthesised by Motterlini (**52**); new iron(II) dicarbonyl-thiolate-ethylamine complex (**53**); tungsten(0) pentacarbonyl synthesised in the Weserhausen (**54**) and a manganese(I) tricarbonyl complex synthesised in the Schatzschneider group (**55**).

However, limitations of this current line of therapy are due to the majority of PhotoCORMs activated with short wavelengths of light, typically 300-370 nm. The future of PhotoCORMs involves lowering their energy to wavelengths of ca. 600 nm, nearer to the therapeutic window.[166] These latest studies suggest the wide utility of photo-chemotherapy using transition metal complexes and their potential in the treatment in a variety of cancer types.

1.9 Aims of thesis

The main objectives of this thesis were as follows.

1. To identify radical species generated from the photo-activation of platinum(IV) diazido anticancer complexes using spin trapping electron paramagnetic resonance (EPR) spectroscopy.

2. To vary the nitrone spin trap, solvent, wavelength of activation and source of radiation to establish an optimum spin trapping EPR system for photo-activatable platinum(IV) diazido anticancer complexes.

3. Establish the consequence of photo-activation of a platinum(IV) diazido complex in the presence of various amino acids and antioxidants and identify the potential reactivity of the formed radical(s).

4. To determine the effect of sulfur-containing molecules on the photo-irradiation of a photo-activatable platinum(IV) diazido complex.

1.10 References

(1)   World Health Organisation (WHO), Fact sheet on cancer assessed via http://www.who.int/mediacentre/factsheets/fs297/en/, on 27-Feb-2013.

(2)   Reuter, S.; Gupta, S. C.; Chaturvedi, M. M.; Aggarwal, B. B. *Free Radic. Biol. Med.* **2010**, *49*, 1603.

(3)   Friedman, J. In *Oxidative Stress and Free Radical Damage in Neurology*; Gadoth, N., Göbel, H. H., Eds.; Humana Press: New York, USA, 2011, p 1.

(4)   Choudhari, S. K.; Chaudhary, M.; Gadbail, A. R.; Sharma, A.; Tekade, S. *Oral Oncol.* **2014**, *50*, 10.

(5)   Valko, M.; Rhodes, C. J.; Moncol, J.; Izakovic, M.; Mazur, M. *Chem. Biol. Interact.* **2006**, *160*, 1.

(6)   Martin, L. P.; Hamilton, T. C.; Schilder, R. J. *Clin. Cancer. Res.* **2008**, *14*, 1291.

(7)   Sies, H. *Angew. Chem. Int. Ed.* **1986**, *25*, 1058.

(8)   Janzen, E. G.; Kotake, Y.; Randall D, H. *Free Radic. Biol. Med.* **1992**, *12*, 169.

(9)   Marnett, L. J. *Carcinogenesis* **2000**, *21*, 361.

(10)   Sova, H.; Jukkola-Vuorinen, A.; Puistola, U.; Kauppila, S.; Karihtala, P. *Br. J. Cancer* **2010**, *102*, 1018.

(11)   Karihtala, P.; Soini, Y. *Acta. Path. Micro. Immunol. Scand.* **2007**, *115*, 81.

(12)   Brown, G. C.; Borutaite, V. *IUBMB Life* **2001**, *52*, 189.

(13)   Banerjee, K.; Ganguly, A.; Chakraborty, P.; Sarkar, A.; Singh, S.; Chatterjee, M.; Bhattacharya, S.; Choudhuri, S. K. *Eur. J. Pharma. Sci* **2014**, *52*, 146.

(14)   Telser, J. In *Encyclopedia of Inorganic and Bioinorganic Chemistry*; John Wiley & Sons, Ltd: Chicago, USA, 2011.

(15)   Höfer, P.; Grupp, A.; Nebenführ, H.; Mehring, M. *Chem. Phys. Lett.* **1986**, *132*, 279.

(16)   Regulla, D. F. *Appl. Radiat. Isot.* **2005**, *62*, 117.

(17)   Thompson, J.; Schwarcz, H. P. *Radiat. Meas.* **2008**, *43*, 1219.

(18)   Moen, R. J.; Klein, J. C.; Thomas, D. D. *Exerc. Sport Sci. Rev.* **2014**, *42*, 30.

(19)   Davies, M. J. In *Electron Paramagnetic Resoance: A Practitioner's Toolkit*; Brustolon, M., Giamello, E., Eds.; John Wiley & Sons: New Jersey, 2009, p 427.

(20)   Corvaja, C. In *Electron Paramagnetic Resonance: A Practitioner's Toolkit*; Brustolon, M., Giamello, E., Eds.; John Wiley & Sons: New Jersey, 2009, p 120.

(21)   Weil, J. A.; Bolton, J. R. In *Electron Paramagnetic Resonance: Elementary Theory and Practical Applications*; 2nd ed.; Bolton, I., James, R., Eds.; John Wiley & Sons: New Jersey, 2007, p 1.

(22)   Eaton, G. R.; Eaton, S. R.; Barr, D. P.; Weber, R. T. In *Quantitative EPR:A Practitioners Guide*; Springer-Verlag/Wien: Germany, 2010, p 2.

(23)   Weber, T. R.; Jiang, J. J.; Barr, P. D. In *EPR Division Bruker Instrumentation Manual* 1998, p 2.

(24)   Eaton, S. S.; Eaton, G. R. *J. Magn. Reson.* **2012**, *223*, 151.

(25)   Jeschke, G. In *ESR Spectroscopy in Membrane Biophysics*; Springer US: 2007; Vol. 27, p 17.

(26)   Bunce, N. J. *J. Chem. Educ.* **1987**, *64*, 907

(27)   Ōishi, Y.; Mukai, K.; Nishiguchi, H.; Deguchi, Y.; Takaki, H. *Tetrahedron Lett.* **1968**, *9*, 4773.

(28)   Eaton, S. S.; Eaton, G. R. *Bull. Magn. Reson.* **1979**, *1*, 130.

(29)   Atkins, P. W. *Physical Chemistry*; 3rd ed.; Oxford University Press: Oxford, UK, 1986, p 458.

(30)   Gescheidt, G. In *Electron Paramagnetic Resonance: A Pracititoner's Toolkit*; Brustolon, M., Giamello, E., Eds.; John Wiley & Sons: New Jersey, 2009, p 109.

(31)   Bačić, G.; Spasojević, I.; Šećerov, B.; Mojović, M. *Spectrochim. Acta, Part A* **2008**, *69*, 1354.

(32)   Mjos, K. D.; Orvig, C. *Chem. Rev.* **2014**, *114*, 4540.

(33)   Ronconi, L.; Sadler, P. J. *Coord. Chem. Rev.* **2007**, *251*, 1633.

(34)   Senthilingam, M. In *Chemistry World*; Robinson, P., Ed.; Royal Society of Chemistry: United Kingdom, 2013.

(35)   Anderson, C. J.; Welch, M. J. *Chem. Rev.* **1999**, *99*, 2219.

(36)   Barry, N. P. E.; Sadler, P. J. *ACS Nano* **2013**, *7*, 5654.

(37)   Barry, N. P. E.; Sadler, P. J. *Chem. Commun.* **2013**, *49*, 5106.

(38)   Arblaster, J. W. *Platinum Met. Rev.* **2000**, *44*, 173.

(39)   Rosenberg, B.; Van Camp, L.; Krigas, T. *Nature* **1965**, *205*, 698.

(40)   Barnard, J. F. C. *Platinum Met. Rev.* **1989**, *33*, 162.

(41)   Alderden, A. R.; Hall, D. M.; Hambley, W. T. *J. Chem. Educ.* **2006**, *83*, 728.

(42)   Berners-Price, S. J.; Sadler, P. J. *Coord. Chem. Rev.* **1996**, *151*, 1.

(43)   Binks, P. S.; Dobrota, M. *Biochem. Pharmacol.* **1990**, *40*, 1329.

(44)   Arnesano, F.; Natile, G. *Coord. Chem. Rev.* **2009**, *253*, 2070.

(45)   Kuo, M.; Chen, H. W.; Song, I.-S.; Savaraj, N.; Ishikawa, T. *Cancer Metast. Rev.* **2007**, *26*, 71.

(46)   Ciarimboli, G.; Deuster, D.; Knief, A.; Sperling, M.; Holtkamp, M.; Edemir, B.; Pavenstädt, H.; Lanvers-Kaminsky, C.; Zehnhoff-Dinnesen, A. A.; Schinkel, A. H.; Koepsell, H.; Jürgens, H.; Schlatter, E. *Am. J. Pathol.* **2010**, *176*, 1169.

(47)   Ciarimboli, G.; Ludwig, T.; Lang, D.; Pavenstädt, H.; Koepsell, H.; Piechota, H.-J.; Haier, J.; Jaehde, U.; Zisowsky, J.; Schlatter, E. *Am. J. Pathol.* **2005**, *167*, 1477.

(48)   Jennerwein, M.; Andrews, P. A. *Drug Metab Dispos* **1995**, *23*, 178.

(49)   Davies, M. S.; Berners-Price, S. J.; Hambley, T. W. *J. Inorg. Biochem.* **2000**, *79*, 167.

(50)   Berners-Price, S. J.; Frenkiel, T. A.; Frey, U.; Ranford, J. D.; Sadler, P. J. *J. Chem. Soc., Chem. Commun.* **1992**, 789.

(51)   Jamieson, E. R.; Lippard, S. J. *Chem. Rev.* **1999**, *99*, 2467.

(52)   Eastman, A. *Biochemistry.* **1983**, *22*, 3927.

(53)   Eastman, A. *Biochemistry.* **1986**, *25*, 3912.

(54)   Zamble, D. B.; Lippert, S. J. In *Cisplatin: Chemistry and Biochemistry of a Leading Anticancer Drug*; Lippert, B., Ed.; Verlag Helvetica Chimica Acta and Wiley-VCH: Zurich and Weinheim, 1999, p pp. 73

(55)   Eastman, A. In *Cisplatin: Chemistry and Biochemistry of a Leading Anticancer Drug*; Lippert, B., Ed.; Verlag Helvetica Chimica Acta and Wiley-VCH: Zurich and Weinheim, 1999, p pp. 111

(56)   Barnham, K. J.; Sadler, P. J.; Berners-Price, S. J.; Frenkiel, T. A.; Frey, U. *Angew. Chem. Int. Ed.* **1995**, *34*, 1874.

(57)   Fichtinger-Schepman, A. M. J.; Van der Veer, J. L.; Den Hartog, J. H. J.; Lohman, P. H. M.; Reedijk, J. *Biochemistry.* **1985**, *24*, 707.

(58)   Kelland, R. L. *Nat. Rev. Cancer* **2007**, *7*, 573.

(59)   Huang, H.; Zhu, L.; Reid, B. R.; Drobny, G. P.; Hopkins, P. B. *Science* **1995**, *270*, 1842.

(60)   Takahara, M. P.; Rosenzweig, C. A.; Frederick, A. C.; Lippard, J. S. *Nature* **1995**, *377*, 649.

(61)   Teuben, J.-M.; Bauer, C.; Wang, A. H. J.; Reedijk, J. *Biochemistry.* **1999**, *38*, 12305.

(62)   Gelasco, A.; Lippard, S. J. *Biochemistry.* **1998**, *37*, 9230.

(63)   Wood, K. A.; Youle, R. J. *Ann. N.Y. Acad. Sci.* **1994**, *738*, 400.

(64)   Reedijk, J.; Teuben, J. M. In *Cisplatin: Chemistry and Biochemistry of a Leading Anticancer Drug*; Lippert, B., Ed.; Verlag Helvetica Chimica Acta and Wiley-VCH: Zurich and Weinheim, 1999, p pp. 339

(65)   Shoeib, T.; Sharp, B. L. *Inorg. Chim. Acta.* **2013**, *405*, 258.

(66)   Ishikawa, T.; Ali-Osman, F. *J. Biol. Chem.* **1993**, *268*, 20116.

(67)   Wang, X.; Guo, Z. *Anti-cancer Agents Med. Chem.* **2007**, *7*, 19.

(68)   Hall, M. D.; Okabe, M.; Shen, D.-W.; Liang, X.-J.; Gottesman, M. M. *Annu. Rev. Pharmacol. Toxicol.* **2008**, *48*, 495.

(69)   Bose, R. *Mini-Rev. Med. Chem.* **2002**, *2*, 103

(70)   Dos Santos, N. A. G.; Rodrigues, M. A. C.; Martins, N. M.; Dos Santos, A. C. *Arch. Toxicol.* **2012**, *86*, 1233.

(71)   Weiss, B. R.; Christian, C. M. *Drugs* **1993**, *46*, 360.

(72)   Lebwohl, D.; Canetta, R. *Eur. J. Cancer* **1998**, *34*, 1522.

(73)   *Martindale: The complete drug reference*; 35th ed.; Pharmaceutical Press: London, 2007.

(74)   Jakupec, M. A.; Galanski, M.; Keppler, B. K. In *Reviews of Physiology, Biochemistry and Pharmacology*; Springer Berlin Heidelberg: 2003; Vol. 146, p 1.

(75)   Penson, R. T.; Dizon, D. S.; Cannistra, S. A.; Roche, M. R.; Krasner, C. N.; Berlin, S. T.; Horowitz, N. S.; DiSilvestro, P. A.; Matulonis, U. A.; Lee, H.; King, M. A.; Campos, S. M. *J. Clin. Oncol.* **2010**, *28*, 154.

(76)   Laurie, S. A.; Siu, L. L.; Winquist, E.; Maksymiuk, A.; Harnett, E. L.; Walsh, W.; Tu, D.; Parulekar, W. R. *Cancer* **2010**, *116*, 362.

(77)   Wu, B.; Davey, G. E.; Nazarov, A. A.; Dyson, P. J.; Davey, C. A. *Nucleic Acids Res.* **2011**, *39*, 8200.

(78)   Zayed, A.; Jones, G. D. D.; Reid, H. J.; Shoeib, T.; Taylor, S. E.; Thomas, A. L.; Wood, J. P.; Sharp, B. L. *Metallomics* **2011**, *3*, 991.

(79)   Wheate, N. J.; Walker, S.; Craig, G. E.; Oun, R. *Dalton Trans.* **2010**, *39*, 8113.

(80)   Boudvillain, M.; Dalbiès, R.; Aussourd, C.; Leng, M. *Nucleic Acids Res.* **1995**, *23*, 2381.

(81)   Natile, G.; Coluccia, M. *Coord. Chem. Rev.* **2001**, *216–217*, 383.

(82)   Farrell, N.; Ha, T. T. B.; Souchard, J. P.; Wimmer, F. L.; Cros, S.; Johnson, N. P. *J. Med. Chem.* **1989**, *32*, 2240.

(83)   Van Beusichem, M.; Farrell, N. *Inorg. Chem.* **1992**, *31*, 634.

(84)   Coluccia, M.; Nassi, A.; Loseto, F.; Boccarelli, A.; Mariggio, M. A.; Giordano, D.; Intini, F. P.; Caputo, P.; Natile, G. *J. Med. Chem.* **1993**, *36*, 510.

(85)   Zou, Y.; Van Houten, B.; Farrell, N. *Biochemistry.* **1993**, *32*, 9632.

(86)   Coluccia, M.; Boccarelli, A.; Mariggiò, M. A.; Cardellicchio, N.; Caputo, P.; Intini, F. P.; Natile, G. *Chem. Biol. Interact.* **1995**, *98*, 251.

(87)   Aris, S. M.; Farrell, N. P. *Eur. J. Inorg. Chem.* **2009**, *2009*, 1293.

(88)   Frybortova, M.; Novakova, O.; Stepankova, J.; Novohradsky, V.; Gibson, D.; Kasparkova, J.; Brabec, V. *J. Inorg. Biochem.* **2013**, *126*, 46.

(89)   Kalinowska-Lis, U.; Ochocki, J.; Matlawska-Wasowska, K. *Coord. Chem. Rev.* **2008**, *252*, 1328.

(90)   Cleare, M. J.; Hoeschele, J. D. *Platinum Met. Rev.* **1973**, *17*, 2.

(91)   Rosenberg, B.; Van Camp, L.; Grimley, B. E.; Thomson, J. A. *J. Biol. Chem.* **1967**, *242*, 1347.

(92)   Cleare, M. J.; Hoeschele, J. D. *Bioinorg. Chem.* **1973**, *2*, 187.

(93)   Quiroga, A. G. *J. Inorg. Biochem.* **2012**, *114*, 106.

(94)   Reithofer, M. R.; Bytzek, A. K.; Valiahdi, S. M.; Kowol, C. R.; Groessl, M.; Hartinger, C. G.; Jakupec, M. A.; Galanski, M.; Keppler, B. K. *J. Inorg. Biochem.* **2011**, *105*, 46.

(95)   Kostrhunova, H.; Kasparkova, J.; Gibson, D.; Brabec, V. *Mol. Pharmaceutics* **2010**, *7*, 2093.

(96)   Banfić, J.; Legin, A. A.; Jakupec, M. A.; Galanski, M.; Keppler, B. K. *Eur. J. Inorg. Chem.* **2014**, *2014*, 484.

(97)   Pérez, J. M.; Kelland, L. R.; Montero, E. I.; Boxall, F. E.; Fuertes, M. A.; Alonso, C.; Navarro-Ranninger, C. *Mol. Pharmacol.* **2003**, *63*, 933.

(98)   Martínez, A.; Lorenzo, J.; Prieto, M. J.; de Llorens, R.; Font-Bardia, M.; Solans, X.; Avilés, F. X.; Moreno, V. *ChemBioChem* **2005**, *6*, 2068.

(99)   Min, Y.; Mao, C.; Xu, D.; Wang, J.; Liu, Y. *Chem. Commun.* **2010**, *46*, 8424.

(100)   Brown, S. D.; Nativo, P.; Smith, J.-A.; Stirling, D.; Edwards, P. R.; Venugopal, B.; Flint, D. J.; Plumb, J. A.; Graham, D.; Wheate, N. J. *J. Am. Chem. Soc.* **2010**, *132*, 4678.

(101)   Wang, X.; Guo, Z. *Chem. Soc. Rev.* **2013**, *42*, 202.

(102)   Bhirde, A. A.; Patel, V.; Gavard, J.; Zhang, G.; Sousa, A. A.; Masedunskas, A.; Leapman, R. D.; Weigert, R.; Gutkind, J. S.; Rusling, J. F. *ACS Nano* **2009**, *3*, 307.

(103)   Graf, N.; Mokhtari, T. E.; Papayannopoulos, I. A.; Lippard, S. J. *J. Inorg. Biochem.* **2012**, *110*, 58.

(104)   Margiotta, N.; Denora, N.; Ostuni, R.; Laquintana, V.; Anderson, A.; Johnson, S. W.; Trapani, G.; Natile, G. *J. Med. Chem.* **2010**, *53*, 5144.

(105)   Dhar, S.; Lippard, S. J. *Proc. Natl. Acad. Sci. USA.* **2009**, *106*, 22199.

(106)   Abramkin, S.; Valiahdi, S. M.; Jakupec, M. A.; Galanski, M.; Metzler-Nolte, N.; Keppler, B. K. *Dalton Trans.* **2012**, *41*, 3001.

(107)   Huxley, M.; Sanchez-Cano, C.; Browning, M. J.; Navarro-Ranninger, C.; Quiroga, A. G.; Rodger, A.; Hannon, M. J. *Dalton Trans.* **2010**, *39*, 11353.

(108)   Sýkora, J.; Šima, J. *Coord. Chem. Rev.* **1990**, *107*, 1.

(109)   Farrer, N. J.; Salassa, L.; Sadler, P. J. *Dalton Trans.* **2009**, *48*, 10690.

(110)   Ackroyd, R.; Kelty, C.; Brown, N.; Reed, M. *Photochem. Photobiol.* **2001**, *74*, 656.

(111)   Moan, J.; Peng, Q. In *Photodynamic Therapy*; Patrice, T., Ed.; The Royal Society of Chemistry: Cambridge, UK, 2003, p 1.

(112)   Dougherty, T. J.; Gomer, C. J.; Henderson, B. W.; Jori, G.; Kessel, D.; Korbelik, M.; Moan, J.; Peng, Q. *J. Natl. Cancer Inst.* **1998**, *90*, 889.

(113)   Dolmans, D. E. J. G. J.; Fukumura, D.; Jain, R. K. *Nat. Rev. Cancer* **2003**, *3*, 380

(114)   Shaili, E. *Sci. Prog.* **2014**, *97*, 20.

(115)   Robertson, C. A.; Evans, D. H.; Abrahamse, H. *J. Photchem. Photobiol. B: Biol.* **2009**, *96*, 1.

(116)   Bown, S. G. *Phil. Trans. Soc. A.* **2013**, *371*.

(117)   Yano, S.; Hirohara, S.; Obata, M.; Hagiya, Y.; Ogura, S.-i.; Ikeda, A.; Kataoka, H.; Tanaka, M.; Joh, T. *J. Photochem. Photobiol. C* **2011**, *12*, 46.

(118)   Pereira, S. P.; Ayaru, L.; Ackroyd, R.; Mitton, D.; Fullarton, G.; Zammit, M.; Grzebieniak, Z.; Messmann, H.; Ortner, M. A.; Gao, L.; Trinh, M. M.; Spénard, J. *Aliment. Pharmacol. Ther.* **2010**, *32*, 821.

(119)   Ball, D. J.; Vernon, D. I.; Brown, S. B. *Photochem. Photobiol.* **1999**, *69*, 360.

(120)   McLear, P. W.; Hayden, R. E. *Am. J. Otolmynol.* **1989**, *10*, 92.

(121)   Arnaut, L. In *Advances in Inorganic chemistry*; Rudi van, E., Grazyna, S., Eds.; Elsevier: USA, 2011; Vol. 63, p 188.

(122)   Moan, J.; Berg, K. *Photochem. Photobiol.* **1991**, *53*, 549.

(123)   Guise, C. P.; Mowday, A. M.; Ashoorzadeh, A.; Yuan, R.; Lin, W. H.; Wu, D. H.; Smaill, J. B.; Patterson, A. V.; Ding, K. *Chin. J. Cancer* **2014**, *33*, 80.

(124)   Casas, A.; Di Venosa, G.; Hasan, T.; Batlle, A. *Curr. Med. Chem.* **2011**, *18*, 2486.

(125)   Mayhew, S.; Vernon, D. I.; Schofield, J.; Griffiths, J.; Brown, S. B. *Photochem. Photobiol.* **2001**, *73*, 39.

(126)   Gomer, C. J.; Ryter, S. W.; Ferrario, A.; Rucker, N.; Wong, S.; Fisher, A. M. R. *Cancer Res.* **1996**, *56*, 2355.

(127)   Kratochwil, N. A., *PhD Thesis*, University of Regensburg, 1996.

(128)   Ferraudi, G. J. *Elements of Inorganic Photochemistry*; Wiley Interscience: New York, 1988.

(129)   Kratochwil, N. A.; Bednarski, P. J. *Arch. Pharm.* **1999**, *332*, 279.

(130)   Kratochwil, N. A.; Zabel, M.; Range, K.-J.; Bednarski, P. J. *J. Med. Chem.* **1996**, *39*, 2499.

(131)   Vogler, A.; Kern, A.; Hüttermann, J. *Angew. Chem. Int. Ed.* **1978**, *17*, 524.

(132)   Vogler, A.; Wright, R. E.; Kunkely, H. *Angew. Chem. Int. Ed.* **1980**, *19*, 717.

(133)   Vogler, A.; Hlavatsch, J. *Angew. Chem. Int. Ed.* **1983**, *22*, 154.

(134)   Farrer, N. J.; Gierth, P.; Sadler, P. J. *Chem. Eur. J.* **2011**, *17*, 12059.

(135)   Bednarski, P. J.; Korpis, K.; Westendorf, A. F.; Perfahl, S.; Grünert, R. *Phil. Trans. Soc. A.* **2013**, *371*.

(136)   Müller, P.; Schröder, B.; Parkinson, J. A.; Kratochwil, N. A.; Coxall, R. A.; Parkin, A.; Parsons, S.; Sadler, P. J. *Angew. Chem. Int. Ed.* **2003**, *42*, 335.

(137)   Westendorf, A. F.; Bodtke, A.; Bednarski, P. J. *Dalton Trans.* **2011**, *40*, 5342.

(138)   Mackay, F. S.; Woods, J. A.; Moseley, H.; Ferguson, J.; Dawson, A.; Parsons, S.; Sadler, P. J. *Chem. Eur. J.* **2006**, *12*, 3155.

(139)   Ronconi, L.; Sadler, P. J. *Chem. Commun.* **2008**, 235.

(140)   Farrer, N. J.; Woods, J. A.; Munk, V. P.; Mackay, F. S.; Sadler, P. J. *Chem. Res. Toxicol.* **2009**, *23*, 413.

(141)   Mackay, F. S.; Woods, J. A.; Heringová, P.; Kašpárková, J.; Pizarro, A. M.; Moggach, S. A.; Parsons, S.; Brabec, V.; Sadler, P. J. *Proc. Natl. Acad. Sci. USA.* **2007**, *104*, 20743.

(142)   Westendorf, A. F.; Woods, J. A.; Korpis, K.; Farrer, N. J.; Salassa, L.; Robinson, K.; Appleyard, V.; Murray, K.; Grünert, R.; Thompson, A. M.; Sadler, P. J.; Bednarski, P. J. *Mol. Cancer Ther.* **2012**, *11*, 1894.

(143)   He, C.; Klionsky, D. J. *Annu. Rev. Genet.* **2009**, *43*, 67.

(144)   Westendorf, A. F.; Zerzankova, L.; Salassa, L.; Sadler, P. J.; Brabec, V.; Bednarski, P. J. *J. Inorg. Biochem.* **2011**, *105*, 652.

(145)   Farrer, N. J.; Woods, J. A.; Salassa, L.; Zhao, Y.; Robinson, K. S.; Clarkson, G.; Mackay, F. S.; Sadler, P. J. *Angew. Chem. Int. Ed.* **2010**, *49*, 8905.

(146)   Pracharova, J.; Zerzankova, L.; Stepankova, J.; Novakova, O.; Farrer, N. J.; Sadler, P. J.; Brabec, V.; Kasparkova, J. *Chem. Res. Toxicol.* **2012**, *25*, 1099.

(147)   Zhao, Y.; Farrer, N. J.; Li, H.; Butler, J. S.; McQuitty, R. J.; Habtemariam, A.; Wang, F.; Sadler, P. J. *Angew. Chem. Int. Ed.* **2013**, *52*, 13633.

(148)   Zhao, Y., Ph.D. Thesis, University of Warwick, 2012.

(149)   Mlcouskova, J.; Stepankova, J.; Brabec, V. *J. Biol. Inorg. Chem.* **2012**, *17*, 891.

(150)   Mitra, K.; Basu, U.; Khan, I.; Maity, B.; Kondaiah, P.; Chakravarty, A. R. *Dalton Trans.* **2014**, *43*, 751.

(151)   Saha, S.; Majumdar, R.; Hussain, A.; Dighe, R. R.; Chakravarty, A. R. *Phil. Trans. Soc. A.* **2013**, *371*, 20120190.

(152)   Goswami, T. K.; Gadadhar, S.; Gole, B.; Karande, A. A.; Chakravarty, A. R. *Eur. J. Med. Chem.* **2013**, *63*, 800.

(153)   Banik, B.; Somyajit, K.; Hussain, A.; Nagaraju, G.; Chakravarty, A. R. *Dalton Trans.* **2014**, *43*, 1321.

(154)   Betanzos-Lara, S.; Salassa, L.; Habtemariam, A.; Novakova, O.; Pizarro, A. M.; Clarkson, G. J.; Liskova, B.; Brabec, V.; Sadler, P. J. *Organometallics* **2012**, *31*, 3466.

(155)   Kastl, A.; Dieckmann, S.; Wähler, K.; Völker, T.; Kastl, L.; Merkel, A. L.; Vultur, A.; Shannan, B.; Harms, K.; Ocker, M.; Parak, W. J.; Herlyn, M.; Meggers, E. *ChemMedChem* **2013**, *8*, 924.

(156)   Wähler, K.; Ludewig, A.; Szabo, P.; Harms, K.; Meggers, E. *Eur. J. Inorg. Chem.* **2014**, *2014*, 807.

(157)   Prasad, P.; Khan, I.; Kondaiah, P.; Chakravarty, A. R. *Chem. Eur. J.* **2013**, *19*, 17445.

(158)   Kastl, A.; Wilbuer, A.; Merkel, A. L.; Feng, L.; Di Fazio, P.; Ocker, M.; Meggers, E. *Chem. Commun.* **2012**, *48*, 1863.

(159)   Peng, P.; Wang, C.; Shi, Z.; Johns, V. K.; Ma, L.; Oyer, J.; Copik, A.; Igarashi, R.; Liao, Y. *Organic & Biomolecular Chemistry* **2013**, *11*, 6671.

(160)   Motterlini, R.; Otterbein, L. E. *Nat. Rev. Drug Discov.* **2010**, *9*, 728.

(161)   Kretschmer, R.; Gessner, G.; Görls, H.; Heinemann, S. H.; Westerhausen, M. *J. Inorg. Biochem.* **2011**, *105*, 6.

(162)   Niesel, J.; Pinto, A.; N'Dongo, H. W. P.; Merz, K.; Ott, I.; Gust, R.; Schatzschneider, U. *Chem. Commun.* **2008**, 1798.

(163)   Schatzschneider, U. *Inorg. Chim. Acta.* **2011**, *374*, 19.

(164)   Pfeiffer, H.; Rojas, A.; Niesel, J.; Schatzschneider, U. *Dalton Trans.* **2009**, 4292.

(165)   Dordelmann, G.; Meinhardt, T.; Sowik, T.; Krueger, A.; Schatzschneider, U. *Chem. Commun.* **2012**, *48*, 11528.

(166)   Schatzschneider, U. *Eur. J. Inorg. Chem.* **2010**, *2010*, 1451.

Chapter II

Experimental Methods

This chapter describes the main materials, instrumentation and experimental procedures used throughout this Thesis. Specific experimental methods will be detailed appropriately in the proceeding Chapters.

2.1 Experimental

2.1.1 Materials

Complex **40**, *trans,trans,trans*-[Pt(N$_3$)$_2$(OH)$_2$(py)$_2$] and ^{15}N-**40** were synthesised and characterised as described below. K$_2$[PtCl$_4$] (99%) was obtained from Precious Metals Online, pyridine, ammonium chloride and 1,4 dioxane were purchased from Fischer Scientific. Na^{14}N$_3$ (99%), 4-hydroxy-2,2,6,6-tetramethyl-piperidine-1-oxyl (Tempol EPR standard), deuterium oxide (D$_2$O), H$_2$O$_2$ (30 % v/v), phosphate buffered saline (PBS) tablets were purchased from Sigma Aldrich. Silver nitrate (AgNO$_3$) from Fluka, d$_6$-acetone from Goss Scientific, and Na^{15}N$_3$ (with one terminal nitrogen 100% ^{15}N labelled) from Cambridge Isotope Laboratories. EPR inner quartz tubes (1.2 mm O.D), outer quartz tubes (2.0 mm O.D) and high precision amber NMR tubes were purchased from Wilmad Labglass. Nitrone spin trap 5,5-dimethyl-pyrroline-N-oxide (DMPO) was purchased from Enzo Life Sciences obtained in the highest purity ($\geq$ 99 %) and used without any further purification. HPLC Hamilton syringe 500 µL was purchased from Hamilton Ltd. ICP platinum standard was obtained from Inorganic Ventures.

2.2 Synthesis and characterisation of *trans,trans,trans*-[Pt(N$_3$)$_2$(OH)$_2$(py)$_2$]

! Caution metal azides are known as shock sensitive detonators and synthesis of such compounds were handled with care.

2.2.1 Synthesis of *trans*-[Pt(py)$_2$(Cl)$_2$]

K$_2$PtCl$_4$ (1 g, 2.4 mmol) in H$_2$O (25 mL) was added to pyridine (2 ml, 24 mmol, 10× excess) and the solution heated at 358 K changing colour from deep red – through orange, then white – until colourless and transparent (ca. 1 h 15 min). The solution was allowed to cool on ice and was filtered (IM). IM filtration using a membrane-bound filter was employed to remove any Pt^0 from the reaction mixture. The solvent was removed by rotary evaporator. HCl (2 M, 25 mL) was added and the solution was heated at 348 K for 24 h to give a yellow suspension. This was allowed to cool on ice, filtered under suction and washed with cold minimal solvents (H$_2$O, ethanol and ether) to give a pale yellow product (0.88 g, 2.08 mmol, 86 %).

trans-[Pt(py)$_2$(Cl)$_2$]: ^{1}H NMR (d$_6$–acetone, 400 MHz): δ = 8.86 (dd, J_{1H1H} = 5 Hz, $J_{1H195Pt}$ = 32 Hz, 4H, H$_O$), 8.11 (t, J_{1H1H} = 14 Hz, 2H, H$_p$), 7.66 ppm (dd, J_{1H1H} = 13 Hz, 4H, H$_m$)

From here synthesis was performed under dim controlled lighting conditions.

2.2.2 Synthesis of *trans*-[Pt(py)$_2$(N$_3$)$_2$]

Trans-[PtCl$_2$(py)$_2$] (0.4 g, 0.95 mmol) was suspended in H$_2$O (68 mL), AgNO$_3$ (0.32 g, 1.9 mmol, 2 mol equiv) was added and the reaction stirred at 333 K overnight. The grey solution was filtered by celite to remove the silver chloride (AgCl)

precipitate. Then, the solution was filtered by IM filtration. NaN$_3$ (0.62 g, 9.5 mmol, 5 mol equiv) was added and the reaction was stirred at ambient temperature. After 4 h additional NaN$_3$ (5 mol equiv) was added, and the reaction mixture was stirred for another 4 h. The solution was placed on ice, suction-filtered and the yellow product washed with cold, minimal solvents (H$_2$O, ethanol, ether) to give the crude product (0.37 g, 0.85 mmol, 90 %). The product was purified by crystallisation from pyridine (pre-heated to 313 K; in the ratio 0.34 g/12.9 mL), followed by filtration (IM), and cooling to 269 K. The yellow product was isolated by filtration, washed and dried under suction (51 %).

Trans-[Pt(py)$_2$(N$_3$)$_2$]: ^{1}H NMR (d$_6$-acetone, 400 MHz): δ = 8.8 (d, $J_{1H195Pt}$ = 37 Hz, J_{HH} = 6.7, 1.3 Hz, 4H, H$_O$), 8.04 (dd, J_{1H1H} = 7.7, 1.50 Hz, 2H, H$_p$), 7.6 ppm (dd, J_{1H1H} = 6.60, 1.26 Hz, 4H, H$_m$).

*Equivalent synthesis was repeated for ^{15}N-**40** using Na^{15}N$_3$ (where one terminal nitrogen was 100% ^{15}N labelled).

2.2.3 Synthesis of *trans,trans,trans*-[Pt(N$_3$)$_2$(OH)$_2$(py)$_2$]

Trans-[Pt(N$_3$)$_2$(py)$_2$] (0.094 g, 0.21 mmol) was suspended in H$_2$O$_2$ (7.5 mL, 30 %) and stirred at 318 K for 3 h to give a bright yellow solution. The solvent was removed by rotary evaporator (323 K) until ca. 3 mL remained (*ca*. 40 min). Ethanol (3.75 mL) was added and the solution filtered (IM). Ether (11.30 mL) was added, the solution briefly mixed and left to cool at room temperature and then at 277 K. The yellow crystals were filtered and washed with ice cold ether/ethanol (0.060 g, 0.13 mmol, 59 %).

$C_{10}H_{12}N_8O_2Pt$ (471.37, confirmed by ESI-MS): ^1H NMR (D_2O, 400 MHz): $\delta = 8.76$ (dd, $^3J_{1H195Pt} = 27$ Hz, $^3J_{HH} = 6$ Hz, 2H, H_O), 8.24 (t, $^3J_{1H1H} = 7$ Hz, 1H, H_p), 7.8 ppm (t, $^3J_{1H1H} = 7$ Hz, 2H, H_m). ^{195}Pt NMR (D_2O, 129 MHz): $\delta = 941$ ppm.

This synthesis was reported by Farrer[1]; however the procedure was scaled down. Herein, both *trans,trans,trans*-[Pt(N_3)_2(OH)_2(py)_2] and *trans,trans,trans*-[Pt(^{15}N_3)_2(OH)_2(py)_2] will be denoted as complex **40** and ^{15}N-**40**, respectively

2.3 Instrumentation

2.3.1 Electron Paramagnetic Resonance (EPR) spectroscopy[2-4]

All EPR spectra were recorded at ambient temperature (ca. 291 K) on a Bruker EMX (X-band) continuous wave mode spectrometer. A cylindrical TM110 mode cavity (Bruker 4103TM) was used. This cavity is particularly useful for studies of aqueous or other solvents exhibiting high dielectric loss.[5,6] Samples *ca.* 75-85 μL were transferred using a 500 μL Hamilton syringe needle to a spectrosil quartz tubes with inner diameter of 1.0 mm and outer diameter (O.D.) of 1.2 mm (Wilmad Labglass), sealed with T-Blu Tac® at one end (Figure 2.1**A**). This tube was placed inside a larger quartz tube (O.D. 2.0 mm) so that the sample could be accurately and reproducibly positioned inside the resonator (Figure 2.1**B**). These filled sample tubes were longer than the active length of the TM110 cavity and were chosen such that when the tube was filled with water the cavity could still be critically coupled. Samples were transported in aluminium foil to the EPR spectrometer site to prevent photo-activation of the platinum(IV) diazido complex by sunlight, prior to performing EPR measurements.

A. Inner Quartz Tube

B. Outer Quartz Tube

2 cm

Figure 2.1 EPR tubes used in this work; (**A**) inner quartz EPR tubes with inset depicting the EPR tubes sealed with T-Blu Tac® at one end, and (**B**) larger 2.0 mm O.D outer quartz EPR tubes.

Typical key EPR spectrometer settings were modulation amplitude 2.0 G, microwave power 0.63 mW, 1.0×10^4 receiver gain, conversion time 40.96 ms, time constant 81.92 ms, sweep width 200 G. An incremental sweep mode was used in this work to monitor the formation and decay of the formed spin adduct. A repeated number of 10 X-scans were obtained in the x-axis at a rate of 42 s/scan and resolution in Y of 6. However, scans were analysed up to resolution in Y of 4, as these were deemed biologically relevant given the total irradiation dose after this time was *ca.* 107.9 J cm^{-2}, with 463 nm LED light source (64 mW cm^{-2}).

The LED light irradiation source was mounted between the EPR magnets, supported by a foam sponge (Figure 2.2), to maintain its position throughout the EPR sample measurements. The distance from the tip of the irradiation light bulb to the EPR cavity was *ca.* 8.5 cm (Figure 2.2). In this work, this distance was maintained for all subsequent irradiations. The TM110 EPR cavity used is equipped with a grid on one side allowing optical access (approximately 50%) transmission.

72

The refractive index of quartz is approximately 1.55;[7] hence at normal incidence approximately 5% of the incident light is reflected at an air quartz interface.
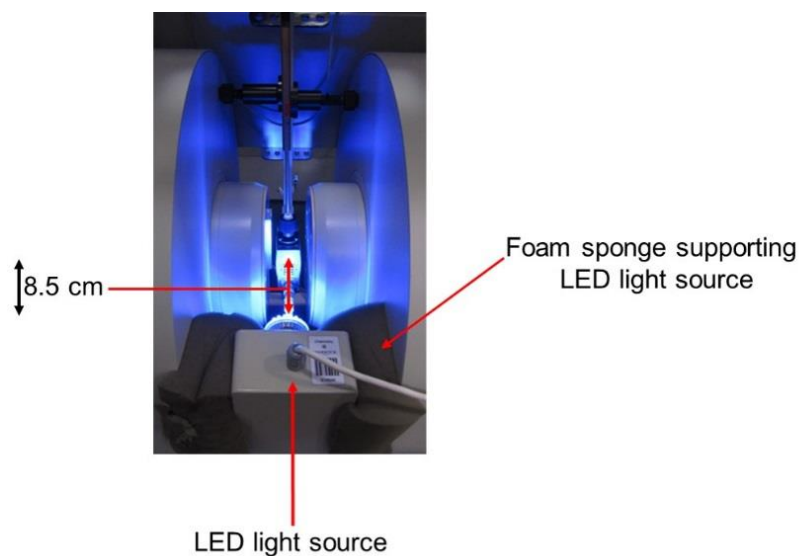
Figure 2.2 Setup of the X-band EPR cavity used in this work with mounted LED light source supported by a foam sponge at each side the EPR magnet. The distance from the LED light source bulb to the EPR sample cavity is *ca.* 8.5 cm.

2.3.1.1 Quantification of spin adducts

The free radical 4-hydroxy-2,2,6,6-tetramethyl-piperidine-1-oxyl (tempol, Figure 2.3) was used to quantify the formed spin adducts, as previously reported.[8,9] This free radical exhibits a triplet EPR spectrum (Figure 2.3), due to the unpaired electron coupling with the nitroxide nitrogen (^{14}N) with a nuclear spin of I = 1.[10]
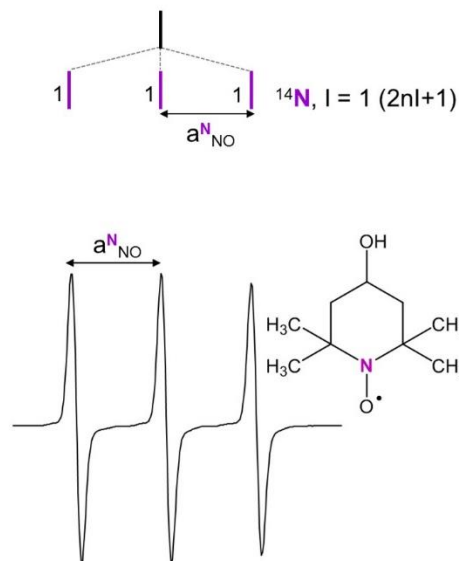
Figure 2.3 EPR spectrum together with the line diagram of the standard free radical, tempol.

For quantitative EPR spectroscopy, recording the free radical as close to the experimental conditions of the system under study is essential.[11,12] Solvents have been reported to have a direct effect on the nitrogen (a_N) hyperfine splitting values.[13,14] Consequently, the EPR spectrum of tempol was recorded in equivalent sample tubes, sample volume and temperature with varying solvent between H_2O, PBS/D_2O and cell culture medium RPMI-1640.

The concentrations prepared for the standard calibration curves were 300, 200, 100, 75, 50, 25, 12.5 and 5 µM. The EPR spectrum of each solution was recorded and after a baseline correction, double integration (DI) was performed using the Bruker WINEPR software programme,[15] providing the area under the curve.[12] In this thesis, EPR spin adduct spectra were quantified at 7 min intervals, where each interval represents an accumulation of 10 X-scans in the x-axis.

2.3.2 Nuclear Magnetic Resonance (NMR) spectroscopy[16]

2.3.2.1 ^{1}H NMR

In this thesis, ^{1}H NMR spectra were recorded on a Bruker DPX-400 (^{1}H, 399.10 MHz), Bruker DRX-500 (^{1}H, 500.13 MHz) or Bruker AV III-600 (^{1}H, 600.13 MHz) spectrometers at ambient 298 K. Spectra were recorded with standard ^{1}H NMR zg30 pulse program and acquired with 32 transients into 65 k data points with a spectral width of 20 ppm. Irradiated samples were performed in a transparent glass vial and transferred to the NMR tube to record the NMR spectrum. Any formed precipitates were removed prior to recording NMR spectra. Spectra were processed with an exponential line-broadening of 0.5 with *J* values quoted in Hz. All ^{1}H NMR spectra were internally calibrated to 1,4 dioxane (3.75 ppm in D_2O),[17] unless otherwise stated.

2.3.2.2 ^{14}N NMR[18-20]

NMR spectra were recorded on a Bruker AV III-600 (^{14}N, 43.36 MHz) instrument with a BBO probe. Due to the rapid quadrupolar relaxation of the ^{14}N nucleus, an anti-ringing pulse sequence "aring" and the digitization mode in "baseopt" were used for improvement of baselines.[21] Spectra were recorded with a pre-scan delay (DE) of 6.5 μs, with a relaxation delay (D1) of 0 s, with 8 k time domain with 32 k transients and spectral width of 100 ppm. Irradiated samples were performed in a transparent glass vial and any formed precipitates were removed prior to recording the NMR spectrum. Irradiated samples *ca.* 550 μL were transferred into the NMR tube to record the NMR spectrum. Data were processed with an exponential line broadening of 30 Hz unless otherwise stated. Similar to the external referencing previously reported by Farrer *et al.,* in this work external referencing was carried

out with D_2O solutions in a capillary tube, inserted into a 5 mm tube containing either $^{14}NH_4Cl$ (1.5 M) in 1 M HCl ($\delta = 0$). The $^{14}NH_4Cl$ signal was found 360.13 ppm (298 K) upfield of the standard ^{14}N reference (neat $MeNO_2$, D_2O in a Shigemi tube), and this value can be used to convert literature shifts referenced to CH_3NO_2 to the $^{14}NH_4Cl$ reference. Similarly, chemical shifts may be converted from $MeNO_2$ to NH_3 referencing (the latter is common for biological NMR spectroscopy) by subtraction of 380.23 ppm.[21,22]

2.3.3 UV-visible spectroscopy[23]

UV-visible electronic absorption spectra were recorded on a Varian Cary 300 UV-visible (V9.0) spectrophotometer in 1 cm path-length dark cuvettes purchased from Starna Scientific. Prior to sample measurement, cell alignment and a baseline correction were performed. Spectra were recorded with scan rate 600 nm/min, 200-800 nm spectral width, 2.0 nm bandwidth and temperature controller set at *ca.* 25.2 °C. Typical sample volume was *ca.* 650 μL. Irradiated samples were performed in a transparent glass vial and transferred to the cuvette to record the UV-visible spectrum.

2.3.4 Irradiations

The majority of irradiations were carried out using a blue light-emitting-diode (LED) source with a power outage measured at 64 mW cm^{-2} using an International Light Technologies Power meter (ILT1400-A) equipped with a SEL033 detector and either a UVA/TD filter (315-390 nm) for a flat response visible filter F/W (400-1064 nm)for visible wavelengths. To confirm irradiation with 463 nm blue LED light source, the spectral output was measured (Figure A2.1). Continuous

irradiation implies the irradiation source was switched on during the entire time of the experiment, unless otherwise stated. Irradiation setup for NMR and UV-visible spectroscopy is depicted in Figure 2.4, where the distance of the LED light bulb to the centre of the sample was measured to *ca.* 8.5 cm, consistent with the EPR spectroscopy irradiation setup. Light doses were determined using the Equation 2.1, below.
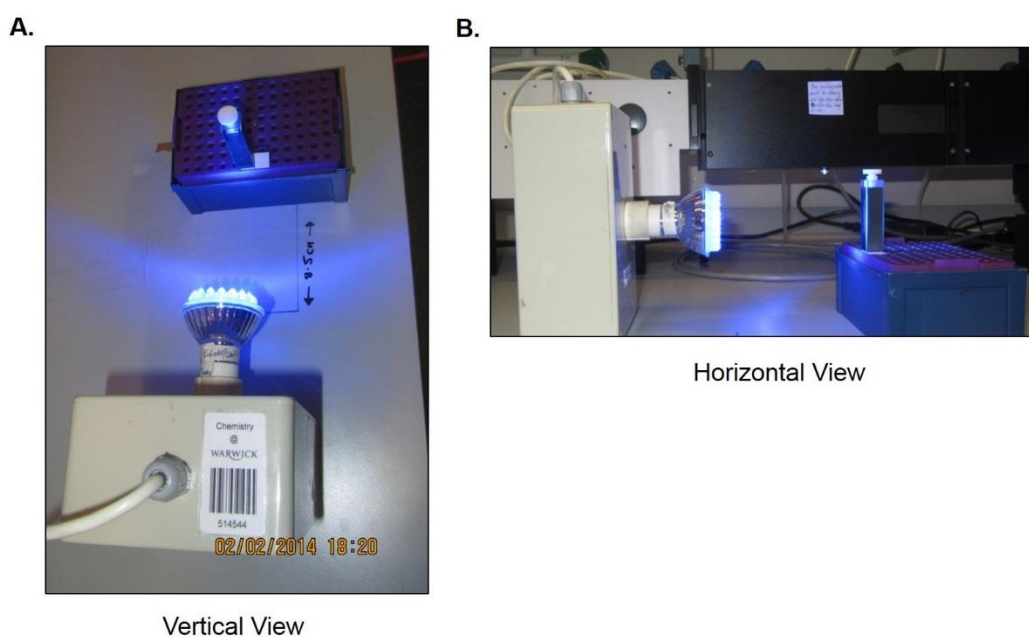
Figure 2.4 Irradiation setup used in this work for both NMR and UV-visible spectroscopy experiments from both (**A**) vertical and (**B**) horizontal viewpoints. The distance from the tip of the LED light bulb to the centre of the cuvette was *ca.* 8.5 cm. This distance is equivalent to that used for EPR spectroscopy irradiations.

$$\text{Dose (mJ cm}^{-2}) = \frac{\text{Time (s)} \times \text{Irradiance (mW cm}^{-2})}{1000}$$

2.3.5 Mass Spectrometry

2.3.5.1 Electrospray Ionisation Mass Spectrometry[24] (ESI-MS)

Electrospray ionisation mass spectrometry was performed on an Agilent 1630 single quad ESI spectrometer with a mass range of 50 - 3,000 *m/z*. Due to components in PBS able to supress the electrospray signal,[25] mass spectra samples were H_2O only and irradiated with 463 nm (64 mW cm^{-2}). Solutions were not prepared in PBS due to components The stock solution under investigation was irradiated, prior to performing a 100-fold serial dilution, to produce a solution in the low micro-molar range, suitable for the mass spectrometer instrument. The 100-fold diluted solution was transferred into a 2 ml amber mass spectroscopy vial. Typically 2 µL of the irradiated sample was injected into the machine. Samples were run in positive mode between the range of 50-500 *m/z*, and 500-1000 *m/z*. Automatic washes were pre-programmed by the computer software and one scan typically took 3 min 21 sec. Data were processed using the Bruker Daltonics software data analysis programme.

2.3.5.2 Inductively Coupled Plasma Mass Spectrometry (ICP-MS)

ICP-MS was performed to determine the platinum (^{195}Pt isotope) content of cell sample solutions provided by Dr. Julie Woods. ICP-MS solutions were recorded with the assistance of Dr. Isolda Romero on Aligent Technology series 7500, a part of the Mass Spectrometry facility at Warwick University. All solutions were prepared in doubly deionised (DDI) water with 5% nitric acid (HNO_3). The standard solutions were freshly prepared in DDI water with 5% HNO_3. The concentrations prepared for the standard calibration curve were 500, 200, 100, 50, 10, 5, 1, 0.5 and 0.2 ppb.

2.3.6 pH measurements

pH values were determined using a Corning 240 pH meter equipped with a micro combination electrode calibrated with Aldrich buffer solutions of pH 4, and 7. For solutions in D_2O, these are given as pH* values, pH meter readings without correction for effects of deuterium on glass electrode. The pH values of solutions were adjusted using 1 mM KOH and 1 mM NaCl.

2.4 Deuterated phosphate buffered saline (PBS/D_2O) solution

The phosphate buffered solutions were prepared by dissolving a PBS tablet in H_2O giving 0.01 M phosphate, 0.0027 M KCl, pH 7.4 at 298 K. Likewise a PBS/D_2O buffer refers to the above prepared by dissolving the PBS tablet in D_2O. A resultant PBS/D_2O at pH* 7.4 was obtained, where pH* refers to pH meter reading without correction effects for deuterium on a glass electrode.

2.5 Cell studies

All cellular studies were performed in the laboratory of Dr. Julie Woods, Photobiology Unit, Ninewell's Hospital, Dundee, UK.

2.5.1 Cell maintenance

Cell culture and other chemicals were obtained from Sigma-Aldrich Ltd (Poole, UK) unless otherwise stated. Disposable sterile cell culture plastics were obtained from Greiner Bio-One (Cambridge, UK). Cell lines were obtained from both the European Collection of Animal Cell Cultures, and the American Cell Culture Collection. HaCaT keratinocytes cells were donated to the Photobiology Laboratory by Professor N. E. Fusenig (Heidelberg, Germany). Cell lines were maintained in

culture medium containing 5-10% foetal bovine serum and other additives as specified by the supplier. Cells were free of mycoplasma and were maintained in antibiotic-free conditions in a humidified atmosphere of 5% CO_2/95% air.

2.5.2 Cell irradiation

Visible light was delivered from a bank of 2 x 2 feet TL03 fluorescent tubes. Wavelengths shorter than 400 nm were blocked by filtering. The spectral output was centred at 420 nm and the irradiance measured with a Gigahertx Optik meter calibrated to the source using a spectroradiometer (Bentham, UK). Irradiances were measured through filters, and where appropriate, cell culture plate lids. Test compounds were prepared immediately before use in warm Earle's balanced salt solution (EBSS) and sterile filtered, or in dimethyl sulfoxide. All procedures were carried out in a specially adapted photobiology laboratory with ambient light levels measured below 1 lux (Solatell, UK).

2.5.3 Photo-toxicity

The neutral red photo-toxicity test was performed to determine the photo-toxic index (PI). This assay is used to assess the cell viability, where uptake of neutral red indicates viable cells.[26] Test compounds were treated as previously described,[1] briefly co-incubated with the cells for 60 min in the dark, before irradiation. The test compounds were *in-situ* during the irradiation with visible light (5 J cm^{-2}). Two identical plates were prepared, one of which was irradiated while the second was covered in aluminium foil and sham irradiated. Cell viability was measured using the uptake of neutral red dye as an endpoint after 24 h.

2.5.4 Data Analysis

The concentration of test compound required to inhibit neutral red dye retention by 50% (IC_{50} value) was calculated from the log-transformed concentration-response curves, constrained to 100% at the maximal value (Prism, Graphpad). The photo-toxicity index was calculated as previously described. The data represent the mean of at least two independent experiments performed in triplicate.

2.6 References

(1)   Farrer, N. J.; Woods, J. A.; Salassa, L.; Zhao, Y.; Robinson, K. S.; Clarkson, G.; Mackay, F. S.; Sadler, P. J. *Angew. Chem. Int. Ed.* **2010**, *49*, 8905.

(2)   Corvaja, C. In *Electron Paramagnetic Resonance: A Practitioner's Toolkit*; Brustolon, M., Giamello, E., Eds.; John Wiley & Sons: New Jersey, 2009, p 120.

(3)   Jeschke, G. In *ESR Spectroscopy in Membrane Biophysics*; Springer US: 2007; Vol. 27, p 17.

(4)   Gescheidt, G. In *Electron Paramagnetic Resonance: A Pracititoner's Toolkit*; Brustolon, M., Giamello, E., Eds.; John Wiley & Sons: New Jersey, 2009, p 109.

(5)   Dalal, D. P.; Eaton, S. S.; Eaton, G. R. *J. Magn. Reson.* **1981**, *44*, 415

(6)   Eaton, S. S.; Eaton, G. R. *Bull. Magn. Reson.* **1979**, *1*, 130.

(7)   Bertino, A. J. *Forsenic Science: Fundamentals and Investigations 2012 Update*; Cengage Learning: Mason, USA, 2012, p 403.

(8)   Akaike, T.; Yoshida, M.; Miyamoto, Y.; Sato, K.; Kohno, M.; Sasamoto, K.; Miyazaki, K.; Ueda, S.; Maeda, H. *Biochemistry.* **1993**, *32*, 827.

(9)   Akaike, T.; Sato, K.; Ijiri, S.; Miyamoto, Y.; Kohno, M.; Ando, M.; Maeda, H. *Arch. Biochem. Biophys.* **1992**, *294*, 55.

(10)   Yordanov, N. D.; Ranguelova, K. *Spectrochim. Acta. A. Mol. Biomol. Spectrosc.* **2000**, *56*, 373.

(11)   Mazur, M. *Anal. Chim. Acta* **2006**, *561*, 1.

(12)   Eaton, G. R.; Eaton, S. R.; Barr, D. P.; Weber, R. T. In *Quantitative EPR:A Practitioners Guide*; Springer-Verlag/Wien: Germany, 2010, p 2.

(13)   Janzen, E. G.; Coulter, G. A. *Tetrahedron Lett.* **1981**, *22*, 615.

(14)   Janzen, E. G.; Coulter, G. A. *Can. J. Chem.* **1982**, *60*, 2725.

(15)   Thiele, H.; Erstling, J.; Such, P.; Hofer, P.; 921201 ed. Germany, 1992.

(16)   Hore, P. J. *Nuclear Magnetic Resonance*; Oxford University Press: New York, 2001.

(17)   Gottlieb, H. E.; Kotlyar, V.; Nudelman, A. *J. Org. Chem.* **1997**, *62*, 7512.

(18)   Seok, W. K.; Klapötke, T. M. *Bull. Korean Chem. Soc.* **2010**, *31*, 781.

(19)   Westendorf, A. F.; Woods, J. A.; Korpis, K.; Farrer, N. J.; Salassa, L.; Robinson, K.; Appleyard, V.; Murray, K.; Grünert, R.; Thompson, A. M.; Sadler, P. J.; Bednarski, P. J. *Mol. Cancer Ther.* **2012**, *11*, 1894.

(20)   Phillips, H. I. A.; Ronconi, L.; Sadler, P. J. *Chem. Eur. J.* **2009**, *15*, 1588.

(21)   Farrer, N. J.; Gierth, P.; Sadler, P. J. *Chem. Eur. J.* **2011**, *17*, 12059.

(22)   Mitchell, T. N.; Costisella, B. *NMR - from Spectra to Stuctures an Experimental Approach*; 2nd ed.; Springer-Verlag: Dortmund, Germany, 2007, p 60.

(23)   Brisdon, A. K. *Inorganic Spectroscopic Methods*; Oxford University Press: New York, 1998.

(24)   P, A. In *The Encyclopedia of Mass Spectrometry*; Gross, M. L., Caprioli,

R. M., Eds.; Elsevier Science: USA, 2003; Vol. 1, p 940.

(25)   Iavarone, A. T.; Udekwu, O. A.; Williams, E. R. *Anal. Chem.* **2004**, *76*,

3944.

(26)   Repetto, G.; del Peso, A.; Zurita, J. L. *Nat. Protocols.* **2008**, *3*, 1125.

Chapter III

EPR Spin Trapping of

Photoactivated Platinum(IV)

Diazido Anticancer Complexes

This chapter initially investigates the photo-generation of radical species from the photo-activation of platinum(IV) diazido anticancer complexes characterised by electron paramagnetic resonance (EPR) spectroscopy. Experimental conditions were varied to optimise spin trapping EPR. Finally, photo-activation of complex **40** at longer wavelengths and using gamma-rays was investigated.

3.1 Introduction

3.1.1 Metal diazido complexes

Photo-irradiation of *trans,trans,trans*-[Pt(OH)$_2$(N$_3$)$_2$(py)$_2$] (complex **40**, py = pyridine) leads to a decrease in the intensity of the ligand-to-metal charge transfer (N$_3$→Pt^{IV}, LMCT) transition, previously assigned as the loss of the azide ligands.[1] Photo-activation studies of metal diazido complexes of the type [M^{n+}(N$_3$)$_2$(X)$_2$(Y)$_2$] (where M = Pd^{II}, Pt^{II}, Sn^{II}, Au^{III}, Co^{III}, Fe^{III} and Mo^{IV}; X = OH/OR; Y = amine-based ligands) have reported on azidyl ($^\bullet$N$_3$) radical formation through one-electron reduction of the M^{n+} centre,[2-6] as shown below (Figure 3.1).

X = -OH/-OR ligands
Y = amine-based ligands
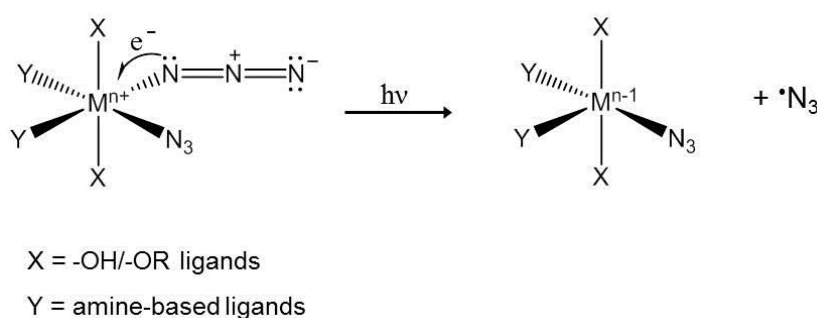
Figure 3.1 One-electron reduction of the metal centre (M^{n+}) induced from the photo-irradiation of a metal-diazido complex.

The observation of bubbles, proposed to be N$_2$ gas, has been reported as evidence to support $^\bullet$N$_3$ radical formation, where $^\bullet$N$_3$ radical dimerisation was the suggested

mechanism for N_2 formation.[7-9] Thermodynamically favourable ($\Delta H = -210 \pm 6$ kcal mol^{-1}), $^\bullet N_3$ radical dimerisation leading to N_2 gas was suggested to proceed through an intermediate N_6 species;[10]

$$2(^\bullet N_3) \xrightarrow{k_1} N_6 \xrightarrow{k_2} N_2 + N_4$$
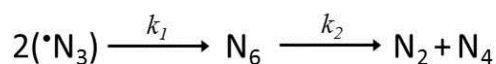
where k_1 and k_2 are rate constants of 1.3×10^{10} M^{-1} s^{-1} and 3.6×10^3 M^{-1} s^{-1}, respectively and the N_6 intermediate species possesses a half-life ($t_{1/2}$) of ca. 200 μs.[11] Whilst detection of N_2 gas may be postulated by the observation of bubbles or more accurately by gas chromatography, the formation of metal-nitrene intermediates may also account for the detection of N_2 gas.[12] Additional loss of azide ligands can also proceed *via* direct solvent substitution through a non-redox photo-substitution pathway, typically characterised by the formation of free azide (N_3^-).[8] Consequently, the most reliable method to establish $^\bullet N_3$ radical formation is by EPR spin trapping spectroscopy.

Previous photo-irradiation studies of complex **40** in the presence of guanosine 5′-monophosphate (5′-GMP, a model for the nucleobase guanine in DNA) identified both mono- and bi-functional Pt^{II}-GMP adducts suggesting the stepwise loss of the azide ligands.[1,13,14] It was suggested that the formed N_2 gas detected by ^{14}N NMR spectroscopy was due to $^\bullet N_3$ radical dimerisation.[15] The reduction of the Pt^{IV} to Pt^{II} metal centre of complex **40** has also been suggested to involve hydroxyl ($^\bullet OH$) radical formation (Figure 3.2**B**).[1] Interestingly, photo-irradiation of *trans,trans,trans*-[Pt(N$_3$)$_2$(OH)$_2$(MA)(py)] (**44**, where MA = methylamine), an analogue of complex **40**, has been reported to generate singlet oxygen ($^1O_2$) through $^\bullet OH$ radical dimerisation leading to the formation of hydrogen peroxide

(H_2O_2), which upon disproportionation generated both $^1O_2$ and H_2O.[16] Consequently, various different photo-activation pathways of platinum(IV) diazido complexes appear to exist.
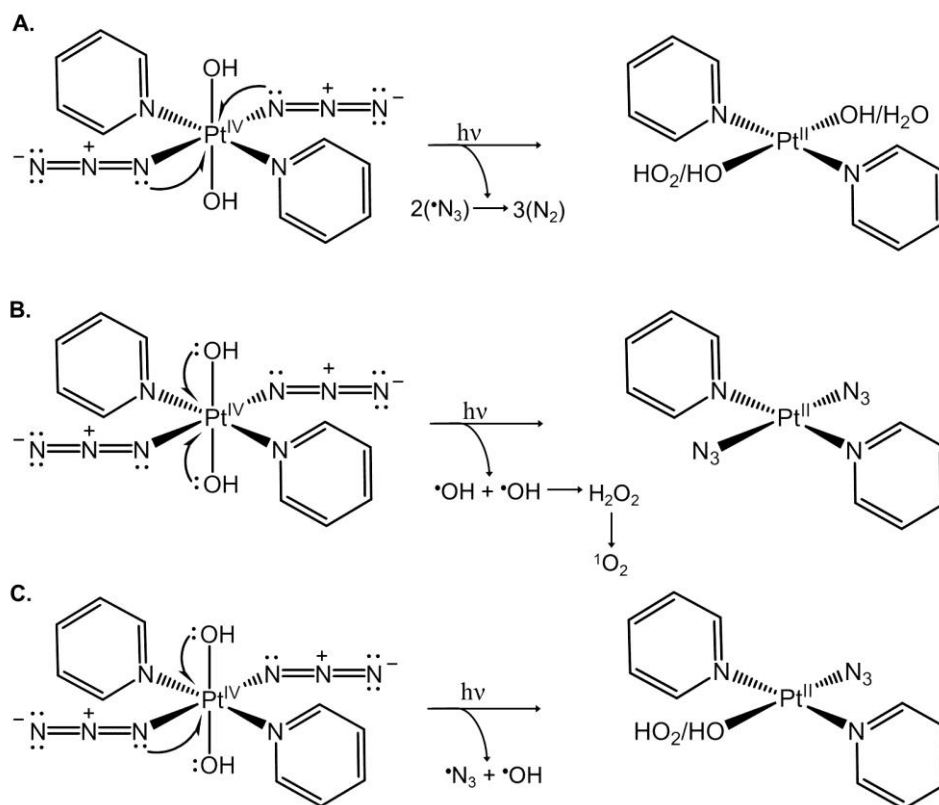
Figure 3.2 Photo-activation of complex **40** through two successive one electron reductions from (**A**) the azide (**B**) hydroxyl (**C**) one azide and one hydroxyl ligands, all in turn generating a Pt^{II} photo-species.

A useful method to detect and characterise radical species is electron paramagnetic resonance (EPR) spectroscopy. In **Chapter I**, a brief description of the theory and characterisation of EPR spectra was given. This Chapter will focus on EPR spin trapping of radicals. Radical species possessing short life-times (*ca.* 10^{-9} s) such as ROS and RNS radicals,[17] cannot be directly detected by EPR spectroscopy and are referred to as transient species. These transient species can undergo uni-molecular (fragmentation) or bimolecular (addition) reactions prior to detection by

EPR spectroscopy. Consequently, EPR spin trapping spectroscopy, developed in the late 1960's, is a more appropriate technique for their detection.

3.1.2 Spin trapping Electron Paramagnetic Resonance

3.1.2.1 Spin adduct formation

Spin trapping EPR involves the use of a diamagnetic compound, commonly referred to as a spin trap (ST), typically a nitroso or nitrone compound. This ST covalently interacts with an unstable radical ($^\bullet$R) leading to the generation of a longer lived radical species, referred to as a spin adduct (ST-R$^\bullet$).[18]

$$ST + {}^\bullet R \xrightarrow{\ k_1\ } ST\!-\!R^\bullet$$
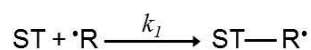
where k_1 is the rate of the radical being trapped by the spin trap and varies dependent on the experimental conditions.[19]

3.1.2.2 Choice of spin trap

Both nitroso and nitrone spin traps are available for spin trapping EPR. They possess the ability to trap oxygen-, carbon-, nitrogen- and sulfur-based radicals. However, the information obtained about the composition of the trapped radical is directly dependent on the chosen spin trap. Nitroso spin traps, such as 2-methyl-2-nitrosopropane (MNP), provide direct information on the trapped radical (Figure 3.3**A**),[20] in contrast, nitrone spin traps such as 5,5-dimethyl-1-pyrroline-N-oxide (DMPO) provide indirect information on the trapped radical (Figure 3.3**B**).[21,22] In this instance, although the nitrogen hyperfine splitting is not as specific to the trapped radical, the presence of the β-hydrogen provides a wealth of information on the radical trapped.
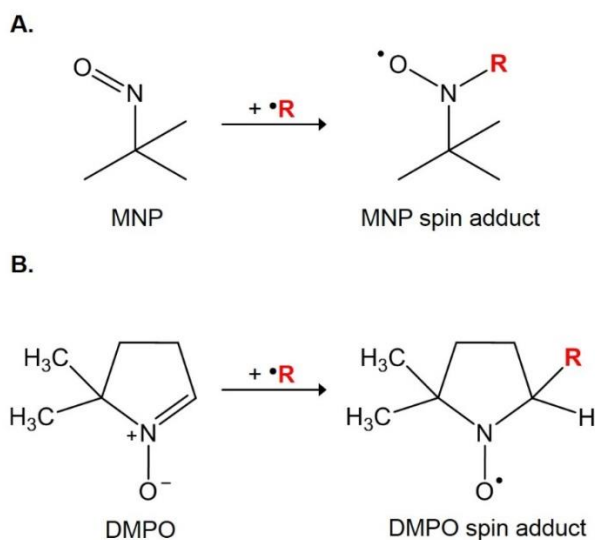
Figure 3.3 Trapping of a radical (•**R**) species by (**A**) nitroso and (**B**) nitrone spin traps, showing the position at which the •**R** species covalently attaches in the resultant spin adduct.

The photo-lability of MNP spin trap limited its use in this work. Irradiation of MNP with visible light leads to the formation of both nitric oxide and *tert*-butyl radicals, subsequently trapped by MNP, obscuring the radical species under investigation. Additionally, various EPR-active impurities have been identified from the reduction of nitroso spin traps.[23] Consequently, nitrone spin (Figure 3.4) traps were selected for this work.
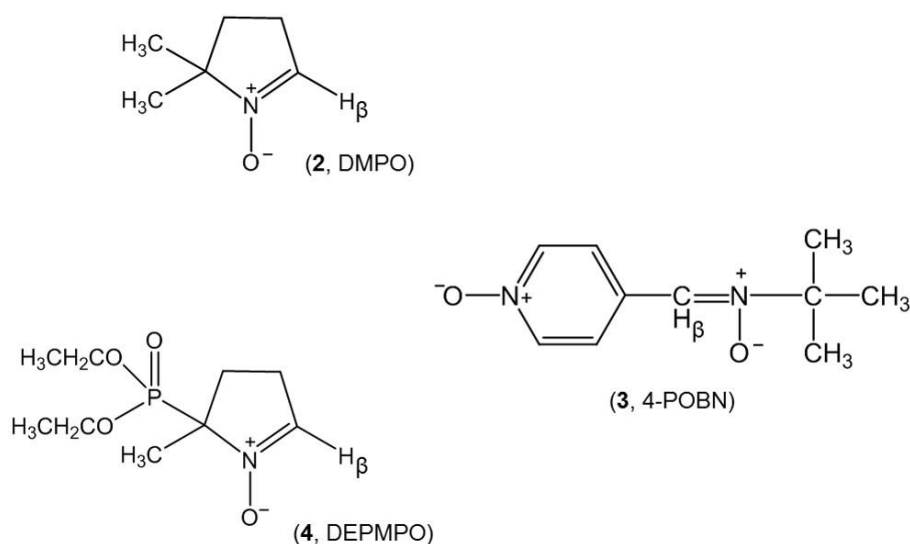
Figure 3.4 Structures of the nitrone spin traps used in this study; (**2**) 5,5-dimethyl-pyrroline-*N*-oxide (DMPO); (**3**) α-4-pyridyl-1-oxide-*N-tert*-butylnitrone (POBN) and (**4**), 5-diethoxyphosphoryl-5-methyl-1-pyrroline-*N*-oxide (DEPMPO).

3.1.2.3 McConnell equation[24]

Regardless of which nitrone spin trap is chosen, all generate nitroxide radicals (Figure 3.5**A**), from the covalent interaction with an unstable radical. Nitroxide radicals possess resonance structures (Figure 3.5).
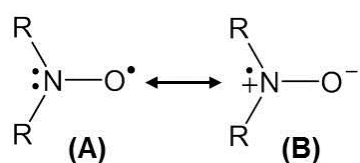
Figure 3.5 Resonance structures of nitroxide spin adduct. Radical is based on the (**A**) oxygen atom (^{16}O, I $=0$), and (**B**) nitrogen atom (^{14}N, I $=1$).

As described in **Chapter I**, hyperfine coupling arises from the interaction of the unpaired electron spin with the nuclear spin of a magnetically-active nucleus, whose spin (I) is greater than zero (I $\neq$ 0). Depending on the position of the proton

coupling to the unpaired electron, the spin density in the 2pπ orbital can be calculated. The standard McConnell equation (Equation 3.1) determines an α-proton coupling (Figure 3.6**A**), where Q^H_{CH} is the proportionality constant (mT) and varies dependent on the atom.[24]

$$a^H = Q^H_X \rho_c \qquad \text{Eq 3.1}$$

However, in nitroxide spin adducts, a β-proton coupling is present (Figure 3.6**B**), which is dependent on the dihedral angle (θ) of the C-H bond w.r.t to the z axis. This dihedral angle (θ) can vary dependent on the orientation of trapped radical species (**R**).[25]
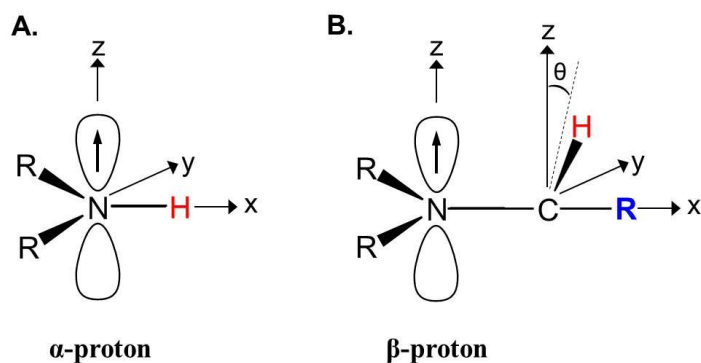
Figure 3.6 Illustrations of (**A**) α-proton and (**B**) β-proton coupling to the unpaired electron (↑). Where β-proton coupling is dependent on the dihedral angle θ and varies according to the trapped radical (**R**) (figure adapted from ref 21).

Therefore, determining the spin density in spin systems such as nitroxide radicals, the standard McConnell equation has been modified to incorporate this dihedral angle parameter (Eq 3.2).

$$\alpha^H_\beta = Q^H_{CH} \rho_c (\cos^2\theta) \qquad \text{Eq 3.2}$$

However, in this thesis the spin density of obtained nitroxide radicals were accessed *via* density functional theory (DFT) calculations. Previous DFT calculations were performed on both the DMPO-O$_2$$^{-\bullet}$ and DEPMPO-O$_2$$^{-\bullet}$ spin adducts to investigate the dependence of the $a_{\beta\text{-H}}$ value with the spin density on the nitrogen atom.[25]

3.1.2.4 Decay of spin adducts

The decomposition of spin adducts has been reported to proceed through a disproportionation pathway generating a nitrone and hydroxylamine species (Figure 3.7).[22] This process requires a β-hydrogen and is retarded by the presence of bulky substituents at the C5-position in cyclic nitrone spin traps.[21]
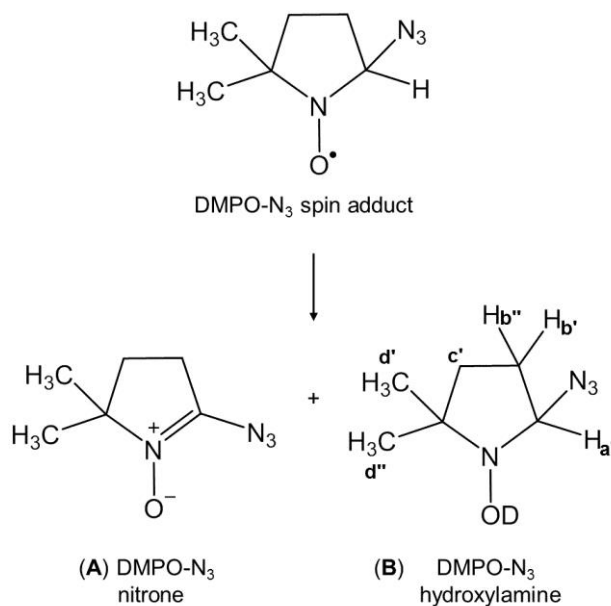
Figure 3.7 Decomposition pathway of a DMPO spin adduct forming a (**A**) nitrone and (**B**) hydroxylamine species in aqueous solution.

3.1.2.5 Azidyl and hydroxyl radicals

The trapping of $^\bullet$N$_3$ radicals has been investigated using a variety of spin traps. In particular, the DMPO-N$_3$ spin adduct has been well characterised.[2,26,27] The quartet-of-triplets EPR spectrum indicates $^{14\bullet}$N$_3$ radicals, in contrast to the quartet-of-doublets EPR spectrum reported for the $^{15\bullet}$N$_3$ radicals, trapped by DMPO.[28] The resultant change in these EPR spectra is due to the change in their nuclear spin (I) of each isotope (^{14}N, I = 1; ^{15}N, I = ½).

The trapping of the $^\bullet$OH radical by DMPO generates a quartet EPR signal.[29] However, this EPR spectrum can also be detected from the spontaneous decomposition of unstable DMPO-R spin adducts.[30] This has been distinguished by the addition of $^\bullet$OH radical scavengers, such as ethanol (EtOH) or dimethyl-sulfoxide (Me$_2$SO). Interaction of the formed $^\bullet$OH radicals with these radical scavengers leads to the formation of carbon-centred radicals, generating distinct EPR spectra.[31,32] The 4-POBN (**4**, Figure 3.4) spin trap has been shown to be the most efficient spin trap for the detection of the α-hydroxy-ethyl ($^\bullet$CHCH$_3$OH) radicals.[33,34]

3.1.2.6 Wavelength of activation

The choice of the irradiation source in photo-chemotherapy is important for achieving sufficient penetration into the tissue, where longer wavelengths of light (white, red and NIR) penetrate more deeply (refer to Figure 1.23, p 36).[35,36] Photo-activation of complex **40** with 463 nm and 517 nm light limits the potential application of complex **40** to thin-walled organ cancers such as bladder and oesophagus cancers.[1] Therefore, activating complex **40** with alternative radiation

sources, such as gamma rays (widely used clinically) has potential to widen the types of tumours treatable by complex **40**. The main aim of radiotherapy is to achieve cancer cell death with minimal damage to normal "healthy" tissue(s), through the use of high energy particles or waves such as X-rays, gamma-rays, electron beams or photons. Commonly used radiation sources are radioactive cobalt-60 (^{60}Co) and cesium-137 (^{137}Cs) isotopes. ^{137}Cs emits gamma (γ) rays of energy 0.66 MeV.[37] Currently used in chemotherapy, *cis*-platin and carboplatin have been shown also to be efficient radiosensitisers. Their cytotoxicity is sometimes enhanced by activation with a radiation source compared to conventional treatment procedures.[38,39] However, the activation of platinum(IV) diazido anticancer complexes with gamma-rays has not been previously reported.

In this Chapter, the detection of radical species from the photo-activation of complex **40** was investigated through the use of spin trapping (EPR) spectroscopy, using a variety of nitrone spin traps. Successful trapping of $^{\bullet}N_3$ radicals led to varying experimental conditions to best mimic a biological environment. The spin trapping of azidyl radicals was extended to other photo-activatable platinum(IV) diazido anticancer complexes. Finally, spin trapping studies of photo-activated complex **40** with longer wavelengths of light (green and yellow LED light sources) and a gamma-ray irradiation source were investigated.

3.2 Experimental

Below are the experimental sample preparation and instrumentation set up specific to this Chapter. More details regarding instrumentation and the irradiation setup are described in **Chapter II**.

3.2.1 Materials

Complex **40**, *trans,trans,trans*-[Pt(N$_3$)$_2$(OH)$_2$(py)$_2$] and ^{15}N-**40** were synthesised and characterised as described in **Chapter II**. *Trans,trans,trans*-[Pt N$_3$)$_2$(OH)$_2$(MA)(py)] (complex **44**, MA = methylamine) was provided by Dr. Yao Zhao[40] and *trans,trans,trans*-[Pt(N$_3$)$_2$(OH)(SAD)(py)$_2$] (complex **56**, SAD = succinate), *trans,trans,trans*-[Pt(N$_3$)$_2$(OH)(ethyl-methyl-SAD)(py)$_2$] (complex **57**) and *trans,trans,trans*-[Pt(N$_3$)$_2$(OH)(N-MI)(py)$_2$] (complex **58**, N-MI = N-methylisatoate) were provided by Dr. Evyenia Shaili.[41] Nitrone spin traps α-4-pyridyl-1-oxide-*N-tert*-butylnitrone (4-POBN) and 5-diethoxyphosphoryl-5-methyl-1-pyrroline-*N*-oxide (DEPMPO) were purchased from Enzo Life Sciences, obtained in the highest purity ($\geq$ 99 %) and used without any further purification. The fully prepared cell culture medium RPMI-1640 (without L-glutamine) was purchased from PAA Laboratories Gmbh.

3.2.2 Instrumentation

3.2.2.1 X-band Electron Paramagnetic Resonance

All EPR spectra were recorded on a 9.5 GHz X-band EPR spectrometer at ambient temperature (ca. 291 K). More specific details regarding EPR acquisition and spin adduct quantification are described in **Chapter II**.

3.2.2.2 Irradiation Sources

The majority of irradiations were performed using a blue LED light source (λ = 463 nm, 64 mW cm^{-2}) commonly denoted herein as "463 nm" unless otherwise stated; the spectral output is shown in Figure A2.1. Additional irradiations involving green LED light source (λ = 517 nm, 33 mW cm^{-2}) and yellow LED light source (λ = 593 nm, 17 mW cm^{-2}) were used with spectral outputs shown in

Figure A3.1 and Figure A3.2, respectively. More specific details regarding irradiation setup, times and light power intensity measurements are described in **Chapter II**.

3.2.2.3 Gamma-ray irradiations

Gamma-ray irradiations were performed by Dr. Rebecca Carter at the Gray Institute in Oxford. Plates were irradiated using a ^{137}Cs irradiator (dose rate 1.81 Gy min^{-1}) at room temperature.

3.2.3 Sample preparation

3.2.3.1 Varying solvent

Solutions of complex **40** and spin trap were both prepared in deuterated phosphate buffer (PBS/D$_2$O) and Roswell Memorial Park Institute medium (RPMI-1640), the latter to represent a more physiologically relevant environment. The phosphate-buffered saline (PBS) solution was prepared in D$_2$O as opposed to H$_2$O. D$_2$O was chosen essentially for direct comparison purposes between EPR and NMR spectroscopic data (in subsequent **Chapters IV-IV**).

3.2.3.2 UV-visible spectroscopy

The UV-visible spectrum of a solution of complex **40** (50 μM) prepared in PBS/D$_2$O was recorded in the dark and after 5 min, 15 min, 30 min and 60 min irradiation with both 463 nm and 517 nm light. UV-visible instrumentation and irradiation setup were as described in **Chapter II**.

3.2.3.3 Gamma ray samples

Complex **40** was transported from Warwick University to the Gray Institute in Oxford in an amber Eppendorf tube and wrapped in aluminium foil to prevent photo-activation from sunlight. Spin traps were stored under dry ice in an appropriate container and sealed to maintain the spin traps viability during transit. An aqueous stock solution of complex **40** (5 mM) in the presence of spin trap (10 mM) was prepared immediately prior to performing the experiment. An aliquot of the stock solution (ca. 1 mL) was transferred on a plastic cell plate and placed inside the irradiation source. The selected irradiation doses, some of therapeutic relevance were delivered by specific placement of the cell plate containing the solution on the appropriate shelf and positioned near the gamma-ray source. After irradiation, the solution was transferred to a transparent vial, covered with aluminium foil to reduce additional light exposure. It was transported back to Warwick University where EPR analysis was undertaken, ca. 1.5 h after the initial irradiation was performed.

3.2.4 Density functional theory (DFT) calculations

Density functional theory calculations were performed by Miss Nichola Smith. Geometry optimisations were performed using Gaussian03[42] in the gas phase using Becke's three-parameter hybrid functional[43] with Lee-Yang-Parr's gradient-corrected correlation functional (B3LYP).[44] The split valence 6-31G** basis set was applied to all atoms. Electrostatic potential surfaces (EPS) were calculated and mapped on electron density (isovalue 0.001) of the molecules. The selected spin density maps for the spin adducts, DMPO-N_3, DEPMPO-N_3 and 4-POBN-N_3 are

provided where green indicates a decrease in spin density, while dark blue indicates an increase.

3.3 Results

3.3.1 Dark and irradiated controls

The spin traps used in this work (Figure 3.4) were purchased with the highest degree of purity (> 99 %). However, some commercially available spin traps contain hydroxylamines, which, under oxidising conditions, can generate EPR spectra obscuring the radical species under investigation.[17] To investigate the presence of background EPR signals from the different spin traps used in this work, both dark and irradiated controls of the spin traps were performed.

No EPR signals were detected from either the dark or after 30 min irradiation with 463 nm (blue), 517 nm (green) and 593 nm (yellow) LED light for all of the spin traps DMPO (**2**, Figure 3.4), 4-POBN (**3**, Figure 3.4) and DEPMPO (**4**, Figure 3.4) in H_2O, deuterated phosphate buffer (PBS/D_2O) and in cell culture medium (Figure A3.3). The stability of these spin traps rendered them suitable for the potential detection of radicals generated from the photo-irradiation of complex **40**.

Furthermore, solutions of *trans,trans,trans*-[Pt(N$_3$)$_2$(OH)$_2$(py)$_2$] (complex **40**) were prepared in all three solvents and did not display an EPR spectrum in either the dark or upon irradiation. Additionally, the dark EPR spectrum of complex **40** in the presence of spin traps (**2**-**4**) in all three solvents did not display an EPR signal (Figure A3.4), confirming no radical detection from complex **40** in the dark.

The cyclic nitrone spin trap, DMPO is the most commonly used spin trap in both *in vitro*[45] and *in vivo*[46] studies. Therefore, primary photo-activation of complex **40** was performed in the presence of this spin trap.

3.3.2 EPR spectroscopy with 5,5-dimethyl-pyrroline-*N*-oxide (DMPO)

3.3.2.1 Azidyl radical trapping

A solution of complex **40** (4 mM) in the presence of DMPO (8 mM, 2 mol equiv) was prepared in H_2O at pH 7.4 and irradiated at 463 nm. An EPR signal was observed after 42 s (2.7 J cm^{-2}) irradiation at 463 nm (Figure 3.8**A**). After 7 min irradiation, this EPR signal became more pronounced in its intensity in the ratio of 1:1:1:2:2:2:2:2:2:1:1:1 (Figure 3.8**B**) and was assigned to a quartet of triplets EPR spectrum. An equivalent EPR spectrum was generated after performing a simulation (Figure 3.8**B**) using the experimentally determined hyperfine coupling constants. The observed hyperfine coupling values were similar to previously reported values for the DMPO-$^{14}N_3$ spin adduct (Table 3.1).[28] Therefore, this spectrum is assigned to the DMPO-$^{14}N_3$ spin adduct. Differences between the experimental and previously reported hyperfine coupling constants values will be discussed in section **3.4.2**.

To confirm that the $^{\bullet}N_3$ radicals arose from the platinum(IV)-bound azide, the experiment was repeated with ^{15}N-complex **40**, prepared from azide labelled with ^{15}N at one of the terminal nitrogen atoms ($[^{15}N=N=N]^-$). The coupling of the unpaired electron to the ^{15}N possessing a spin of I=½, is expected to alter the resultant EPR spectrum.
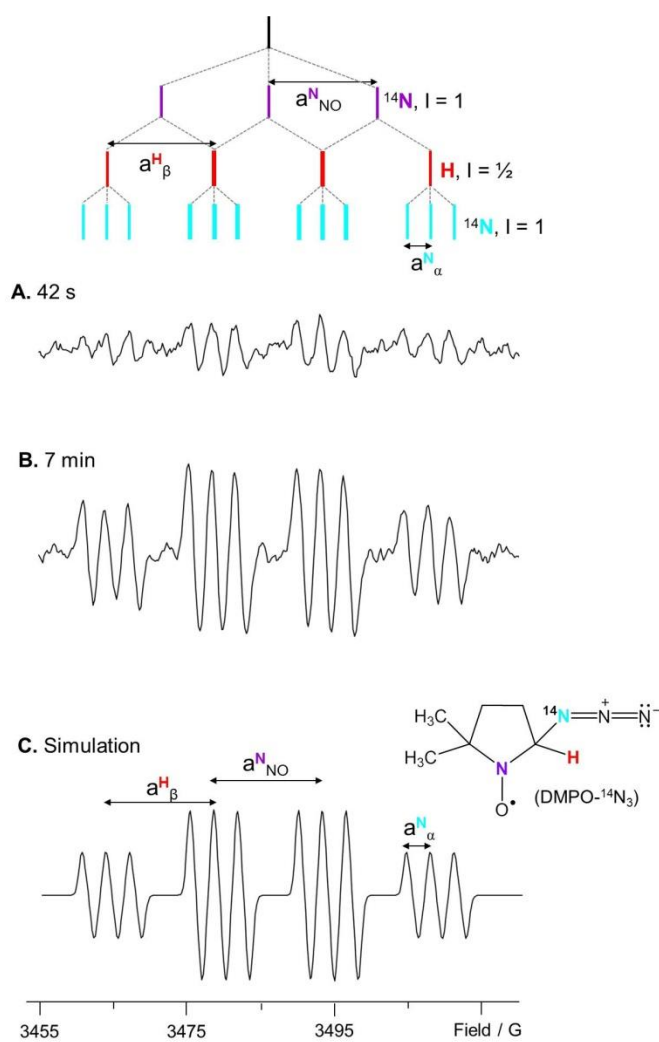
Figure 3.8 EPR spectra together with the line diagram of the DMPO-N$_3$ spin adduct formed from a solution of complex **40** (4 mM) in the presence of DMPO (8 mM, 2 mol equiv) at pH 7.4 after (**A**) 42 s; (**B**) 7 min irradiation at 463 nm and (**C**) a simulation using experimental values as depicted in Table 3.1, together with the structure of the DMPO-^{14}N$_3$ spin adduct.

Table 3.1 Hyperfine coupling constants and g-factor determined for the DMPO-N$_3$ spin adduct shown in Figure 3.8 with literature values for the DMPO-^{14}N$_3$ spin adduct (in brackets).

DMPO-^{14}N$_3$	a^N_{NO} / (G)	a^H / (G)	$a^{14}N_\alpha$ / (G)	g-factor
Experimental[a]	14.76 ± 0.02	14.49 ± 0.04	3.15 ± 0.02	2.011 ± 0.0004
Published[b]	(14.8)	(14.2)	(3.1)	-[c]

[a]data represent means $\pm$ standard deviation of three independent experiments; [b]ref 28; [c]not determined.

3.3.2.2 Confirmation of $^\bullet$N$_3$ radical formation

A solution containing ^{15}N-**40** (4 mM, 50% labelled at N$_\alpha$ position) in the presence of 2 mol equiv DMPO was prepared in H$_2$O at pH 7.4 and irradiated at 463 nm, which generated the spectrum shown in Figure 3.9**A**. This spectrum contains a quartet of doublets[28] superimposed with peaks from residual DMPO-^{14}N$_3$ spin adduct due to 50% ^{14}N at the N$_\alpha$ position, as evidenced through the presence of the central ($-$) lines. These central lines assigned to DMPO-^{14}N$_3$ spin adduct were confirmed, from the parallel alignment of both the DMPO-^{14}N$_3$ and DMPO-^{15}N$_3$ line diagrams (Figure 3.9). The presence of the DMPO-^{14}N$_3$ spin adduct, meant that not all hyperfine splitting values were accurately resolved, in particular the a^{15N}_α splitting. The remaining hyperfine coupling constants for the DMPO-^{15}N$_3$ spin adduct were determined and were similar to previously reported hyperfine splitting values[28] (Table 3.2). The ratio between a^{15N} / a^{14N} was ca. 1.6, was similar to the gyromagnetic ratios of $\gamma^{15N}/\gamma^{14N} = 1.40$. The minor difference is attributed to the crude determination of the a^{15N}_α value due to the presence of the DMPO-^{14}N$_3$ spin adduct.
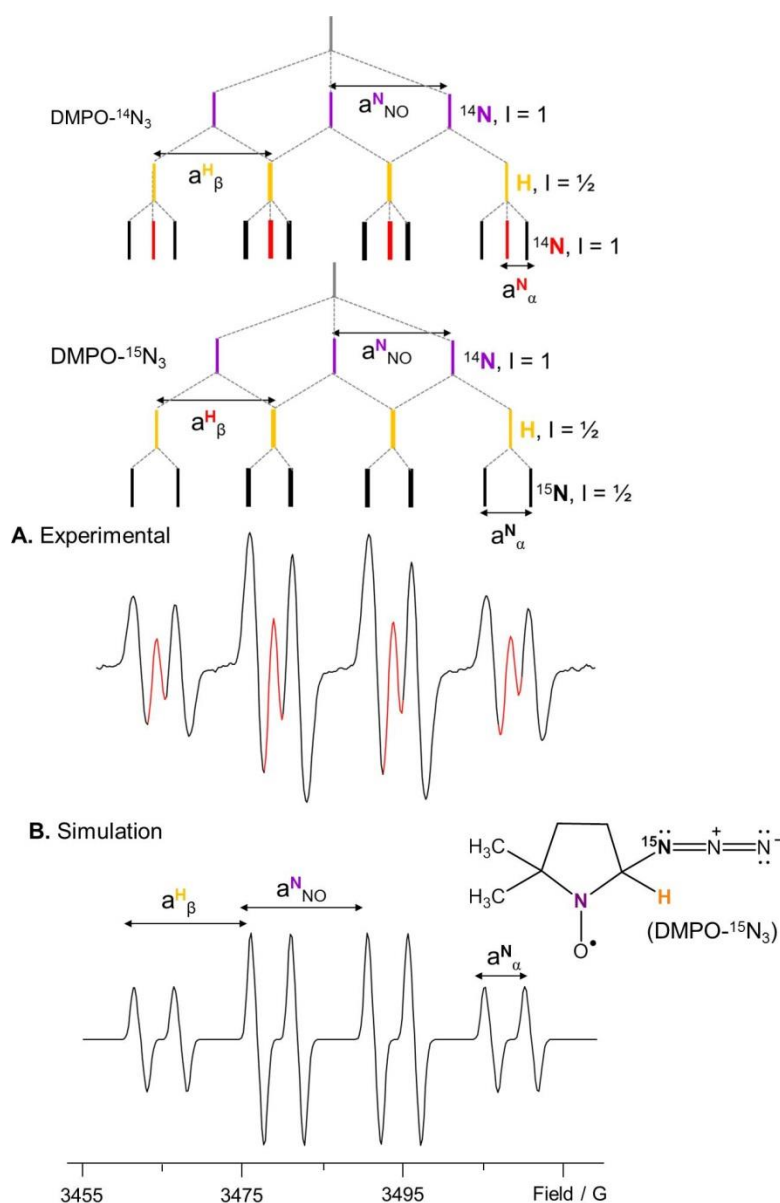
Figure 3.9 EPR spectra together with the line diagrams of both the DMPO-^{14}N$_3$ and DMPO-^{15}N$_3$ spin adducts generated from the (**A**) photo-irradiation of an aqueous solution of ^{15}N-**40** (4 mM) in the presence of DMPO (8 mM) at pH 7.4 with 463 nm light for 7 min and, (**B**) simulation generated using experimental values depicted in Table 3.2, together with the structure of the DMPO-^{15}N$_3$ spin adduct. Contribution of the DMPO-^{14}N$_3$ (−) spin adduct due to only one terminal end of coordinated azide ligand being ^{15}N labelled.

Table 3.2 Hyperfine coupling constants and g-factor determined from Figure 3.9 with literature values for the DMPO-$^{15}N_3$ spin adduct (in brackets).

DMPO-$^{15}N_3$	a^N_{NO} / (G)	a^H / (G)	a^{15N}_α / (G)	g-factor
Experimental[a]	14.72 ± 0.1	14.5 ± 0.00	5.26 ± 0.01	1.934 ± 0.105
Published[b]	(14.8)	(14.7)	(4.5)	-[c]

[a]data represent means $\pm$ standard deviation of two independent experiments; [b]ref 28; [c]not determined.

Similar to the DMPO-$^{14}N_3$ spin adduct, differences between the experimental and previously reported hyperfine coupling constants values will be discussed in section **3.4.2**.

3.3.2.3 Quantification of the DMPO-N_3 spin adduct

Successful trapping and characterisation of the $^\bullet N_3$ radicals, led to monitoring the formation and photo-decomposition of the DMPO-N_3 spin adduct after 21 min irradiation at 463 nm. EPR signals were quantified at 7 min intervals over a total irradiation period of 21 min (80.7 J cm^{-2}). Quantification of the EPR spectra was performed as described as **Chapter II**. The photo-irradiation of complex **40** in the presence of spin trap DMPO was monitored over a series of concentrations, maintaining the spin trap in excess. Irradiating a 9 mM solution complex **40** with DMPO (18 mM, 2 mol equiv) at 463 nm for 14 min led to ca. 237 μM of formed DMPO-$^{14}N_3$ spin adduct (Figure 3.10). Lowering the concentration of complex **40** to 5 mM led to a maximum concentration of DMPO-N_3 spin adduct of ca. 369 μM after 14 min irradiation with 463 nm light (ca. 1.5-fold higher compared to the spin adduct formed from the photo-irradiation of complex **40** at 9 mM).

Figure 3.10 Quantification of the DMPO-N$_3$ spin adduct formed from the photo-irradiation at 463 nm after 7 min, 14 min and 21 min intervals from a solution containing complex **40** (different concentrations, see legend) in the presence of DMPO (2 mol equiv relative to complex **40**) prepared in H$_2$O at pH 7.4. No spin adduct was observed in the dark (0 min). Error bars represent standard error of three independent experiments.

This reduced $^\bullet$N$_3$ radical trapping by DMPO at higher concentrations of complex **40**, is likely to be due to azidyl radical dimerisation ($2k = 9 \times 10^9 \, M^{-1} \, s^{-1}$).[11] Despite varying the concentration of complex **40**, the photo-decomposition profile of the DMPO-N$_3$ spin adduct remained consistent with the maximum trapping after 14 min irradiation (Figure 3.10).

Due to the position of the EPR tube in the EPR spectrometer cavity, it was not possible to observe *in situ* formation of bubbles, previously assigned to the formation of dinitrogen gas (N$_2$). However, upon removal of the quartz tube from the EPR cavity, bubbles were observed.

Primarily, solutions in water were studied to ascertain the formation of the $^\bullet$N$_3$ radicals from the photo-irradiation of complex **40**. Next $^\bullet$N$_3$ radical formation generated from the photo-irradiation of complex **40** under more physiologically relevant conditions was investigated.

3.3.2.4 DMPO-N$_3$ formation in phosphate buffered saline solution

A solution of complex **40** (5 mM) and DMPO (2 mol equiv) were prepared in PBS/H$_2$O at pH 7.4 and irradiated at 463 nm for 21 min. The amount of formed DMPO-N$_3$ spin adduct appeared to be unaffected by the PBS components, 0.01 M phosphate and 0.0027 M KCl (Figure A3.5). Next, a solution of complex **40** (4 mM) in the presence of DMPO (2 mol equiv, 8 mM) prepared in PBS/D$_2$O at pH* 7.4 (where pH* is the pH meter reading in D$_2$O, refer to **Chapter II**) was irradiated with 463 nm light, which led to the formation of the quartet-of-triplets EPR spectrum, as previously observed in water. Interestingly, the amount of the DMPO-N$_3$ spin adduct formed was ca. two-fold higher in PBS/D$_2$O (Figure 3.11). This increase is possibly due to the deuterated (D$_2$O) solvent.

The increase in the DMPO-N$_3$ spin adduct in PBS/D$_2$O (ca. 20% higher per mol of complex **40** compared to water) was also observed from the photo-irradiation of complex **40** at both 1 mM and 0.6 mM concentrations prepared in PBS/D$_2$O at pH* 7.4. Next, the trapping of the $^\bullet$N$_3$ radicals in RPMI-1640 cell culture medium was investigated.
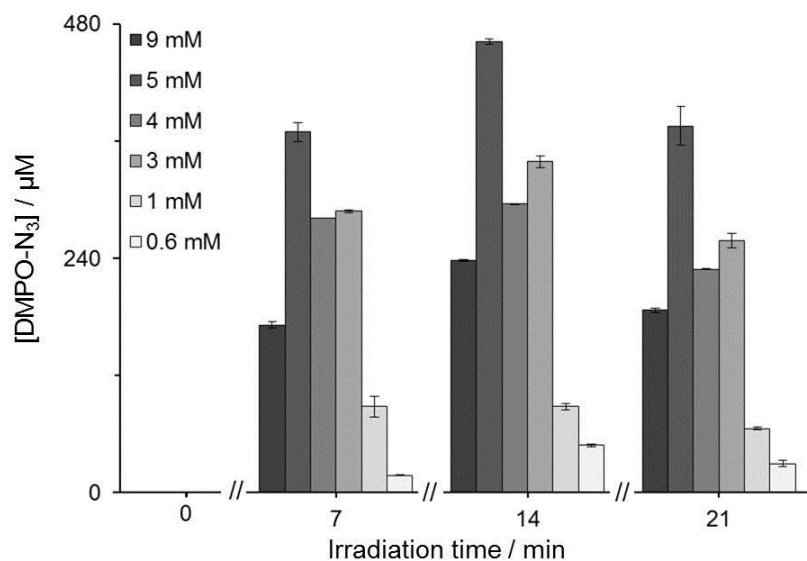
Figure 3.11 Quantification of the DMPO-N_3 spin adduct formed from the photo-irradiation at 463 nm after 7 min, 14 min and 21 min intervals from a solution containing complex **40** (different concentrations, see legend) and DMPO (2 mol equiv relative to complex **40**) prepared in PBS/D_2O at pH* 7.4. No EPR signal was observed in the dark (0 min). Error bars represent the standard error of three independent experiments.

3.3.2.5 DMPO-N_3 formation in cell culture medium

A solution of complex **40** (5 mM) with DMPO (2 mol equiv) prepared in RPMI-1640 was irradiated at 463 nm for 21 min. The quantity of the DMPO-N_3 spin adduct generated after 14 min irradiation was ca. two and four-fold lower, compared to the DMPO-N_3 spin adduct formed in water and PBS/D_2O, respectively, summarised in Figure 3.12. This reduction in the DMPO-N_3 spin adduct in RPMI-1640 may to be due to both the viscosity change and the presence of various components in the cell culture medium (Figure A3.6). Despite this reduced trapping, this result illustrated the release of the azide ligands from photo-irradiated complex **40** in cell culture medium.
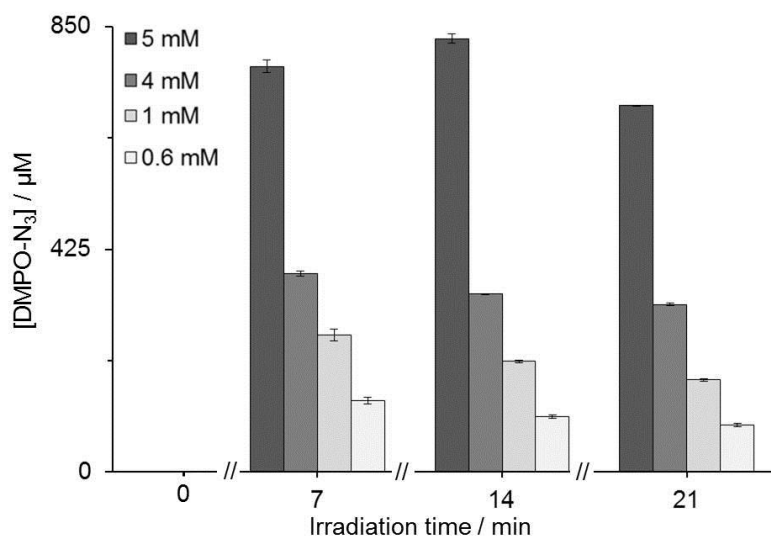
106
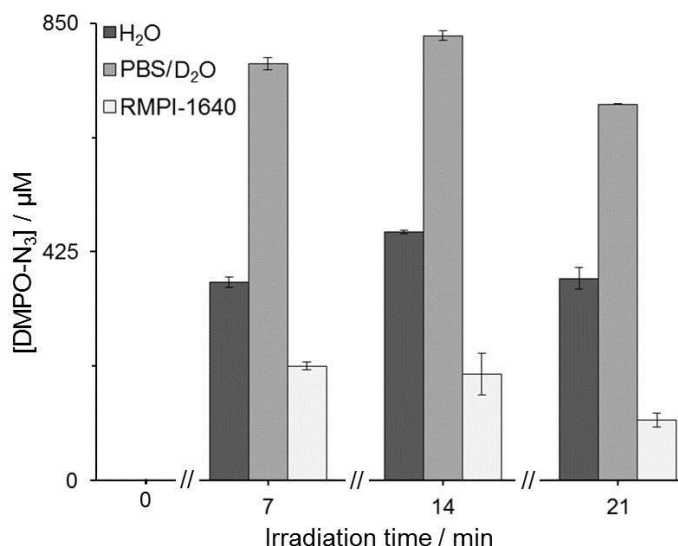
Figure 3.12 Quantification of the DMPO-N$_3$ spin adduct formed from the photo-irradiation at 463 nm after 7 min, 14 min and 21 min intervals from a solution containing complex **40** (5 mM) and DMPO (2 mol equiv) prepared in (■) H$_2$O (■) PBS/D$_2$O and (□) RPMI-1640. No EPR signal was observed in the dark (0 min). Error bars represent standard error of three independent experiments.

These results illustrate the effect of changing from H$_2$O and PBS/D$_2$O to a medium can directly influence the amount of $^\bullet$N$_3$ radicals trapped by DMPO. Next, the generation of $^\bullet$N$_3$ radicals from the photo-activation of related platinum(IV) diazido anticancer complexes was investigated.

3.3.3 Related platinum(IV) diazido complexes

3.3.3.1 Modified equatorial ligand

Spin trapping EPR spectroscopy of photo-activatable platinum(IV) diazido anticancer complexes with varying ligands in both the equatorial and axial positions compared to complex **40** (Figure 3.13) was performed. Initial work was performed on a solution of *trans,trans,trans*-[Pt(N$_3$)$_2$(OH)$_2$(MA)(py)] (4 mM, complex **44**, Figure 3.13) in the presence of DMPO (2 mol equiv) prepared in

107

water at pH 7.4 irradiated with 450 nm light (10 mW cm^{-2}) at a distance of ca. 30

cm from the EPR sample cavity. An identical EPR spectrum to the previously

assigned DMPO-N$_3$ spin adduct was obtained (Figure 3.8**A**).
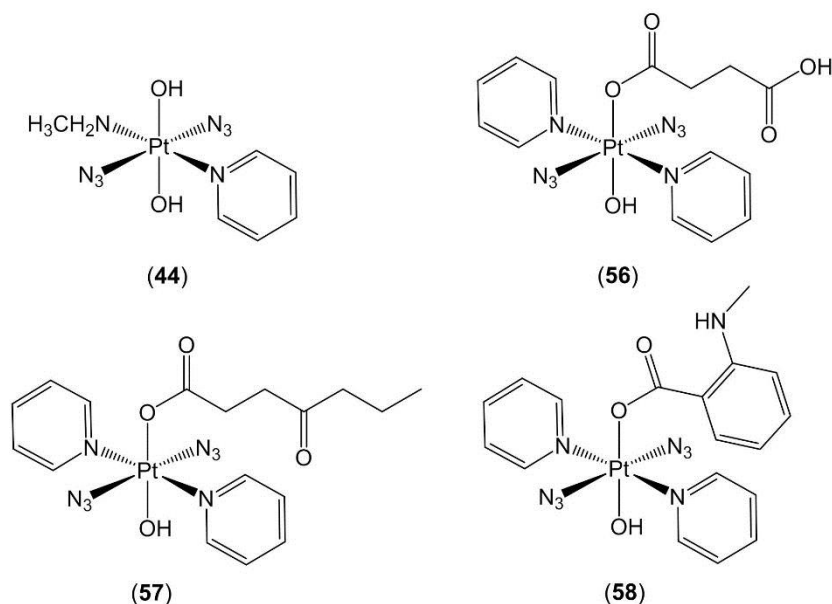
Figure 3.13 Photo-activatable platinum(IV) diazido complexes with various ligands in the axial (complex **44**) and equatorial (complexes **56**-**58**) positions.

Therefore, it appeared that the replacement of the equatorial pyridine ligand for methylamine (MA) did not affect the release of the azide ligand in azidyl radical form from the photo-irradiation of complex **44**.

3.3.3.2 Modified axial ligands

The release of azidyl radicals from complexes **56**-**58** (Figure 3.13) was also investigated. Two of these complexes possess carboxylate functional groups (complexes **56** and **57**) and the third complex possesses an N-methylisatoate group (complex **58**). Both carboxylate compounds **56** and **57** were soluble in phosphate buffered saline (PBS) solution. However, complex **58** was soluble only in

dimethyl-formamide (DMF). Therefore, two separate investigations were performed.

Initially, the yield of the DMPO-N_3 spin adduct formed from photo-irradiation of complex **40** with 517 nm light was compared with the photo-irradiation of complexes **56** and **57**. From these results, it was observed that complex **40** does not generate $^\bullet N_3$ radicals from photo-irradiation with 517 nm light in PBS/H_2O. However, both carboxylate complexes generated the DMPO-N_3 spin adduct (Figure 3.14).
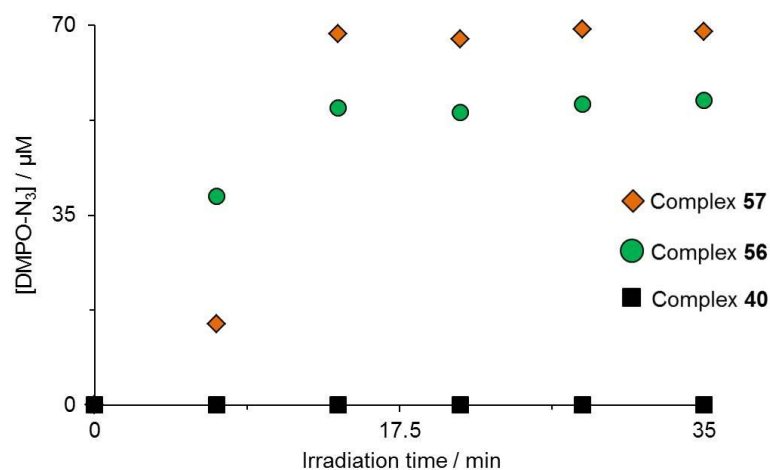
Figure 3.14 Quantification of the DMPO-N_3 spin adduct formed from the photo-irradiation of 2 mM (♦) complex **57**; (●) complex **56**; (■) complex **40** and DMPO (4 mM, 2 mol equiv) prepared in PBS/H_2O at pH 7.4 at 517 nm. No EPR signal observed in the dark (0 min) or from photo-irradiated complex **40**. Refer to Figure 3.2 and Figure 3.13 for structures of complexes **40** and **56** & **57**, respectively.

To compare complexes **40** and **56**-**58**, under equivalent experimental conditions, the solvent was changed to aid the dissolution of complex **58**. As a result, 2 mM solutions of complexes **40** and **56**-**58** were prepared in DMF/H_2O (75%/25%, v/v)

in the presence of DMPO (4 mM, 2 mol equiv) and irradiated at 517 nm. Interestingly, all complexes (including complex **40**) generated the DMPO-N$_3$ spin adduct (Figure 3.8**A**). The detection of the DMPO-N$_3$ spin adduct from complex **40**, under these experimental conditions, suggested photo-activation of platinum(IV) diazido anticancer complexes are directly dependent on the irradiation environment. As can be seen from Figure 3.15, a slight reduction in the DMPO-N$_3$ spin adduct formed from the photo-irradiation of complex **58** is observed. This reduction will be discussed in more detail in **Chapter IV**.
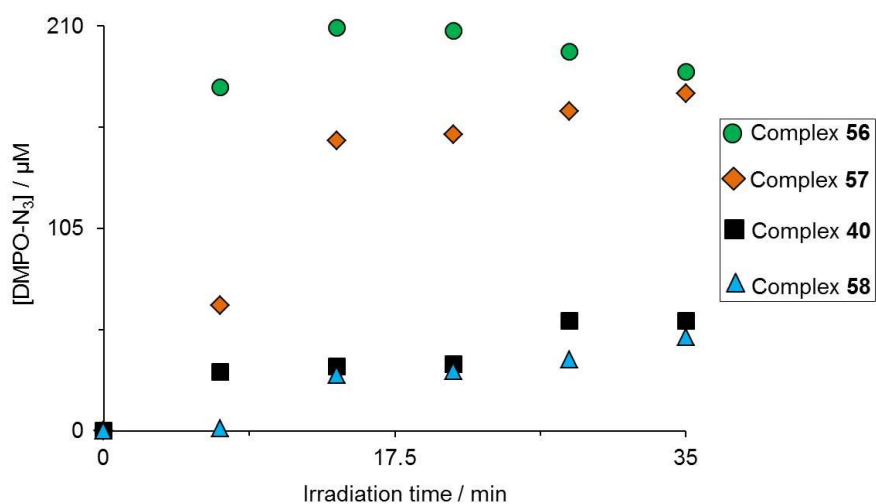
Figure 3.15 Quantification of the DMPO-N$_3$ spin adduct formed from the photo-irradiation of 2 mM (●) complex **56** (♦) complex **57** (■) complex **40** and (▲) complex **58** in the presence of DMPO (2 mol equiv, 4 mM) prepared in DMF/H$_2$O (75%/25%, v/v) at 517 nm. No EPR signal observed in the dark (0 min). Refer to Figure 3.2 and Figure 3.13 for structures of complexes **40** and **56**-**58**, respectively.

In summary, the trapping of •N$_3$ radicals using the nitrone spin trap, DMPO was successfully demonstrated. The release of the azide ligand in azidyl radical form was not limited to complex **40**, but extended to other photo-activatable platinum(IV) diazido anticancer complexes, possessing varied axial and equatorial

ligands. Next, spin trap analogues of DMPO were examined for their ability to trap

$^\bullet$N$_3$ radicals and/or additional radical-based species formed from the photo-

irradiation of complex **40**.

3.3.4 Alternative nitrone spin traps

3.3.4.1 α-4-Pyridyl-1-oxide-*N*-tert-butylnitrone (4-POBN)

A solution of complex **40** (5 mM) with 4-POBN (2 mol equiv, 10 mM) prepared

in water at pH 7.4 was irradiated with 463 nm light for 28 min. This led to the

formation of a triplet-of-quartets EPR signal (Figure 3.16**A**). This EPR

spectroscopic signal exhibited similar hyperfine coupling constants to previously

published data of the 4-POBN-N$_3$ spin adduct (Table 3.3).[47] Consequently, this

spin adduct is assigned to the 4-POBN-N$_3$ spin adduct. Minor variations between

the experimental and previously reported hyperfine coupling constants values will

be discussed in section **3.4.2**.

In this EPR spectrum, the two central lines of the quartet in the overall triplet of

quartets were unresolved, appearing as shoulders (Figure 3.16**A**). This has been

attributed to a sterically induced alternation between the dihedral angle between

the β-hydrogen, α-carbon, nitrone nitrogen plane with the plane defined by the α-

carbon, nitrone nitrogen and its *p*-orbitals as reported by Walter *et al.*.[48]

The amount of the 4-POBN-N$_3$ spin adduct formed from the photo-irradiation of

complex **40** (5 mM) in the presence of 4-POBN (2 mol equiv, 10 mM) was ca.

four-fold lower than the DMPO-N$_3$ spin adduct (refer to Figure 3.17).
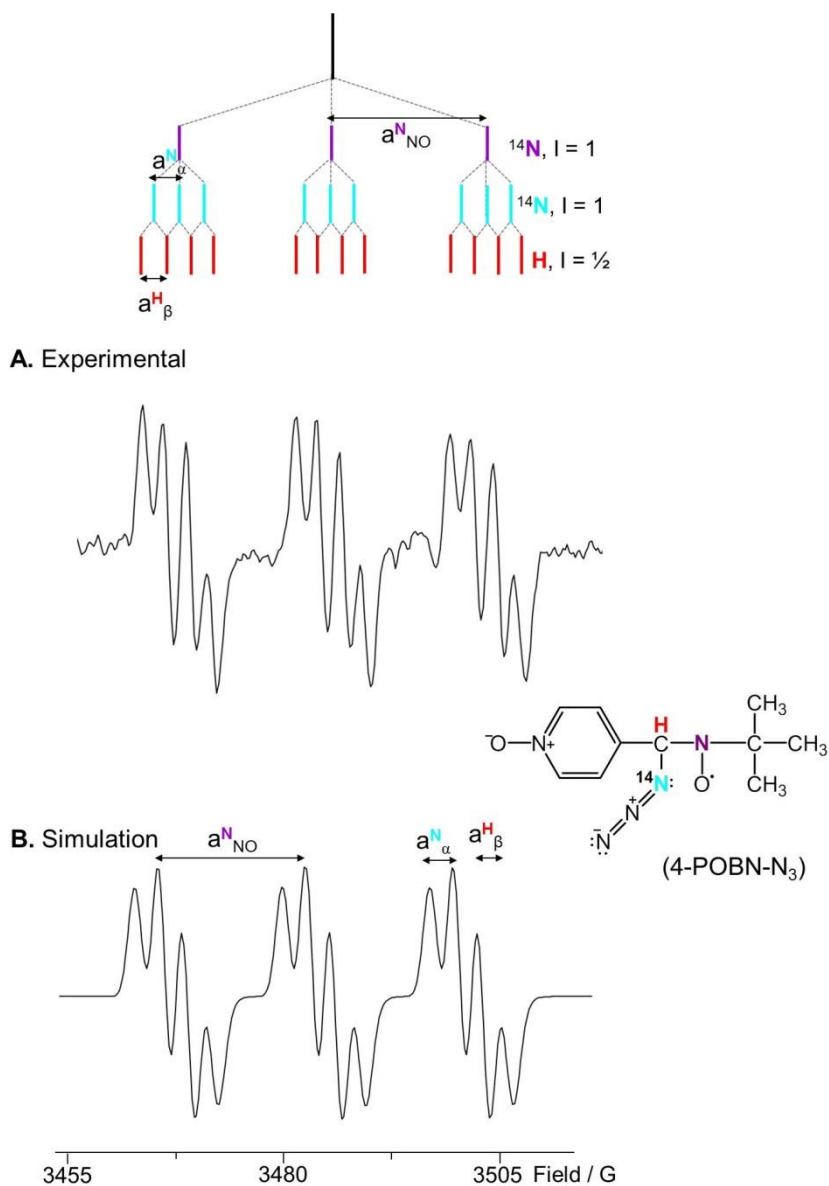
Figure 3.16 EPR spectra together with line diagram of the 4-POBN-N$_3$ spin adduct formed from (**A**) a solution of complex **40** (5 mM) and 4-POBN (2 mol equiv) prepared in water at pH 7.4 irradiated at 463 nm for 7 min and (**B**) simulation performed using experimental values depicted in Table 3.3, together with structure of the 4-POBN-N$_3$ spin adduct.

Table 3.3 Hyperfine coupling constants and g-factor determined from Figure 3.16 with literature values for the 4-POBN-$^{14}N_3$ spin adduct (in brackets).

4-POBN-N$_3$	a^N_{NO} / (G)	a^H / (G)	$a^{14}N_\alpha$ / (G)	g-factor
Experimental[a]	14.66 ± 0.01	1.92 ± 0.10	2.06 ± 0.08	2.0119 ± 0.0003
Published[b]	(14.68)	(1.95)	(1.95)	-[c]

[a]data represent means $\pm$ standard deviation of two independent experiments; [b]ref 47; [c]not determined.

Changing the solvent from water to PBS/D$_2$O, led to a two-fold higher formation of the 4-POBN-N$_3$ spin adduct (Figure 3.17), which gradually decayed after 21 min irradiation at 463 nm. This increase in spin adduct formation was similar to that observed in the presence of DMPO, which suggests that PBS/D$_2$O induces an equivalent effect regardless of the spin trap present in solution.

The primary use of 4-POBN in this work, was to determine the release of $^\bullet$OH radicals from the photo-irradiation of complex **40**. However, the 4-POBN-OH spin adduct has a short life-time of ca. < 1 min.[49] A useful method for $^\bullet$OH radical detection is from the reaction of the $^\bullet$OH radicals with ethanol, which forms a unique carbon-centred radical. Therefore, the addition of ethanol (EtOH) to the system was investigated as an indirect method to confirm the presence of $^\bullet$OH radicals.
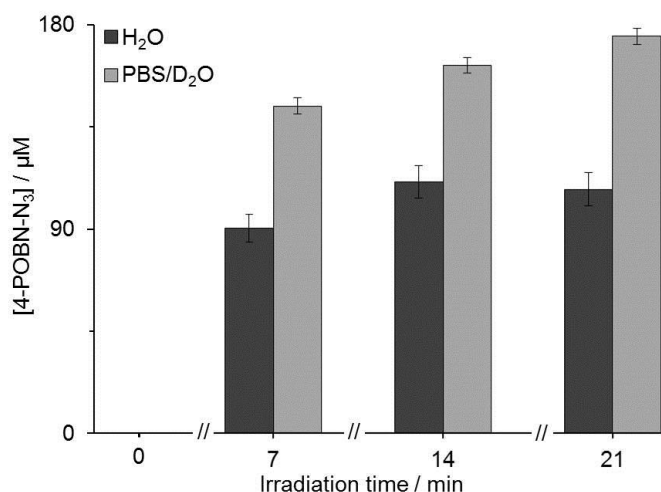
Figure 3.17 Quantification of the 4-POBN-N$_3$ spin adduct formed from the photo-irradiation at 463 nm after 7 min, 14 min and 21 min intervals from a solution of complex **40** (5 mM) with 4-POBN (2 mol equiv, 10 mM) prepared in (■) H$_2$O and (■) PBS/D$_2$O. No spin adduct was observed in the dark (0 min). Error bars shown represent standard error of three independent experiments.

3.3.4.2 Addition of ethanol

Pou *et al.* reported on the optimum concentrations of both 4-POBN and EtOH for the detection of the $^\bullet$OH radical.[34] Ideally working with 4-POBN (10 mM) in conjunction with EtOH concentration ranging from 17 – 170 mM were optimum for the indirect detection of the $^\bullet$OH radicals. Therefore, a solution containing complex **40** (2.5 mM) and 4-POBN (4 mol equiv, 10 mM) prepared in water at pH 7.4 was irradiated at 463 nm for 14 min in both the absence and presence of EtOH (17 mM).

A similar amount of 4-POBN-N$_3$ spin adduct was formed in both the absence and presence of ethanol (Figure 3.18), but no new EPR signals were detected in the

presence of ethanol. In view of these results, this spin trap was not investigated further in the photo-irradiation studies of complex **40**.
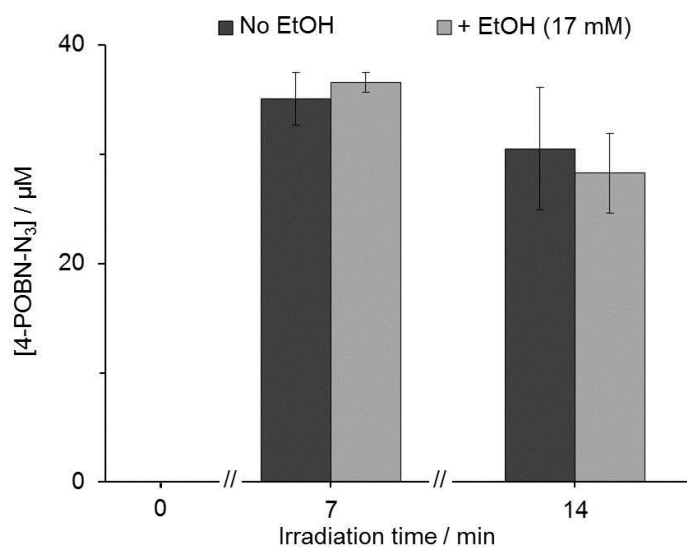
Figure 3.18 Quantification of the 4-POBN-N$_3$ spin adduct formed after 7 min and 14 min intervals from the photo-irradiation at 463 nm of a solution containing complex **40** (2.5 mM) with 4-POBN (10 mM) prepared in water at pH 7.4 in (■) the absence and (■) presence of ethanol (17 mM). No EPR signal was observed in the dark (0 min). Error bars represent the standard error of three independent experiments.

3.3.4.3 Phosphorus nitrone spin trap

A solution of complex **40** (5 mM) in the presence of DEPMPO (**4**, Figure 3.4, 2 mol equiv) prepared in water at pH 7.4 was irradiated at 463 nm for 21 min. A more complex EPR spectrum was generated (Figure 3.19**A**) compared to previously observed spin adducts, studied in this work. The additional lines are attributed to the unpaired electron coupling to the magnetically active, phosphorus atom (^{31}P, I = ½). The generated EPR spectrum is assigned to the DEPMPO-N$_3$ spin adduct, in agreement with previously published data of the DEPMPO-N$_3$ spin

adduct (Figure 3.19**B**).[50] Differences between the experimental and previously reported hyperfine coupling constants values will be discussed in section **3.4.2**.
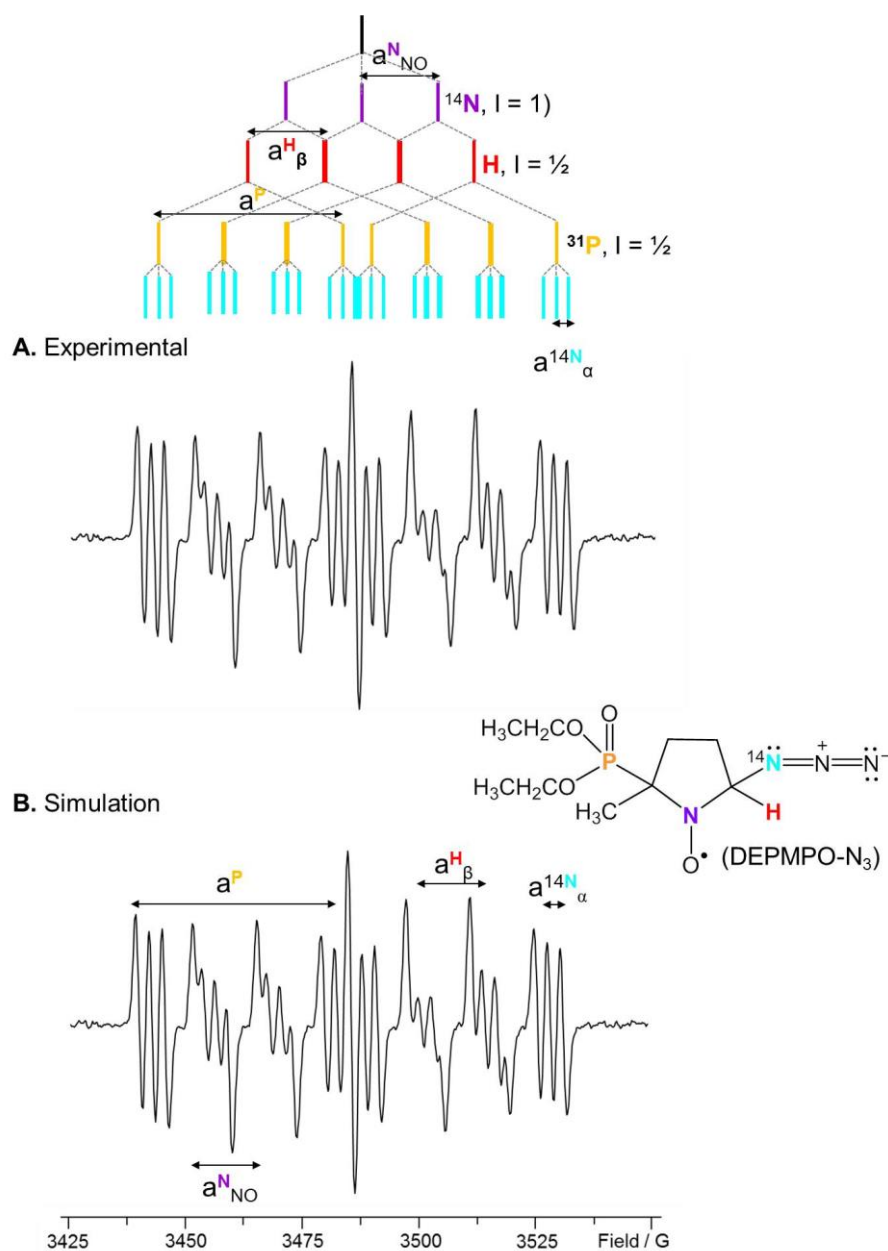
Figure 3.19 EPR spectra together with the line diagram of the DEPMPO-N$_3$ spin adduct generated from the (**A**) a solution of complex **40** (5 mM) and DEPMPO (10 mM) prepared in water at pH 7.4 irradiated at 463 nm for 7 min and (**B**) simulation using experimental values depicted in Table 3.4, together with the structure of the DEPMPO-N$_3$ spin adduct.

Table 3.4 Hyperfine coupling constants and g-factor determined from Figure 3.19 with literature values for the DEPMPO-^{14}N$_3$ spin adduct (in brackets).

DEPMPO-N$_3$	a^N_{NO} / (G)	a^H / (G)	a^P / (G)	a^N_{α} / (G)	g-value
Experimental[a]	13.82 ± 0.05	13.76 ± 0.13	45.94 ± 0.09	2.93 ± 0.06	2.013 ± 0.0003
Published[b]	(13.93)	(12.39)	(46.05)	(2.80)	-[c]

[a]data represent means ± standard deviation of two independent experiments; [b]ref 50; [c]not determined.

The DEPMPO-N$_3$ spin adduct generated was ca. three-fold higher than the DMPO-N$_3$ spin adduct formed, under similar experimental conditions (Figure 3.20).
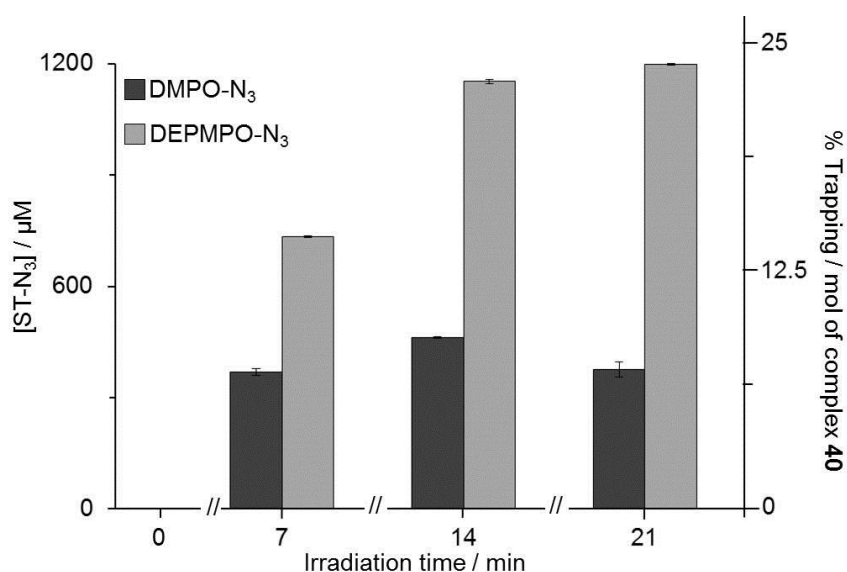
Figure 3.20 Quantification (μM) and % trapping per mol of complex **40** for both (■) DMPO-N$_3$ and (■) DEPMPO-N$_3$ spin adducts generated from the photo-irradiation of a solution of complex **40** (5 mM) and spin trap (2 mol equiv) with 463 nm light after 7 min, 14 min and 21 min prepared in H$_2$O at pH 7.4. No EPR signal was observed in the dark (0 min). Error bars represent the standard error of three independent experiments.

The DEPMPO-N_3 spin adduct was observed at a concentration of ca. 580 μM after 2 h irradiation with 463 nm light. This illustrated the persistency of the DEPMPO-N_3 spin adduct in contrast to both DMPO-N_3 and 4-POBN-N_3 spin adducts, which photo-decomposed within ca. 1 h after irradiation with 463 nm light. Consequently, the DEPMPO spin trap proved to be the most efficient in the trapping of the $^\bullet N_3$ radicals, generated from the photo-irradiation of complex **40**.

The efficiency of the phosphorus spin trap for trapping $^\bullet N_3$ radicals (17% higher per mol of complex **40** compared to DMPO) prompted investigation of $^\bullet N_3$ radical trapping by DEPMPO at more biologically-relevant conditions. Individual solutions of complex **40** (0.8 mM and 0.4 mM) in the presence of DEPMPO (2 mol equiv relative to complex **40**) were prepared in water at pH 7.4 and irradiated at 463 nm light for 21 min (Figure 3.21). Photo-irradiation of complex **40** (0.8 mM) with DEPMPO (1.6 mM) led to the trapping of ca. 24% per mol of complex **40**, equivalent to that observed from the photo-irradiation of complex **40** (5 mM). The yield of the DEPMPO-N_3 spin adduct was ca. two-fold lower from the irradiation of a 0.4 mM solution of complex **40**. Interestingly, an equivalent ca. 14% per mol of complex **40** was obtained after 21 min irradiation from solutions containing 0.8 mM and 0.4 mM complex **40**. After 21 min irradiation, the DEPMPO-N_3 spin adduct formed in both solutions gradually decayed.
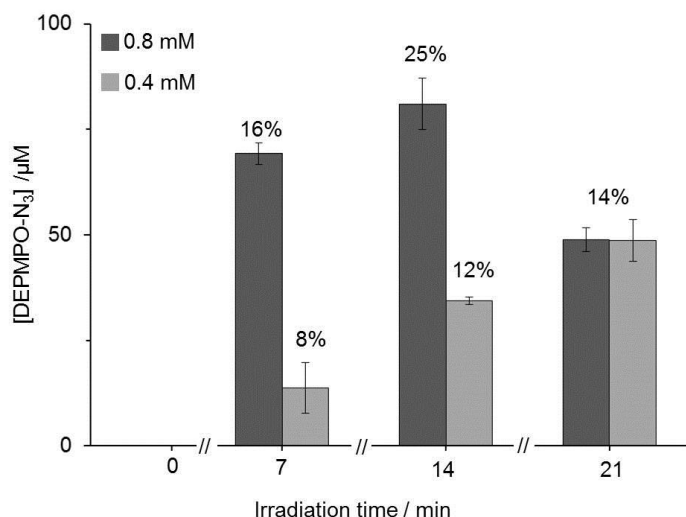
Figure 3.21 Quantification (μM) and % trapping per mol of complex **40** of the DEPMPO-N_3 spin adduct formed from irradiation at 463 nm after 7 min, 14 min and 21 min from solutions containing complex **40** (■) 0.8 mM and (■) 0.4 mM in the presence of DEPMPO (2 mol equiv relative to complex **40**) prepared in H_2O at pH 7.4. No EPR signals observed in the dark (0 min). Error bars represent the standard error of three independent experiments.

Moreover, a solution containing complex **40** (100 μM) and DEPMPO (2 mol equiv) prepared in H_2O at pH 7.4 was irradiated at 463 nm light for 21 min, which led to the detection of the DEPMPO-N_3 spin adduct (Figure 3.22). Whilst under these conditions, owing to high signal-to-noise (S/N) ratio not all lines of the DEPMPO-N_3 spin adduct were clearly visible. Consequently a crude quantification the DEPMPO-N_3 spin adduct of ca. 2.0 ± 0.3 μM was determined. This result did suggest the potential use of this spin trap for *in cellulo* studies, due to its ability to trap the $^{\bullet}N_3$ radical at low micro-molar concentrations of complex **40**. Next, the formation of the DMPO-N_3 and DEPMPO-N_3 spin adducts was investigated from the photo-irradiation of complex **40** with longer wavelengths of light.
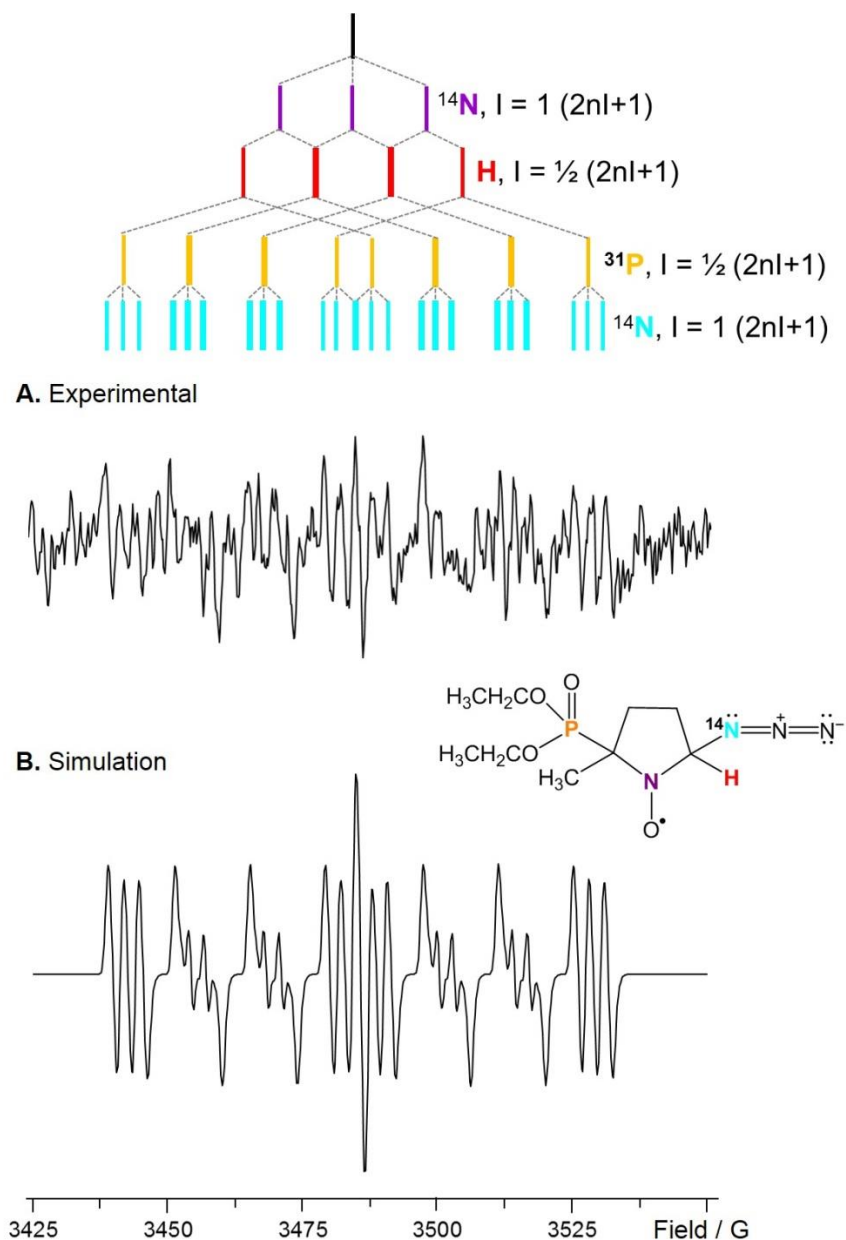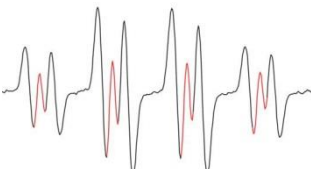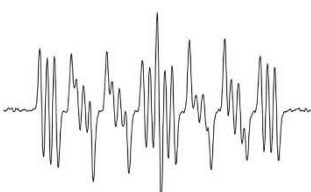
Figure 3.22 EPR spectra together with the line diagram of the DEPMPO-N$_3$ spin adduct generated from (**A**) the photo-irradiation of an aqueous solution of complex **40** (100 μM) and DEPMPO (200 μM) with 463 nm light after 21 min and, (**B**) simulation generated as per Figure 3.19 with the structure of the DEPMPO-N$_3$ spin adduct.

Table 3.5 Summary of spin adducts detected in this Chapter.

EPR spectra	Spin Adduct	H₂O	PBS (D₂O)	RPMI	463 nm	517 nm
Figure 3.8 **Quartet-of-triplets**	DMPO-^{14}N$_3$	✓	✓	✓	✓	✓
Figure 3.9 **Quartet-of-doublets**	DMPO-^{15}N$_3$	✓	✗	✗	✓	✗
Figure 3.16 **Triplet-of-quartets**	4-POBN-N$_3$	✓	✗	✗	✓	✗
Figure 3.19 **Octet-of-triplets**	DEPMPO-N$_3$	✓	✗	✗	✓	✓

✓, spin adduct detected; ✗, experiment not performed.

3.3.5 Longer wavelength of activation

Irradiating a solution of complex **40** (5 mM) with DMPO (2 mol equiv) in both protiated solvent and PBS/D$_2$O buffer with green 517 nm light (33 mW cm^{-2}) for 21 min did not produce any EPR signal. However, irradiating an equivalent solution of complex **40** with DMPO prepared in RPMI-1640 led to the detection of the quartet of triplets EPR spectrum (Figure 3.23).
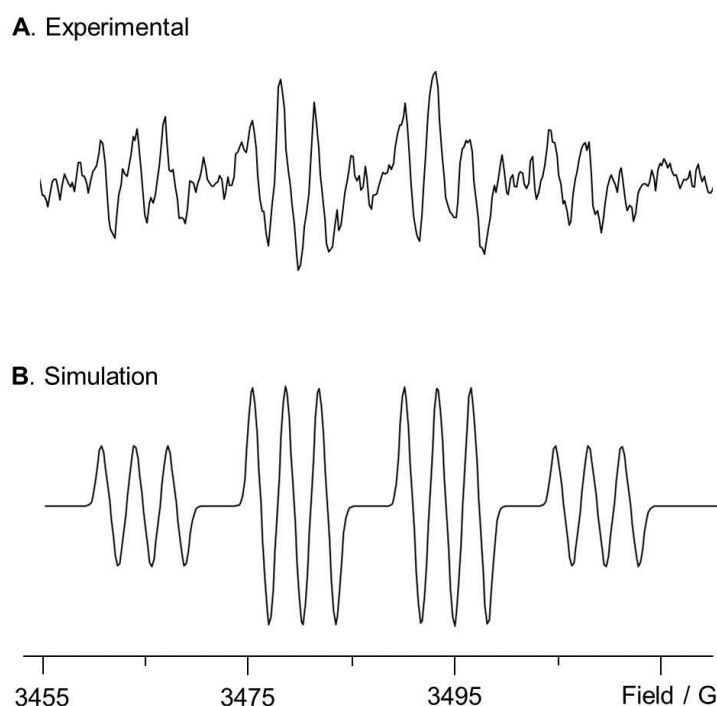
Figure 3.23 EPR spectra of the DMPO-N$_3$ spin adduct formed from (**A**) a solution of complex **40** (5 mM) and DMPO (2 mol equiv) prepared in RPMI-1640 medium irradiated for 21 min at 517 nm and (**B**) simulation of DMPO-N$_3$ (generated as Figure 3.8) to aid experimental peak assignment.

The DMPO-N$_3$ spin adduct formed from the photo-irradiation of complex **40** with 517 nm light was ca. ten-fold lower in comparison to the DMPO-N$_3$ spin adduct formed with 463 nm light, summarised in Figure 3.24**A**. Despite this reduction in the DMPO-N$_3$ spin adduct formed, these results effectively demonstrate the release

of the $^\bullet N_3$ radicals from photo-irradiated complex **40** by green light in cell culture RPMI-1640 medium.
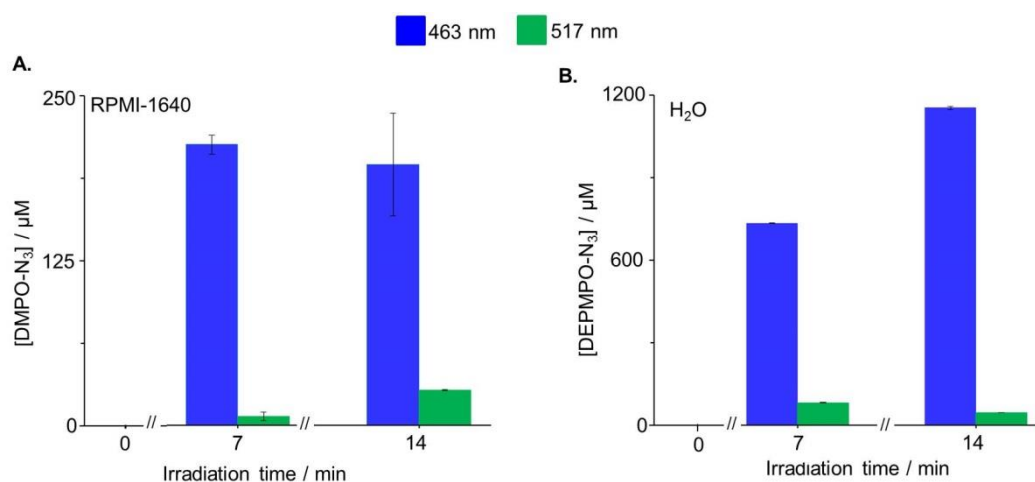
Figure 3.24 Quantification of the (**A**) DMPO-N$_3$ and (**B**) DEPMPO-N$_3$ spin adduct formed from the photo-irradiation with either (■) 463 nm and (■) 517 nm light after 7 min and 14 min intervals from a solution containing complex **40** (5 mM) with DMPO (2 mol equiv) prepared in (**A**) RPMI-1640 medium and (**B**) H$_2$O. No EPR signal was observed in the dark (0 min). Error bars represent the standard error of three independent experiments.

Photo-irradiation of complex **40** in the presence of DMPO at 593 nm (17 mW cm^{-2}) in H$_2$O, PBS/D$_2$O and RPMI-1640 was also performed. However, no EPR signal for the DMPO-N$_3$ spin adduct was observed.

Next, a solution of complex **40** (5 mM) with DEPMPO (2 mol equiv, 10 mM) was irradiated at 517 nm prepared in H$_2$O at pH 7.4. Despite the observation of the DEPMPO-N$_3$ spin adduct EPR spectrum, the amount generated was 9- and 27-fold lower after 7 and 14 min, respectively, compared to the DEPMPO-N$_3$ spin adduct formed from irradiation with 463 nm light (Figure 3.24**B**).

Photo-irradiation of complex **40** at 517 nm light, led to a reduction in the amount of both the DMPO-N$_3$ and DEPMPO-N$_3$ spin adducts. The N$_3 \rightarrow$ Pt^{IV} ligand-metal-charge-transfer (LMCT) transition present in complex **40**, has been shown to decrease upon photo-irradiation, assigned to the loss of the azide ligands in azidyl radical form (**Chapter I**).[1] Consequently, the decrease in the N$_3 \rightarrow$ Pt^{IV} LMCT band of complex **40** photo-irradiated with both 463 nm (Figure 3.25**A**) and 517 nm (Figure 3.25**B**) light was monitored by UV-visible spectroscopy. It was determined that ca. 60% of complex **40** photo-decomposed after 60 min irradiation with 463 nm light, compared to ca. 3% from irradiation with 517 nm light (Figure 3.25**C**). Therefore, photo-irradiation of complex **40** with 517 nm light leads to a reduction in azidyl radical formation, thereby rationalising the reduction in spin adduct formation.
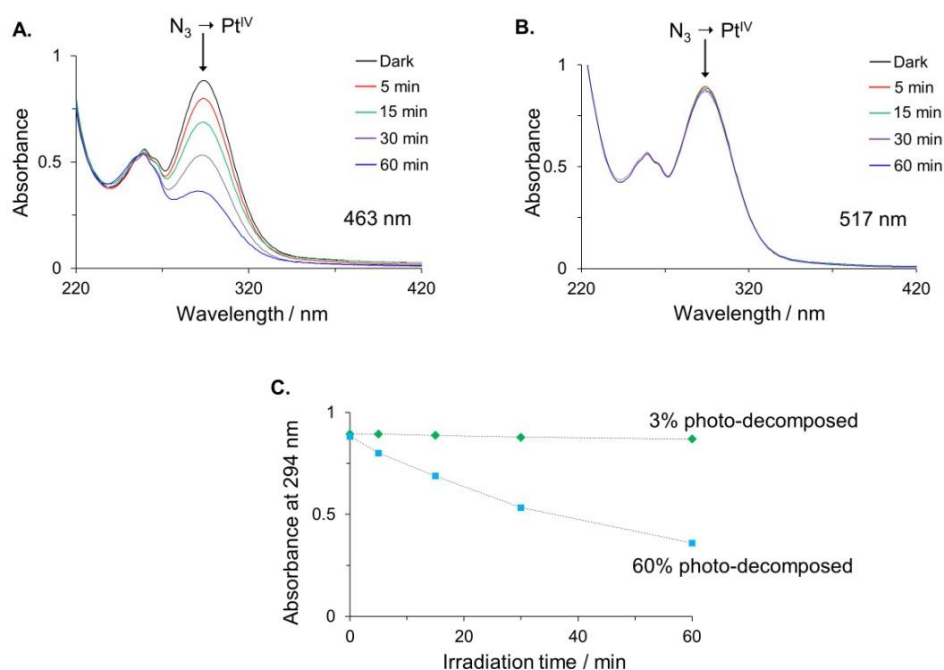
Figure 3.25 UV-visible spectra of complex **40** (50 μM) prepared in PBS/D$_2$O at pH* 7.4 in the (–) dark and after (–) 5; (–) 15; (–) 30 and (–) 60 min irradiation with (**A**) 463 nm; (**B**) 517 nm light. Decrease (↓) in the N$_3 \rightarrow$ Pt^{IV} LMCT band (**C**) extent of photo-decomposition in the N$_3 \rightarrow$ Pt^{IV} LMCT transition.

3.3.6 Density Functional Theory (DFT) calculations

The spin density in the formed spin adducts was determined from DFT calculations, performed by Miss Nichola Smith. The spin densities on atoms involved in the hyperfine coupling were the focus of this study. The spin density map of the DMPO-N_3 spin adduct is shown in Figure 3.26**A1** and displays the spin density on the O1, N_{NO}, H_β and N_α atoms (blue coloured orbitals). A similar spin density map is observed for the DEPMPO-N_3 spin adduct (Figure 3.26**A2**). However, the DEPMPO-N_3 spin adduct exhibits an additional spin density of ca. 0.027 on the phosphorus atom. This additional spin density on the phosphorus atom is believed to account for the greater lifetime of the DEPMPO-N_3 spin adduct. The spin densities are summarised in Table 3.6.

Interestingly, the 4-POBN-N_3 spin adduct exhibited a different spin density distribution, compared to both the DMPO-N_3 and DEPMPO-N_3 spin adducts (Figure 3.27). The spin density on the β-proton (H_β) is about seven- and nine-fold lower, compared to the DMPO-N_3 and DEPMPO-N_3 spin adducts, respectively, (Table 3.6). Furthermore, the spin density on N_α atom (N3) of 4-POBN-N_3 spin adduct was ca. eleven-fold lower in contrast to the N_α atom (N3) of the DMPO-N_3 spin adduct. Interestingly, the 4-POBN-N_3 spin adduct exhibited spin density on other atoms present in the spin adduct, not involved in the hyperfine coupling (Figure 3.27**A**). These differences are believed to explain the reduced lifetime of 4-POBN-N_3 compared to the DMPO-N_3 and DEPMPO-N_3 spin adducts. The spin density on all atoms present in DMPO-N_3, DEPMPO-N_3 and 4-POBN-N_3 are summarised in Tables A3.7-3.9.
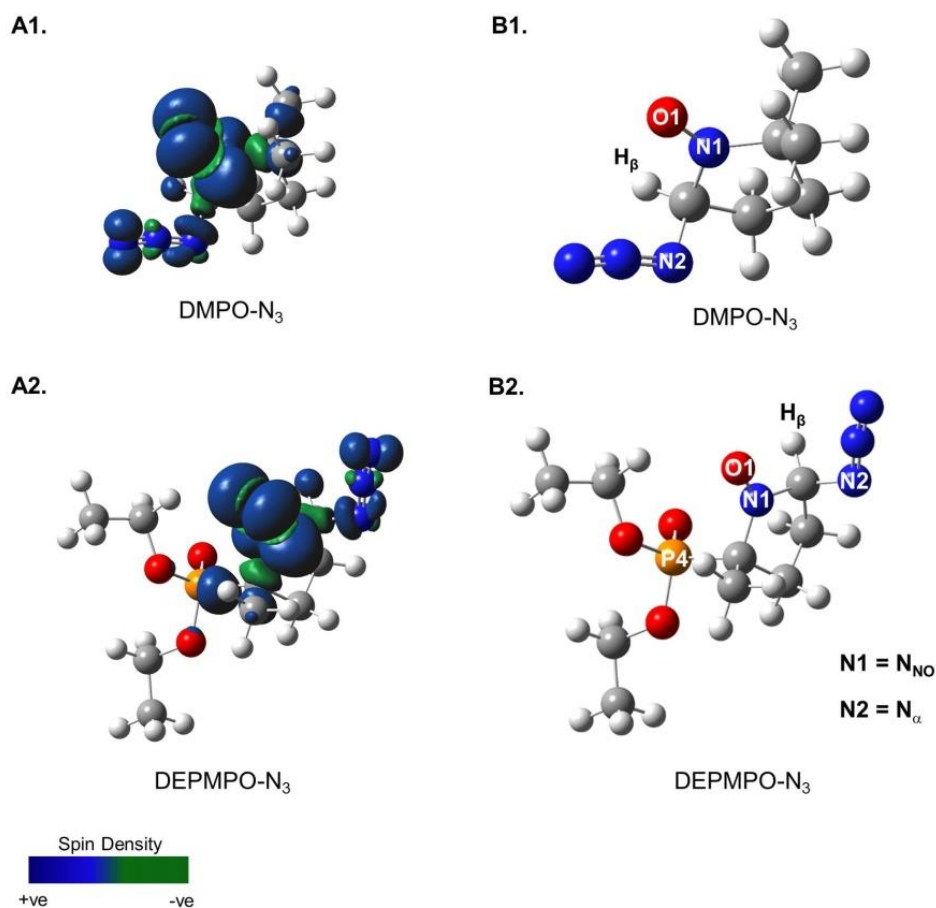
Figure 3.26 Spin density maps together with 2D orientation of both (**A1** and **B1**) DMPO-N_3 and (**A2** and **B2**) DEPMPO-N_3 spin adducts. Green indicates a decrease in spin density, while dark blue indicates an increase values summarised in Table 3.6. Spin densities were calculated by DFT as described in experimental section. Atom labels: red, oxygen; blue, nitrogen; orange, phosphorus, light grey, hydrogen; dark grey, carbon.

Table 3.6 Localisation of spin density in the DMPO-N_3, DEPMPO-N_3 and 4-POBN-N_3 spin adducts.

Atom	DMPO-N_3	DEPMPO-N_3	4-POBN-N_3
O1	0.5288	0.5153	0.5335
[a]N2	0.4115	0.4226	0.4421
H_β	0.0126	0.0148	0.0017
[b]N3	0.1356	0.0124	0.0115
P3	-	0.0267	-

[a]refers to nitroxide nitogen, N_{NO} atom; [b]refers to α-nitrogen of the trapped azidyl radical, N_α.
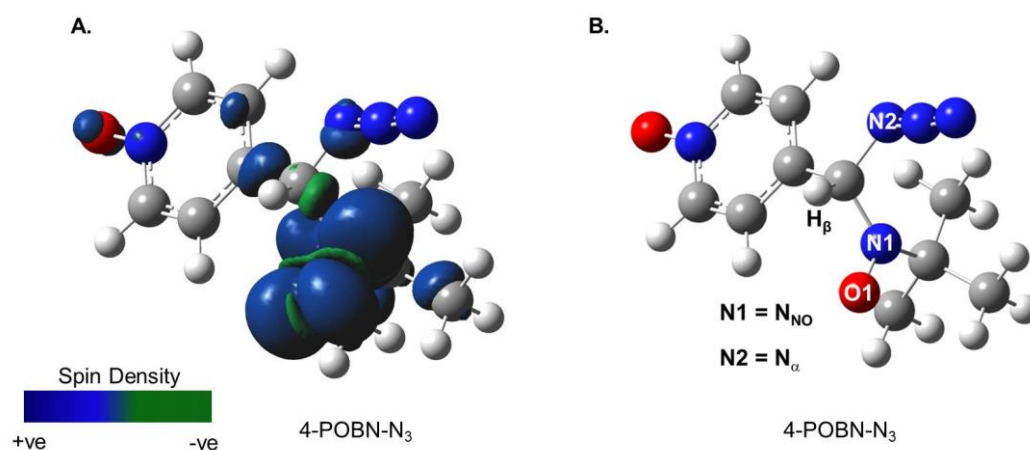
Figure 3.27 Spin density map together with 2D orientation of the 4-POBN-N_3 spin adduct. Green indicates a decrease in spin density, while dark blue indicates an increase. The values are summarised in Table 3.6. Spin densities were calculated by DFT as described in experimental section.

3.3.7 Alternative radiation source

Longer wavelengths of light are preferred therapeutically, owing to their deeper tissue penetration. Photo-activation of complex **40** has been limited to 517 nm

(green) light, with longer wavelengths of light not reported for the photo-activation

of complex **40**. In the clinic, combination of both chemotherapy and radiotherapy

is commonly used. An investigation of the activation of complex **40** with a gamma-

ray source was therefore carried out.

3.3.7.1 Gamma-ray irradiation in the presence of DMPO

An aqueous stock solution of complex **40** (5 mM) with DMPO (10 mM) was

prepared at pH 7.4 under dim lighting conditions. An aliquot (ca. 1 mL) was

transferred onto a cell culture plate. The flat surface of the cell culture plate

provided an optimum setup for exposure to the gamma-rays. Gamma irradiations

were performed by Dr. Rebecca Carter. In an attempt to establish the photo-

activation of complex **40**, various doses ranging from $2 - 100$ Gy were chosen

(Table 3.7).

Table 3.7 Gamma (γ) radiation doses used in this work.

γ-Dose / Gy	Time of radiation / s
1	10
2	34
4	68
8	216
100	7.42 min

Irradiated samples were compared to both a dark control and the DMPO-N$_3$ spin

adduct formed with 463 nm light. No EPR signals were detected for samples

radiated with 4, 8, 16 or 100 Gy. Interestingly, irradiation with 2 Gy gave rise to

an EPR signal (Figure 3.28). The low S/N ratio of this EPR spectrum meant that full characterisation and quantitative EPR spectroscopy could not be performed. This EPR signal did not resemble that of the quartet of triplets EPR signal assigned to the DMPO-N_3 spin adduct. This suggested the possible trapping of an alternative radical species from irradiated complex **40** with gamma-rays. A crude estimation of the formed spin adduct was determined to be ca. 10 ± 0.4 μM. These results provided strong evidence for the activation of complex **40** with a ^{137}Cs gamma-ray irradiation source.

3455   3475   3495   Field / G
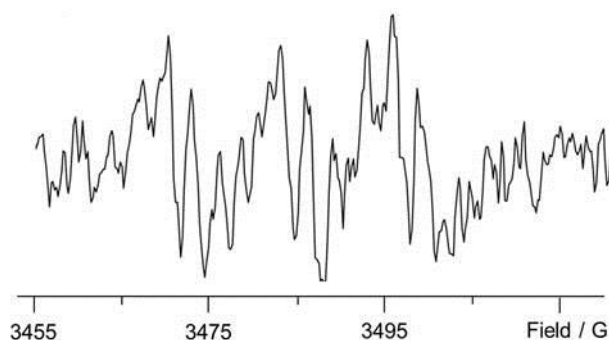
Figure 3.28 EPR spectra generated from (**A**) a solution of complex **40** (5 mM) with DMPO (2 mol equiv) prepared in water at pH 7.4 irradiated with 2 Gy dose of ^{137}Cs gamma radiation source. Formed spin adduct was roughly quantified to ca. 10 ± 0.4 μM.

3.3.7.2 Gamma-ray irradiation in the presence of DEPMPO

Additional gamma-ray irradiation studies were performed with spin trap, DEPMPO, owing to its greater efficiency at $^{\bullet}N_3$ radical trapping, as previously observed in section **3.3.4**. Solutions containing complex **40** (5 mM) and DEPMPO (10 mM, 2 mol equiv) were prepared in water at pH 7.4 and irradiated with varying doses of the ^{137}Cs gamma-ray irradiation source (Figure 3.29). Irradiated solutions generated an EPR signal assignable to DEPMPO-N_3 (Figure 3.29**G**), as previously

observed in Figure 3.19. The observation of the DEPMPO-N$_3$ spin adduct from the irradiation of complex **40** (5 mM) with DEPMPO (2 mol equiv) with a ^{137}Cs gamma source is the first report of the activation of complex **40** with gamma rays.
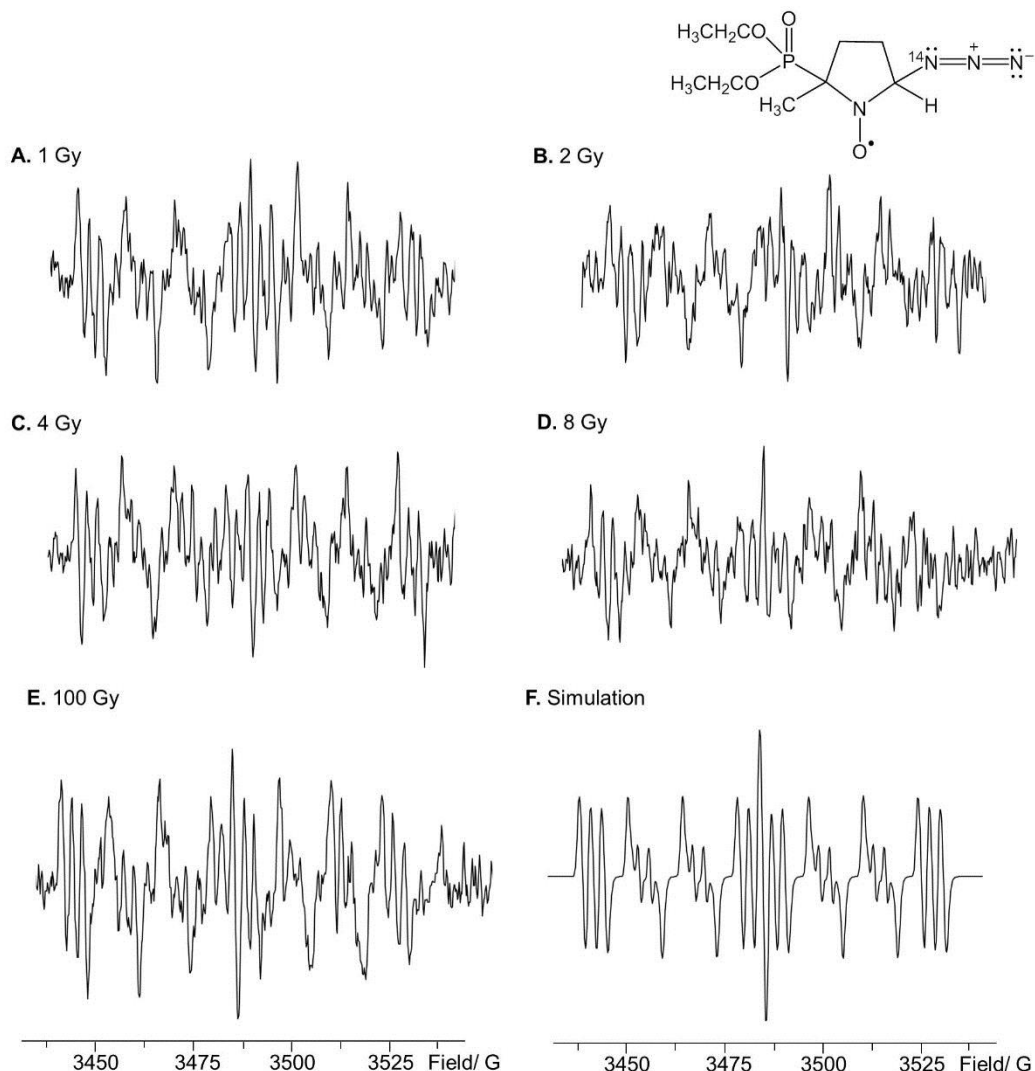
Figure 3.29 EPR spectra generated from the gamma irradiation of complex **40** (5 mM) with DEPMPO (2 mol equiv) with ^{137}Cs gamma source with doses of (**A**) 1 Gy; (**B**) 2 Gy; (**C**) 4 Gy; (**D**) 8 Gy; (**E**) 100 Gy and (**F**) simulation of DEPMPO-N$_3$ using experimentally-obtained parameters listed in Table 3.4. EPR signal assigned to the DEPMPO-N$_3$ spin adduct, refer to Figure 3.19 for spin adduct formation.

Table 3.8 Quantification of the DEPMPO-N$_3$ spin adduct formed from gamma-ray irradiation of complex **40** at varying doses.

γ-Dose / (Gy)	[DEPMPO-N$_3$][a] / μM	% Mol complex 40
1	31.8	0.6
2	18.0	0.4
4	41.6	0.8
8	45.1	0.9
100	50.0	1.0

[a]spin adduct formed from the gamma-ray irradiation of a solution of complex **40** (5 mM) with DEPMPO (2 mol equiv) prepared in water at pH 7.4 recorded 1.5 h after initial irradiation.

These results prompted the investigation of the cytotoxicity of complex **40** irradiated with the ^{137}Cs gamma-ray irradiation source. Complex **40** (up to 80 μM) incubated in DLD1 colorectal adenocarcinoma cell line did not exhibit any cytotoxic effect, either in the dark or after irradiation with the ^{137}Cs gamma-ray source. This study has to be repeated to confirm this observation. However, this preliminary result suggests that despite the detection of the DEPMPO-N$_3$ spin adduct, activated complex **40** is incapable of inducing a cytotoxic effect. Consequently, activation of complex **40** with a ^{137}Cs gamma-ray irradiation source may activate the platinum(IV) diazido anticancer complex by an alternative pathway.

3.4 Discussion

3.4.1 Efficiency and stability of formed spin adducts

It was shown that the DEPMPO spin trap was more efficient at trapping $^\bullet N_3$ radicals formed from the photo-irradiation of complex **40** with 463 nm light, compared to spin traps, DMPO and 4-POBN (summarised in Figure 3.30). This effect is thought to be due to the rate at which $^\bullet N_3$ radicals are trapped by each spin trap which is determined by their chemical composition.
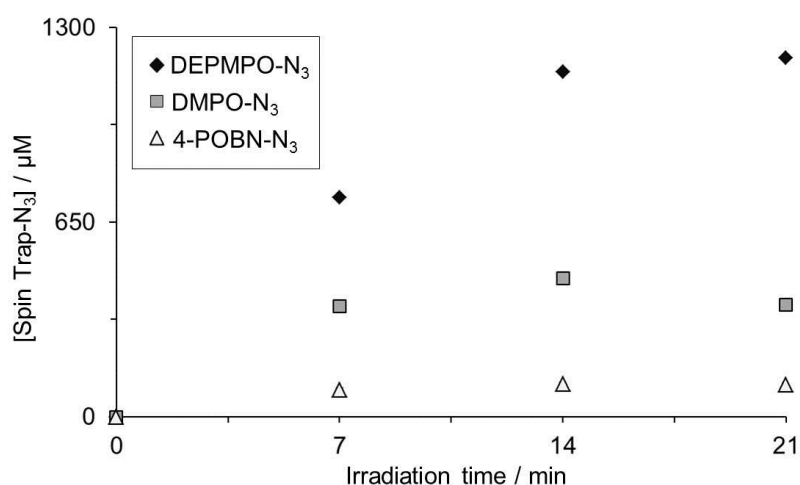
Figure 3.30 Quantification of the spin trap-N_3 spin adduct formed from the photo-irradiation of complex **40** (5 mM) in the presence of spin trap (2 mol equiv, see legend) prepared in H_2O at pH 7.4 with 463 nm light.

3.4.1.1 DEPMPO

Substituting a methyl group in DMPO for a diethoxy-phosphoryl group generating the DEPMPO spin trap has been previously reported to exhibit a faster rate for the trapping of the hydroxyl ($^\bullet OH$) radical, $k_{DEPMPO} = 7.8 \times 10^9$ M^{-1} s^{-1} vs. $k_{DMPO} = 3.4 \times 10^9$ M^{-1} s^{-1}.[51] This has been attributed to the electron-withdrawing effect of the diethoxy-phosphoryl group and it is believed that DEPMPO also possesses a faster rate than DMPO and 4-POBN for the trapping of the $^\bullet N_3$ radicals. This rate

is also thought to be faster than $^{\bullet}N_3$ radical dimerisation ($2k = 9 \times 10^9 \, M^{-1} \, s^{-1}$) rationalising the higher trapping of the $^{\bullet}N_3$ radicals.[28] Moreover, the DEPMPO-N_3 spin adduct was the most persistent spin adduct detected in this work. The increased stability is attributed to the presence of the diethoxy-phosphoryl group shielding the unpaired electron on the NO functional group, as reported previously for $^{\bullet}OH$, $^{\bullet}OOH$ and $^{\bullet}O_2^-$ radicals trapped by DEPMPO.[52,53]

3.4.1.2 4-POBN

The reduced trapping of the $^{\bullet}N_3$ radicals by 4-POBN is thought to be a result of steric hindrance due to the presence of both the 4-pyridyl and *t*-butyl groups present in 4-POBN, inhibiting the covalent bonding of the $^{\bullet}N_3$ radicals to the α-carbon of the nitrone spin trap. As a result, azidyl radical dimerisation ($2k = 9 \times 10^9 \, M^{-1} \, s^{-1}$)[28] is suggested to proceed in preference to 4-POBN-N_3 spin adduct formation. The use of 4-POBN has been commonly reported for spin trapping of oxygen- and carbon-centred radicals. Thus, it is thought that nitrogen-centred radicals, such as $^{\bullet}N_3$ radicals exhibit a lower affinity for spin trapping by 4-POBN.

3.4.1.3 DMPO

A rate constant of $k = 1.6 \times 10^9 \, M^{-1} \, s^{-1}$ for the trapping of $^{\bullet}N_3$ radicals by DMPO has been reported.[54] This lower rate constant in comparison to $^{\bullet}N_3$ radical dimerisation indicates that DMPO does not trap all $^{\bullet}N_3$ radicals generated from the photo-irradiation of complex **40**. However, the DMPO spin trap is more stable in solution compared to the phosphorus analogue. Therefore, this spin trap was still used throughout this study. Moreover, the stability of the formed DMPO-N_3 spin adduct was enhanced by the β-methyl groups present on C5 of the nitrone spin

adduct. These bulky substituents delayed the decomposition the DMPO-N$_3$ spin adduct.

3.4.1.4 Spin density

The DMPO-N$_3$ spin adduct, exhibited similar spin densities on the nitroxide nitrogen (N$_{NO}$), β-proton (H$_β$) and α-nitrogen of the trapped azidyl radical (N$_α$) atoms to that of the DEPMPO-N$_3$ spin adduct. However, the DEPMPO-N$_3$ spin adduct possessed additional spin density on the phosphorus atom. This extra spin density is believed to account for the longer lifetime of the DEPMPO-N$_3$ spin adduct compared to the DMPO-N$_3$ spin adduct. Interestingly, a difference in spin density distribution was obtained by DFT for the 4-POBN-N$_3$ spin adduct compared to the DMPO-N$_3$ and DEPMPO-N$_3$ spin adducts. Lower spin densities were observed on the N$_α$ and H$_β$ atoms present in 4-POBN-N$_3$ spin adduct in contrast to both to the DMPO-N$_3$ and DEPMPO-N$_3$ spin adducts. Moreover, in contrast to both DMPO-N$_3$ and DEPMPO-N$_3$ spin adducts, where the majority of spin density was localised on atoms involved in the hyperfine coupling, in the 4-POBN-N$_3$ spin adduct, the spin density appeared to be distributed throughout the spin adduct molecule (Figure A3.9).

Consequently, these observations are thought to account for the reduced lifetime of the 4-POBN-N$_3$ spin adduct, compared to both DMPO-N$_3$ and DEPMPO-N$_3$ spin adducts. These spin density distributions for each spin adduct are in agreement with the experimental data on DEPMPO-N$_3$ > DMPO-N$_3$ >4-POBN-N$_3$, where DEPMPO-N$_3$ is the longest lived spin adduct, under these experimental conditions. Complete spin density values are summarised in Figures A3.7 – A3.9.

Consequently, it appears spin density on the atoms involved in the hyperfine coupling can directly correlate with the lifetime of each respective spin adduct.

3.4.2 Hyperfine coupling constants

Increasing the solvent polarity has been correlated with the increase in both the a^N_{NO} and a^H_β values, which is attributed the spin adduct residing in resonance form **B** (refer to Figure 3.5).[19,55] For example, Ozawa *et al.* detected the quartet EPR spectrum assigned to DMPO-OH spin adduct in acetonitrile possessing hyperfine couplings of $a^N_{NO} = 14.10$ G and $a^H_\beta = 12.29$ G.[56] In contrast, the equivalent quartet EPR spectrum was observed by Lai *et al.* in water, however the spin adduct possessed hyperfine couplings values of $a^N_{NO} = a^H_\beta = 15.0$ G.[57] Despite this difference of ca. 0.9 G and 2.7 G between the a^N_{NO} and a^H_β values, respectively, both studies concluded the trapping of the $^\bullet$OH radicals by DMPO. Consequently, it would be expected that spin adducts recorded in the same solvent would exhibit identical hyperfine coupling constants. However, a variety of hyperfine coupling constants have been reported for the DMPO-N_3 spin adduct recorded in water (Table 3.9).[58-60] From these data, it is evident that the hyperfine splitting constants appear to be also influenced by the EPR spectrometer parameters such as modulation amplitude, microwave power and experimental conditions.[61]

Table 3.9 Comparison of the hyperfine coupling constants (G) from the DMPO-N_3 spin adduct formed in water under non-identical experimental conditions.

Radical	a^N_{NO} / G	a^H_β / G	a^N_α / G	Conditions	Ref
$^\bullet N_3$	14.9	14.9	3.0	HP,[a] N_3^- , light	60
$^\bullet N_3$	14.5	14.5	3.1	MB,[b] light	61
$^\bullet N_3$	15.0	14.3	3.17	AP,[c] N_3^- , light	62

[a] horse-radish peroxidase; [b] methylene blue; [c] antrapyrazole.

Therefore, it appears no two independent EPR spin trapping studies will generate equivalent hyperfine coupling values, unless identical experimental conditions are used. Consequently, this rationalises the minor differences in hyperfine coupling constants determined in this thesis compared to previous literature.

3.4.3 Solvent effects

An equivalent formation of the DMPO-N_3 spin adduct was detected in both (H_2O) and PBS/H_2O (Figure A3.5). Consequently, it appeared the PBS components (phosphate and potassium chloride) did not affect the trapping of the azidyl radical. However, changing from water to deuterated phosphate buffer led to an increase (ca. two-fold higher) in both the DMPO-N_3 and 4-POBN-N_3 spin adduct concentrations. An increasing yield in radical species in deuterated solvent has been previously reported, ca. 5% higher in deuterated solvent compared to aqueous solution.[62,63]

Collectively, increasing radical yields and extended lifetimes are postulated to be due to the Brownian motion (diffusion) of the formed radicals. Previous literature

has described the higher tumbling rates of molecules in less viscous solvents.[15] Furthermore, Harbour *et al.* determined a three-fold increase in the DMPO-N_3 spin adduct upon changing the solvent from H_2O to D_2O. Therefore, in this work it is proposed that changing from protiated (H_2O) solvent (η = 0.8903 cP s at 25 ºC) to deuterated (η = 1.100 cP at 25 ºC) deuterated (D_2O) solvent,[64] is the reason for the concentration increase in the formed spin adducts.

The reduction of the DMPO-N_3 spin adduct generated in the cell culture medium RPMI-1640 may be at least partially attributed to its low viscosity (η = 0.7 cP at 310 K).[65] However, the $^\bullet N_3$ radicals are reactive towards a variety of amino acids, in particular L-tyrosine (L-Tyr) and L-tryptophan (L-Trp).[62,66] RPMI-1640 contains various components including amino acids (L-Tyr and L-Trp) (Figure A3.6). However, their concentrations in the cell culture medium are thought to be too low to induce reactivity with the formed $^\bullet N_3$ radicals. Nevertheless, other substituents in the cell culture medium may be strong azidyl radical quenchers at low concentrations. Owing to the array of substituents present in RPMI-1640, this effect was not investigated in greater depth.

3.4.4 Irradiation sources

3.4.4.1 Longer wavelength of activation

Green (33 mW cm^{-2}) LED light of 517 nm is ca. two-fold lower in power than the corresponding 463 nm blue (64 mW cm^{-2}) LED light source. This lower power is envisaged to reduce the rate of photo-activation of complex **40**. This was confirmed by monitoring the photo-decomposition of complex **40** with 517 nm light by UV-visible spectroscopy. The reduced decrease in the $N_3 \rightarrow Pt^{IV}$ LMCT

band coincides with a reduction in $^{\bullet}N_3$ radical release, leading to a reduction in the amount of $^{\bullet}N_3$ radicals to be trapped by both DMPO and DEPMPO.

Changing the wavelength of irradiation to 517 nm (green) light led only to the formation of the DMPO-N$_3$ spin adduct in RPMI-1640 medium compared to water and PBS/D$_2$O solvents. This was suggested to be due to the presence of the various substituents present in the cell culture medium. It is probable that one or more components in the cell culture medium enhance the light-dependent generation of $^{\bullet}N_3$ radicals. The reason why activation at the longer wavelength was successful only in the culture medium is not clear, although perhaps it could be related to the behaviour of very weak bands at longer wavelength found in density functional theory calculations.[1] Longer wavelengths are of interest because of their deeper penetration into tissues, and both blue and green light are effective in activating related pyridyl/ammine Pt^{IV} complexes in cancer cells.[1,67]

The trapping of the $^{\bullet}N_3$ radicals formed from the photo-irradiation of complex **40** prepared in DMF/H$_2$O (75% / 25% v/v) with 517 nm light is suggested to be due to both the higher solvent-mixture viscosity inducing a lower rate of molecular tumbling, subsequently leading to an increase in the amount of the $^{\bullet}N_3$ radicals trapped by DMPO.

It was also established that the release of the azide ligands depends on the ligands coordinated to the platinum(IV) metal centre. As observed, the photo-irradiation with 517 nm LED light of complexes **56** and **57** (refer to Figure 3.13 for structures) prepared in PBS/H$_2$O led to the trapping of the $^{\bullet}N_3$ radicals, in contrast to complex

40 photo-activated under similar conditions. Both of these carboxylate compounds exhibited an ability to be photo-activated with green light, suggesting equatorial ligand modification influence the wavelength of activation of platinum(IV) diazido complexes. This is in agreement with previous DFT calculations performed on complexes **56** and **57** which exhibited bands at longer wavelengths compared to complex **40**.[41] The trapping of the $^\bullet N_3$ radicals from photo-irradiated complexes **40**, **44** and **57-59** suggested the release of the azide ligands in azidyl ($^\bullet N_3$) radical form is a common photo-decomposition pathway for platinum(IV) diazido complexes.

3.4.4.2 Gamma ray irradiation

Cis-platin was first reported to be a radio-sensitiser by Zák and Drobník.[68] Second and third generation platinum anticancer complexes are also efficient radio-sensitisers.[69,70] However, this appears to be the first report on the activation of complex **40** with a gamma-ray irradiation source. Initial gamma-ray irradiation of complex **40** in the presence of spin trap, DMPO, did not generate EPR spectra suitable for full characterisation or qualitative analysis. It is most probably a decay product from the initial trapping of the $^\bullet N_3$ radicals by DMPO.

Employing the phosphorus spin trap, DEPMPO was more efficient in allowing the resultant EPR spectra to be interpreted in terms of $^\bullet N_3$ radical trapping. The detection of the DEPMPO-N_3 spin adduct suggests gamma-ray irradiation is effective in photo-activating complex **40**. Two probable activation pathways of complex **40** with the ^{137}Cs gamma-ray irradiation source have potential to occur. Firstly, the ^{137}Cs gamma-ray irradiation source has potential to ionise the solvent,

H$_2$O, leading to the generation of aqueous free radicals, hydrogen ion and low amounts of H$_2$ and H$_2$O$_2$ (Equation 3.3). Previous studies by Khan reported on the one-electron reduction of *trans*-[Pt^{IV}(NH$_3$)$_4$(OH)$_2$]$^{2+}$ by the aquated electron generated from pulse radiolysis, leading to the formation of a *trans*-[Pt^{III}(NH$_3$)$_4$(OH)$_2$]$^+$ species. This platinum(III) species underwent additional reaction with the hydroxyl radicals generated from the pulse radiolysis of water, forming *trans*-[Pt(NH$_3$)$_4$(H$_2$O)$_2$]$^{3+}$.[71] Additionally, free ammonia was also detected in these reactions.

$$H_2O \xrightarrow{e^-} e^-_{aq}, H^+, {}^\bullet OH, H_2, H_2O_2 \qquad \text{Eq. 3.3}$$

In this work, gamma-ray irradiations were performed in water, therefore ionisation of the solvent as shown in Equation 3.3 is possible. Through the hydrated electron, a one-electron reduction of the Pt^{IV} metal centre of complex **40** could occur, generating a platinum(III) intermediate. Although it is not fully understood, it is proposed the reactive nature of this platinum(III) transient species may result in the loss of the azide ligand in azidyl radical form, which is subsequently trapped by DEPMPO. Alternatively, the ^{137}Cs, parent nuclide spontaneously decays via beta decay to the daughter nuclide, ^{137}Ba and emits a β$^-$ particle, an antineutrino ($\bar{\upsilon}$e) and Q_{β^-} energy (Equation 3.4). The *β$^-$* particle corresponds to an electron (e$^-$), where its presence satisfies the energy conservation.[72]

$$^{137}_{55}Cs \longrightarrow {}^{137}_{56}Ba + \beta^- + \bar{\upsilon}_e + Q_{\beta^-} \qquad \text{Eq. 3.4}$$
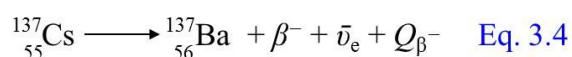
Therefore, the reduction of the Pt^{IV} metal centre may also be initiated from this electron in a similar pathway as described above. One-electron reduction of *cis*-platin has also been reported with the hydrated electron, forming a platinum(I) type species.[73] Free ammonia from *trans*-[Pt^{IV}(NH$_3$)$_4$(OH)$_2$]$^{2+}$ was also detected in the

study by Khan *et al.*. Therefore in this work, the lack of cytotoxicity in DLD-1 cells from gamma-ray irradiated complex **40** may be due to the loss of coordinated pyridine. The loss of carrier ligands from platinum anticancer complexes has been associated with reduced cytotoxicity.[74-76]

Interestingly, the detection of the DEPMPO-N$_3$ spin adduct from complex **40** was obtained using clinically relevant gamma-ray irradiation doses. To date, the maximum dosage applied to patients is 45 Gy, given in aliquots of $1.8 - 2$ Gy over a period of 5-8 weeks.[37] However, despite the detection of the DEPMPO-N$_3$ spin adduct, it should be noted that the ^{137}Cs gamma-ray irradiation source emitting a photon with energy of ca. 662 keV is more destructive towards complex **40**, compared to visible light with a power outage of ca. 64 mW cm^{-2}. Therefore, the detection of the DEPMPO-N$_3$ spin adduct has potential to be due to complete molecular fragmentation of complex **40** irradiated with ^{137}Cs gamma-ray irradiation source. Additional UV-visible and NMR spectroscopy studies of complex **40** irradiated with gamma-rays are required to fully comprehend these preliminary results and elucidate the mechanism of action.

3.5 Conclusion

In this Chapter, photo-activation of complex **40** with blue light gave rise to the release of the azide ligand in azidyl ($^\bullet$N$_3$) radical form, which was detected by spin trapping EPR spectroscopy using a variety of nitrone spin traps namely: DMPO, 4-POBN and DEPMPO. Varying the spin trap led to differences in efficiency and life-times of the resultant spin adducts. The phosphorus spin trap DEPMPO appeared to exhibit the fastest rate towards $^\bullet$N$_3$ radicals. In contrast, the spin trap,

4-POBN displayed the lowest level of $^{\bullet}N_3$ radical trapping, this was attributed to steric hindrance due to the presence of the 4-pyridyl and *t*-butyl groups present in 4-POBN.

The first generation cyclic nitrone spin trap, DMPO generated the quartet of triplets spectrum, indicative of DMPO-N_3 spin adduct formation. However, with a known rate slower than $^{\bullet}N_3$ radical dimerisation, a portion of formed $^{\bullet}N_3$ radicals are believed to undergo radical dimerisation. The distribution of spin density on the atoms involved in the hyperfine coupling was correlated with the lifetime of the spin adducts under investigation.

Interestingly, Brownian motion of the formed $^{\bullet}N_3$ radicals appears to account for the observed increase in the amount of spin adduct formed upon changing the solvent from PBS/H_2O to PBS/D_2O. In contrast, the reduction in the DMPO-N_3 spin adduct formed in RPMI-1640 was attributed to the various components in cell culture medium which have potential to behave as azidyl radical quenchers. Furthermore, the trapping of $^{\bullet}N_3$ radicals from related photo-activatable platinum(IV) diazido complexes, *trans,trans,trans*-[Pt(N_3)$_2$(OH)$_2$(MA)(py)] (**44**, MA = methylamine), *trans,trans,trans*-[Pt(N_3)$_2$(OH)(SAD)(py)$_2$] (**56**, SAD = succinate), *trans,trans,trans*-[Pt(N_3)$_2$(OH)(ethyl-methyl-SAD)(py)$_2$] (**57**) and *trans,trans,trans*-[Pt(N_3)$_2$(OH)(N-MI)(py)$_2$] (**58**, N-MI = N-methylisatoate) suggested the release of the azide ligand(s) as a common photo-decomposition pathway of platinum(IV) diazido complexes. Finally, it was shown that complex **40** could be activated by gamma-rays from a ^{137}Cs gamma radiation source at doses of therapeutic relevance.

In this Chapter, photo-irradiation of a family of platinum(IV) diazido anticancer complexes with visible light led to the trapping of the $^\bullet$N$_3$ radicals using a variety of spin traps. $^\bullet$N$_3$ radicals are regarded as reactive nitrogen species (RNS), which suggests their potential involvement in the photo-cytotoxic nature of platinum(IV) diazido anticancer complexes. These formed $^\bullet$N$_3$ radicals have potential to react with various amino acids, proteins and peptides, leading to a potential disruption in cell homeostasis inducing an acute phase cytotoxic effect. These results suggest platinum(IV) diazido complexes have the ability to exhibit a dual mechanism of action involving both an acute (radical based) and chronic (DNA platination at N^7 of guanine) phase.

3.6 References

(1)   Farrer, N. J.; Woods, J. A.; Salassa, L.; Zhao, Y.; Robinson, K. S.; Clarkson, G.; Mackay, F. S.; Sadler, P. J. *Angew. Chem. Int. Ed.* **2010**, *49*, 8905.

(2)   Beck, W.; Schorpp, K. *Angew. Chem. Int. Ed.* **1970**, *9*, 735.

(3)   Hennig, H.; Stich, R.; Rehorek, D.; Thomas, P.; Kemp, T. J. *Inorg. Chim. Acta.* **1988**, *143*, 7.

(4)   Bartocci, C.; Scandola, F. *J. Chem. Soc.* **1970**, 531a.

(5)   Hennig, H.; Ritter, K.; Chibisov, A. K.; Görner, H.; Grevels, F.-W.; Kerpen, K.; Schaffner, K. *Inorg. Chim. Acta.* **1998**, *271*, 160.

(6)   Knoll, H.; Stich, R.; Hennig, H.; Stufkens, D. J. *Inorg. Chim. Acta.* **1990**, *178*, 71.

(7)   Šima, J.; Ducárová, T.; Šramko, T.; Kotočová, A. *Bull. Soc. Chim. Belg.* **1991**, *100*, 193.

(8)   Šima, J. *Coord. Chem. Rev.* **2006**, *250*, 2325.

(9)   Šima, J. *Comments Inorg. Chem.* **1992**, *13*, 277.

(10)   Workentin, M. S.; Wagner, B. D.; Lusztyk, J.; Wayner, D. D. M. *J. Am. Chem. Soc.* **1995**, *117*, 119.

(11)   Hayon, E.; Simic, M. *J. Am. Chem. Soc.* **1970**, *92*, 7486.

(12)   Gafney, H. D.; Reed, J. L.; Basolo, F. *J. Am. Chem. Soc.* **1973**, *95*, 7998.

(13)   Mackay, F. S.; Woods, J. A.; Moseley, H.; Ferguson, J.; Dawson, A.; Parsons, S.; Sadler, P. J. *Chem. Eur. J.* **2006**, *12*, 3155.

(14)   Mackay, F. S.; Moggach, S. A.; Collins, A.; Parsons, S.; Sadler, P. J. *Inorg. Chim. Acta.* **2009**, *362*, 811.

(15)   Farrer, N. J.; Gierth, P.; Sadler, P. J. *Chem. Eur. J.* **2011**, *17*, 12059.

(16)   Zhao, Y.; Farrer, N. J.; Li, H.; Butler, J. S.; McQuitty, R. J.; Habtemariam, A.; Wang, F.; Sadler, P. J. *Angew. Chem. Int. Ed.* **2013**, *52*, 13633.

(17)   Bačić, G.; Spasojević, I.; Šećerov, B.; Mojović, M. *Spectrochim. Acta, Part A* **2008**, *69*, 1354.

(18)   Janzen, E. G. *Acc. Chem. Res.* **1971**, *4*, 31.

(19)   Buettner, G. R. *Free Radic. Biol. Med.* **1987**, *3*, 259

(20)   Alberti, A.; Macciantelli, D. In *Electron Paramagnetic Resonance: A Practitioner's Toolkit*; Brustolon, M., Giamello, E., Eds.; Wiley&Sons: New Jersey, 1999, p 291.

(21)   Alberti, A.; Macciantelli, D. In *Electron Paramagnetic Resonance: A Practitioner's Toolkit*; Brustolon, M., Giamello, E., Eds.; Wiley&Sons: New Jersey, 1999, p 305.

(22)   Alberti, A.; Macciantelli, D. In *Electron Paramagnetic Resonance: A Practitioner's Toolkit*; Brustolon, M., Giamello, E., Eds.; Wiley&Sons: New Jersey, 1999, p 293.

(23)   Mottley, C.; Kalyanaraman, B.; Mason, R. P. *FEBS Lett.* **1981**, *130*, 12.

(24)   Atkins, P. W. *Physical Chemistry*; 3rd ed.; Oxford University Press: Oxford, UK, 1986, p 458.

(25)   Villamena, F. A.; Liu, Y.; Zweier, J. L. *J. Phys. Chem. A* **2008**, *112*, 12607.

(26)   Chen, Y.-R.; Sturgeon, B. E.; Gunther, M. R.; Mason, R. P. *J. Biol. Chem.* **1999**, *274*, 24611.

(27)   Partridge, R. S.; Monroe, S. M.; Parks, J. K.; Johnson, K.; Parker, W. D.; Eaton, G. R.; Eaton, S. S. *Arch. Biochem. Biophys.* **1994**, *310*, 210.

(28)   Kalyanaraman, B.; Janzen, E. G.; Mason, R. P. *J. Biol. Chem.* **1985**, *260*, 4003.

(29)   Finkelstein, E.; Rosen, G. M.; Rauckman, E. J. *Arch. Biochem. Biophys.* **1980**, *200*, 1.

(30)   Villamena, F. A.; Zweier, J. L. *J. Chem. Soc., Perkin Trans. 2,* **2002**, 1340.

(31)   Finkelstein, E.; Rosen, G. M.; Rauckman, E. J. *Mol. Pharmacol.* **1982**, *21*, 262.

(32)   Koulkes-Pujo, A. M.; Moreau, M.; Sutton, J. *FEBS Lett.* **1981**, *129*, 52.

(33)   Kuchitsu, K.; Kosaka, H.; Shiga, T.; Shibuya, N. *Protoplasma* **1995**, *188*, 138.

(34)   Pou, S.; Ramos, C. L.; Gladwell, T.; Renks, E.; Centra, M.; Young, D.; Cohen, M. S.; Rosen, G. M. *Anal. Biochem.* **1994**, *217*, 76.

(35)   Dai, T.; Gupta, A.; Murray, C. K.; Vrahas, M. S.; Tegos, G. P.; Hamblin, M. R. *Drug Resis. Update* **2012**, *15*, 223.

(36)   Hofmann, N.; Hugo, B.; Klaiber, B. *Eur. J. Oral Sci.* **2002**, *110*, 471.

(37)   Cao, W.; Gu, Y.; Meineck, M.; Xu, H. *Chem. Asian. J.* **2014**, *9*, 48.

(38)   Candelaria, M.; Garcia-Arias, A.; Cetina, L.; Dueñas-Gonzalez, A. *Radiat. Oncol.* **2006**, *1*, 1.

(39)   Douple, E. B. *Platinum Met. Rev.* **1985**, *29*, 118.

(40)   Zhao, Y., Ph.D. Thesis, University of Warwick, 2012.

(41)   Shaili, E., Ph.D. Thesis, University of Warwick, 2013.

(42)   Frisch, M. J.; Trucks, G. W.; Schlegel, H. B.; Scurseria, G. E.; Robb, M. A.; Cheeseman, J. R.; Montgomery, J. A.; Vreven, J., T. ; Kudin, K. N.; Burant, J. C.; *et al.*, Gaussian 03, revision D.01, Gaussian Inc. Wallingford, CT, **2004**.

(43)   Becke, A. D. *J. Chem. Phys.* **1993**, *98*, 5648.

(44)   Lee, C.; Yang, W.; Parr, R. G. *Phys. Rev. B* **1988**, *37*, 785.

(45)   Janzen, E. G.; Liu, J. I. P. *J. Magn. Reson.* **1973**, *9*, 510.

(46)   Samuni, A.; Samuni, A.; Swartz, H. M. *Free Radic. Biol. Med.* **1989**, *6*, 179.

(47)   Kremers, W., Singh, Ajit., *Can. J. Chem.* **1980**, *58*, 1592.

(48)   Walter, T. H.; Bancroft, E. E.; McIntire, G. L.; Davis, E. R.; Gierasch, L. M.; Blount, H. N. *Can. J. Chem.* **1982**, *60*, 1621.

(49)   Eaton, S. S.; Eaton, G. R. *J. Magn. Reson.* **2012**, *223*, 151.

(50)   Paciolla, M. D.; Kolla, S.; Jansen, S. A. *Adv. Environ. Res.* **2002**, *7*, 169.

(51)   Frejaville, C.; Karoui, H.; Tuccio, B.; le Moigne, F.; Culcasi, M.; Pietri, S.; Lauricella, R.; Tordo, P. *J. Chem. Soc., Chem. Commun.* **1994**, 1793.

(52)   Khan, N.; Wilmot, C. M.; Rosen, G. M.; Demidenko, E.; Sun, J.; Joseph, J.; O'Hara, J.; Kalyanaraman, B.; Swartz, H. M. *Free Radic. Biol. Med.* **2003**, *34*, 1473.

(53)   Mojović, M.; Vuletić, G.; Bačić, G. *J. Serb. Chem. Soc.* **2005**, *1048*, 471.

(54)   Ram, M. S.; Stanbury, D. M. *Inorg. Chem.* **1985**, *24*, 4233.

(55)   Ōishi, Y.; Mukai, K.; Nishiguchi, H.; Deguchi, Y.; Takaki, H. *Tetrahedron Lett.* **1968**, *9*, 4773.

(56)   Ozawa, T.; Hanaki, A.; Matsumoto, S.; Matsuo, M. *Biochim. Biophys. Acta* **1978**, *531*, 72.

(57)   Lai, C.-S.; Grover, T. A.; Piette, L. H. *Arch. Biochem. Biophys.* **1979**, *193*, 373.

(58)   Buettner, G. R.; Oberley, L. W. *FEBS Lett.* **1980**, *121*, 161.

(59)   Harbour, J. R.; Issler, S. L. *J. Am. Chem. Soc.* **1982**, *104*, 903.

(60)   Reszka, K.; Kolodziejczyk, P.; Lown, J. W. *Journal of Free Radicals in Biology & Medicine* **1986**, *2*, 267.

(61)   Eaton, G. R.; Eaton, S. R.; Barr, D. P.; Weber, R. T. In *Quantitative EPR:A Practitioners Guide*; Springer-Verlag/Wien: Germany, 2010, p 115.

(62)   S.Solar; N. Getoff; P.S. Surdhar; D.A. Armstrong; Singh., A. *J. Phys. Chem.* **1991**, *95*, 3639.

(63)   Draganic, I. G.; Draganic, Z. D. *Radiation Chemistry of Water*; Elsevier Science & Technology: Oxford/US, 1971.

(64)   Cho, C. H.; Urquidi, J.; Singh, S.; Robinson, G. W. *J. Phys. Chem. B* **1999**, *103*, 1991.

(65)   Biggerstaff, J.; Weidow, B.; Vidosh, J.; Dexheimer, J.; Patel, S.; Patel, P. *Thrombosis J* **2006**, *4*, 1.

(66)   Butler, J.; Land, E. J.; Swallow, A. J.; Prutz, W. *Radiat. Phys. Chem.* **1984**, *23*, 265

(67)   Mackay, F. S.; Woods, J. A.; Heringová, P.; Kašpárková, J.; Pizarro, A. M.; Moggach, S. A.; Parsons, S.; Brabec, V.; Sadler, P. J. *Proc. Natl. Acad. Sci. USA.* **2007**, *104*, 20743.

(68)   Zák, M.; Drobník, J. *Strahlentherapie* **1971**, *142*, 112.

(69)   Hill, E. J.; Nicolay, N. H.; Middleton, M. R.; Sharma, R. A. *Crit. Rev. Oncol. Hemat.* **2012**, *83*, 353.

(70)   Kvols, L. K. *J. Nucl Med.* **2005**, *46*, 187S.

(71)   Khan, H. M.; Waltz, W. L.; Lilie, J.; Woods, R. J. *Inorg. Chem.* **1982**, *21*, 1489.

(72)   Baltos, D.; Sakelliou, L.; Zauboglou, L. In *Medical Physics and Biomedical Engineering*; Webster, J. G., Mould, R. F., Eds.; Taylor and Francis: London, 2007, p 75.

(73)   Swancutt, K. L.; Mezyk, S. P.; Kiddle, J. J. *Radiat. Res.* **2007**, *168*, 423.

(74)   Coluccia, M.; Natile, G. *Anti-cancer Agents Med. Chem.* **2007**, *7*, 111.

(75)   Lau, J. K.-C.; Deubel, D. V. *Chem. Eur. J.* **2005**, *11*, 2849.

(76)   Li, H.; Zhao, Y.; Phillips, H. I. A.; Qi, Y.; Lin, T.-Y.; Sadler, P. J.; O'Connor, P. B. *Anal. Chem.* **2011**, *83*, 5369.

Chapter IV

Reactivity of Azidyl Radicals

This chapter investigates the potential biological target(s) of azidyl radicals in an attempt to elucidate their reactivity within cancer cells.

4.1 Introduction

Platinum(IV) diazido anticancer complexes such as *trans,trans,trans-*[Pt(OH)$_2$(N$_3$)$_2$(py)$_2$] (complex **40**) exert potent photo-cytotoxicity towards a number of cancer cell lines including parental (A2780) and cisplatin-resistant (A2780cis) ovarian carcinoma cells following irradiation with blue/green wavelengths of light, whilst being non-toxic in the dark.[1] The mechanism of action of complex **40** and similar photo-activatable platinum(IV) diazido complexes (Figure 4.1) may involve a number of different pathways, including the platination of DNA nucleobases (such as guanine) which was discussed in **Chapter I**, and the formation of radical species, which was the subject of **Chapter III**.

Similar to reactive oxygen species (ROS), reactive nitrogen species (RNS) are equally capable of inducing biochemical disorders including major tissue/cell damage.[2,3] As shown in **Chapter III**, azidyl radicals ($^\bullet$N$_3$) were characterised by spin trapping EPR spectroscopy upon the photo-irradiation of complex **40** and related platinum(IV) diazido complexes. Once formed, these RNS are readily available to interact with near biological targets in cells. Prütz *et al.* reported the reactive nature of the $^\bullet$N$_3$ radicals towards aromatic functionalised amino acids in addition to noting their unreactive nature towards nucleic acid derivatives.[4]
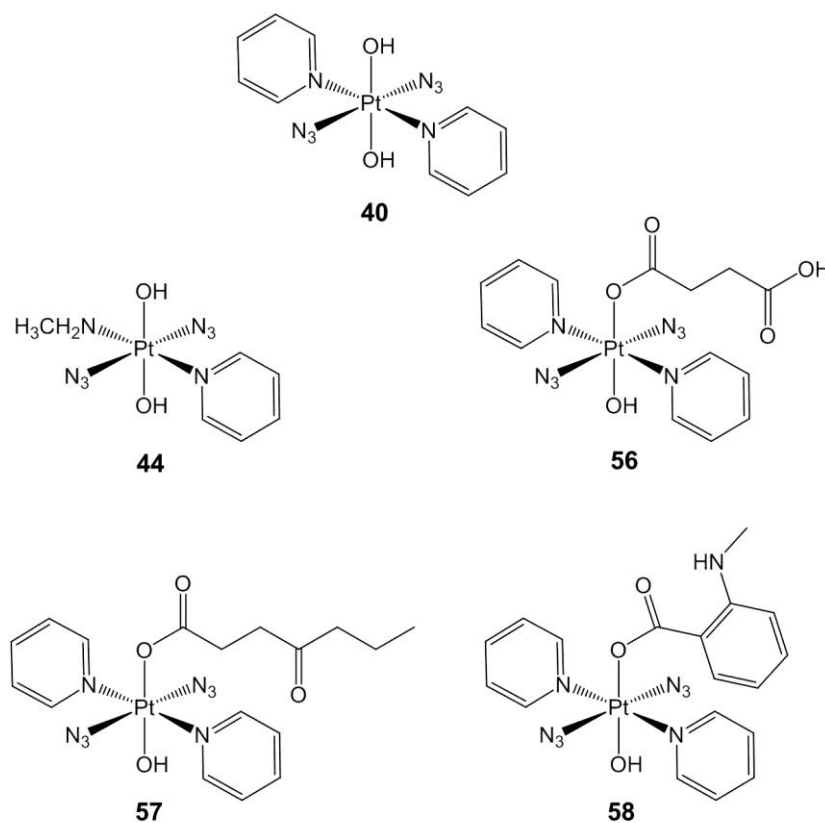
Figure 4.1 Photo-activatable platinum(IV) diazido complexes studied in this work.

Amino acids are involved in a variety of biochemical pathways. For example, L-tyrosine (L-Tyr) possesses important roles in protein synthesis, including the production of neurotransmitters responsible for nerve cell communication and mood influence; it also acts as a precursor to melanin pigment.[5] In contrast, L-tryptophan (L-Trp) is transformed into various biomolecules including nicotinic acid (a vitamin), serotonin (a neuro-hormone) and indole acetic acid (a phyto-hormone).[6] Furthermore, L-Trp is a precursor for nicotine-aminde adenosine dinucleotide (NAD$^+$), a coenzyme found in living cells, involved in redox reactions and cellular processes such as post-translational modifications of proteins.[6,7]

Previous reports on the reactivity of $^\bullet N_3$ radicals have been on the interaction with L-Trp, L-Tyr,[8] *N*-methylindole (NMI), various styrenes and olefin derivatives.[8] Thermodynamically, the reaction between $^\bullet N_3$ radicals with L-Trp was reported to proceed via a hydrogen-atom abstraction process (Scheme 4.1**A**), leading to the formation of a neutral L-Trp$^\bullet$ radical and hydrazoic acid (HN$_3$).[9] However, reacting near the diffusion-controlled limit, $^\bullet N_3$ radicals favour an electron-transfer mechanism (Scheme 4.1**B**).[9] One-electron oxidation of L-Trp by $^\bullet N_3$ radicals generates both free azide (N$_3^-$) and the corresponding amino acid radical cation (L-Trp$^{\bullet+}$).

A.

B.
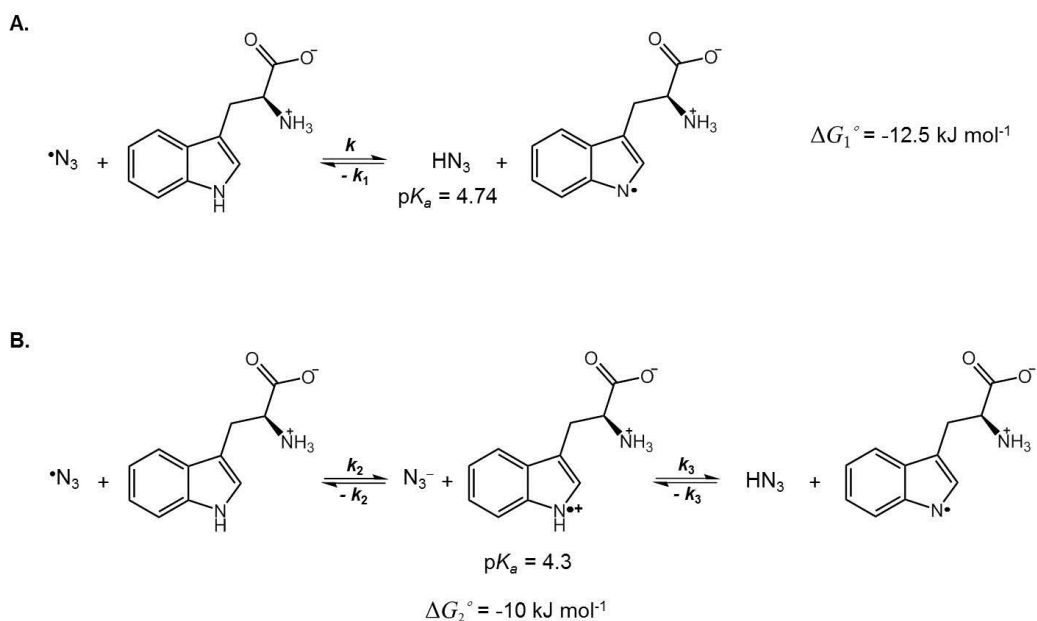
Scheme 4.1 Azidyl radical reaction with L-Trp through (**A**) hydrogen atom abstraction and (**B**) electron transfer pathways with included pK_a and Gibbs Free Energy ($\Delta G°$) values shown. The rate constants for the forward (k_n) and back directions ($-k_n$) are depicted.

L-Trp$^{\bullet+}$ with a pK_a of ca. 4.3, deprotonates within nanoseconds at pH > 5, leading to the formation of L-Trp$^\bullet$ and HN$_3$. The hydrogen atom belonging to the NH

amine functional group of the indole ring is abstracted from L-Trp$^{\bullet+}$.[9] These one-electron oxidation reactions of amino acids by $^{\bullet}N_3$ radicals have been reported in numerous instances with the formation of the corresponding amino acid radical.[9,10] The redox couples (Trp$^{\bullet+}$ / Trp) with a reported reduction potential (E°) of ca. 1.24 ± 0.02 V,[11] is a stronger oxidant than the redox couple (Tyr$^{\bullet+}$ / Tyr) with a E° value of 0.94 V.[12] Moreover, at pH 7, redox potential values for the redox couples (Trp/Trp$^{\bullet}$) and (Tyr/Tyr$^{\bullet}$) have been reported to be ca. 0.94 V and > 0.8 V, respectively.[13] Despite the reduction potentials showing a marked pH dependence,[14] the above reduction potentials are weaker than the redox couple ($^{\bullet}N_3$/ N_3^-) with a E° value of ca. 1.33 V. The reduction potentials for the redox couples, (Trp$^{\bullet+}$/Trp), (Tyr$^{\bullet+}$/Tyr), (Trp/Trp$^{\bullet}$) and (Tyr/Tyr$^{\bullet}$) together with the pK_a values of 4.74 for HN$_3$ suggest it is favourable for either L-Trp or L-Tyr to donate an electron to the $^{\bullet}N_3$ radicals. Therefore, potential reaction of $^{\bullet}N_3$ radicals with either amino acid has potential to subsequently render partial or complete inhibition in their biochemical pathways. This could result in an overall disruption of the cell homeostasis, possibly inducing a series of unwanted side effects, compromising cell viability.

In this Chapter the reactivity of $^{\bullet}N_3$ radicals generated from the photo-activation of *trans,trans,trans*-[Pt(N$_3$)$_2$(OH)$_2$(py)$_2$] (complex **40**) towards various amino acids was investigated using various spectroscopic techniques including UV-visible, EPR, ^{1}H and ^{14}N NMR spectroscopy. The reactivity of $^{\bullet}N_3$ radicals towards L-Trp led to a further investigation of their activity in A2780 ovarian cancer cells. Additionally, the reactive nature of $^{\bullet}N_3$ radicals generated from

trans,trans,trans-[Pt(N$_3$)$_2$(OH)(N-MI)(py)$_2$] (complex **58**, Figure 4.1) was also briefly investigated.

4.2 Experimental

Below are the experimental sample preparation and instrumentation set up specific to this Chapter. More details regarding instrumentation and the irradiation setup are described in **Chapter II**.

*Note

Unless otherwise stated all experiments were undertaken in deuterated phosphate buffered saline solution (PBS/D$_2$O) at pH* 7.4. Deuterated solvent was selected to allow comparison between the various spectroscopic techniques used. The effect of D$_2$O on the system was previously discussed in **Chapter III**. It was shown not to affect the photo-activation pathway of complex **40** but rather prolong the lifetime of the generated free radical in solution in comparison to protiated solvent. A similar effect to has been observed for ^{1}O$_2$ generated in D$_2$O.[15]

4.2.1 Materials

Complex **40** was synthesised and characterised as previously described in **Chapter II**. *Trans,trans,trans*-[Pt(N$_3$)$_2$(OH)(N-MI)(py)$_2$] (complex **58**, Figure 4.1) was provided by Dr. Evyenia Shaili and was synthesised and characterised as previously described.[16] L-tryptophan was purchased from Sigma Aldrich. L-tyrosine was purchased from Acros Organics and glycine from BDH Ltd. A2780 human ovarian carcinoma cells were obtained from the European Collection of Animal Cell Cultures (Porton Down, UK) and grown as 6 monolayers in RPMI-1640 containing 10 % (v/v) foetal calf serum.

4.2.2 Sample preparation

All solutions were freshly prepared prior to performing experiments.

4.2.2.1 UV-visible spectroscopy

The concentration of complex **40** was kept constant at 50 μM while varying the mol equiv. of the added amino acids, Gly, L-Tyr and L-Trp were prepared in PBS/D_2O at pH* 7.4.

4.2.2.2 Electron Paramagnetic Resonance (EPR) spectroscopy

Solutions were prepared containing complex **40** (4 mM), DMPO (8 mM) in addition to amino acid (Gly, L-Tyr and L-Trp) present at a final concentration of either 0.5 mM or 1 mM prepared in PBS/D_2O at pH* 7.4.

4.2.2.3 Nuclear Magnetic Resonance Spectroscopy

- **^1H NMR**

Complex **40** (4 mM), DMPO (8 mM) in both the absence and presence of L-Trp (2 mol equiv) were prepared in PBS/D_2O at pH* 7.4. Dark stability was monitored at 0 h and 24 h time intervals.

- **^{14}N NMR**

The ^{14}N NMR resonance of L-Trp was monitored by preparing a solution of L-Trp (18 mM) in PBS/D_2O at pH* 7.4. Additional solutions containing complex **40** (9 mM) in both the absence and presence of L-Trp (2 mol equiv) were prepared in PBS/D_2O at pH* 7.4. All ^{14}N NMR spectra were externally referenced to $^{14}NH_4Cl$ (1.5 M) in 1 M HCl ($\delta = 0$).

4.2.3 Cell studies

All biological experiments were carried out by Dr. Julie Woods (Photobiology Unit, Ninewells Hospital, Dundee UK).

4.2.3.1 A2780 ovarian cancer cells

Cell irradiations were performed with 420 nm (5 J cm^{-2}) irradiation source, as described in **Chapter II**.

4.2.3.2 Photo-toxicity

A2780 cells were seeded at a density of 6-7 x 10^4 cells cm^{-2} in 96 well plates 24 h before the initiation of the experiment. The neutral red photo-toxicity test was performed as previously described.[1] Cell viability was measured using the uptake of neutral red dye as an end point 24 h later.

4.2.3.3 Data analysis

Goodness-of-fit of dose response curves were determined from R^2 values and the 95% confidence interval of the IC$_{50}$ value. The IC$_{50}$ value was defined as the concentration of test compound required to inhibit dye uptake by the cells by 50% (Graph pad Prism v5). Exposures were performed in triplicate and experiments were repeated at least twice, as stated in the figure legends.

4.3 Results

4.3.1 UV-visible spectroscopy - Glycine

Prior to irradiating in the presence of functionalised amino acids, the amino acid glycine (Gly, Figure 4.2) was studied. Glycine, the simplest amino acid, possesses

both amino and carboxylate groups, present in all amino acids. It was chosen to investigate a possible interaction between photo-activated complex **40** with Gly, either through formation of a Pt^{II}-Gly species or a reaction with the formed $^\bullet N_3$ radicals with either the carboxylate or amino group (or both). Establishing an interaction between photo-activated complex **40** and Gly has potential to suggest photo-activated complex **40** would behave similarly towards all amino acids.
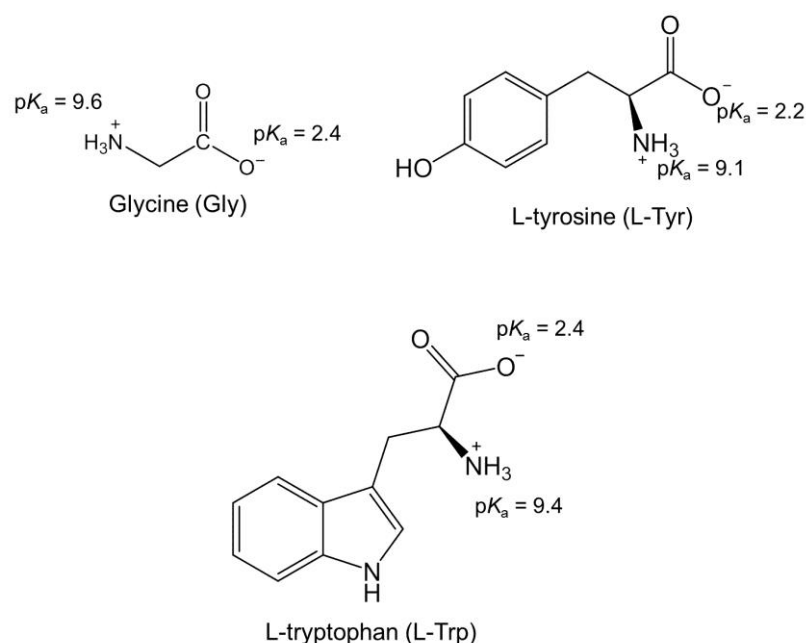

Figure 4.2 Structures of amino acids studied in this work at physiological pH.

As shown in **Chapter III**, the UV-visible spectrum of complex **40** in the dark displayed an absorption at 294 nm (Figure 4.3**A**) assigned as a ligand-to-metal charge transfer ($N_3 \rightarrow Pt^{IV}$, LMCT) transition.[1] After 30 min irradiation at 463 nm, the decrease of ca. 40% in this LMCT band is attributed to the release of the azide ligands (Figure 4.3**B**). Consequently, the decrease in the intensity of the LMCT band was used to monitor the photo-decomposition of the platinum complex.
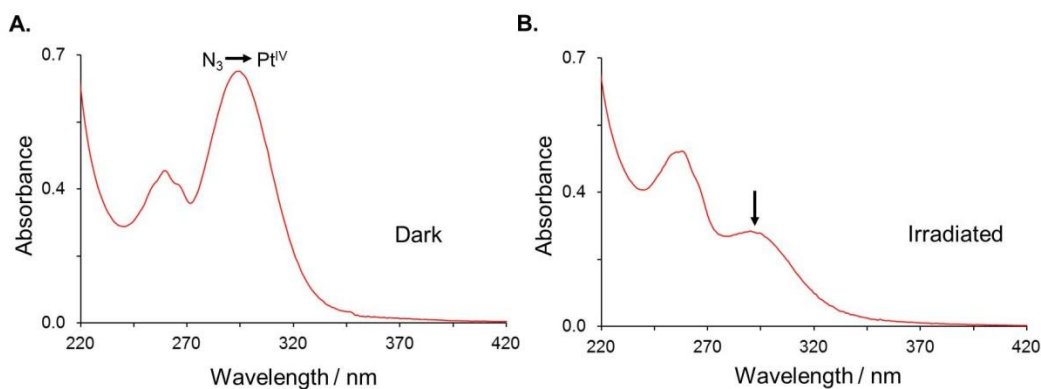
Figure 4.3 Absorption spectrum of complex **40** (50 μM) prepared in PBS/D$_2$O at pH* 7.4 in the (**A**) dark; N$_3$→Pt^{IV} LMCT band at ca. 294 nm ($\varepsilon_{294nm} = 1.35 \times 10^4$ M^{-1} cm^{-1}) and (**B**) after 30 min irradiation with 463 nm light, ↓ shows a decrease in the LMCT band ($\varepsilon_{294nm} = 0.5 \times 10^4$ M^{-1} cm^{-1}).

There is no absorption from Gly over the range shown (Figure 4.4**A**), as such, subsequent mol equiv additions of Gly to a solution of complex **40** (50 μM) did not affect the absorption of the LMCT band of complex **40**, in the dark (Figure 4.4**B**). Irradiating complex **40** in both the absence and presence of Gly (0.5 and 4 mol equiv) for 30 min with 463 nm light led to a decrease of ca. 40% in the LMCT band (Figure 4.4**C**). This equivalent photo-decomposition of complex **40** in the presence of Gly (up to 4 mol equiv), suggests that Gly does not affect the photo-activation of complex **40**.
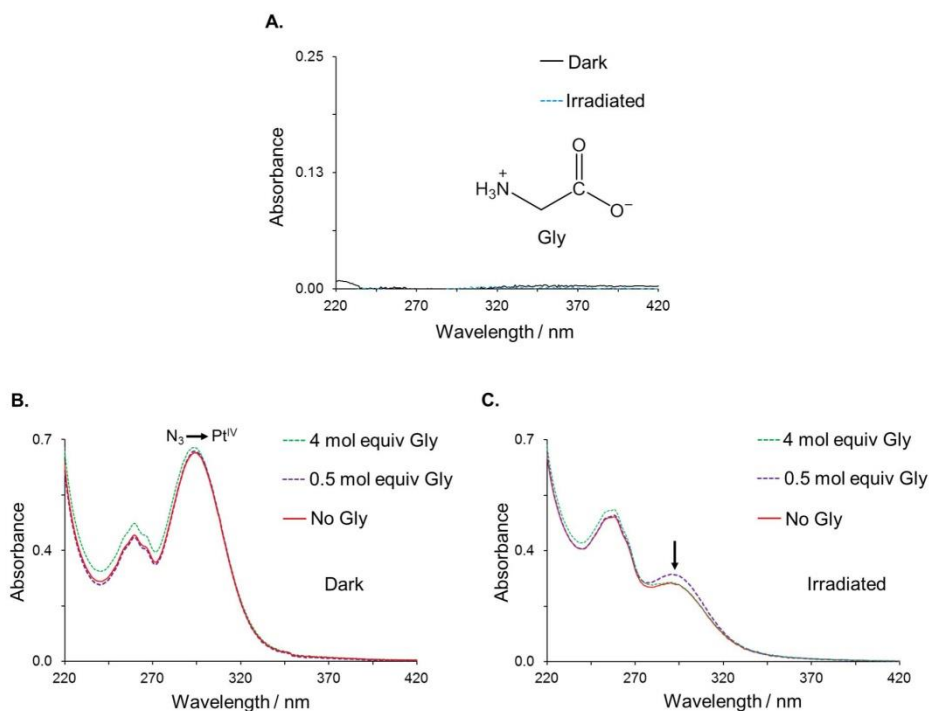
Figure 4.4 Absorption spectrum of solutions of (**A**) glycine (50 μM) prepared in PBS/D$_2$O at pH* 7.4 in the dark and after 30 min irradiation with 463 nm light; and solutions of complex **40** (50 μM) in the presence of Gly (0.5 and 4 mol equiv) prepared in PBS/D$_2$O at pH* 7.4 in the (**B**) dark; (**C**) after 30 min irradiation with 463 nm, ↓ shows a decrease in the LMCT band.

4.3.1.2 In the presence of aromatic amino acids.

Next, aromatic amino acids L-Tyr and L-Trp were studied (Figure 4.2). Aromatic amino acids have an absorbance in the region of < 300 nm. L-Tyr and L-Trp exhibit maximum absorbance's at ca. 274 nm and 278 nm, respectively, as reported by Fasman.[17]

L-Tyr (50 μM) prepared in PBS/D$_2$O at pH* 7.4, was photo-stable exhibiting an extinction coefficient of ca. 1.8×10^4 M^{-1} cm^{-1} at ca. 274 nm, both before and after irradiation with 463 nm light (Figure 4.5**A**). Supplementing a solution of complex

40 (50 μM) with L-Tyr (0.5 and 4 mol equiv) enhanced the absorbance in the dark (Figure 4.5**B**). This increase was attributable to the sum of both complex **40** and L-Tyr absorbance's. Photo-irradiation of solutions containing complex **40** (50 μM) in the presence of L-Tyr (0.5 and 4 mol equiv) with 463 nm light for 30 min, led to a decrease of ca. 40% in the LMCT band, comparable to the photo-decomposition of complex **40** alone (Figure 4.5**C**). From this result, it is reasonable to deduce that L-Tyr does not affect the photo-activation of complex **40**.
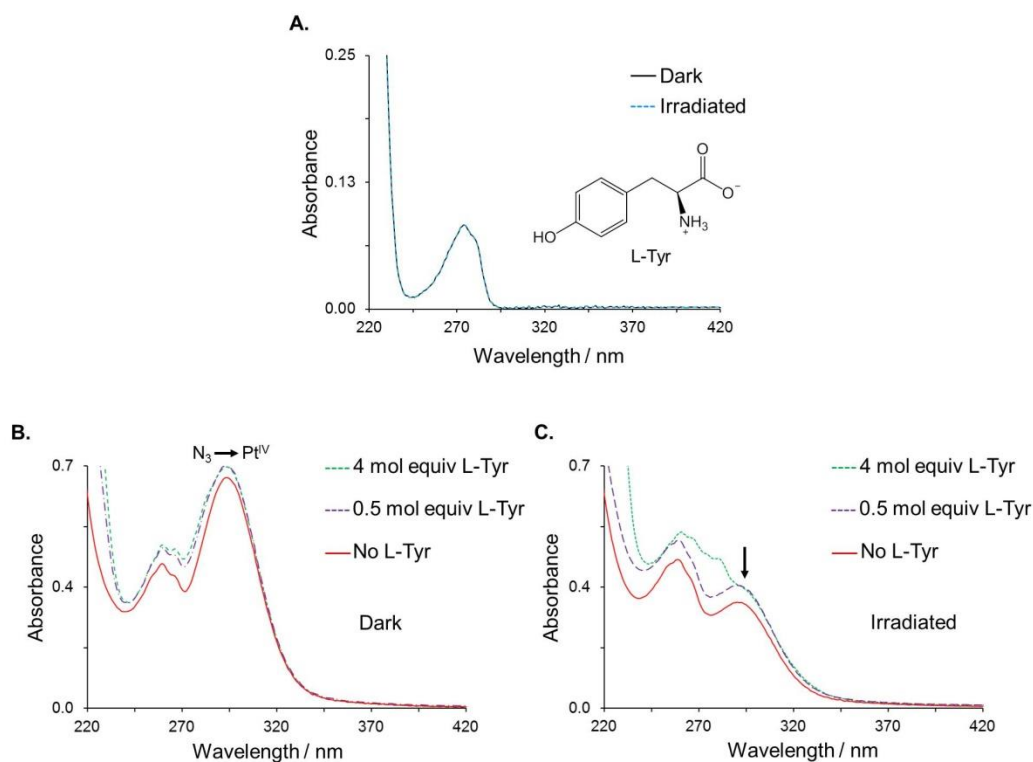

Figure 4.5 Absorption spectra of (**A**) L-Tyr (50 μM) prepared in PBS/D_2O at pH* 7.4 in the dark and after 30 min irradiation with 463 nm light; and solutions containing complex **40** (50 μM) in the presence of L-Tyr (0.5 and 4 mol equiv) prepared in PBS/D_2O at pH* 7.4 in the (**B**) dark and (**C**) after irradiation at 463 nm for 30 min, ↓ shows a decrease in the LMCT band.

L-Trp exhibits two absorption bands due to both the $\pi\rightarrow\pi^*$ (190 nm) and $n\rightarrow\pi^*$ (278 nm)[17] transitions (Figure 4.6**A**). L-Trp was photo-stable towards irradiation at 463 nm light, displaying a constant absorption at ca. 278 nm (Figure 4.6**A**). Solutions containing complex **40** (50 μM) and L-Trp (various mol equiv) were prepared in PBS/D$_2$O at pH* 7.4. As can be seen from Figure 4.6**B**, successive additions of L-Trp led to an increase in the absorbance region of the $N_3\rightarrow Pt^{IV}$ LMCT band absorption. This increase was attributable to the absorption by L-Trp.
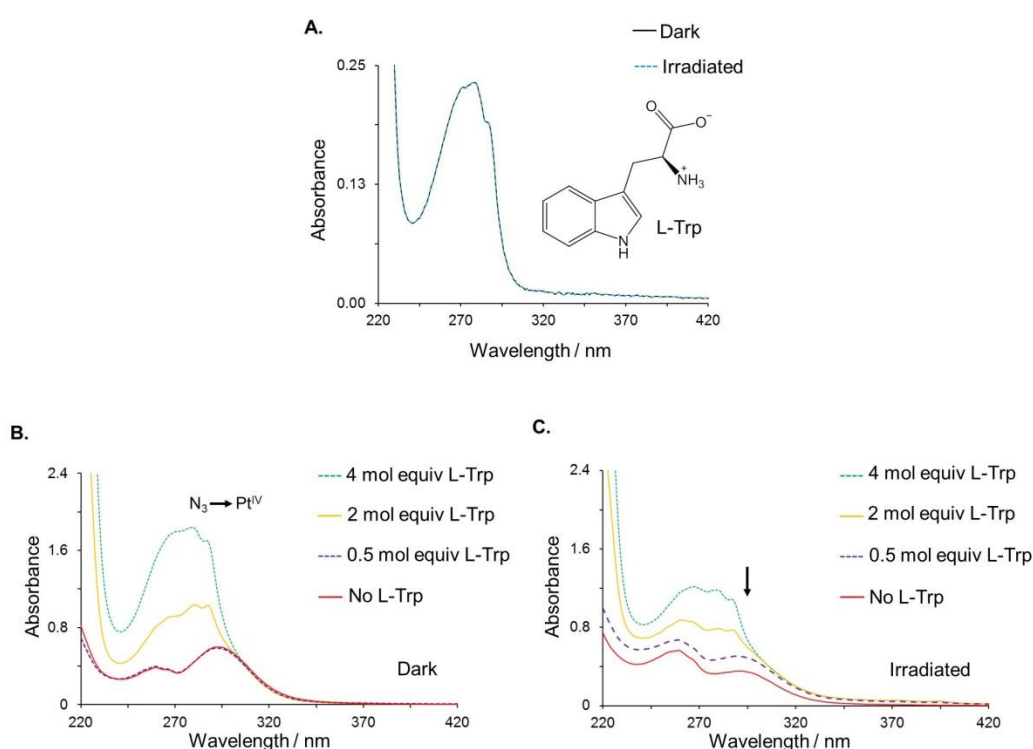

Figure 4.6 Absorption spectra of (**A**) L-Trp (50 μM) prepared in PBS/D$_2$O at pH* 7.4 in the dark and after 30 min irradiation with 463 nm light; and solutions containing complex **40** (50 μM) in the presence of L-Trp (different mol equiv) prepared in PBS/D$_2$O at pH* 7.4 in the (**B**) dark and (**C**) after irradiation at 463 nm for 30 min, ↓ shows a decrease in the LMCT band.

The $N_3 \rightarrow Pt^{IV}$ LMCT band of complex **40** decreased to a similar extent in both the absence and presence of L-Trp, attributable to an equivalent release of the azide ligands (Figure 4.6**C**). As a result, the UV-visible data suggest that photo-irradiation of complex **40** in the presence of amino acids; Gly, L-Tyr and L-Trp proceeds through two one-electron donations from the azide ligands to the Pt^{IV} metal centre. $^\bullet N_3$ radicals are reported to undergo one-electron transfer reactions with amino acids. This possible interaction was investigated by performing spin trapping EPR spectroscopy.

4.3.2 EPR spectroscopy

The EPR spectrum of complex **40** in the presence of amino acids Gly, L-Tyr and L-Trp was recorded and did not produce any EPR signals in the dark (Figure A4.1). Therefore, photo-irradiation experiments were performed.

Solutions of complex **40** (4 mM), DMPO (8 mM) were irradiated with 463 nm light prepared in PBS/D_2O at pH* 7.4 in the presence of 0.5 mM and 1 mM Gly. A comparable concentration of the DMPO-N_3 spin adduct was formed in both the absence and presence of Gly (Figure 4.7**A**). The quantity and decomposition of the DMPO-N_3 spin adduct followed a similar trend despite the presence of Gly.

Similarly, continuous irradiation for 28 min of complex **40** with 463 nm light in the presence of 0.5 mM and 1 mM L-Tyr did not induce any effect in the trapping of the azidyl radicals by DMPO (Figure 4.7**B**).
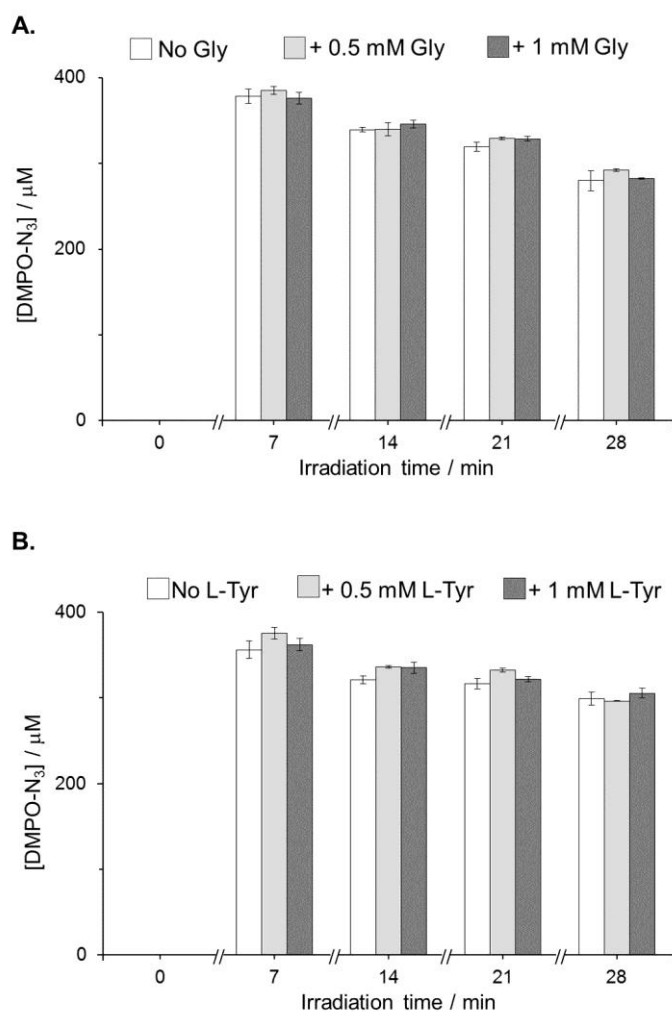
Figure 4.7 Quantification of the DMPO-N_3 spin adduct formed after 7 min, 14 min, 21 min and 28 min of irradiation at 463 nm of a solution containing complex **40** (4 mM) with DMPO (8 mM) in the (□), absence and presence of (▨), 0.5 mM; (▨), 1 mM (**A**) Gly and (**B**) L-Tyr prepared in PBS/D_2O at pH* 7.4 at 291 K. No EPR spectrum was observed in the dark (0 min). Error bars represent the standard deviation from three independent experiments.

The DMPO-N_3 spin adduct exhibited a concentration maximum of ca. 360 μM in both the absence and presence of Gly and L-Tyr after 7 min irradiation with 463 nm light. These results suggest that under these conditions the $^\bullet N_3$ radicals are unreactive to either the carboxylate or the amino group(s) present in these amino

acids, which may extend across the range amino acids. Previous literature has reported on the inert nature of the $^\bullet N_3$ radicals towards phenylalanine, alanine and valine.[18]

Irradiation of complex **40** (4 mM) and DMPO (8 mM) at 463 nm generates the DMPO-N_3 spin adduct, quartet of triplets EPR spectrum (Figure 4.8**A**), previously characterised in **Chapter III**. However, in presence of 0.5 mM (Figure 4.8**B**) and 1 mM (Figure 4.8**C**) L-Trp, a partial and complete suppression in the DMPO-N_3 spin adduct was observed, respectively.

Interestingly, in the presence of 0.5 mM L-Trp, the DMPO-N_3 spin adduct was suppressed by ca. 85%, determined after 7 min irradiation. This was reduced to ca. 70% after 14 min irradiation. The effect of L-Trp on the trapping of the $^\bullet N_3$ radicals produced from photo-irradiated complex **40** can be seen quantitatively in Figure 4.9.

This result above differed from that observed for the photo-irradiation of complex **40** in the presence of Gly or L-Tyr. Thus, these EPR data suggested a possible interaction of the $^\bullet N_3$ radicals with L-Trp. To further investigate this potential interaction, NMR spectroscopy was performed.
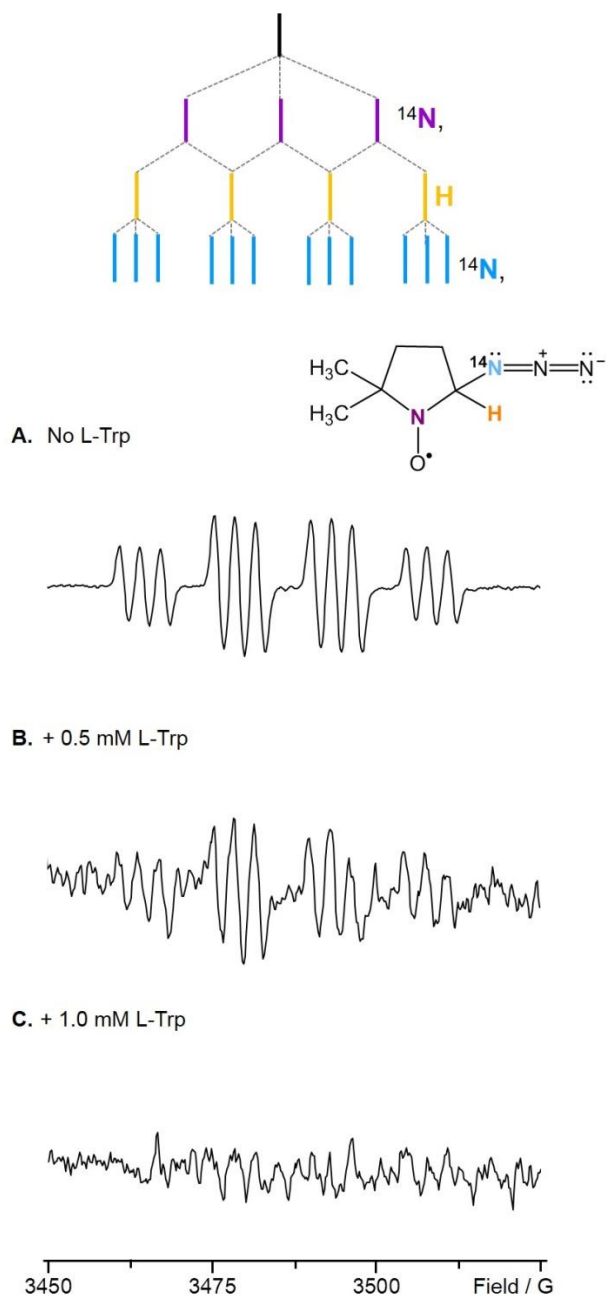
Figure 4.8 DMPO-N$_3$ spin adduct EPR spectra formed from the photo-irradiation of complex **40** (4 mM) and DMPO (8 mM) in (**A**) absence; (**B**) in the presence of 0.5 mM and (**C**) 1 mM L-Trp prepared in PBS/D$_2$O at pH* 7.4 at 291 K with 463 nm light after 7 min.
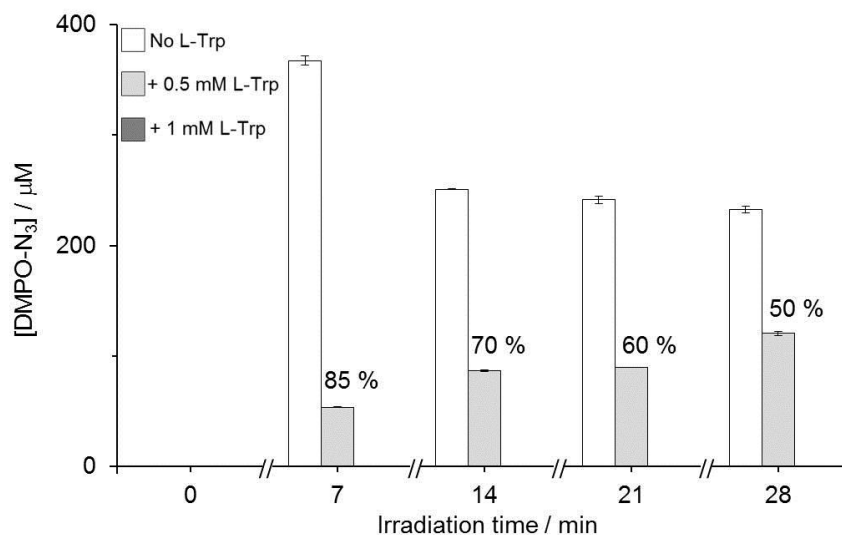
Figure 4.9 Quantification and percentage suppression of the DMPO-N$_3$ spin adduct formed after 7 min, 14 min, 21 min and 28 min from irradiation with 463 nm light of a solution containing complex **40** (4 mM) and DMPO (8 mM) in the (□) absence and presence of (▢) 0.5 mM; (■) 1 mM L-Trp prepared in PBS/D$_2$O at pH* 7.4 at 291 K. No EPR spectra were observed in the dark (0 min) in the absence or in the presence of 1 mM L-Trp. Error bars represent the standard deviation from three independent experiments.

4.3.3 ^{1}H NMR spectroscopy

4.3.3.1 Absence of L-Trp

Prior to studying the photo-irradiation of complex **40** with L-Trp, the photo-irradiation of complex **40** in the presence of the spin trap DMPO was initially studied. A solution containing complex **40** (4 mM) and DMPO (8 mM) was prepared in PBS/D$_2$O at pH* 7.4. The ^{1}H NMR spectrum of the diamagnetic spin trap DMPO alone displayed four resonances (Figure 4.10), unaffected by irradiation with 463 nm light. Additionally, the ^{1}H NMR resonances showed that

both complex **40** and DMPO were stable in the dark prior to photo-irradiation (Figure 4.11**A**).
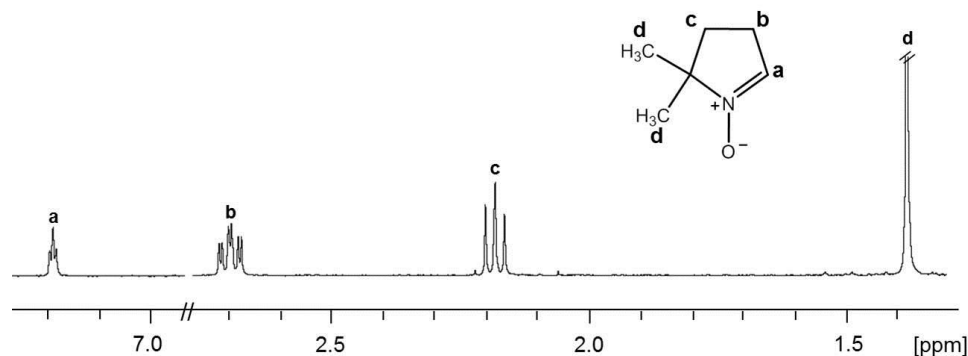

Figure 4.10 ^{1}H NMR spectrum of 5,5-dimethyl-1-pyrroline-*N*-oxide (DMPO, 5 mM) in PBS/D$_2$O at pH* 7.4 at 298K.

Irradiation of complex **40** (4 mM) and DMPO (8 mM) with 463 nm light for 30 min led the solution to lighten in colour and generate a yellow coloured precipitate (Figure 4.12). The precipitate was removed by centrifugation and filtration, prior to recording the ^{1}H NMR spectrum. Bubbles thought to be due to N$_2$ gas, from the dimerisation of the $^\bullet$N$_3$ radicals were observed, as previously reported.[1] The extracted precipitate could not be dissolved in a variety of either polar (water, ethanol, methanol) or non-polar (benzene, toluene) solvents.

Photo-irradiation of complex **40** led to ca. 40% reduction in the pyridine proton resonances consistent with previous reports[1] on the photo-decomposition of complex **40**. Furthermore, new photo-generated peaks (**e′-i′**) were observed after 30 min irradiation of complex **40** with 463 nm light (Figure 4.11**B**).
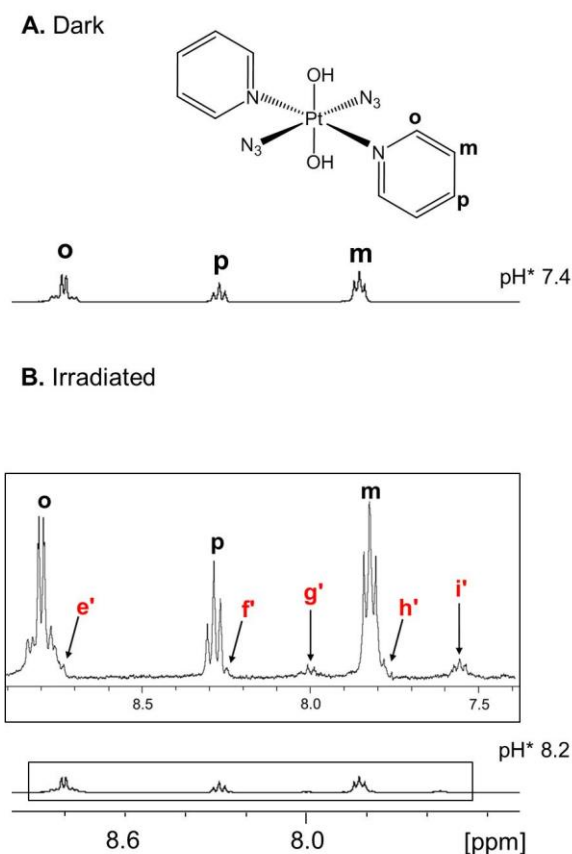
Figure 4.11 The aromatic region of the ^{1}H NMR spectra from a solution of complex **40** (4 mM) and DMPO (8 mM) prepared in PBS/D$_2$O buffer at pH* 7.4 in (**A**) dark and (**B**) after 30 min irradiation with 463 nm light. Assignments: Pt-py peaks, (**o/p/m**); platinum photoproducts, (**e'-i'**). Inset (6× magnification) is an expansion of the 8.9 – 7.4 ppm region of the formed photo-products. Refer to Figure 4.13 for DMPO ^{1}H NMR resonances.

Figure 4.12 Precipitate from the photo-irradiation of complex **40** (4 mM) with DMPO (8 mM) with 463 nm light prepared in PBS/D$_2$O at pH* 7.4. Magnified (4x) image of precipitate in the included inset.

The assignment of photo-generated peaks **e′-i′** (Figure 4.11**B**) was made by comparison of the Pt-py resonances of complex **40**, Pt^{II}-py intermediates (intermediate complexes formed during the synthesis of complex **40**) and free pyridine ^{1}H NMR chemical shifts. It is postulated that the ^{1}H resonances **e′**, **f′** and **h′** are in close agreement with those belonging to a Pt^{IV}-py based species, whereas, **g′** and **i′** resonances are in closer agreement being assigned to the H_p and H_m resonances of a Pt^{II}-py based species, respectively (Table 4.1).

None of the platinum photo-generated peaks (**e′-i′**) corresponded to that of free pyridine, suggesting all new peaks are likely to arise from coordinated pyridine. This is in agreement with previous reports on the photo-stability of the Pt-py bond, both before and after irradiation.[1]

Table 4.4 Assignment of the platinum photo-products (**e′- i′**) shown in Figure 4.11**B**.

Photo-products	δ / ppm	^{1}H Resonance
e′	8.73	H_O (Pt^{IV}-py)
f′	8.25	$-^b$ (Pt^{IV}-py)
g′	8.01	H_p (Pt^{II}-py)
h′	7.77	$-^b$ (Pt^{IV}-py)
i′	7.56	H_m (Pt^{II}-py)

^{b}complete peak assignment not feasible.

The photo-irradiation of complex **40** (4 mM) in the presence of DMPO (8 mM) with 463 nm light was repeated in D_2O. Equivalent photo-products (**e′-i′**) were identified (Figure A4.2), confirming that the presence of the chloride (0.0027 M) and phosphate (0.01 M) in the PBS buffer did not affect the photo-activation or photo-decomposition of complex **40**. This is a similar chloride concentration as in the cell nucleus (ca. 4 mM), which suggests that an equivalent photo-decomposition pathway of complex **40** could occur in cells.

As shown in **Chapter III** (Figure 3.8, p 106), the DMPO-N_3 spin adduct decayed with prolonged irradiation. The decomposition of spin adducts has been reported to proceed via a disproportionation reaction pathway, forming both a nitrone and hydroxylamine species (Figure 4.13), with the latter reported to be the main decomposition product.[19-21]
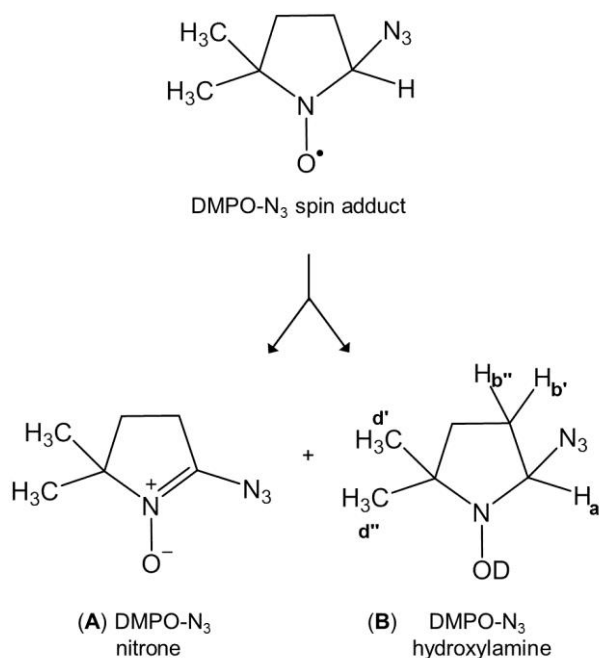

Figure 4.13 Decomposition pathway of the DMPO-N_3 spin adduct into either a DMPO-N_3 (**A**) nitrone, or (**B**) hydroxylamine species, both NMR detectable.

Therefore, photo-products (**a'-d''**) formed from the photo-irradiation of complex **40** (4 mM) with DMPO (8 mM) at 463 nm for 30 min prepared in PBS/D$_2$O at pH* 7.4 (Figure 4.14), are believed to be related to the DMPO-N$_3$ hydroxylamine species (Figure 4.13**B**). Assignments of the ^{1}H NMR resonances of the photo-products **a'** - **d''** are summarised in Table 4.2, and are in close agreement with previous ^{1}H NMR studies of a DMPO-SO$_3$ hydroxylamine species.[22]
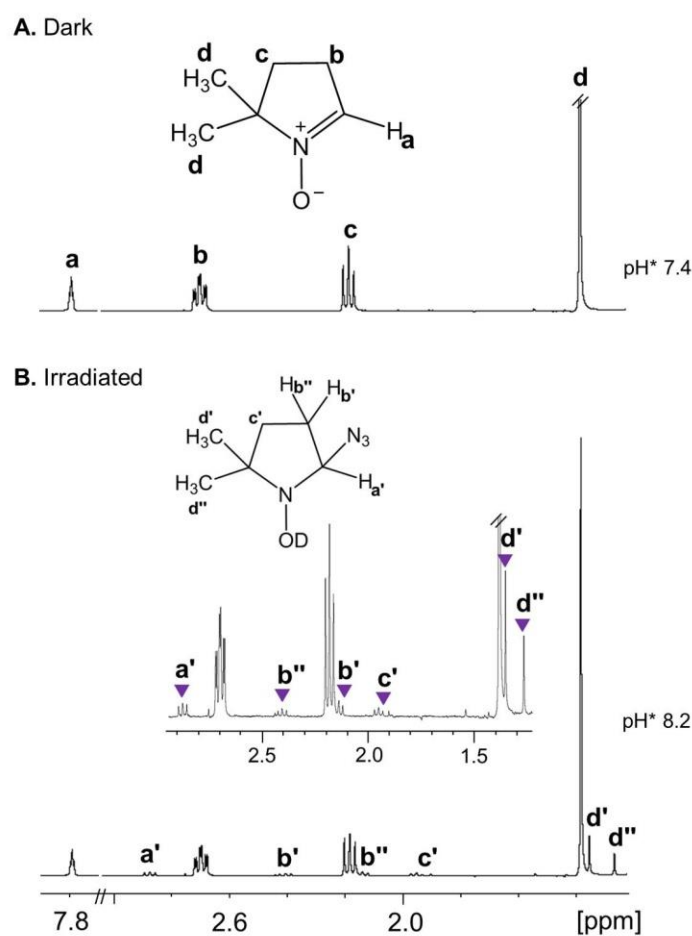

Figure 4.14 The ^{1}H NMR spectra from a solution of complex **40** (4 mM) and DMPO (8 mM) prepared in PBS/D$_2$O buffer at pH* 7.4 in (**A**) dark and (**B**) after irradiation at 463 nm for 30 min. Assignments: DMPO peaks, (**a-d**); DMPO-N$_3$ hydroxylamine peaks, (**a'- d''**). Inset (×4) is an expansion of the 2.9 − 1.3 ppm region of the formed photo-products. Refer to Figure 4.11 for complex **40** region.

Table 4.2 Assignment of the photo-products (**a′**- **d″**) shown in Figure 4.14**B** to the DMPO-N$_3$ hydroxylamine species.

δ / ppm	Assignment	DMPO-N$_3$ Hydroxylamine
2.872	C^{2}H (**a'**)	
2.406	C^{3}H$_A$ (**b'**)	
2.139	C^{3}H$_B$ (**b''**)	
1.952	C^{4}H$_2$ (**c'**)	
1.352	C^{6}H$_3$ (**d'**)	
1.266	C^{7}H$_3$ (**d''**)	

Through ^{1}H NMR integration, it was determined ca. 40% of complex **40** had photo-decomposed after 30 min irradiation with 463 nm light (Figure 4.11**B**), whilst the spin trap, DMPO photo-decomposed by ca. 12% (Figure 4.14**B)**. This decrease in the ^{1}H NMR resonances of DMPO is attributed to the transformation of diamagnetic DMPO into the paramagnetic DMPO-N$_3$ spin adduct. It was determined *via* ^{1}H NMR integration that ca. 0.74 mM of the DMPO-N$_3$ hydroxylamine species was present in solution. Integrals of both parental and photo-products generated in both Figures 4.11 and 4.14 are summarised in Table 4.3.

Table 4.3 Quantification of the species observed in both Figures 4.11 and 4.14 determined by ^{1}H NMR integration.

Species	Conc Start / (mM)	Conc After[b] / (mM)
Complex **40** (**o/m/p**)	4	2.4
DMPO (**a-d**)	8	7.0
Pt-photoproducts (**e'-i'**)	-[a]	0.6
DMPO-N$_3$ hydroxylamine (**a'-d"**)	-[a]	0.7

[a]peaks not present in the dark; [b]solutions irradiated for 30 min with 463 nm light and precipitate removed prior to recording the ^{1}H NMR.

4.3.3.2 In the presence of L-Trp

The photo-stability of L-Trp was previously reported in **section 4.3.1**, however it was further confirmed *via* ^{1}H NMR spectroscopy (Figure 4.15).
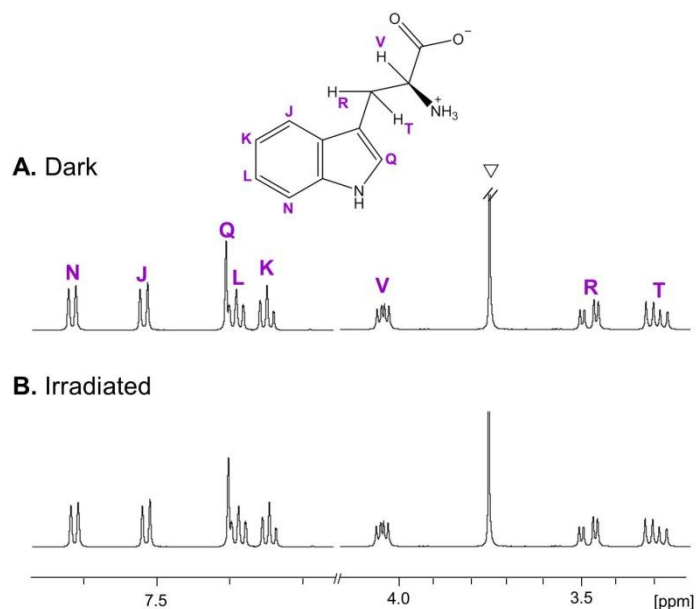

Figure 4.15 ^{1}H NMR spectra of L-Trp (8 mM) prepared in PBS/D$_2$O at pH* 7.4 in (**A**) the dark and (**B**) after irradiation at 463 nm for 30 min. Assignments: L-Trp peaks, (**J-V**); internal reference 1,4 dioxane, ($\triangledown$).

The ^{1}H NMR resonances of complex **40** (4 mM) with DMPO (2 mol equiv) in the dark remained unchanged in the presence (Figure 4.16**A**) of L-Trp (2 mol equiv), indicating no dark interaction. The overlap between L-Trp (H$_\mathbf{K}$) and the DMPO spin trap (H$_\mathbf{a}$) slightly obscured their ^{1}H resonances (◆, Figure 4.16**A**). Irradiation of complex **40** (4 mM) with DMPO (8 mM) in the presence of L-Trp (2 mol equiv, 8 mM) at 463 nm led the solution to lighten in colour and generate a yellow-brown dark coloured precipitate (Figure 4.17). The precipitate was removed by centrifugation and filtration prior to recording the ^{1}H NMR spectrum. The precipitate was insoluble in a variety of solvents, so solution-phase NMR spectroscopy was not feasible. Furthermore, bubbles were observed in the NMR tube consistent with previous reports on the radical dimerisation of two $^\bullet$N$_3$ radicals forming N$_2$ gas.[1]

Integrating the signals present in Figure 4.16 revealed that ca. 40% of complex **40** had photo-decomposed after 30 min irradiation with 463 nm light, similar to that observed in the absence of L-Trp (Table 4.7). Furthermore, platinum photo-products (**e'**-**i'**) were observed in the presence of L-Trp (inset Figure 4.16**B**). Additionally, only in the presence of irradiated complex **40**, was a decrease of ca. 20% in the L-Trp peaks observed. Moreover, the ^{1}H NMR resonances of spin trap DMPO remained consistent both before and after irradiation, with no detection of new peaks previously assigned to the DMPO-N$_3$ hydroxylamine species. All species present in Figure 4.16 were quantified by ^{1}H NMR integration and are summarised in Table 4.7.
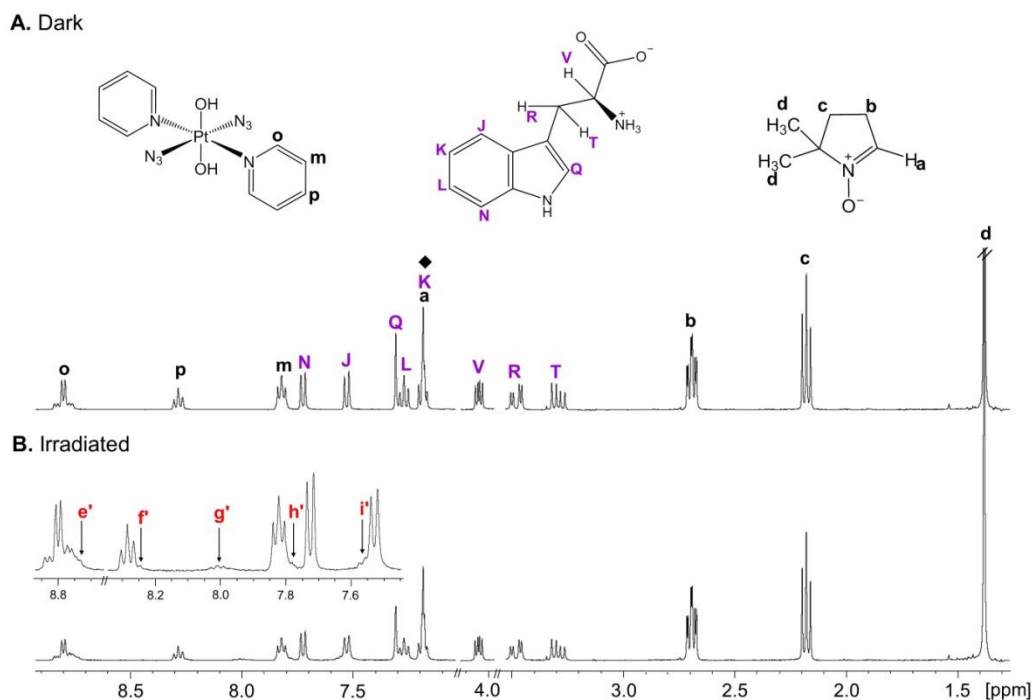
Figure 4.16 ^{1}H NMR spectra of a solution of complex **40** (4 mM) and DMPO (8 mM) in the presence of L-Trp (2 mol equiv, 8 mM) prepared in PBS/D$_2$O buffer at pH* 7.4 in the (**A**) dark and (**B**) after 30 min irradiation with 463 nm light. Assignments: Pt-py peaks, (**o**/**p**/**m**); L-Trp peaks, (**J**-**V**); DMPO peaks, (**a-d**); Pt-photo-products, (**e'-i'**); (◆), overlap of peaks from L-Trp (H$_K$) and DMPO (H$_a$).

Figure 4.17 Precipitate from the photo-irradiation of complex **40** (4 mM) and DMPO (8 mM) in the presence of L-Trp (2 mol equiv) with 463 nm light prepared in PBS/D$_2$O at pH* 7.4. Magnified (4x) image of precipitate in the included inset.

Table 4.7 Quantification of the species observed in Figure 4.16 by ^{1}H NMR integration.

Peaks Assignment	Conc Start/ (mM)	Conc After^b /(mM)
Complex **40** (**o/m/p**)	4	2.4
DMPO (**a-d**)	8	8
L-Trp (**J-V**)	8	6.2
Pt-photoproducts (**e'-i'**)	$-^a$	0.6

^{a}peaks not present in the dark; ^{b}solutions irradiated for 30 min and precipitate removed prior to recording the ^{1}H NMR spectrum.

The lack of detection of the ^{1}H NMR resonances related to the DMPO-N$_3$ hydroxylamine species in the presence of L-Trp, further supports the potential reaction between photo-activated complex **40** and L-Trp. As described in section **4.3.1**, the interaction between $^•$N$_3$ radicals and L-Trp has been reported to proceed via one-electron transfer generating both free azide (N$_3^-$) and L-Trp$^{•+}$, the latter readily deprotonates to L-Trp$^•$ at pH 7.[9] In an attempt to establish such an interaction between $^•$N$_3$ radicals generated from photo-activated complex **40** with L-Trp, ^{14}N NMR spectroscopy was performed.

4.3.4 Free azide (N$_3^-$) detection

Due to the lower sensitivity (receptivity relative to ^{1}H at 100 % = 1.01 $\times10^{-3}$) and quadrupolar nature[23] of the ^{14}N nucleus, ^{14}N NMR spectroscopy was performed at higher concentrations (ca. 2.25 fold higher mol equiv). The ^{14}N NMR spectrum of L-Trp displayed a peak at 17.1 ppm (Figure 4.18**A**), assigned to the nitrogen (**N**H) atom present in the indole ring. The additional ^{14}N NMR resonance for the α-

amino ($^+$NH$_3$) group was not observed in the region shown. This was in agreement with previous ^{14}N NMR spectroscopic reports on Gly, Glu (glutamic acid) and Arg (arginine) in which the α-amino group ($^+$NH$_3$) ^{14}N NMR resonance was reported at ca. > -300 ppm.[24] Irradiation of L-Trp for 30 min with 463 nm light did not have any effect on its ^{14}N NMR resonance (Figure 4.18**B**) consistent with its photo-stability.
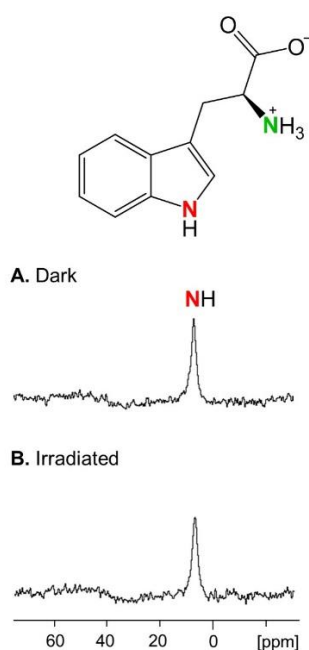

Figure 4.18 The ^{14}N NMR spectra of L-Trp (18 mM) in PBS/D$_2$O at pH* 7.4 in (**A**) the dark and (**B**) after 30 min irradiation with 463 nm light. The resonance at 17.1 ppm is assigned to the amine (**N**H) group present in L-Trp. This resonance remains unchanged after irradiation confirming the photo-stability of L-Trp. The amino group present in the side chain of L-Trp is not observed in this range ($^+$**N**H$_3$, δ ~ -300 ppm).[24]

Dark solutions containing complex **40** (9 mM) both in the presence (Figure 4.19**A**) and absence (Figure 4.19**B**) of L-Trp (2 mol equiv, 18 mM) prepared in PBS/D$_2$O at pH* 7.4, exhibited resonances related to the coordinated azide (**N**$_\beta$

and $N\gamma$) and pyridine (**N**) ligands of complex **40**. In the presence of L-Trp, an additional resonance was observed at 15.7 ppm and is assigned to the nitrogen atom of the indole ring (**N**H) functional group.
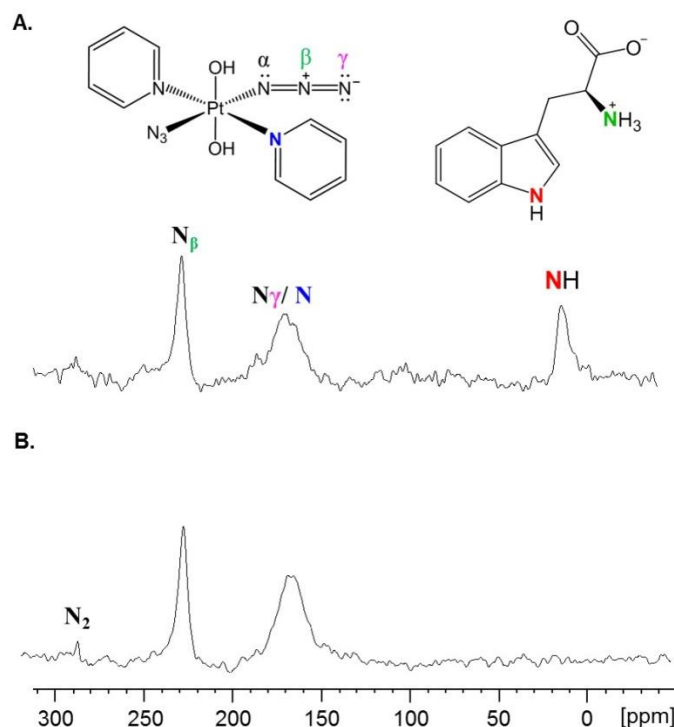

Figure 4.19 Dark ^{14}N NMR spectra of complex **40** (9 mM) in (**A**) the presence and (**B**) absence of L-Trp (2 mol equiv, 18 mM) prepared in PBS/D$_2$O at pH* 7.4. The peak for the terminal nitrogen atom of the coordinated azide (**N**γ) is overlapped with the pyridine (**N**) at ca. 168.1 ppm. The appearance of the Nα peak of complex **40** (expected at ca. 60 ppm) is dependent on viscosity and temperature and is too broad to observe under the conditions used due to a strong inhomogeneity in the electric field at N$_\alpha$.[25] Assignments: δ = 288.9 (N$_2$, atmospheric nitrogen gas), 227.5 (N$_\beta$, central N of coordinated azide), 15.7 (indole **N**H of L-Trp).

The **N**H resonance of L-Trp was slightly upfield-shifted in the presence of complex **40** and is attributed to a weak interaction with the platinum(IV) diazido

complex. Irradiation of complex **40** (9 mM) in the presence of L-Trp (2 mol equiv, 18 mM) with 463 nm light for 30 min resulted in the formation of a new peak (**N$_\beta'$**) at 77.3 ppm (Figure 4.20**A**) assigned as the central nitrogen of free azide.
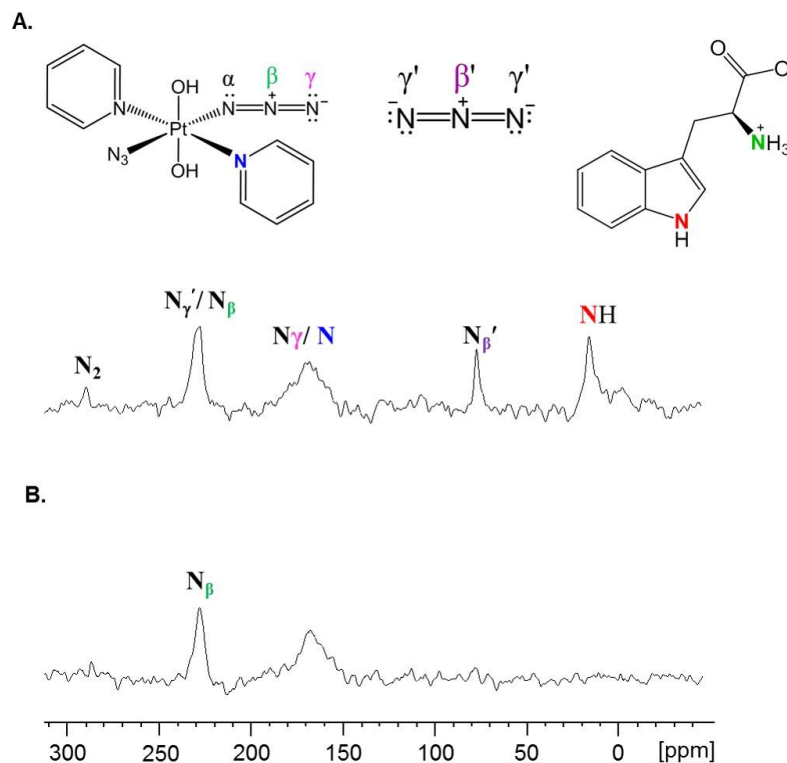

Figure 4.20 ^{14}N NMR spectra of complex **40** (9 mM) irradiated at 463 nm for 30 min in the (**A**) presence and (**B**) absence of L-Trp (2 mol equiv, 18 mM) prepared in PBS/D$_2$O at pH* 7.4. The new ^{14}N NMR resonance at 77.3 ppm (**N$_\beta'$**) is assigned to the central N of free azide. Overlap between the terminal nitrogen of N$_3^-$ (Nγ', δ = 228.2) with the central nitrogen of coordinated azide (**N$_\beta$**, 228.7). Assignments: δ = 288.9 (N$_2$), 77.3 (**N$_\beta'$** central nitrogen of N$_3^-$) and as labelled in Figure 4.19.

The overlap between the resonances for the terminal (Nγ') nitrogen of free azide ($^-$N$_3$) with the central nitrogen of coordinated azide, meant this peak alone was not indicative of the formation of free azide ($^-$N$_3$). Comparison of the spectra in

Figures 4.19 and 4.20, observed a decrease in the ^{14}N NMR resonances of both complex **40** and L-Trp. The **N**H resonance of L-Trp at ca. 15.7 ppm decreased in its intensity by ca. two-fold, only in the presence of irradiated complex **40**. This decrease and the subsequent detection of N_3^- supports the postulated one-electron transfer reaction between the $^•N_3$ radicals generated from photo-irradiated complex **40** with L-Trp. N_3^- is generally considered to be a species with toxicity comparable to that of cyanide.[26] Therefore, photo-irradiation of complex **40** in the presence of L-Trp was thought to enhance the photo-cytotoxicity profile of complex **40**. To examine this hypothesis, photo-irradiation studies in A2780 ovarian cancer cells were undertaken.

4.3.5 Cell studies

4.3.5.1 Photo-irradiation in A2780 ovarian cancer cells

Cell studies performed by Dr. Julie Woods showed that neither complex **40** alone nor complex **40** in the presence of L-Trp exhibited any effects on the cell growth in the dark under the experimental conditions used (■, Figure 4.21). Similarly, blue light (λ = 420 nm, 5 J cm^{-2}) did not produce any observable effects towards A2780 ovarian cancer cells (cell viability of 115.7 ± 9.4%). However, it can be seen that co-incubation of complex **40** (42.5 μM) in variable concentrations of L-Trp (0 - 2 mM), reduced cell death following irradiation at 420 nm (■, Figure 4.21). This photo-protective effect enhanced with successive addition of L-Trp (62.5 μM – 500 μM). However, the extent of photo-protection appeared to reach a plateau at ca. 85%, in the presence of L-Trp (0.5 -2 mM).
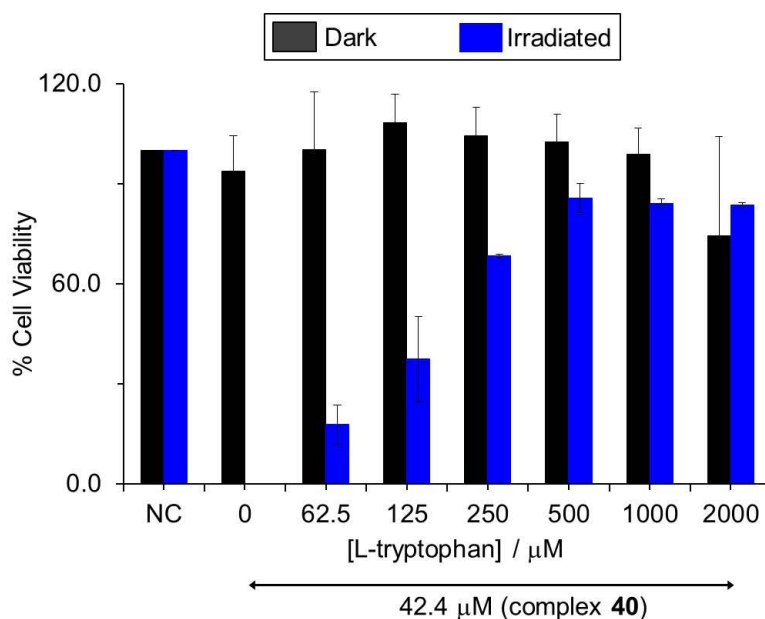
Figure 4.21 Ability of photo-activated complex **40** (42.4 μM, n = 3 independent experiments) to reduce the cell viability in A2780 ovarian cancer cells in the presence of L-Trp (varied concentrations) in the (■) dark and (■) after irradiation at λ_{max} = 420 nm (5 J cm^{-2}). NC: negative control (no L-Trp or complex **40**). Data represent means ± standard errors of the mean for three independent experiments performed in triplicate.

Co-incubation of 0.5 mM L-Trp with a variable concentration of complex **40** (0-105 μM) reduced cell death (Figure 4.22), leading to a protection factor of ca. 7 based on IC$_{50}$ values (Table 4.8).
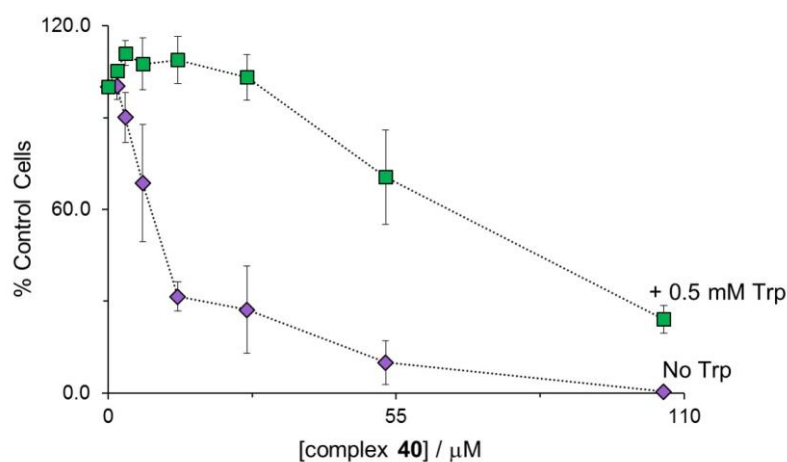
Figure 4.22 Ability of photo-activated complex **40** (varied concentration) to reduce the viability of A2780 human ovarian cancer cells (◆) in the absence and (■) presence of 0.5 mM L-Trp at 420 nm (5 J cm^{-2}). Data represent means ± standard errors of the mean for three independent experiments performed in triplicate.

Table 4.8 Ability of photo-activated complex **40** to reduce the viability of A2780 ovarian cancer cells in both the absence and presence of L-Trp (0.5 mM).

Treatment	IC$_{50}$/(μM)^a	95% interval /(μM)	Confidence R^2
No L-Trp	8.3	3.4-20.4	0.85
+ 0.5 mM L-Trp	59.4	34.7-101.8	0.86

^{a}IC$_{50}$ = concentration of complex **40** that inhibited uptake of the neutral red dye by 50%. Data represent the mean of three independent experiments.

Furthermore, the implication of this photo-protective effect was examined morphologically on A2780 ovarian cancer cells by Dr. Julie Woods using the neutral red uptake dye. The assay is based on the principle that it is absorbed only by viable cells.[27] Interestingly, irradiation of complex **40** (42.4 μM) in the

182

presence of 0.5 mM L-Trp at 420 nm led to the neutral red dye being taken up by the cells 24 h after exposure, indicating viability (Figure 4.23**A**), whereas few viable cells could be seen in the absence of L-Trp (Figure 4.23**B**). Surprisingly, photo-activation of complex **40** in the presence of L-Trp led to a photo-protective effect in A2780 ovarian cancer cells. Despite earlier spectroscopic methods detecting N_3^-, its formation appeared not to induce a cytotoxic effect in A2780 ovarian cancer cells.
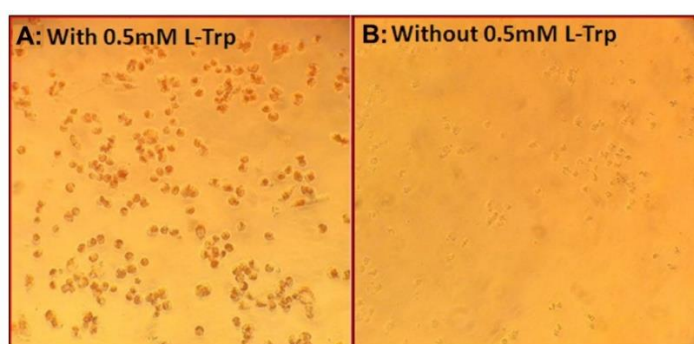

Figure 4.23 Microscopy image of both (**A**) viable and (**B**) non-viable A2780 ovarian cancer cells. Images were obtained from A2780 cells treated with complex **40** (42.4 μM) in the (**A**) presence; (**B**) absence of 0.5 mM L-Trp 24 h after irradiation at 420 nm. The clearly visible intracellular red staining in the left-hand image is neutral red dye (Leica DMIL microscope, 200× magnification).

This photo-protection is postulated to be induced by the quenching of the $^\bullet N_3$ radicals by L-Trp, but could also be due to a reduced Pt uptake of complex **40**. Therefore, ICP-MS was performed to determine the amount of platinum accumulation from complex **40** in both the absence and presence of L-Trp.

4.3.5.2 Platinum accumulation in A2780 ovarian cancer cells

Dark and irradiated cell samples containing complex **40** (42.4 µM) in the absence and presence of L-Trp in A2780 ovarian cancer cells were provided by Dr. Julie Woods. These cell samples for ICP-MS were prepared as described in **Chapter II** for the detection of ^{195}Pt metal. As can be seen from Figure 4.24, in both the dark and irradiated samples, the accumulation of Pt from complex **40** was equivalent in both the (**A**) absence and (**B**) presence of 0.5 mM L-Trp.
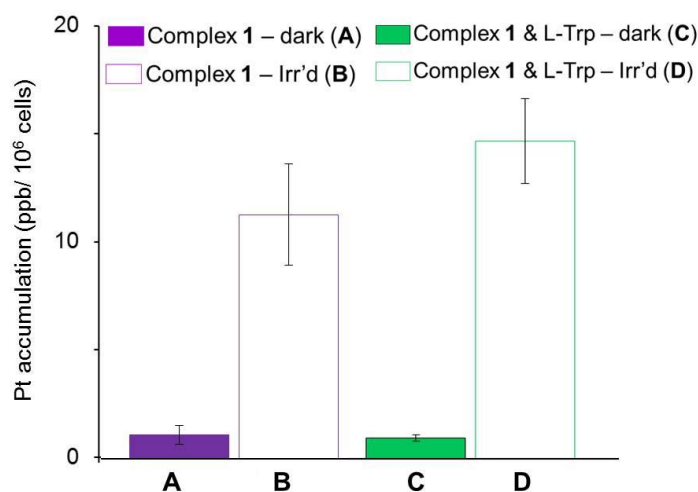

Figure 4.24 ICP-MS of platinum accumulation in A2780 ovarian cancer cells treated with complex **40** (42.4 µM) in the absence (purple bars) and presence (green colour) of L-Trp (0.5 mM) in A2780 ovarian cancer cells. Accumulation was determined for cell samples in the dark (**A** and **C**) and after irradiation (**B** and **D**) at 420 nm. Error bars represent ± standard error of the mean for two independent experiments performed in duplicate.

This confirms that the photo-protective effect of complex **40** in the presence of L-Trp is not due to a reduced uptake of complex **40** in the presence of L-Trp,

suggesting the photo-protective effect is due to the quenching process of the $^\bullet$N$_3$ radicals by L-Trp.

4.3.6 Azidyl radical quenching for a related Pt^{IV} diazido complex

As shown in **Chapter III**, the trapping of the $^\bullet$N$_3$ radicals was not limited to photo-irradiated complex **40** but extended across a range of platinum(IV) diazido complexes (Figure 4.1). Interestingly, photo-irradiation of *trans,trans,trans-*[Pt(N$_3$)$_2$(OH)(*N*-MI)(py)$_2$] (**58**, *N*-MI = methylisatoate 2 mM, Figure 4.1) in the presence of DMPO (4 mM) with 517 nm light generated the lowest yield of the DMPO-N$_3$ spin adduct compared to complexes **56** and **57** (Figure 4.1). This reduction in the DMPO-N$_3$ was suggested to be due to the presence of the methylisatoate (*N*-MI) ligand. Azidyl radicals have been reported to be reactive towards *N*-methylindole and various olefins,[8] suggesting potential reactivity with the *N*-MI ligand. The quenching ability of *N*-MI ligand towards the $^\bullet$N$_3$ radicals was investigated through the photo-irradiation of complex **40** (2 mM, 75% DMF/ 25% H$_2$O), DMPO (2 mol equiv) in the presence and absence of *N*-MI (1 and 2 mol equiv) with 463 nm light for 35 min. No DMPO-N$_3$ spin adduct was formed in the presence of *N*-MI (Figure 4.25), confirming its ability to quench the formed $^\bullet$N$_3$ radicals.

The photolysis of N-methylisatoate has been previously reported to undergo photo-chemical decarboxylation leading to formation of aniline via hydrogen atom abstraction from the solvent.[28] Recent studies have determined a lower photo-cytotoxic activity of complex **58** (Figure 4.1) in A2780 ovarian cancer cells. This was attributed the quenching of the $^\bullet$N$_3$ radicals by *N*-MI.[16] This further

supports the hypothesis that the photo-cytotoxic nature of platinum(IV) diazido complexes involves a radical-based mechanism.
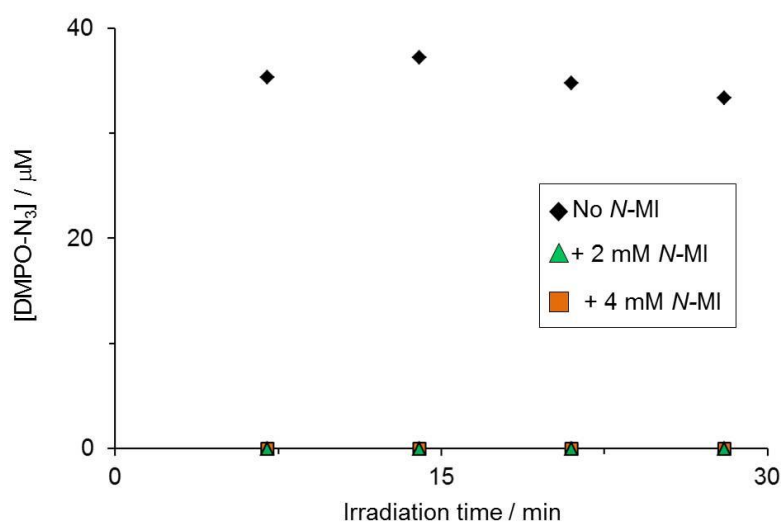

Figure 4.25 Quantification of the DMPO-N$_3$ spin adduct generated from the photo-irradiation of complex **40** (2 mM) in the absence (◆) and presence 1 mol equiv (■); 2 mol equiv (▲) *N*-methylisatoate (*N*-MI) with 463 nm light for 35 min prepared in 75% DMF/ 25% H$_2$O.

4.4 Discussion

4.4.1 Reactivity of the azidyl radicals

The unreactive nature of the $^\bullet$N$_3$ radicals generated by pulse radiolysis towards aliphatic amino acids has been previously reported.[18] Therefore, in this work, the equivalent formation of the DMPO-N$_3$ spin adduct in both the absence and presence of Gly was an expected result. In contrast, previous studies have reported on the oxidation of L-Tyr by $^\bullet$N$_3$ radicals generated by pulse radiolysis,[4,10,18] where the rate of reaction was dependent on the pH of solution (Figure 4.26). Rate constants for pathway **A** of $k_1 = 1.0 \times 10^8$ M^{-1} s^{-1} and pathway **B** of $k_2 = 3.6 \times 10^9$ M^{-1} s^{-1} have been reported for the oxidation of L-Tyr by the $^\bullet$N$_3$ radicals, at

186

different pH values (Figure 4.26). The trapping of $^\bullet N_3$ radicals by DMPO has been reported to proceed with a rate constant of ca. $k = 1.6 \times 10^9 \, M^{-1} \, s^{-1}$.[29] In this work, a competition for reaction of the $^\bullet N_3$ radicals with DMPO and L-Tyr is believed to exist in solution.

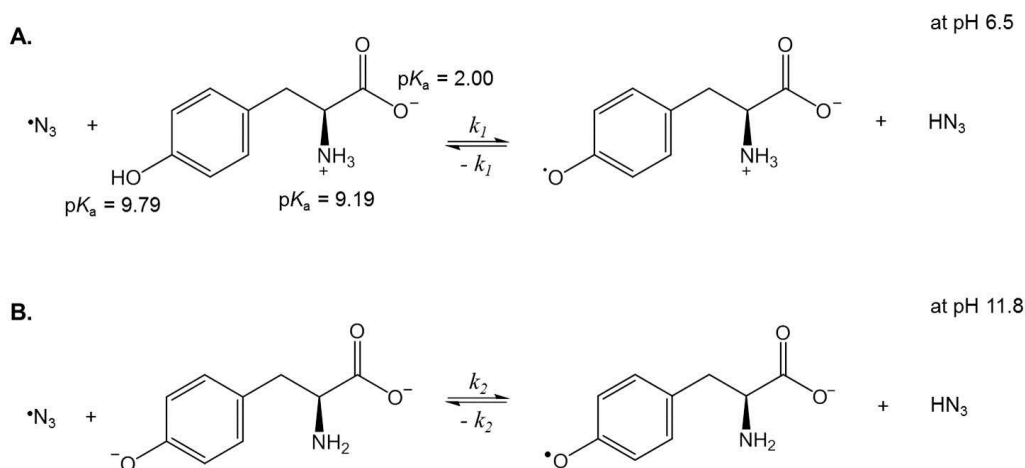**Figure 4.26** Oxidation of L-tyrosine by the $^\bullet N_3$ radicals formed from pulse radiolysis at pH (**A**) 6.5 and (**B**) 11.8, where k_1 and k_2 are the forward and $-k_1$ and $-k_2$ are the backward rate constants of each respective reaction. (Figure based on ref 15).

In this work, photo-irradiation of complex **40** in the presence of L-Tyr led to an increase in pH* from ca. 7.4 to ca. 8.2. Despite this pH* increase, the reaction of $^\bullet N_3$ radicals with L-Tyr is believed to be slower than trapping of $^\bullet N_3$ radicals by DMPO. This rationalises the equivalent formation of the DMPO-N$_3$ spin adduct in both the absence and presence of L-Tyr.

4.4.2 *In vitro* effect of L-Trp on irradiated complex 40

Photo-irradiation of complex **40** in both the absence of L-Trp led to the observation of a yellow coloured precipitate (refer to Figures 4.12). Similar

formation of precipitates have been reported by Ronconi[30] and Mackay[31] from the photo-irradiation of platinum(IV) diazido complexes, **36** and **37** (**Chapter I**). Consequently, the formed precipitate in this work, is thought to be multinuclear oxygen-bridged Pt^{II} species.[31] The observation of the platinum photo-products (**e''** – **i''**) in both the absence and presence of L-Trp supported an equivalent photo-decomposition pathway of complex **40** occurred in the presence of L-Trp.

The dark-brown colour of the formed precipitate (refer to Figure 4.17) in the presence of L-Trp is attributed to a possible L-Trp polymer-type species. Previous literature has reported on the polymerisation of aromatic compounds including, pyrroles,[32-35] aniline,[36] and indoles.[37,38] Additionally, numerous spectroscopic and theoretical studies have reported on the polymerisation of unsubstituted indoles generating poly-indoles through radical cation intermediates.[37] Consequently, the L-Trp[•+] radicals formed from the oxidation of L-Trp by the [•]N_3 radicals are suggested to react with unreacted L-Trp, through an electron transfer pathway, leading to the formation of a poly-tryptophan species. Solar *et al.* reported on the bio-molecular reaction of L-Trp[•+] radicals, providing additional evidence to support the formation of L-Trp polymer-type species.[9] A decrease in the L-Trp ^{1}H NMR resonances supports the potential formation of L-Trp polymer species. Moreover, previous literature has reported on the formation of dark coloured precipitates attributed to poly-pyrroles.[33] This further supports the idea that the observed dark brown colour is due to an L-Trp polymer species. Therefore, the precipitate formed in the presence of L-Trp, is likely to contain both a multinuclear oxygen-bridged Pt^{II} species.[31] Solution-phase analysis of the extracted precipitates was unsuccessful due to their insolubility in a variety of

solvents. Irradiation of complex **40** (≤ 100 µM) in either the absence or presence of L-Trp did not lead to the formation of these precipitates. Additionally, previous photo-irradiation studies of complex **40** (15 µM) have shown that cell death is induced in A2780 ovarian carcinoma cells.[1] This suggests that these precipitates are not a factor contributing to the photo-cytotoxicity of complex **40** but a direct consequent of photo-irradiating platinum(IV) diazido complexes at milli-molar (mM) concentrations.

4.4.3 Azidyl radical quenching

In the absence of L-Trp, photo-irradiation of complex **40** with DMPO led to the detection the DMPO-N$_3$ spin adduct and the corresponding DMPO-N$_3$ hydroxylamine species by EPR and NMR spectroscopy, respectively. Potapenko *et al.* identified a large upfield shift from ca. 7.2 ppm to ca. 4.1 ppm characteristic of a break in the N=CH double bond at the C2 position of spin trap, DMPO.[22] The new ^{1}H NMR resonance, **a'**, at ca. 2.87 ppm (refer to Figure 4.14**B**) is assigned to the H**a'** resonance of the DMPO-N$_3$ hydroxylamine species (refer to Figure 4.14**B**). Additionally, covalent attachment of the $^\bullet$N$_3$ radical leads to the non-equivalence of the protons at the C3 position of the DMPO-N$_3$ hydroxylamine species, generating two ^{1}H NMR resonances at 2.14 ppm (**b'**) and 1.94 ppm (**b''**). The change in the ^{1}H NMR resonance "**c**" at ca. 2.73 ppm from a triplet to a multiplet at ca. 1.94 ppm, further supports the formation of diasterotopic protons at C3 in the hydroxylamine DMPO-N$_3$ species. Additionally, the splitting of the singlet at 1.38 ppm into two signals δ = 1.35 (**d'**) and 1.27 (**d''**) suggests non-equivalence of the methyl groups upon the $^\bullet$N$_3$ radical covalently bonding to the DMPO spin trap.

However, in the presence of L-Trp, the partial and complete suppression of the DMPO-N_3 spin adduct detected by EPR spectroscopy was a primary indicator of $^\bullet N_3$ radical quenching by L-Trp. Moreover, the lack of ^1H NMR resonances attributable to the DMPO-N_3 hydroxylamine species in the presence of L-Trp, further supported the quenching of the $^\bullet N_3$ radicals. The reactivity between the $^\bullet N_3$ radicals with L-Trp was established through the detection of free azide (N_3^-) which proceeded through a one-electron transfer process. This observation is in agreement with Solar *et al.*, who identified that reaction of $^\bullet N_3$ radicals with indole-related compounds favours a one-electron transfer pathway as opposed to an hydrogen atom abstraction pathway.[9]

The reaction of $^\bullet N_3$ radicals with L-Trp at neutral pH 7 has been previously reported to possess a higher rate constant[18] of 4.1×10^9 M^{-1} s^{-1} in comparison to L-Tyr (1.0×10^8 M^{-1} s^{-1} at pH 6.5). This faster rate compared to trapping of $^\bullet N_3$ radicals by DMPO ($k = 1.6 \times 10^9$ M^{-1} s^{-1})[29] rationalises the reduced formation of DMPO-N_3 spin adduct in the presence of L-Trp. The majority of $^\bullet N_3$ radical reactions have been reported to occur at L-Trp residues in proteins such as *β*-lactoglobulin, pepsin, trypsin and yeast alcohol dehydrogenase (yADH).[4,18]

The reduction of the DMPO-N_3 spin adduct from the irradiation of *trans,trans,trans*-[Pt(N_3)$_2$(OH)(*N*-MI)(py)$_2$] (complex **58**, Figure 4.1) at 517 nm was established as being due to the photo-release of the equatorial *N*-methylisatoate (*N*-MI) ligand (refer to Figure 4.25). This released equatorial ligand has been recently reported to react with the $^\bullet N_3$ radicals, prior to reaction with spin trap, DMPO.[16] The nature of this reaction is currently unknown, but is

predicted to proceed through an electron transfer pathway at the NH moiety of the *N*-MI ligand. The quenching of the $^{\bullet}N_3$ radicals by the *N*-MI ligand present in complex **58**, has potential to induce an *in-situ* photo-protective effect *in cellulo*.

It should be noted that determining a possible target of the $^{\bullet}N_3$ radicals *in vitro* does not necessarily render this the primary biological target of $^{\bullet}N_3$ radicals generated *in vivo*. Radicals generated in an intracellular environment are surrounded by an array of amino acids, proteins, peptides, lipids, DNA and vitamins. Nevertheless, these initial results suggest that indoles and derivatives thereof are favourable targets for $^{\bullet}N_3$ radicals generated from photo-irradiated platinum(IV) diazido complexes.

4.4.4 Photo-protection in A2780 ovarian cancer cells

4.4.4.1 Free azide

The presence of L-Trp induced a photo-protective effect in A2780 ovarian cancer cells despite the formation of N_3^-. Azide is considered to be a toxic species, similar to cyanide which binds to Fe^{3+} of cytochrome oxidase leading to enzyme inhibition[26] but also binds to cytochrome *bo*, a quinol oxidase from *Escherichia coli*.[39] Furthermore, numerous publications have reported on azide induced poisoning in recent years.[40,41] The toxicity of azide has been directly correlated with the administered dose. Burger *et al.*[42] reported on the survival of a patient who ingested 150 mg of sodium azide, compared to the documented fatalities upon ingestion of 0.7 - 2.0 g of sodium azide.[43,44] Therefore, in this work it is believed the concentration of N_3^- formed, is below the toxic level to induce a cytotoxic effect.

Moreover, detection of N_3^- suggests the formation of both L-TrpH$^{\bullet+}$ and Trp$^{\bullet}$ radicals. Mediated by amino acid radicals, electron transfer (ET) is paramount to a myriad of biological processes including enzyme cytochrome *c* peroxidase, DNA photolyase and galactose oxidase.[45] L-Trp$^{\bullet}$ radicals are involved in both electron transfer and catalytic processes.[46] L-Trp radicals formed in di-peptides of L-Trp and L-Tyr have been reported to undergo a fast intra-molecular process ($k = 6 \times 10^4 \, \text{M}^{-1} \, \text{s}^{-1}$) either through hydrogen-atom abstraction or electron-transfer resulting in the same overall effect.[4] Furthermore, increasing the distance between the L-Trp and L-Tyr residues lowers the intra-molecular rate constant but not its efficiency. Electron transfer processes in ribo-nucleotide reductase (RNR) have been reported to occur at distances >35Å.[47] However, with the driving force of these reactions being dependent on the protonation of the L-Trp radical, it is important to determine whether the radical is in its cation or neutral form. Previous studies have characterised the neutral L-Trp$^{\bullet}$ radical,[46-49] with only a few publications[50-52] reporting the detection of the cationic L-Trp$^{\bullet+}$ radical, compared to other spectroscopic techniques capable of detecting both species.[10,49,53,54]

4.4.4.2 Amino acid radicals

Recent *in vitro* studies have shown that *trans,trans,trans*-[Pt(N$_3$)$_2$(OH)$_2$(NH$_3$)py] (complex **38**, Figure 4.27) induced autophagy in A2780 ovarian cancer cells.[55] Cell death can be induced either through apoptosis,[56] autophagic[57] or necrosis[58] pathways. Morphological changes in cancer cells have characterised the induction of apoptosis typically through cellular shrinkage, nuclear chromatin condensation and nuclear fragmentation.[59] The widely used anticancer agent c*is*-platin has been reported to induce apoptosis.[60] Previous cellular studies of photo-activated

complex **40** reported on its inability to induce either fragmented or condensed nuclei, both commonly associated with apoptosis.[1] Additionally, the structural similarly between complex **40** and **38**, suggests autophagy as a possible cell death mechanism of photo-activated complex **40**.
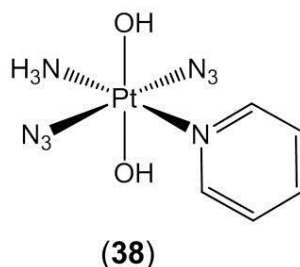

(38)

Figure 4.27 Photo-activatable complex, *trans,trans,trans*-Pt(N₃)₂(OH)₂(NH₃)py] shown to induce autophagy in A2780 ovarian cancer cells.[55]

In contrast, cell death by autophagy is typically determined by increased cellular levels of various autophagic proteins including a protein light chain 3 (LC3-II), p62 and beclin-1 (Bec-1).[57] Decreased expression levels of Bec-1 have been reported in ovarian cancers.[61] Consequently, LC3-II is typically used for establishing the induction of the autophagic pathway in ovarian cancers. The formation of LC3-II has been previously reported. Briefly, essential for autophagy, is the cleavage of the microtubule-associate protein (MAP) light chain 3 (LC3) by a cysteine protease (Atg4) generating cytosolic LC3-I, which is then converted to LC3-II by Atg7.[62] The structure of LC3-I determined by Kouno *et al.* was reported to be composed of four α-helices and a central β-sheet, where three histidine and four tyrosine residues were identified in the H1 helix of LC3-I.[63]

The photo-protective effect observed in this work is proposed to be due to the quenching of the •N₃ radicals by L-Trp, in turn leading to the formation of free

azide and the L-Trp$^\bullet$ radical. This formed L-Trp$^\bullet$ radical has potential to undergo an inter-molecular process with one of four tyrosine residues present in LC3-I, postulated to be through an electron transfer process due to the packing of the L-Tyr resides in LC3-I.[63] Consequently, this is envisaged to disrupt the conversion of LC3-1 to LC3-II effectively inhibiting the process of autophagy and inducing a photo-protective effect. In the absence of L-Trp, cell death was observed. Interestingly, ovarian cancer cells are reported to have depleted levels of L-Trp.[64,65] Consequently, treatment of cancers with depleted serum levels of L-Trp have the potential to enhance the photo-cytotoxicity of complex **40**. Moreover, the extent of the photo-cytotoxicity of complex **40** has potential to be controlled in the presence of L-Trp.

4.5 Conclusion

In this Chapter, the reactivity of azidyl radicals ($^\bullet N_3$) generated from the photo-irradiation of complex **40** towards a variety of amino acids was studied. The $^\bullet N_3$ radicals were unreactive towards glycine. This was consistent with earlier studies on the unreactive nature of $^\bullet N_3$ radicals, generated by pulse radiolysis, towards aliphatic amino acids.[18] Previous literature has reported on the pH dependent oxidation of L-tyrosine by the $^\bullet N_3$ radicals, which is favoured at more alkaline pH. Interestingly, in this work $^\bullet N_3$ radicals were unreactive towards L-tyrosine. This was attributed to a slower rate of $^\bullet N_3$ radical reactivity with L-tyrosine, compared to that of spin trap, DMPO. In the presence of L-tryptophan the trapping of the $^\bullet N_3$ radicals by DMPO suppressed. The extent of $^\bullet N_3$ radical quenching was enhanced with successive addition of L- tryptophan (0.5 – 1 mM).

^{1}H NMR spectroscopy in the absence of L- tryptophan identified various platinum photo-products and ^{1}H NMR resonances assigned to the DMPO-N_3 hydroxylamine species, a photo-decomposition species of the paramagnetic DMPO-N_3 spin adduct. Equivalent platinum photo-products were observed from the photo-irradiation of complex **40** in the presence of L-tryptophan. However, the ^{1}H NMR resonances related to the DMPO-N_3 hydroxylamine species were not detected. This was in agreement with EPR spectroscopic data on the suppression of the DMPO-N_3 spin adduct. Through the use of ^{14}N NMR spectroscopy, this quenching process was attributed to the oxidation of L-Trp tryptophan by the $^•N_3$ radicals through a one-electron transfer pathway, generating free azide (N_3^-) and L-Trp$^•$ (undetected). Free azide was not observed from the photo-irradiation of complex **40** alone, this further supported the one-electron transfer process.

The known cytotoxic nature of N_3^- suggested that an increase in the photo-cytotoxicity of complex **40** in the presence of L-tryptophan would be observed. However, a photo-protective effect was established from the photo-irradiation of complex **40** in the presence of L- tryptophan. Consequently, the formation of N_3^- appears to be below the concentration level required to induce a cytotoxic effect. Detection of N_3^- from the one-electron transfer between the $^•N_3$ radicals with L-tryptophan, also suggested the formation of the L-Trp$^•$ (undetected). The formation of the L-Trp$^•$ radical has potential to interact with the autophagic protein, LC3-I through an electron-transfer process, at one of the L-tyrosine residues present in the H1 α-helix of LC3-I. Consequently, this could augment the suggested autophagic pathway of photo-activated complex **40**. These data suggest

that the photo-toxicity induced by complex **40** involves both acute (radical) and chronic (DNA platination) based mechanisms.

4.6 References

(1)   Farrer, N. J.; Woods, J. A.; Salassa, L.; Zhao, Y.; Robinson, K. S.; Clarkson, G.; Mackay, F. S.; Sadler, P. J. *Angew. Chem. Int. Ed.* **2010**, *49*, 8905.

(2)   Halliwell, B. *Mutat. Res.* **1999**, *443*, 37

(3)   Wiseman, H.; Kaur, H.; Halliwell, B. *Cancer Lett.* **1995**, *93*, 113.

(4)   Butler, J.; Land, E. J.; Prütz, W. A.; Swallow, A. J. *Biochim. Biophys. Acta* **1982**, *705*, 150.

(5)   Fernstrom, J. D.; Fernstrom, M. H. *J. Nutr.* **2007**, *137*, 1539S.

(6)   Chung, K.-T.; Gadupudi, G. S. *Environ. Mol. Mutagen.* **2011**, *52*, 81.

(7)   Radwanski, E. R.; Last, R. L. *Plant Cell.* **1995**, *7*, 921.

(8)   Workentin, M. S.; Wagner, B. D.; Lusztyk, J.; Wayner, D. D. M. *J. Am. Chem. Soc.* **1995**, *117*, 119.

(9)   Solar, S.; Getoff, N.; Surdhar, P. S.; Armstrong, D. A.; A., S. *J. Phys. Chem.* **1991**, *95*, 3639.

(10)   Butler, J.; Land, E. J.; Swallow, A. J.; Prutz, W. *Radiat. Phys. Chem.* **1984**, *23*, 265

(11)   Merenyi, G.; Lind, J.; Shen, X. *J. Phys. Chem.* **1988**, *92*, 134.

(12)   DeFelippis, M. R.; Murthy, C. P.; Broitman, F.; Weinraub, D.; Faraggi, M.; Klapper, M. H. *J. Phys. Chem.* **1991**, *95*, 3416.

(13)   Jovanovic, S. V.; Harriman, A.; Simic, M. G. *J. Phys. Chem.* **1986**, *90*, 1935.

(14)   Harriman, A. *J. Phys. Chem.* **1987**, *91*, 6102

(15)   Hurst, J. R.; McDonald, J. D.; Schuster, G. B. *J. Am. Chem. Soc.* **1982**, *104*, 2065.

(16)   Shaili, E., Ph.D. Thesis, University of Warwick, 2013.

(17)   Fasman, G. D. *Handbook of Biochemistry and Molecular Biology: Proteins*; 3rd ed.; CRC Press: Cleveland, Ohio., 1976; Vol. I, p 183 - 203.

(18)   Land, E. J.; Prütz, W. A. *Int. J. Radiat Biol.* **1979**, *36*, 75.

(19)   Sang, H.; Janzen, E. G.; Poyer, J. L.; McCay, P. B. *Free Radic. Biol. Med.* **1997**, *22*, 843.

(20)   Krainev, A. G.; Williams, T. D.; Bigelow, D. J. *J. Magn. Reson., Ser B* **1996**, *111*, 272.

(21)   Tuccio, B.; Lauricella, R.; Charles, L. *Int. J. Mass Spectrom.* **2006**, *252*, 47.

(22)   Potapenko, D. I.; Bagryanskaya, E. G.; Reznikov, V. V.; Clanton, T. L.; Khramtsov, V. V. *Magn. Reson. Chem.* **2003**, *41*, 603.

(23)   Gan, Z. *J. Am. Chem. Soc.* **2006**, *128*, 6040.

(24)   Thorpe, T. A.; Bagh, K.; Cutler, A. J.; Dunstan, D. I.; McIntyre, D. D.; Vogel, H. J. *Plant Physiol.* **1989**, *91*, 193.

(25)   Farrer, N. J.; Gierth, P.; Sadler, P. J. *Chem. Eur. J.* **2011**, *17*, 12059.

(26)   Suzuki, O.; Watanabe, K. *Drugs and Poisons in Humans: A Handbook of practical analysis*; 1st ed.; Springer: Berlin, Heidelberg., 2005; p 633.

(27)   Repetto, G.; del Peso, A.; Zurita, J. L. *Nat. Protocols.* **2008**, *3*, 1125.

(28)   Yeasmin, L.; MacDougall, S. A.; Wagner, B. D. *J. Photochem. Photobiol. A: Chem* **2009**, *204*, 217.

(29)   Ram, M. S.; Stanbury, D. M. *J. Phys. Chem.* **1986**, *90*, 3691.

(30)   Ronconi, L.; Sadler, P. J. *Chem. Commun.* **2008**, 235.

(31)   Mackay, F. S.; Woods, J. A.; Moseley, H.; Ferguson, J.; Dawson, A.; Parsons, S.; Sadler, P. J. *Chem. Eur. J.* **2006**, *12*, 3155.

(32)   Lacroix, J.-C.; Valente, R.-J.; Maurel, F.; Lacaze, P.-C. *Chem. Eur. J.* **1998**, *4*, 1667.

(33)   Mermilliod, N.; Tanguy, J.; Petiot, F. *J. Electrochem. Soc.* **1986**, *133*, 1073.

(34)   Pfluger, P.; Krounbi, M.; Street, G. B.; Weiser, G. *J. Chem. Phys.* **1983**, *78*, 3212.

(35)   Yurtsever, E. *Synth. Met.* **2001**, *119*, 227.

(36)   Kitani, A.; Kaya, M.; Sasaki, K. *J. Electrochem. Soc.* **1986**, *133*, 1069.

(37)   Choi, K. M.; Jang, J. H.; Rhee, H.-W.; Kim, K. H. *J. Appl. Polym. Sci.* **1992**, *46*, 1695.

(38)   Yurtsever, M.; Yurtsever, E. *Polymer* **2002**, *43*, 6019.

(39)   Little, R. H.; Cheesman, M. R.; Thomson, A. J.; Greenwood, C.; Watmough, N. J. *Biochemistry.* **1996**, *35*, 13780.

(40)   Chiba, Y.; Ohmichi, M.; Inaba, H. *Jpn. J. Hyg.* **1999**, *53*, 572.

(41)   Richardson, S. G. N.; Giles, C.; Swan, C. H. L. *J. Clin. Path.* **1975**, *28*, 350.

(42)   Burger, E.; Bauer, H. M. *Arch. Toxikol* **1965**, *20*, 279.

(43)   Klein-Schwartz, W.; Gorman, R.; Oderda, G.; Massaro, B.; Kurt, T.; Garriott, J. *Med. Toxicol. Adverse Drug Exp.* **1989**, *4*, 219.

(44)   Howard, J. D.; Stogerboe, K. J.; Case, G. A. *J. Forensic. Sci* **1990**, *35*, 193.

(45)   Stubbe, J.; van der Donk, W. A. *Chem. Rev.* **1998**, *98*, 705.

(46)   Shafaat, H. S.; Leigh, B. S.; Tauber, M. J.; Kim, J. E. *J. Phys. Chem. B* **2008**, *113*, 382.

(47)   Bleifuss, G.; Kolberg, M.; Pötsch, S.; Hofbauer, W.; Bittl, R.; Lubitz, W.; Gräslund, A.; Lassmann, G.; Lendzian, F. *Biochemistry.* **2001**, *40*, 15362.

(48)   Barrows, T. P.; Bhaskar, B.; Poulos, T. L. *Biochemistry.* **2004**, *43*, 8826.

(49)   Sheth, S.; Baron, A.; Herrero, C.; Vauzeilles, B.; Aukauloo, A.; Leibl, W. *Photochem. Photobiol. Sci.* **2013**, *12*, 1074.

(50)   Connor, H. D.; Sturgeon, B. E.; Mottley, C.; Sipe, H. J.; Mason, R. P. *J. Am. Chem. Soc.* **2008**, *130*, 6381.

(51)   Huyett, J. E.; Doan, P. E.; Gurbiel, R.; Houseman, A. L. P.; Sivaraja, M.; Goodin, D. B.; Hoffman, B. M. *J. Am. Chem. Soc.* **1995**, *117*, 9033.

(52)   Rigby, S. E. J.; Jünemann, S.; Rich, P. R.; Heathcote, P. *Biochemistry.* **2000**, *39*, 5921.

(53)   Bellina, B.; Compagnon, I.; Houver, S.; Maître, P.; Allouche, A.-R.; Antoine, R.; Dugourd, P. *Angew. Chem. Int. Ed.* **2011**, *50*, 11430.

(54)   Singh, A.; Koroll, G. W.; Cundall, R. B. *Radiat. Phys. Chem.* **1982**, *19*, 137.

(55)   Westendorf, A. F.; Woods, J. A.; Korpis, K.; Farrer, N. J.; Salassa, L.; Robinson, K.; Appleyard, V.; Murray, K.; Grünert, R.; Thompson, A. M.; Sadler, P. J.; Bednarski, P. J. *Mol. Cancer Ther.* **2012**, *11*, 1894.

(56)   Wood, K. A.; Youle, R. J. *Ann. N.Y. Acad. Sci.* **1994**, *738*, 400.

(57)   He, C.; Klionsky, D. J. *Annu. Rev. Genet.* **2009**, *43*, 67.

(58)   Zong, W.-X.; Thompson, C. B. *Genes & Development* **2006**, *20*, 1.

(59)   Su, M.; Mei, Y.; Sinha, S. *J. Oncol.* **2013**, *2013*, 14.

(60)   Qin, L. F.; Ng, I. O. L. *Cancer Lett.* **2002**, *175*, 27.

(61)   Yue, Z.; Jin, S.; Yang, C.; Levine, A. J.; Heintz, N. *Proc. Natl. Acad. Sci. USA.* **2003**, *100*, 15077.

(62)   Dodson, M.; Darley-Usmar, V.; Zhang, J. *Free Radic. Biol. Med.* **2013**, *63*, 207.

(63)   Kouno, T.; Mizuguchi, M.; Tanida, I.; Ueno, T.; Kanematsu, T.; Mori, Y.; Shinoda, H.; Hirata, M.; Kominami, E.; Kawano, K. *J. Biol. Chem.* **2005**, *280*, 24610.

(64)   Lyon, D. E.; Walter, J. M.; Starkweather, A. R.; Schubert, C. M.; McCain, N. L. *BMC Res. Notes* **2011**, *4*.

(65)   Capuron, L.; Ravaud, A.; Neveu, P. J.; Miller, A. H.; Maes, M.; Dantzer, R. *Mol. Psychiatry* **2002**, *7*, 468.

Chapter V

Photoactivation of a Platinum(IV) Diazido Anticancer Complex in the presence of Melatonin

The objective of this work was to establish the effect of melatonin on the photo-irradiation of a platinum(IV) diazido anticancer complex. Melatonin is a metabolite from the biodegradation of the amino acid, L-tryptophan (L-Trp). In **Chapter IV**, the azidyl radical was quenched by L-Trp through a one-electron transfer pathway. Melatonin possesses a methoxy group on the indole ring. It was interesting to investigate whether this functional group would alter the photochemistry of photo-irradiated complex **40**.

5.1 Introduction

Oxygen is essential for most aerobic living organisms. As mentioned in **Chapter I**, through oxidative stress, numerous reactive oxygen species (ROS) including singlet oxygen ($^1O_2$), the superoxide ($O_2^{\bullet-}$) and the hydroxyl ($^\bullet OH$) radicals have been reported to be generated.[1] ROS are known to interact with cell membranes, proteins, lipids and DNA inducing a cascade of unwanted side effects.[2,3] The $^\bullet OH$ radical with a high reduction potential ($E^\circ = 2.31$ V)[4] is regarded as the most aggressive reactive oxygen-based radical, reacting immediately upon formation with nearby target molecules[5] due to its maximum diffusion radius of ca. 3 Å.[6] Various aerobic redox processes generate both hydrogen peroxide (H_2O_2) and the superoxide ($O_2^{\bullet-}$) radical.[7] Interestingly, the Fenton reaction, simplified in Equation 5.1 has been involved in the *in vivo* generation of $^\bullet OH$ radicals,[8] but its formation can also involve highly active copper(II) and iron(II) species.[9] Lloyd *et al.* confirmed using 17-labelled hydrogen peroxide and molecular oxygen that the $^\bullet OH$ radicals were generated from the hydrogen peroxide and did not exchange with the oxygen in the aqueous solvent.[10]

$$Fe^{2+} + H_2O_2 \longrightarrow Fe^{3+} + {}^{\bullet}OH + {}^{-}OH \qquad \text{Eq 5.1}$$
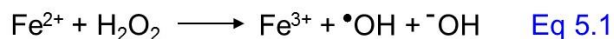
Due to the short lifetime (ca. 10^{-9} s) of ${}^{\bullet}OH$ radicals, direct detection is not feasible. Therefore, the detection of ${}^{\bullet}OH$ radicals has been primarily achieved through the use of EPR spin trapping.[11-14] The most widely used spin trap, DMPO has been reported to trap the ${}^{\bullet}OH$ radical and generate a quartet EPR spectrum (Figure 5.1), indicative on the formation of the DMPO-OH spin adduct.[15]
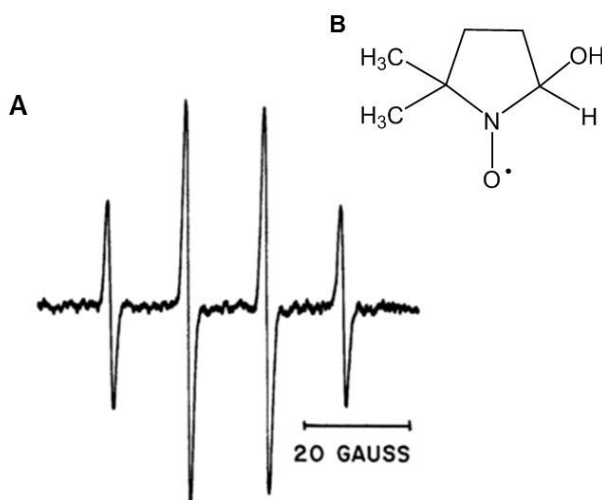
Figure 5.1 EPR spectrum (from ref 11) from the trapping of the hydroxyl (${}^{\bullet}OH$) radical with spin trap, DMPO and (**B**) molecular structure of DMPO-OH spin adduct giving rise to the quartet EPR spectrum.

However, this quartet EPR spectrum has potential to be generated from the decomposition of DMPO-OOH spin adduct.[16] Therefore, the addition of ${}^{\bullet}OH$ radical quenchers, such as dimethyl-sulfoxide (DMSO)[17] or ethanol,[18] have been used to confirm ${}^{\bullet}OH$ radical generation. Reaction of the ${}^{\bullet}OH$ radicals with DMSO and EtOH generate methyl and α-hydroxyl-ethyl radicals, respectively (Figure 5.2). These carbon-centred radicals subsequently trapped by DMPO give rise to unique EPR spectra.
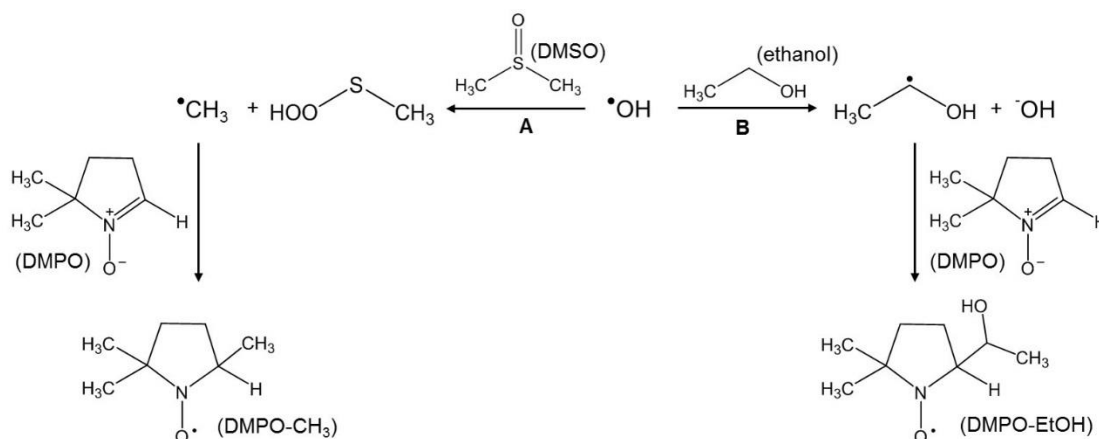
Figure 5.2 Reaction pathway of the hydroxyl ($^\bullet$OH) radical with (**A**) DMSO or (**B**) ethanol. Both lead to unique DMPO-R spin adducts (figure adapted from ref 17 and 18).

Melatonin, N-acetyl-5-methoxytryptamine (Figure 5.3), is a hormone commonly found in plants and animals. In mammals, it is synthesised in the pineal gland.
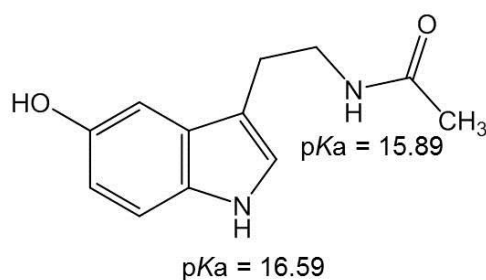

Figure 5.3 Structure of N-acetyl-5-methoxytryptamine (melatonin, MLT) at pH 7.4 together with pK_a values.[19]

A simplified stepwise formation of melatonin is depicted in Figure 5.4. Melatonin is synthesised from serotonin through two enzymatic processes, described in more detail by Cardinali *et al.*[20]
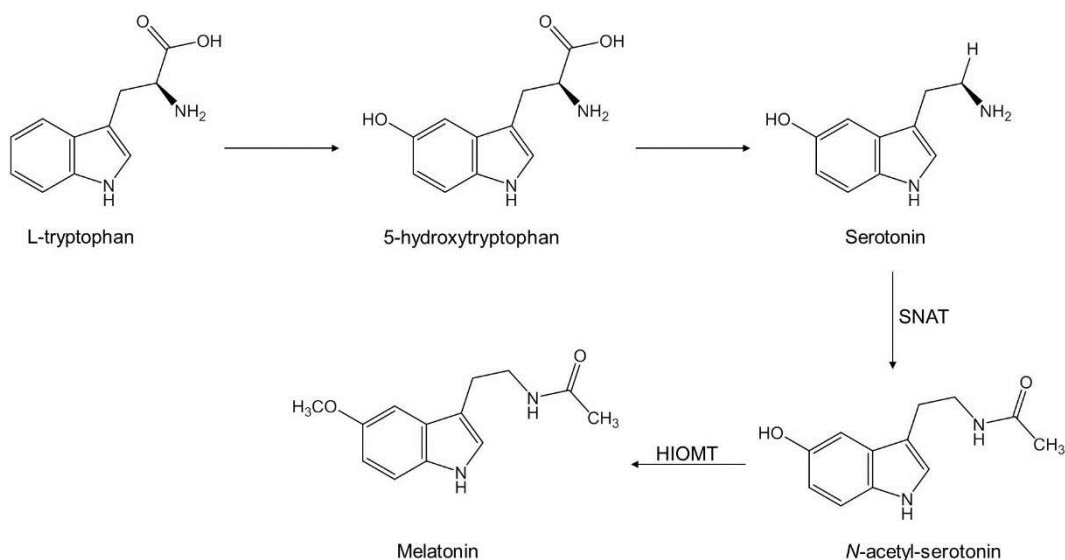
Figure 5.4 Stepwise synthesis of melatonin originating from the amino acid L-tryptophan involving two enzymes serotonin *N*-acetyltransferase (SNAT) and hydroxylindole-O-methyl-transferase (HIOMT) (figure adapted from ref 20).

Regarded as an important biological compound, melatonin is involved in a series of membrane-bound receptor-mediated processes including the regulation of retinal function, circadian rhythms and reproduction cycles.[21,22] In 2003, it was approved as a dietary supplement by the FDA[23] and is commonly used for the treatment of insomnia[20] and jet lag.[24] The intracellular concentration of melatonin has been reported to be dependent on the tissue/organ.[25] The plasma concentration of melatonin has been reported to be in the nanomolar (nM) range.[26] Melatonin has many functions,[27] it is well known for its anti-oxidant properties in reducing both oxidative cellular and molecular damage.[28] Over the last two decades, the ability of melatonin to scavenge the most reactive oxygen radical, the hydroxyl ($^\bullet$OH) radical, has been the subject of numerous reports.[29-31]

Tan *et al.* attributed the reduction in the DMPO-OH spin adduct to the quenching of the •OH radicals by melatonin.[32] Ebelt *et al.* reported on the dose-dependent scavenging ability of melatonin towards the •OH radicals, determined through the use of the phosphorus-based spin trap, DEPMPO (Figure 5.5).[33] The electron-rich indoleamine ring present in melatonin functions as an electron-donating group.
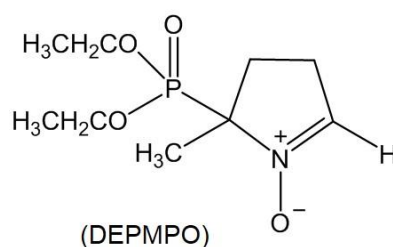

Figure 5.5 Structure of spin trap, 5-(Diethoxyphosphoryl)-5-methyl-1-pyrroline-*N*-oxide (DEPMPO).

This quenching ability of melatonin has been reported to proceed through a one-electron oxidation pathway generating a melatoninyl cation radical (MLT$^{•+}$) and a hydroxide ion ($^-$OH).[22] Numerous spectroscopic data have indirectly confirmed the formation of the MLT$^{•+}$ radical,[30,31,34] whereas to date no direct EPR data have been reported (**A**, Figure 5.6). Similar to L-Trp$^{•+}$ at neutral pH,[35] the MLT$^{•+}$ radical cation has been reported to undergo rapid deprotonation generating a neutral MLT$^{•}$ radical species and H$_2$O (**B**, Figure 5.6).[36] Moreover, the addition of the •OH radicals to the indole ring present in melatonin has also been reported.[37] Furthermore, a novel metabolite, 3-hydroxy-melatonin, was reported by Tan *et al.* from the interaction of the •OH radicals with melatonin.[38] Consequently, from these previous reports it appears the metabolites from the interaction of the •OH radicals with melatonin are dependent on the reaction conditions.
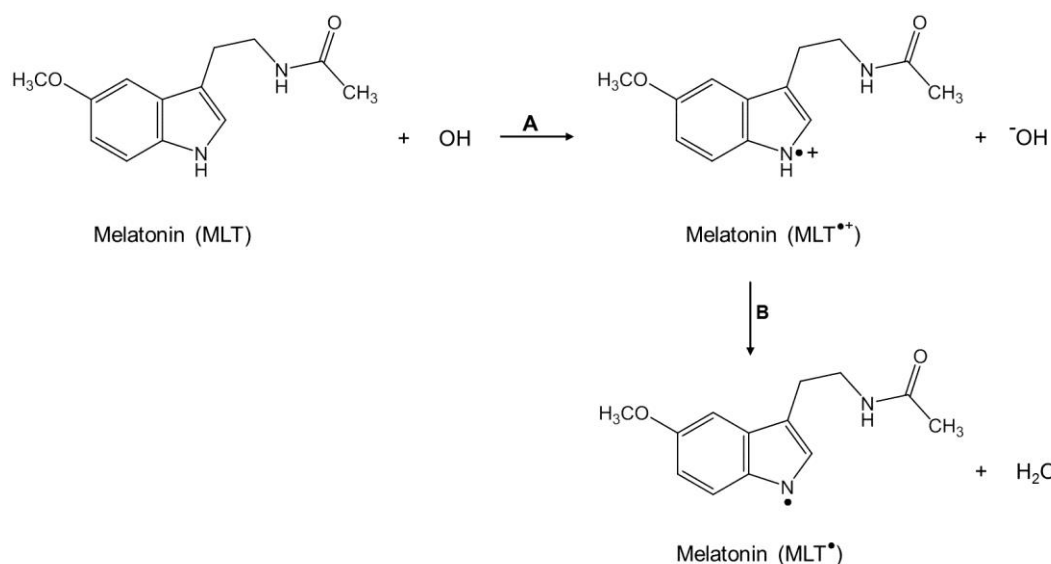
Figure 5.6 Scavenging ability of melatonin (MLT) towards the hydroxyl ($^\bullet$OH) radical generating both a melatoninyl (MLT$^{\bullet+}$) cation and a neutral melatonyl (MLT$^\bullet$) radical species.

Various other studies have reported on the quenching ability of MLT towards the alkoxyl (RO$^\bullet$) and hydroxyl ($^\bullet$OH) radicals using pulse radiolysis and flash photolysis techniques.[39-41] Interestingly, melatonin inhibited oxidative damage induced by 5-aminolevulinic acid (ALA) in male hamster Harderian glands.[42] ALA is a metabolic precursor of the photosensitiser, protoporhyrin(IX). Irradiation at the appropriate wavelength induces a cytotoxic effect due to singlet oxygen ($^1O_2$) formation[43] *via* a PDT based mechanism[44] (**Chapter I**). Interestingly, melatonin does not exhibit a quenching ability towards the superoxide ($O_2^{\bullet-}$) radical.[45]

Melatonin also exhibits a scavenging ability towards reactive nitrogen species (RNS) such as nitric oxide (NO$^\bullet$)[46], peroxynitrite anion (ONOO$^-$)[47] and azidyl ($^\bullet$N$_3$) radicals. Roberts *et al.* reported on the reaction between the azidyl radicals ($^\bullet$N$_3$) and melatonin possessing a second order rate constant ($k = 0.98 \times 10^{10}$ M^{-1} s^{-1})[37]

207

slightly faster to that of $^\bullet N_3$ reaction with L-Trp ($k = 0.41 \times 10^{10}$ M^{-1} s^{-1})[35] and other indole derivatives.[48,49] Oxidation of melatonin by the $^\bullet N_3$ radicals has been postulated to proceed through a similar reaction pathway to that of $^\bullet N_3$ radical reaction with L-Trp.[37]

Melatonin also possesses anti-tumour activity in various types of cancers.[50] Certain cancers, such as breast cancer, are more sensitive towards low (nM) concentrations of melatonin,[51] whereas colon cancer is responsive towards high (mM) concentrations of melatonin.[52] Similarly, a ca. 12% decrease in the cell viability was observed in Chinese ovarian (CHO) cells treated with melatonin (2-3 mM), although lower concentrations (μM) did not induce a cytotoxic effect.[53] The efficiency of various chemotherapeutic agents is enhanced upon administration with melatonin both *in vitro*[54,55] and *in vivo*.[56] To date no serious side-effects have been reported from patients treated with melatonin,[57,58] compared to other chemotherapeutics.[59] Melatonin was shown to induce its anti-tumour activity in colorectal cancer cells through both apoptosis and autophagy,[60] programmed cell death pathways mediated by various melatonin receptors.[61]

In addition to its antioxidant properties, through absorptive stripping voltammetry an electrochemical technique, melatonin has been shown to form complexes with various metal ions including iron(III), zinc(II), sodium(I), calcium(II), lithium(I), arsenic(III), aluminium(III), copper(II), nickel(II) and mercury(II).[62,63] These interactions of melatonin with various metal ions have been reported to be of biological importance, either altering or inhibiting the mechanism of action of the

metal ion.[64] However, neither of these studies identified the metal binding site(s) in melatonin.

In this Chapter, photo-irradiation of *trans,trans,trans*-[Pt(N$_3$)$_2$(OH)$_2$(py)$_2$] (complex **40**) in the presence of melatonin was investigated. The anti-tumour activity of melatonin has potential to enhance the efficiency of platinum(IV) diazido chemotherapeutic drugs. However, the antioxidant and metal-binding effects of melatonin have the ability to alter the mechanism of action of **40**.

5.2 Experimental

Below are the experimental sample preparation and instrumentation set up specific to this Chapter. More details regarding instrumentation and the irradiation setup are described in **Chapter II**.

5.2.1 Materials

Trans,trans,trans-[Pt(N$_3$)$_2$(OH)$_2$(py)$_2$] (complex **40**) was synthesised as described in **Chapter II**. Melatonin (MLT) was purchased from Sigma Aldrich and stored at −20 °C. Absolute ethanol (HPLC grade) was purchased from Fischer Scientific.

5.2.2 Sample preparation
5.2.2.1 UV-visible spectroscopy

Individual deuterated phosphate buffered solutions of melatonin (50, 100 and 200 µM) were prepared to assess its photo-stability towards irradiation at 463 nm (Spectral output, Figure A2.1). Separate solutions of complex **40** (50 µM) in the

presence of melatonin (2.5, 6.25, 50, 100 and 200 μM) were prepared in PBS/D$_2$O at pH* 7.4.

5.2.2.2 EPR spectroscopy

Solutions of complex **40** (different concentrations) containing excess spin trap, DMPO (2 mol equiv relative to complex **40**) were prepared in PBS/D$_2$O at pH* 7.4 in both the absence and presence of melatonin (different concentrations). Additional, spin trapping studies were investigated the both absence and presence of ethanol. Finally, solutions of complex **40** (4 mM) with spin trap, DEPMPO (8 mM, 2 mol equiv) in both the absence and presence of melatonin (0.5 mM) were prepared in PBS/D$_2$O were at pH* 7.4.

5.2.2.3 NMR spectroscopy

- **^{1}H NMR**

A solution of melatonin (5 mM) was prepared in PBS/D$_2$O at pH* 7.4 to assess its photo-stability. Additional, solutions containing complex **40** (9 mM) with melatonin (9 mM, 1 mol equiv) were prepared in PBS/D$_2$O at pH* 7.4.

- **^{13}C-DEPT135 NMR**

Solutions containing complex **40** (9 mM) with melatonin (9 mM, 1 mol equiv) were prepared in PBS/D$_2$O at pH* 7.4.

- **^{14}N NMR**

Similar solutions were prepared for ^{14}N NMR, but at higher concentrations (ca. 6 mM) due to the lower sensitivity of the ^{14}N nucleus compared to the ^{1}H nucleus

(receptivity relative to ^{1}H at 100 % = 1.01 ×10^{-3}). ^{1}H and ^{14}N NMR spectroscopy were performed as described in detail in **Chapter II**.

- **COSY NMR**

[^{1}H, ^{1}H] COSY NMR was recorded on a Bruker DPX-400 MHz (^{1}H, 399.10 MHz) spectrometer at room temperature. Spectra were recorded with standard COSY NMR cosygpqf pulse program and acquired with 32 transients into 65 k data points with a spectral width of 10 ppm. The solution recorded was equivalent to that prepared for ^{1}H NMR analysis. The advantage of COSY is that it determines a correlation between two and three-bonded coupled protons.

5.2.3 Irradiations

All irradiations were performed using a blue LED light source (λ = 463 nm, 64 mW cm^{-2}), spectral output (Figure A2.1) unless otherwise stated. In this Chapter, irradiations were performed in both continuous and semi-continuous mode. Information regarding continuous mode is detailed in **Chapter II**. Semi-continuous irradiation refers to samples irradiated for a set time period (e.g. 14 min) after which the irradiation source is switched off whilst the recording of the EPR spectrum remained continuous throughout. EPR parameters and irradiation setup are as described in **Chapter II**.

5.3 Results

5.3.1 Photo-stability of melatonin

Melatonin exhibits a broad absorbance extending from ca. 240 to 310 nm, with a maximum absorbance at ca. 278 nm (Figure 5.7), attributed to a $\pi \rightarrow \pi^*$ transition.[65]

The determined molar absorption coefficient of ca. 5.6×10^3 $M^{-1}.s^{-1}$, is in agreement with ε values reported by He *et al.*[66] Melatonin (different concentrations) remained stable in solution after 30 min irradiation at 463 nm (Figure 5.7). A mass adduct with *m/z* of 233.1285 was detected both before and after irradiation and assigned to [melatonin+H]$^+$ (Figure 5.8).
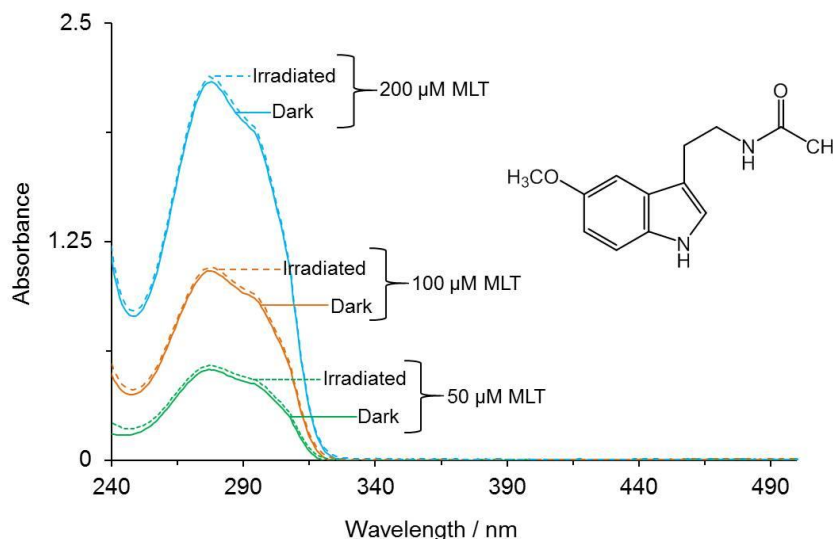

Figure 5.7 UV-visible spectra of solutions of melatonin (50 μM, 100 μM and 200 μM as labelled) prepared in PBS/D_2O at pH* 7.4 in the (solid line) dark and (dashed line) after irradiation at 463 nm for 30 min.
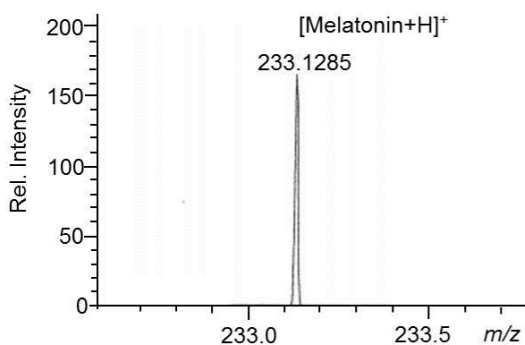
Figure 5.8 HR-MS of melatonin prepared in H_2O solvent irradiated at 463 nm for 30 min. Mass adduct at *m/z* of ca. 233.1285 is assigned to [melatonin+H]$^+$, in agreement with calculated *m/z* of 233.1212.

Furthermore, the photo-stability of melatonin was also monitored by ^{1}H NMR spectroscopy. The ^{1}H NMR spectrum of melatonin (5 mM) prepared in PBS/D$_2$O remained unchanged after irradiation at 463 nm light for 30 min. The photo-stability of melatonin rendered it a suitable molecule for studying its effect on the photo-activation of *trans,trans,trans*-[Pt(N$_3$)$_2$(OH)$_2$(py)$_2$] (**40**).
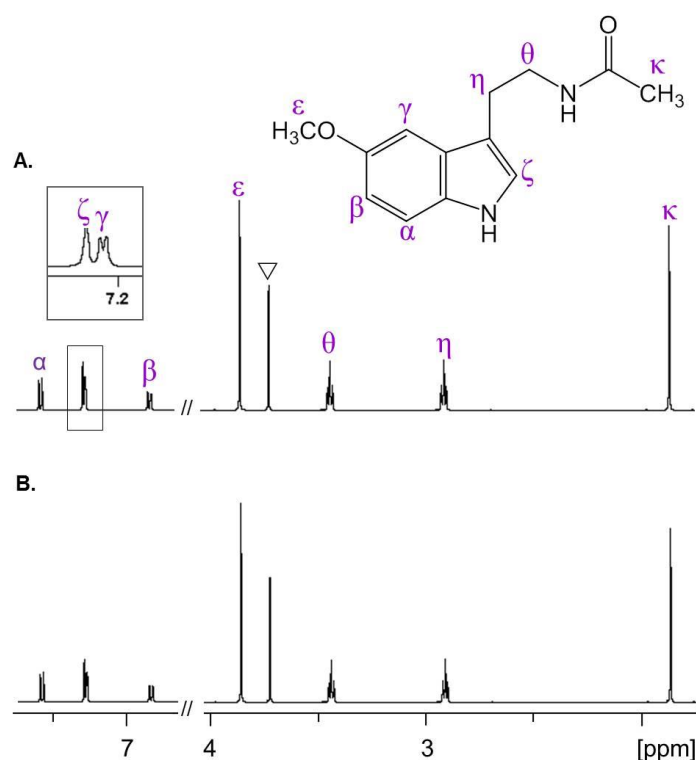

Figure 5.9 ^{1}H NMR spectra showing photo-stability of melatonin (5 mM) prepared in PBS/D$_2$O at pH* 7.4 in (**A**) the dark and (**B**) after irradiation at 463 nm for 30 min. Where ▼ refers to the resonance from the internal reference, 1,4-dioxane.

5.3.2 Irradiation of complex 40 in the presence of melatonin

Solutions of *trans,trans,trans*-[Pt(N$_3$)$_2$(OH)$_2$(py)$_2$] (**40**, 50 µM) in the absence and presence of melatonin (different concentrations) were prepared in PBS/D$_2$O at pH* 7.4. In the absence of melatonin, the N$_3$→Pt^{IV} LMCT band at 294 nm, photo-

decomposed by ca. 40% after irradiation at 463 nm for 30 min (Figure 5.10**A**). Solutions containing complex **40** (50 µM) and melatonin ($\geq$ 50 µM) prepared in PBS/D$_2$O at pH* 7.4, were dominated by the absorbance from melatonin at ca. 278 nm, in the dark. This absorption at ca. 278 nm masked the N$_3$→Pt^{IV} LMCT band from complex **40** at ca. 294 nm. Therefore, to observe the LMCT band in solutions containing complex **40** and melatonin ($\geq$ 50 µM), the absorbance of melatonin over the range of 240 – 410 nm was subtracted. It was determined that an equivalent photo-decomposition of ca. 40% in the N$_3$→Pt^{IV} LMCT band occurred (**B-F**, Figure 5.10).

The formation of an isosbestic point (**a'**) at ca. 330 nm (inset **E40** and **F40**, Figure 5.10), was determined to be dependent on the dose of melatonin. The formation of the isosbestic point only in the presence of melatonin suggests an alternative photo-decomposition pathway of complex **40** occurs in the presence of melatonin.

The equivalent decrease in the N$_3$→Pt^{IV} LMCT band despite the presence of melatonin, suggested an equivalent release of azide ligand. The structural similarity between L-Trp and melatonin, suggests the quenching of the $^\bullet$N$_3$ radicals by melatonin. Furthermore, previous studies have reported on the oxidation of melatonin by the $^\bullet$N$_3$ radicals.[37] This quenching mechanism was investigated by performing EPR spectroscopy.
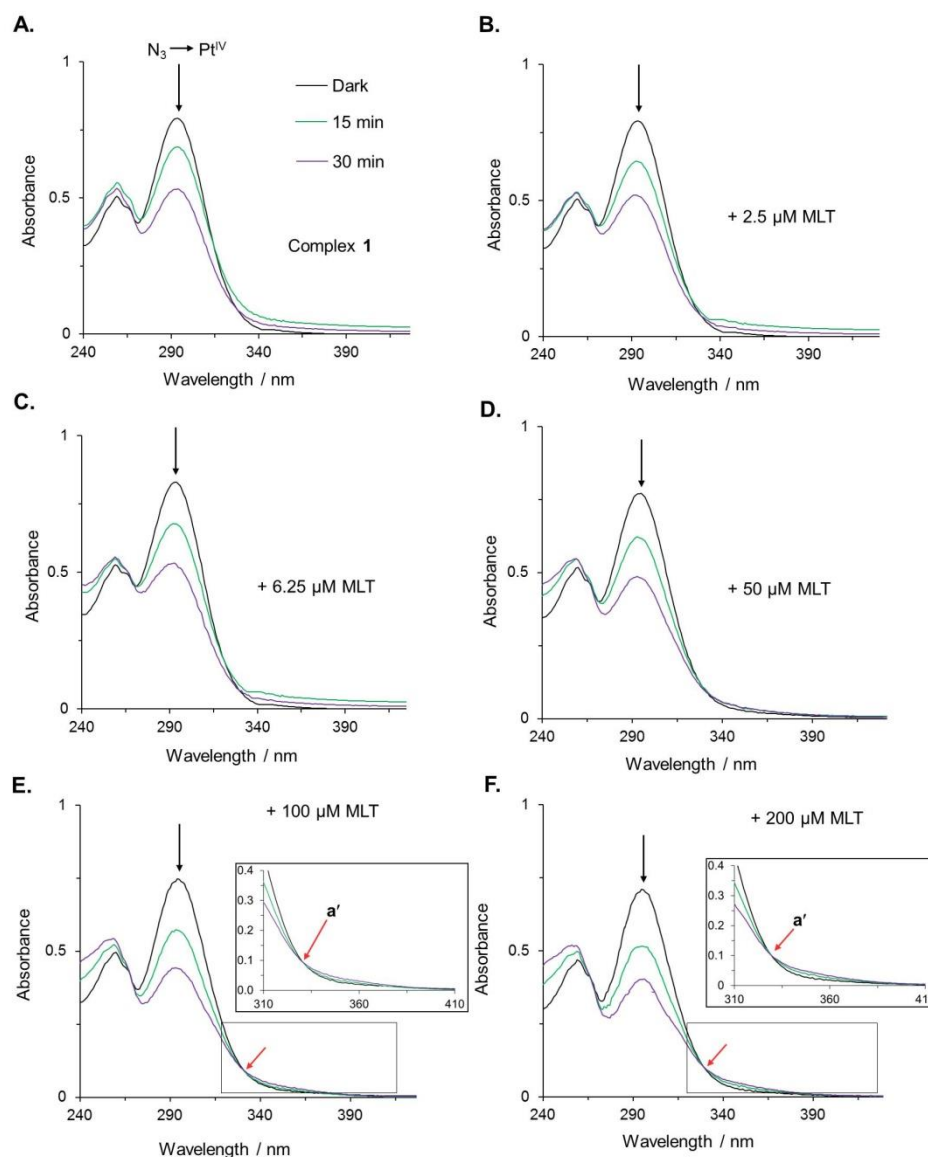
Figure 5.10 UV-visible spectra of complex **40** (50 µM) in the (–) dark and after (–) 15 min; and (–) 30 min irradiation at 463 nm in (**A**) absence and presence of (**B**) 2.5 µM; (**C**) 6.25 µM; (**D**) 50 µM; (**E**) 100 µM and (**F**) 200 µM melatonin (MLT) prepared in PBS/D$_2$O at pH* 7.4. A decrease (↓) of ca. 40% in the N$_3$→Pt^{IV} LMCT band at ca. 294 nm was observed in all spectra (**A**-**G**). Insets (**E40** and **F40**) show isosbestic point (**a'**) at ca. 330 nm.

5.3.3 Radical scavenging ability of melatonin

Solutions containing complex **40** (4 mM) and DMPO (8 mM) in both the absence and presence of melatonin (100 µM, 200 µM and 500 µM) were prepared in PBS/D_2O at pH* 7.4. No EPR spectroscopic signals were observed in the dark (Figure A5.1). In the absence of melatonin, photo-irradiation with 463 nm light for 7 min led to the quartet of triplets EPR spectrum (Figure 5.11**A**), previously assigned to the DMPO-N_3 spin adduct (**Chapter III**). Under similar experimental conditions but in the presence of melatonin, either partial (Figure 5.11**B** and **C**) or complete (Figure 5.11**D**) suppression in the DMPO-N_3 spin adduct was observed, dependent on the concentration of melatonin.
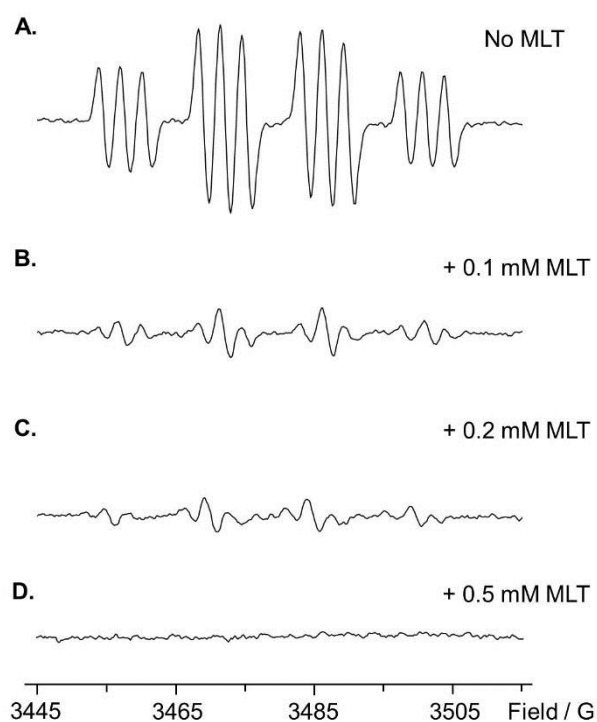

Figure 5.11 EPR spectra generated from a solution containing complex **40** (4 mM) and DMPO (8 mM) in (**A**) absence and presence of (**B**) 0.1 mM; (**C**) 0.2 mM and (**D**) 0.5 mM melatonin (MLT) prepared in PBS/D_2O at pH* 7.4 irradiated at 463 nm for 7 min.

Despite the complete suppression in spectrum **D** (Figure 5.11), prolonged irradiation (> 14 min) led to both an increase in the intensity and formation of a different EPR signal (Figure 5.12). These generated EPR signals were not in agreement with the quartet of triplets DMPO-N$_3$ spin adduct (Figure 5.11**A**). The marked intensity of the red lines (Figure 5.12**C**-**G**) suggests possible superimposition of two nitrone DMPO spin adducts.

As can be deduced from the line diagrams in Figure 5.12**F**, it appears the centre lines of the DMPO-N$_3$ (**R1**) spin adduct are overlapped with a quartet EPR spectrum from a second DMPO-X (**R2**, X = secondary radical species generated from irradiated complex **40**) spin adduct, rationalising the pronounced intensity of the red lines. Moreover, from this assignment the black lines are attributed to the DMPO-N$_3$ (**R1**) spin adduct only.

As shown in **Chapter III** (Figure 3.2, p 86), photo-irradiation of complex **40** has potential to lead to the generation of both reactive oxygen and nitrogen species (ROS/RNS). Moreover, Ronconi *et al*. observed that experimental conditions can greatly affect both the photo-activation and photo-decomposition of platinum(IV) diazido complexes.[67] The presence of residual DMPO-N$_3$ (**R1**) spin adduct appeared to obscure the observation of DMPO-X (**R2**) spin adduct. Harbour *et al* determined the DMPO-N$_3$ spin adduct decays to half its intensity within ca. 2 s after the light source is switched off.[68] Therefore, in an attempt to observe **R2** only, semi-continuous irradiation mode was used. In this mode, the solution under investigation was irradiated for 14 min at 463 nm, after which the light source was switched off whilst the EPR spectrum was continuously recorded.
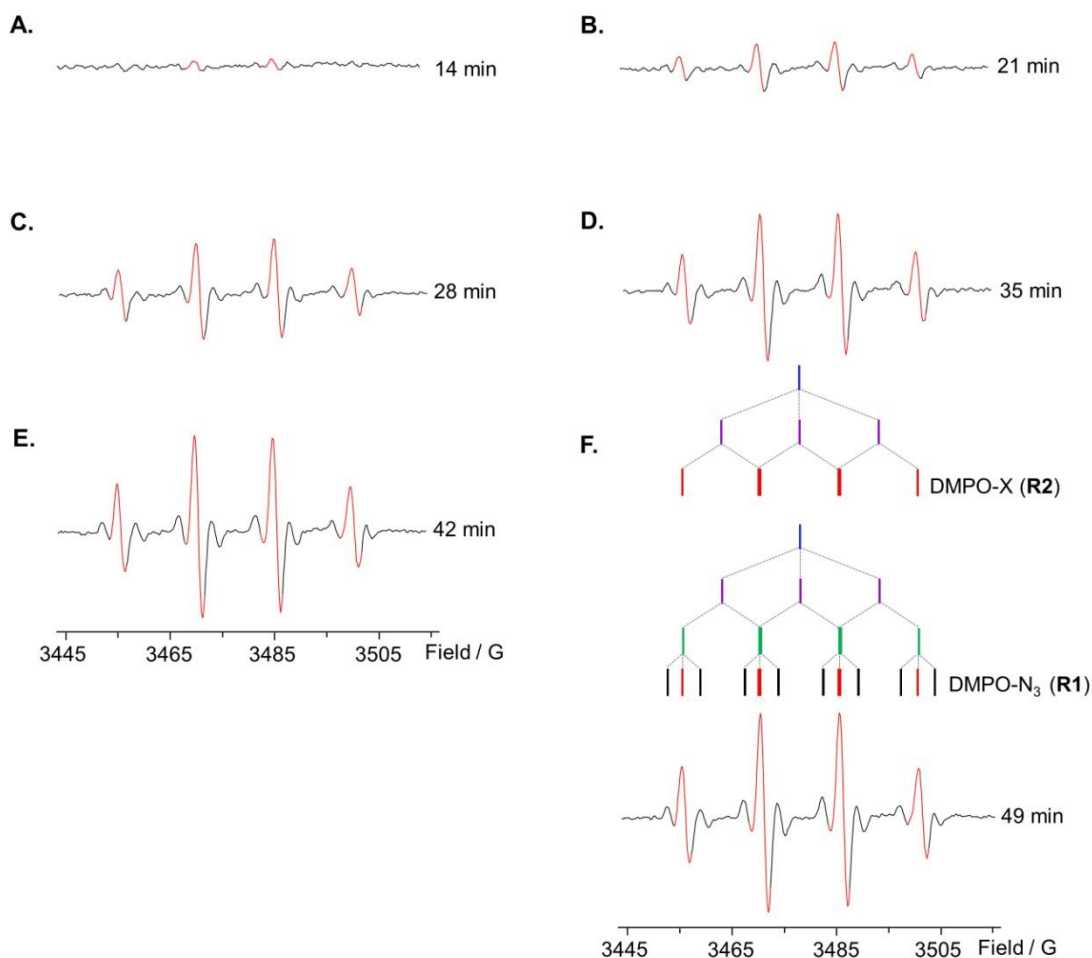
Figure 5.12 EPR spectra generated from the photo-irradiation of complex **40** (4 mM) with DMPO (8 mM) in the presence of melatonin (0.5 mM) prepared in PBS/D$_2$O at pH* 7.4 continuously irradiated for (**A**) 14 min; (**B**) 21 min; (**C**) 28 min; (**D**) 35 min; (**E**) 42 min and (**F**) 49 min at 463 nm. The pronounced intensity of the red lines is assigned to the superimposition of both the DMPO-N$_3$ (**R1**) and DMPO-X (**R2**) spin adducts, deduced from the parallel alignment of the **R1** and **R2** line diagrams as shown in spectrum **F**, where X refers to second radical species.

5.3.3.1 Semi-continuous irradiation

A solution of *trans,trans,trans*-[Pt(N$_3$)$_2$(OH)$_2$(py)$_2$] (**40**, 4 mM) and DMPO (8 mM) in the presence of melatonin (0.5 mM) was prepared in PBS/D$_2$O at pH* 7.4 and irradiated for 14 min at 463 nm, after which the irradiation source was switched off.

218

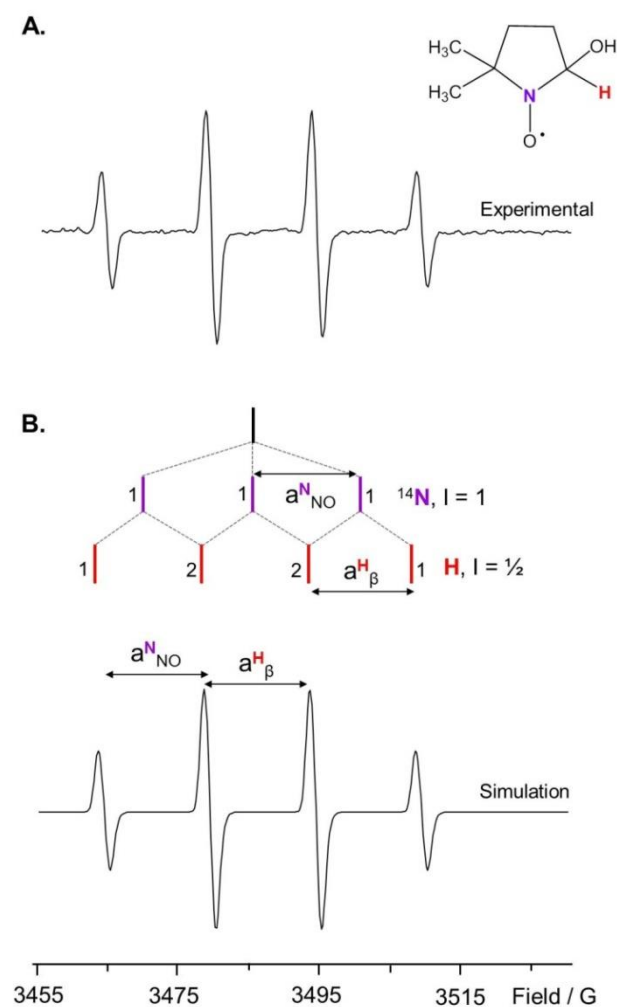Only in the presence of melatonin was a quartet EPR spectrum generated (**R2**, Figure 5.13).

Figure 5.13 EPR spectra generated from (**A**) a solution of complex **40** (4 mM) and DMPO (8 mM) in the presence of melatonin (0.5 mM) irradiated for 14 min at 463 nm, after which the light source was switched off (semi-continuous irradiation mode) prepared in PBS/D$_2$O at pH* 7.4 and (**B**) a simulation using experimental values as depicted in Table 5.1 together with the line diagram of the DMPO-OH spin adduct.

Previous studies have attributed the quartet EPR spectrum in the ratio of 1:2:2:1 to the trapping of the hydroxyl ($^\bullet$OH) radical by DMPO. The experimentally measured

hyperfine coupling constants and g-factor of the unknown DMPO-X (**R2**) spin adduct are similar to those previously reported values for the DMPO-OH spin adduct (Table 5.1),[18] this led **R2** to be assigned to the DMPO-OH spin adduct.

Table 5.1 Hyperfine coupling constants and g-factor determined for the DMPO-OH spin adduct as shown in Figure 5.13 with literature values (in brackets).

DMPO-OH	a^N_{NO} / (G)	a^H_β / (G)	g-value
Experimental[a]	14.96 ± 0.04	14.90 ± 0.03	2.0133 ± 0.0012
Published[b]	(14.9)	(14.9)	-[c]

[a]data represent means $\pm$ the standard deviation of three independent experiments; [b]from ref 20; [c]not determined.

However, the formation of a quartet EPR spectrum has also been reported to form from the decomposition of the DMPO-OOH spin adduct.[15] To confirm the formation of the $^\bullet$OH radicals, the experiment was repeated with substitution of DMPO by spin trap DEPMPO (Figure 5.5). In the absence of melatonin, only the DEPMPO-N_3 spin adduct (**R3**, Figure 5.14**A**) was observed, previously characterised in **Chapter III**. No EPR signal consistent with the trapping of the $^\bullet$OH radicals by DEPMPO was observed. Rather, a gradual photo-decomposition of **R3** was observed (Figure 5.14**B**).
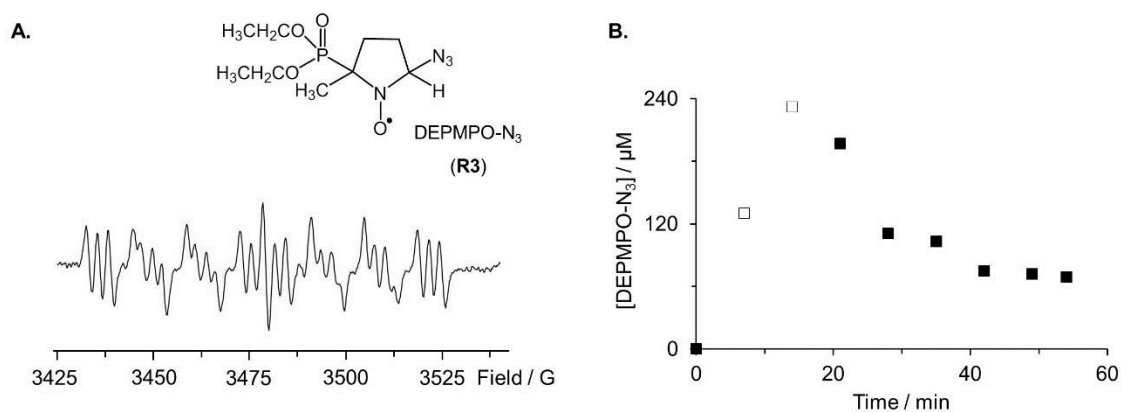
Figure 5.14 (**A**) EPR spectrum of the DEPMPO-N$_3$ spin adduct generated from a solution containing complex **40** (4 mM) with DEPMPO (8 mM) in the absence of melatonin prepared in PBS/D$_2$O at pH* 7.4 irradiated for 14 min at 463 nm (semi-continuous irradiation mode) and (**B**) quantification of DEPMPO-N$_3$ spin adduct obtained in semi-continuous irradiation mode over a total of 54 min, where ■ and □ refer to irradiation source switched off and on, respectively.

However, in the presence of melatonin (0.5 mM) a new 8-lined EPR spectrum (**R4**) was observed (Figure 5.15). This EPR spectrum possessed hyperfine coupling constants (Table 5.2) in agreement with values reported by Paciolla *et al.* for the DEPMPO-OH spin adduct.[69] This led to the assignment of **R4** as the DEPMPO-OH spin adduct.
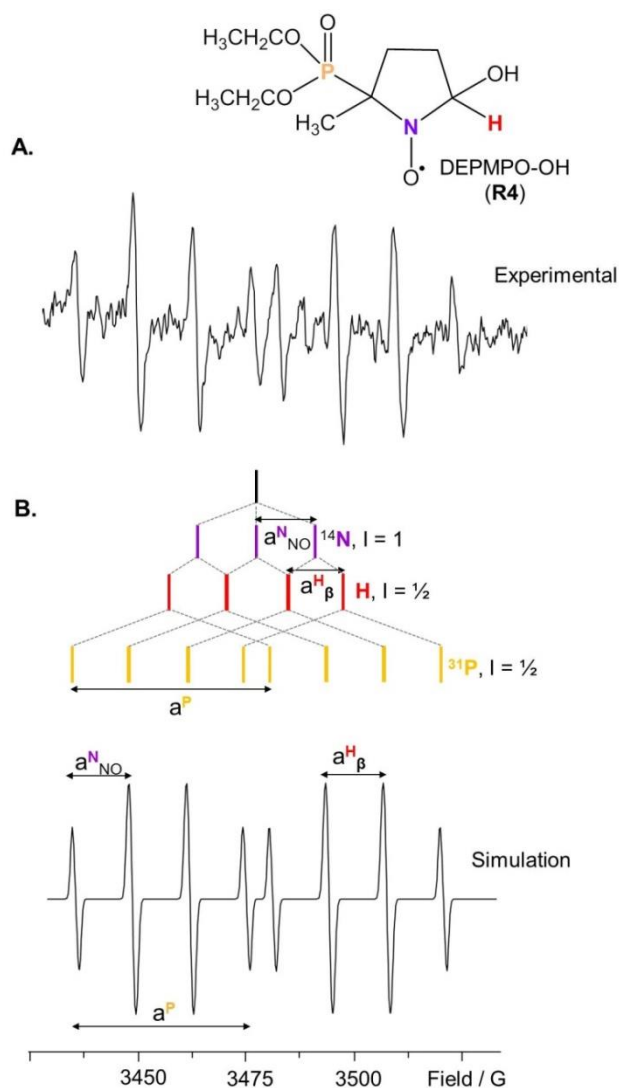
Figure 5.15 EPR spectra generated from (**A**) a solution containing complex **40** (4 mM) and DEPMPO (8 mM) in the presence of melatonin (0.5 mM) irradiated for 14 min at 463 nm (semi-continuous irradiation mode) prepared in PBS/D$_2$O at pH* 7.4 and (**B**) simulation using experimental values as depicted in Table 5.3 together with the line diagram of the DEPMPO-OH spin adduct.

Table 5.3 Hyperfine coupling constants and g-factor determined for the DEPMPO-OH spin adduct as shown in Figure 5.15 with literature values (in brackets).

DEPMPO-OH	a^N_{NO} / (G)	a^H_β / (G)	a^P /(G)	**g-value**
Experimental[a]	13.84 ± 0.03	13.68 ± 0.11	47.48 ± 0.02	2.0209 ± 0.0098
Published[b]	(13.98)	(13.26)	(47.18)	(-)[c]

[a]data represent means $\pm$ the standard deviation of three independent experiments; [b]from ref 75; [c]not determined.

The minor variations in hyperfine coupling values are attributed to the different experimental conditions, as previously discussed in **Chapter III** (section **3.4.2**). Frejaville *et al* reported on the detection of the DEPMPO-OH with hyperfine coupling constants of 14.1 G, 13.2 G and 47.3 G for the a^N_{NO}, a^H and a^P, respectively.[70] Consequently, it appears hyperfine coupling constants within this range and detection of the 8-lined EPR spectrum as shown in Figure 5.15**A**, can be attributed to the DEPMPO-OH spin adduct.

The detection of the DEPMPO-OH spin adduct confirmed the formation of the $^\bullet$OH radicals from irradiated complex **40** in the presence of melatonin. This supported that the quartet EPR signal observed (Figure 5.13) was due to the trapping of the $^\bullet$OH radicals by DMPO. The detection of the α-hydroxyl-ethyl radical ($^\bullet$EtOH) as shown in Figure 5.2 is another method to confirm $^\bullet$OH radical formation. As described in **Chapter III**, the spin trap 4-POBN is the most efficient spin trap in the detection of the α-hydroxyl-ethyl radical.[71,72] However, due to a dark reaction between 4-POBN with melatonin, this spin trap was unsuitable. Consequently, the

detection of the α-hydroxyl-ethyl radical was investigated using the spin trap DMPO.

5.3.4 Detection of the α-hydroxyl-ethyl radical

In the absence of ethanol (EtOH), the red lines (−, Figure 5.16) were quantified to ca. 9.7 µM from the photo-irradiation of a solution of complex **40** (4 mM), DMPO (8 mM) and melatonin (0.5 mM) at 463 nm. Addition of EtOH (1.2 mM) led to ca. a four-fold reduction in the red lines, quantified to ca. 2.1 µM (---, Figure 5.16). The black lines in both the absence and presence of ethanol retained their intensity. This supports the earlier suggestion that these outer lines belong to DMPO-N$_3$ (**R1**) and do not contribute to the **R2** spin adduct.
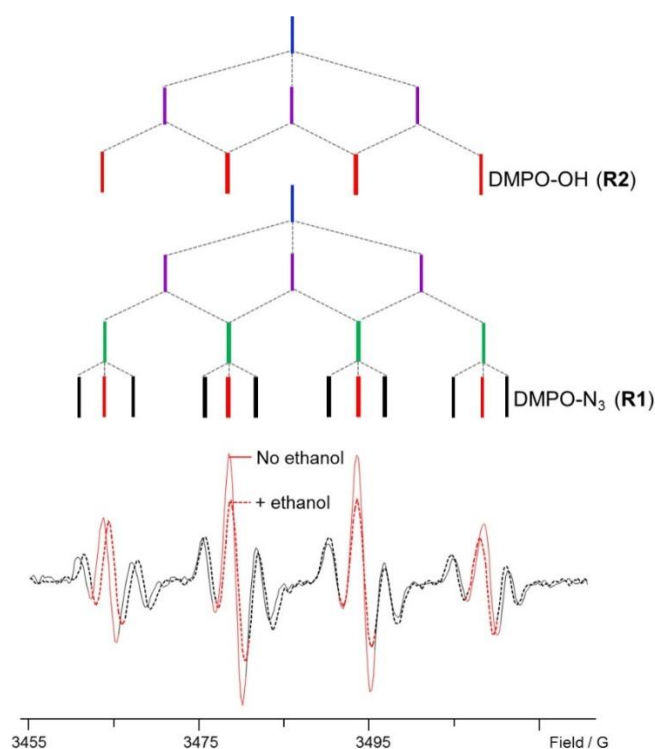

Figure 5.16 EPR spectra generated from the continuous photo-irradiation of complex **40** (4 mM), DMPO (8 mM) and melatonin (0.5 mM) in (−) absence and (----) presence of ethanol (1.2 mM) with 463 nm after 35 min prepared in PBS/D$_2$O at pH* 7.4 together with line diagrams of **R1** and **R2**.

224

The presence of residual DMPO-N$_3$ (**R1**) spin adduct appears to prevent the observation of the potential DMPO-EtOH (**R5**) spin adduct. Therefore, semi-continuous irradiation was used to observe **R5**. Only upon the addition of ethanol (1.2 mM) were new EPR signals observed (−, Figure 5.17**A**). These new peaks exhibited similar hyperfine couplings to those previously reported for the DMPO-EtOH (**R5**) spin adduct (Table 5.4).[72] Consequently, these new peaks were assignable to the DMPO-EtOH spin adduct.
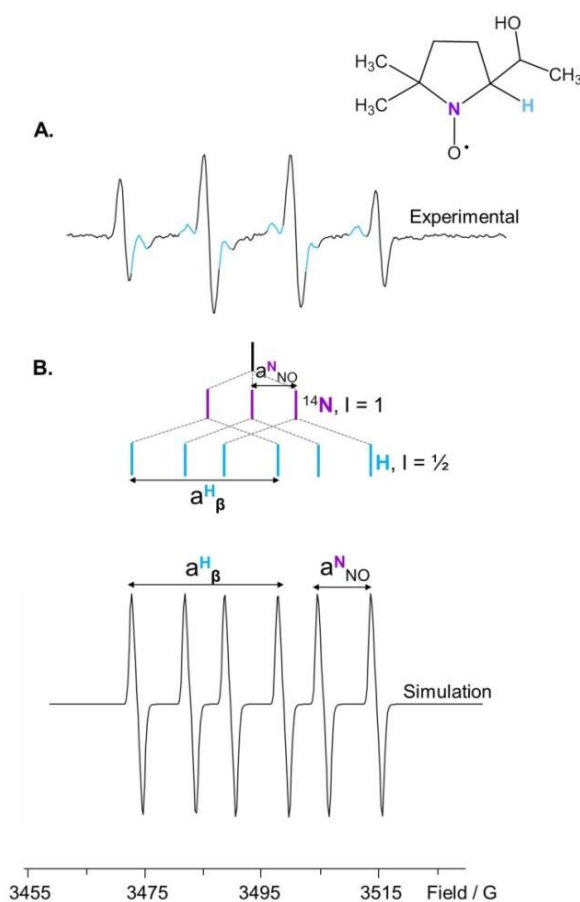

Figure 5.17 EPR spectra generated from (**A**) a solution of complex **40** (4 mM), DMPO (8 mM) and melatonin (0.5 mM) in the presence of ethanol (1.2 mM) irradiated for 14 min at 463 nm (semi-continuous irradiation mode) prepared in PBS/D$_2$O at pH* 7.4 and (**B**) a simulation using experimental values as depicted in Table 5.4 together with the line diagram of the DMPO-EtOH spin adduct. Blue peaks in **A** refer to the DMPO-EtOH spin adduct.

225

Table 5.4 Hyperfine coupling constants and g-factor determined for the DMPO-EtOH spin adduct as shown in Figure 5.17 with literature values (in brackets).

DMPO-EtOH	a^N_{NO} / (G)	a^H_β / (G)	g-value
Experimental[a]	14.24 ± 0.05	22.75 ± 0.06	2.0106 ± 0.0002
Published[b]	(15.8)	(22.0)	(-)[c]
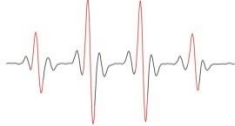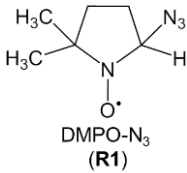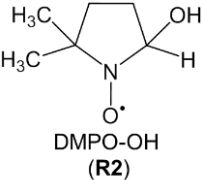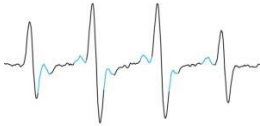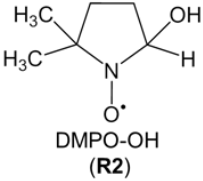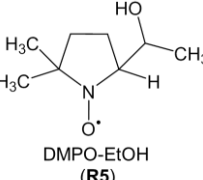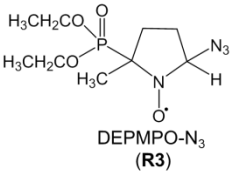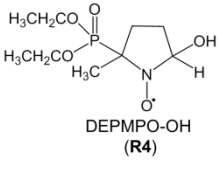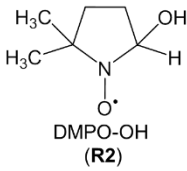
[a]data represent means $\pm$ the standard deviation of three independent experiments; [b]from ref 78; [c] not determined.

As discussed in **Chapter III** (section **3.4.2**), the hyperfine coupling values are dependent on the solvent and EPR spectrometer parameter settings.[73] Consequently, unless recorded under identical experimental conditions, differences between experimental and previously reported values are possible.

Ethanol was also added to the DEPMPO system, however no additional EPR signals were observed. Previous studies have reported on the trapping of the methanol radical formed from the interaction between formed $^\bullet$OH radicals and methanol. This could suggest the DEPMPO spin trap exhibits a low rate for the α-hydroxy-ethyl radical.[70,74] From this section, five spin adducts shown in Table 5.5, were observed. Three of these spin adducts (**R2**, **R4** and **R5**) are observed only in the presence of melatonin. This suggests melatonin contributes to their formation.

Table 5.5 Summary of spin adducts detected in this section

EPR spectra	Adduct	EPR spectra	Adduct
Figure 5.12 **Quartet-of-triplets** **&** **Quartet**	DMPO-N₃ (**R1**) & DMPO-OH (**R2**)	**Figure 5.17** **Quartet** **&** **sextet**	DMPO-OH (**R2**) & DMPO-EtOH (**R5**)
Figure 5.14 **Octet-of-triplets**	DEPMPO-N₃ (**R3**)	**Figure 5.15** **Octet**	DEPMPO-OH (**R4**)
Figure 5.13 **Quartet**	DMPO-OH (**R2**)	-	-

5.3.5 Quantification of the DMPO-N₃ (R1) spin adduct

Irradiation of complex **40** (4 mM) and DMPO (8 mM) with 463 nm light for 14 min led to ca. 378 µM formation of the DMPO-N$_3$ (**R1**) spin adduct (**Chapter III**). In the presence of melatonin (0.1 mM) a decrease of ca. 180- and 11-fold in the DMPO-N$_3$ (**R1**) spin adduct after 7 and 14 min continuous irradiation, respectively, with 463 nm light was observed. Interestingly, it appears a similar quenching effect

on **R1** was observed in the presence of 0.2 mM melatonin. Consequently, this suggests lower concentrations of melatonin (< 0.5 mM) exhibit similar quenching effects on **R1.** However, increasing to the concentration of melatonin to 0.5 mM led to a complete suppression in the **R1** spin adduct after 14 min irradiation at 463 nm (Table 5.6).

Table 5.6 Quantification of **R1** formed from the photo-irradiation of complex **40** (4 mM), DMPO (8 mM) in the absence and presence of melatonin (varied concentration) prepared in PBS/D_2O at pH* 7.4

[Melatonin] / (mM)	[R1][a] / (µM)	[R1][b] / (µM)
No MLT	378.3 ± 0.8	339.3 ± 1.0
0.1	2.1 ± 0.7	30.1 ± 0.4
0.2	1.6 ± 0.9	24.3 ± 1.2
0.5	-[c]	-[c]

R1 refers to the DMPO-N_3 spin adduct after [a]7 min; [b]14 min irradiation at 463 nm (64 mW cm^{-2}); data represent means ± the standard error of three independent experiments [c]no spin adduct formation.

Prolonged irradiation (> 21 min) at 463 nm of the solution containing complex **40** (4 mM), DMPO (8 mM) and melatonin (0.5 mM) prepared in PBS/D_2O at pH* 7.4 led to a successive increase in the EPR signal. The resultant **R1** and **R2** spin adducts were quantified at 7 min intervals up to a total of 54 min continuous irradiation at 463 nm (Figure 5.19). Suppression of **R1** by melatonin appeared to be less potent with prolonged irradiation leading to an increase in its concentration. However, the level of **R1** remained 21-fold lower than the **R1** formed in the absence of melatonin.
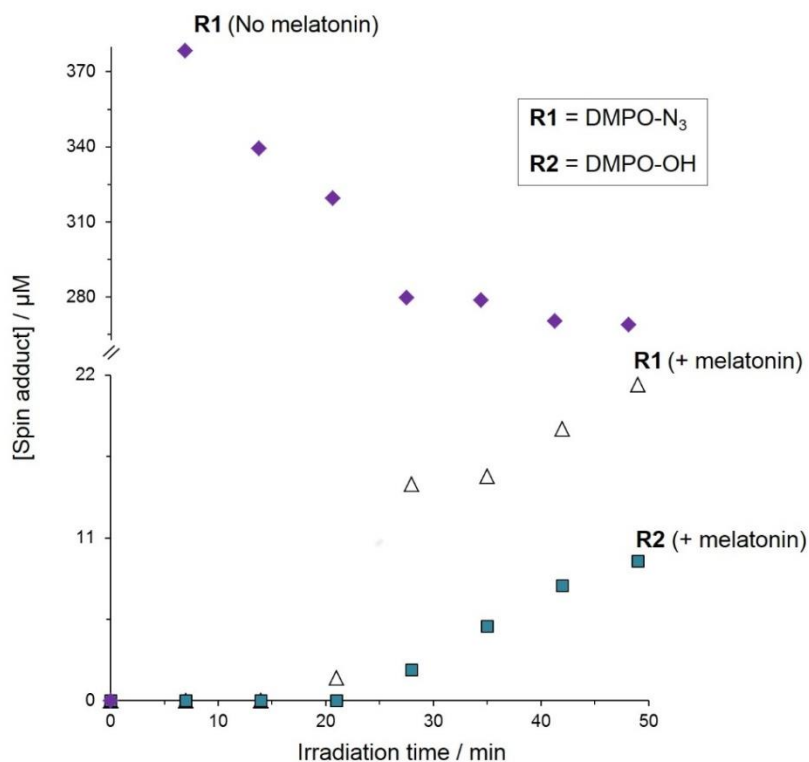
Figure 5.19 Quantification of both the **R1** and **R2** spin adducts formed from a solution containing complex **40** (4 mM), DMPO (8 mM) in the absence (◆) and presence (Δ and ▣) of melatonin (0.5 mM) continuously irradiated at 463 nm for 54 min prepared in PBS/D$_2$O at pH* 7.4. In the presence of melatonin no EPR spectrum is observed until after 21 min irradiation. Spin adduct concentrations determined at 7 min intervals. Refer to Figure 5.18 for structure of **R1** and **R2**.

Hydroxyl (•OH) radicals are regarded as the most aggressive ROS due to their ability to induce DNA, protein and lipid damage.[75] The formation of •OH radicals has potential to enhance the photo-cytotoxicity of complex **40**. Therefore, EPR spin trapping of complex **40** in the presence of melatonin was performed under more physiologically relevant conditions, to determine •OH radical formation.

5.3.6 Physiological concentrations

A solution of *trans,trans,trans*-[Pt(N$_3$)$_2$(OH)$_2$(py)$_2$] (**40**, 300 μM) with DMPO (600 μM) prepared in PBS/D$_2$O at pH* 7.4 was irradiated at 463 nm. In the absence of melatonin, **R1** (DMPO-N$_3$) was generated at ca. 31.5 μM (spectrum **A**, Figure 5.20). A dose dependent suppression in **R1** was observed upon addition of melatonin (spectra **B-D**, Figure 5.20).

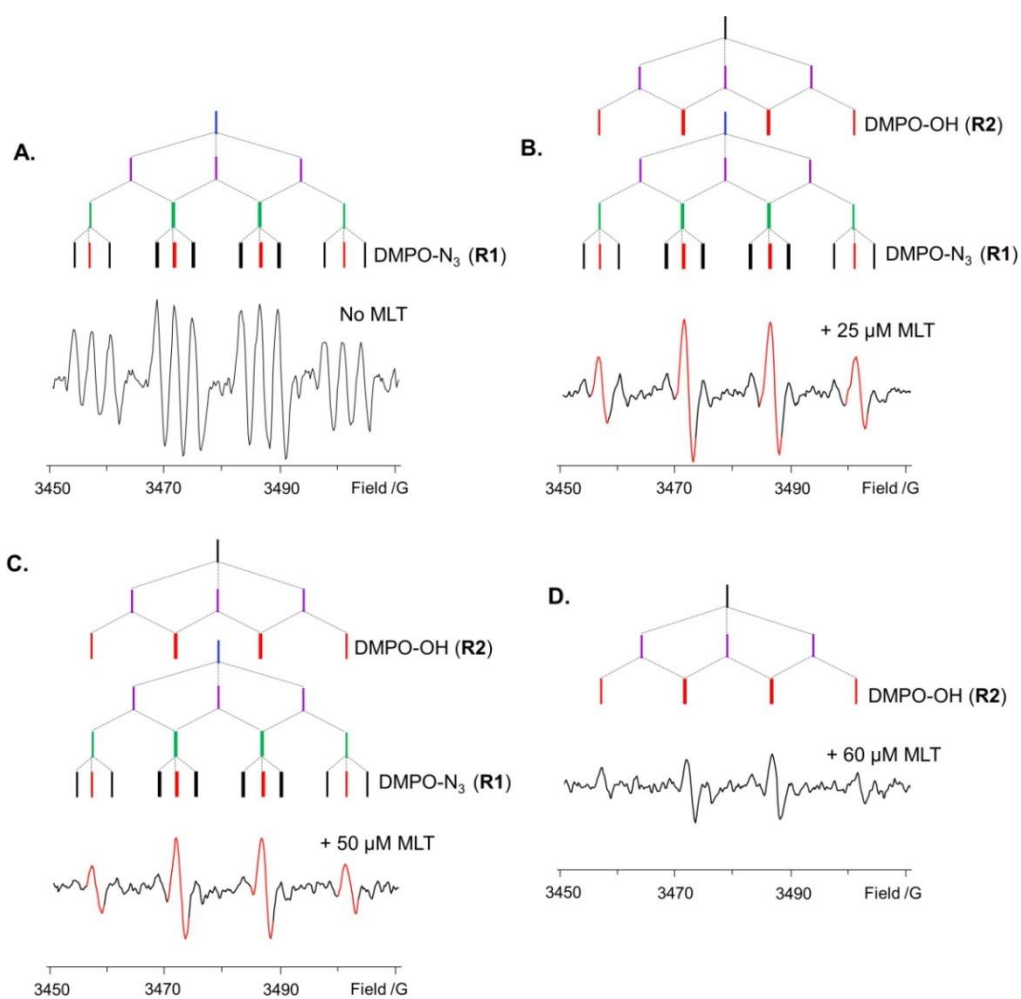**Figure 5.20** EPR spectra generated from the continuous photo-irradiation of complex **40** (300 μM) and DMPO (600 μM) with 463 nm light after 28 min prepared in PBS/D$_2$O at pH* 7.4 in (**A**) absence and presence of (**B**) 25 μM; (**C**) 50 μM; (**D**) 60 μM melatonin (MLT) together with the line diagrams of both **R1** and **R2**. Complete suppression of **R1** in the presence of 60 μM melatonin.

In the presence of 25 µM and 50 µM melatonin, superimposition of both **R1** and **R2** (DMPO-OH) is apparent due to the pronounced intensity of the red lines (**B** and **C**, Figure 5.20), as observed previously at millimolar concentrations of complex **40**. Complete suppression of **R1** was observed upon the addition of 60 µM melatonin, leading only to the formation of **R2** (spectrum **D**, Figure 5.19). As mentioned earlier, the "pharmacological" concentrations of melatonin are reported to be in the nanomolar (nM) range. This suppression of **R1** and formation of **R2** in the presence of melatonin at low micromolar (µM) concentrations suggests the possibility these effects could occur *in vivo*.

Suppression of **R1** has potential to be induced from the scavenging of the $^\bullet N_3$ radicals by melatonin, in agreement with previous literature.[37] Furthermore, the detection of the DMPO-OH (**R2**) spin adduct suggests an alternative photo-decomposition pathway of complex **40** in the presence of melatonin. This was investigated by ^1H NMR spectroscopy.

5.3.7 ^1H NMR spectroscopy

- **Aromatic region**

A solution containing *trans,trans,trans*-[Pt(N$_3$)$_2$(OH)$_2$(py)$_2$] (**40**, 9 mM) and melatonin (9 mM, 1 mol equiv) was prepared in PBS/D$_2$O at pH* 7.4. The ^1H NMR resonances of complex **40** and melatonin remained unchanged in the dark, confirming no dark reaction occurred (Figure 5.21**A**). Photo-irradiation at 463 nm for 60 min led to a brown-coloured precipitate (Figure 5.22**B**), which was removed by centrifugation prior to recording the ^1H NMR spectrum. The extracted precipitate could not be dissolved in a variety of solvents either polar (water,

ethanol, methanol) or non-polar non-polar (benzene, toluene, dimethylformamide). Through ^{1}H NMR integration, ca. a 20% decrease in the Pt-py resonances was determined. Additionally, photo-products (**e′-i′**) were observed (Figure 5.21**B**), equivalent to those previously characterised in **Chapter IV** (refer to p 170), and quantified to ca. 0.9 mM after 60 min irradiation at 463 nm. Interestingly, in the presence of melatonin, ca. a 5% decrease in the ^{1}H NMR resonances of melatonin in the aromatic region were observed (Figure 5.21**B**). Moreover, new photo-products (▼) were observed only from the irradiation of complex **40** in the presence of melatonin. Irradiation for 3 h, induced additional photo-decomposition of complex **40** and melatonin by ca. 50% and 15%, respectively, with, an increase in all the formed photo-products (Figure 5.21**C**). The photo-decomposition of melatonin only in the presence of complex **40**, suggested an interaction between irradiated complex **40** and melatonin. Moreover, the formation of new photo-products (▼) supported that an alternative photo-decomposition pathway of complex **40** occurred in the presence of melatonin.

To further establish this alternative photo-decomposition pathway, the aliphatic region of the ^{1}H NMR spectrum was monitored. The ^{1}H NMR resonances of melatonin in the aliphatic region remained unchanged in the presence of **40**, in the dark (Figure 5.23**A**). Irradiation of **40** in the presence of melatonin, led to photo-decomposition in melatonin of ca. 5% and 20% after 60 min and 3 h irradiation at 463 nm, respectively. Moreover, new photo-products (▼) were observed after 60 min (Figure 5.23**B**), not detected from the irradiation of complex **40** alone. Finally, an additional photo-products were observed in the aliphatic region after 3 h

irradiation at 463 nm (▼, Figure 5.23**C**). The photo-decomposition of **40** and melatonin is summarised in Table 5.7.

Figure 5.21 The aromatic region of the ^{1}H NMR spectrum of a solution containing complex **40** (9 mM) in the presence of melatonin (9 mM, 1 mol equiv) prepared in PBS/D$_2$O at pH* 7.4 in (**A**) the dark and after (**B**) 60 min; (**C**) 3 h irradiation at 463 nm. Assignments: **o**/**p**/**m**, Pt-py peaks; Greek letters, melatonin peaks; **e'-i'**, platinum photo-products generated in the absence and presence of melatonin; ▼, photo-products only formed in the presence of melatonin. Insets are an expansion of the region containing peaks for photo-products. (See Figure 5.23 for aliphatic region).
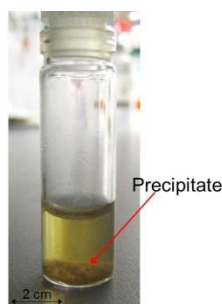
Figure 5.22 Precipitate formed after irradiation of a solution containing complex **40** (9 mM) in the presence of melatonin (9 mM, 1 mol equiv) prepared in PBS/D$_2$O at pH* 7.4 after 60 min irradiation at 463 nm.
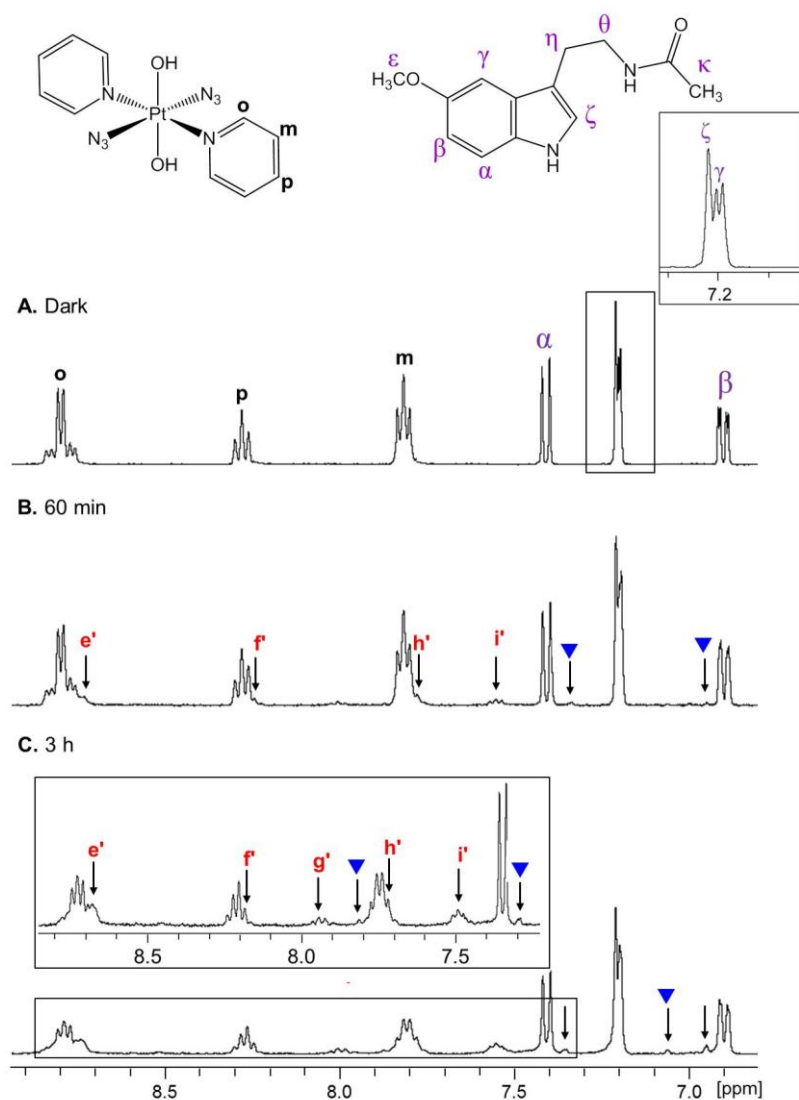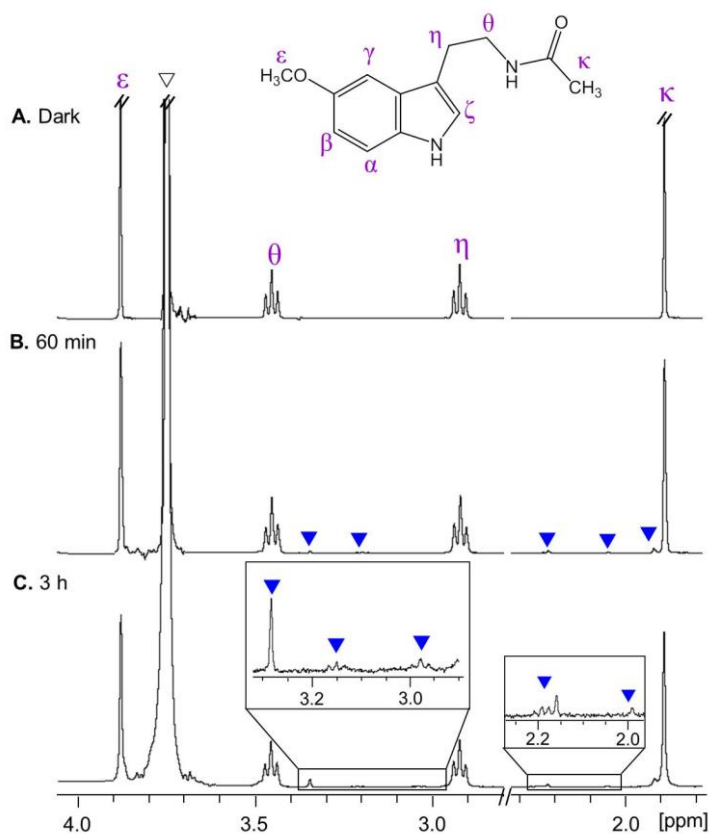

Figure 5.23 The aliphatic region of the ^{1}H NMR spectra of complex **40** (9 mM) in the presence of melatonin (9 mM, 1 mol equiv) prepared in PBS/D$_2$O at pH* 7.4 in the (**A**) dark and after (**B**) 60 min; (**C**) 3 h irradiation at 463 nm. Assignments: Greek letters, melatonin peaks; ▼, photo-products only formed in the presence of melatonin. Insets are an expansion of the region containing peaks for photo-products. (See Figure 5.21 for aromatic region).

Table 5.7 Quantification of the ^{1}H NMR resonances of species shown in Figures 5.21 and 5.23.

Time / min	^{a}[40] / mM	^{b}[MLT] / mM	[e'-i'] / mM	[▼] / mM
Dark	9.0	9.0	$-^c$	$-^c$
60	7.2	8.5	0.9	0.2
3 h	3.0	6.9	1.4	0.6

^{a}**40**, *trans,trans,trans*-[Pt(N$_3$)$_2$(OH)$_2$(py)$_2$]; ^{b}**MLT**, melatonin; **e′-i′**, photo-products generated as shown in Figure 5.21 (previously assigned in **Chapter IV**); coloured triangles, photo-products formed only in the presence of melatonin as shown in Figures 5.21 and 5.23; ^{c}peaks not observed in the dark.

The low S/N ratio of these generated photo-products after 3 h irradiation at 463 nm meant that complete spectral assignment was not feasible by ^{1}H NMR spectroscopy alone. Therefore, HR-MS was performed in an attempt to elucidate the identity of these formed species.

5.3.8 Mass spectrometry and COSY NMR spectroscopy

A solution of *trans,trans,trans*-[Pt(N$_3$)$_2$(OH)$_2$(py)$_2$] (**40**, 9 mM) in the presence of melatonin (9 mM, 1 mol equiv) was prepared in H$_2$O and irradiated at 463 nm for 60 min. After performing a 100-fold dilution of the irradiated solution, mass adducts at *m/z* of 271.085 and 389.103 were detected (Figure 5.24), assigned to [C$_{13}$H$_{16}$N$_2$O$_3$+Na]$^+$ (**59**) and [Pt(OH$_2$)$_2$(py)$_2$]$^{2+}$ (**60**), respectively.

Figure 5.24 HR-MS spectra of a solution of complex **40** (9 mM) in the presence of melatonin (9 mM, 1 mol equiv) prepared in H_2O at pH 7.4 irradiated at 463 nm for 60 min recorded. Labelled mass adducts are summarised in Table 5.8.

Furthermore, mass adducts at *m/z* of 430.0712, 452.0531, 603.1806 and 625.1625 were detected by HR-MS (Figure 5.25), assignable to $[Pt(N_3)(OH)_2(py)_2+H]^{2+}$ (**61**), $[Pt(N_3)(OH)_2(py)_2+Na]^{2+}$, $[Pt(OH_2)(py)_2(MLT)]^{2+}$ (**62**) and $[Pt(OH_2)(py)_2(MLT)+Na]^{3+}$ respectively, in agreement with their simulated mass spectra. The formation of **59** and **62** are suggested to rationalise the photo-products (▼) as shown in Figures 5.21 and 5.23. Mass adducts detected are summarised in Table 5.9.
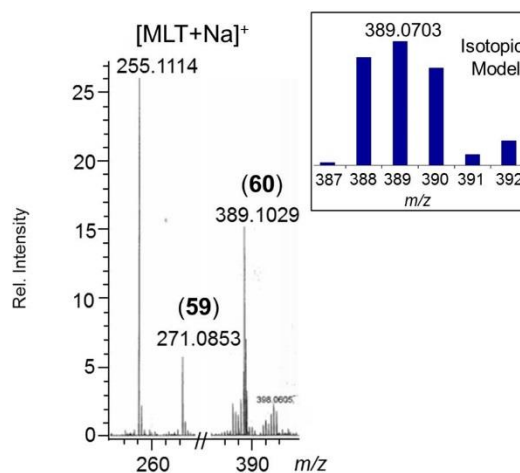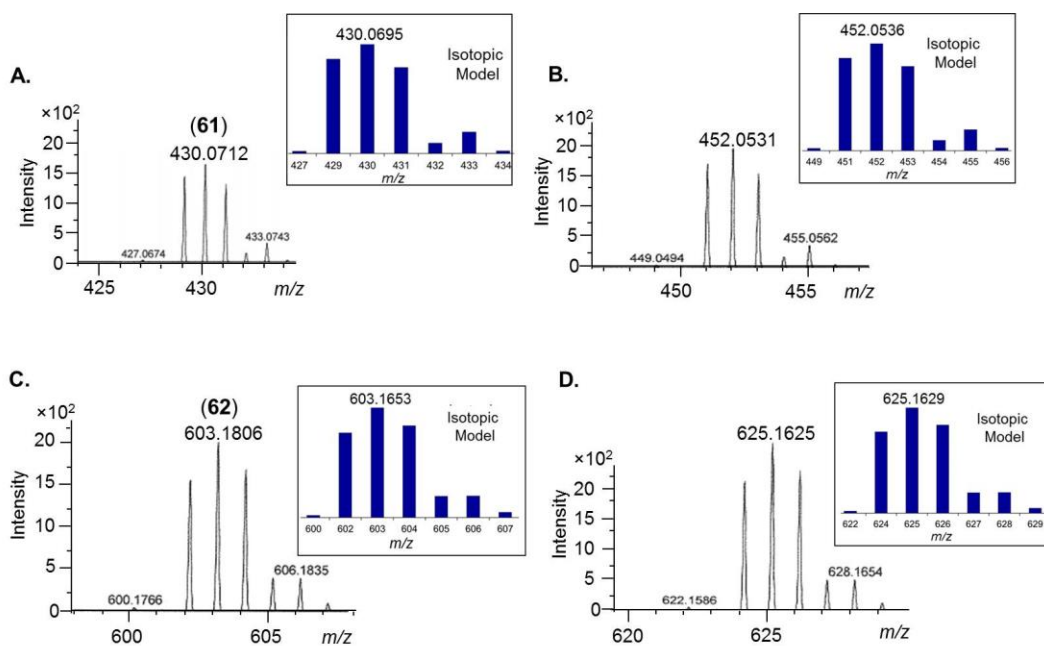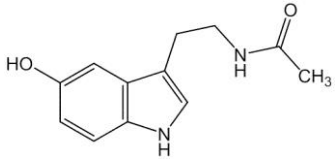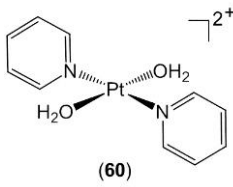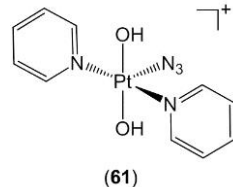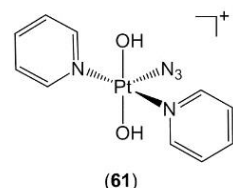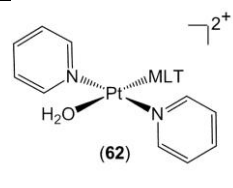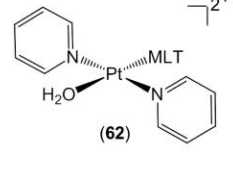
Figure 5.25 HRMS spectra of a solution of complex **40** (9 mM) in the presence of melatonin (9 mM, 1 mol equiv) prepared in H_2O at pH 7.4 irradiated at 463 nm for 60 min recorded. Labelled mass adducts are summarised in Table 5.8.

The detection of the mass adduct at *m/z* 430.0712 (calc. *m/z* 430.0695), assigned to $[Pt(N_3)(OH)_2(py)_2+H]^{2+}$ (**61**), suggested the loss of one azide ligand. This loss of the azide ligand, as free azide, has potential to account for the observed lag-phase in the detection of an EPR signal (Figure 5.19). This mono-azide Pt^{IV} reactive intermediate is suggested to undergo further reaction, leading to the generation of the azidyl and hydroxyl radicals. Moreover, the detection of **62** suggests the binding of melatonin to a Pt^{II} photo-product. This will be discussed later in section **5.4.2**.

237

Table 5.8 Assignment of mass adducts as shown in Figures 5.24 and 5.25.

Found m/z	Structure	Formula	Calc. m/z
255.1114		$C_{13}H_{16}N_2O_2Na$ $[MLT+Na]^+$	255.2830
271.0853	(Structure determined) (**59**)	$C_{13}H_{16}N_2O_3Na$ $[MLT-OH+Na]^+$	271.2224
389.1029	 (**60**)	$C_{10}H_{14}N_2O_2Pt$ $[Pt(OH_2)(py)_2]^{2+}$	389.0703
430.0712	 (**61**)	$C_{10}H_{13}N_5O_2Pt$ $[Pt(OH)_2(N_3)(py)_2+H]^{2+}$	430.0695
452.0531	 (**61**)	$C_{10}H_{12}N_5O_2PtNa$ $[Pt(OH)_2(N_3)(py)_2+Na]^{2+}$	452.0536
603.1806	 (**62**)	$C_{23}H_{28}N_4O_3Pt$ $[Pt(OH)_2(py)_2+H]^{3+}$	603.1653
625.1625	 (**62**)	$C_{23}H_{27}N_4O_3PtNa$ $[Pt(OH)_2(py)_2+Na]^{3+}$	625.1629

The detection of the mass adduct at *m/z* 271.0853 was assigned as $[C_{13}H_{16}N_2O_3+Na]^+$ (**59**), an increase in the sodium adduct of melatonin by 17 mass units, suggesting the addition of "OH" to melatonin. Despite the detection of this mass adduct as 271.0853 *m/z*, based on the ^1H NMR data, complete structural assignment was not feasible. Consequently, a COSY NMR spectrum of the irradiated solution was performed to establish a correlation between the newly formed photo-products generated in the presence of melatonin. However, due to the low S/N ratio of the photo-products, it was not possible to determine correlation between the desired resonances. However, a correlation between photo-products, **e'-i'** was observed (Figure 5.26).
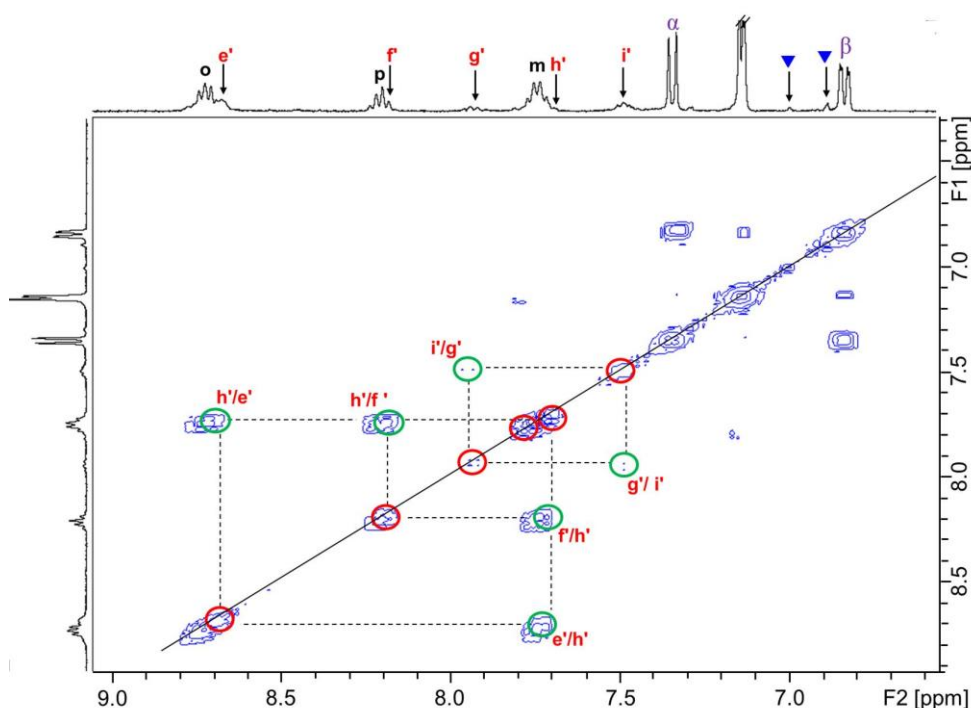
Figure 5.26 The aromatic region of the COSY NMR spectrum obtained from a solution containing complex **40** (9 mM) in the presence of melatonin (9 mM, 1 mol equiv) prepared in PBS/D₂O at pH* irradiated for 3 h at 463 nm. ^1H NMR resonance and cross-peak represented by ○ and ○, respectively. Correlation shown for photo-products **e'-i'**.

Additional, ^{13}C-DEPT135 NMR spectroscopy was also performed to identify the new resonances however no new resonances were observed. The lack of detection of new resonances was attributed to their respective concentrations, believed to be below the limit of detection for ^{13}C-DEPT135 analysis. The possible products of hydroxyl radical addition to melatonin will be discussed in section **5.4.2.**

The DMPO-N$_3$ spin adduct was detected, it was ca. 21-fold lower than the DMPO-N$_3$ detected in the absence of melatonin. Previous literature has reported on the quenching ability of melatonin towards the $^{\bullet}$N$_3$ radicals.[37] To establish this potential interaction in this work, ^{14}N NMR spectroscopy was performed.

5.3.9 Quenching of azidyl radicals

The ^{14}N NMR resonance at 97.9 ppm from a solution of melatonin (18 mM) prepared in PBS/D$_2$O at pH* 7.4 was assigned to the **N**H of the indole ring present in melatonin (Figure 5.27). The other amino resonance is outside the spectral range, as reported for other amino functionalities.[76]
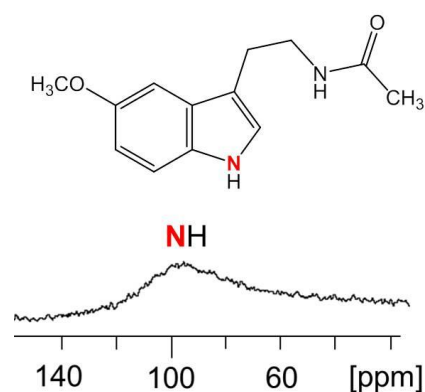
Figure 5.27 The ^{14}N NMR spectrum of a solution of melatonin (18 mM) prepared in PBS/D$_2$O at pH* 7.4. Resonance at ca. 97.9 ppm assigned to the nitrogen atom (**N**H) of the indole ring of the melatonin molecule.

The dark ^{14}N NMR spectrum of a solution of complex **40** (6 mM) in the presence of melatonin (2.5 mM) prepared in PBS/D$_2$O at pH* 7.4 displayed ^{14}N NMR resonances for the coordinated azide ligand (**A**, Figure 5.28). Under these experimental conditions, no ^{14}N NMR resonances were detected for melatonin. Photo-irradiation of this solution of complex **40** (6 mM) in the presence of melatonin (2.5 mM) at 463 nm for 30 min led the observation of an additional peak at *ca.* 77.3 ppm, previously assigned to the central nitrogen (N$_\beta'$) of free azide (**Chapter IV**).
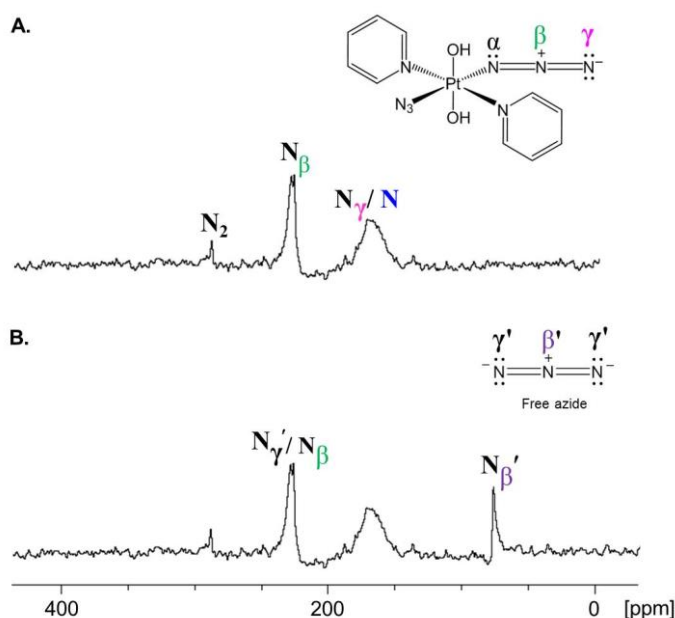
Figure 5.28 The ^{14}N NMR spectrum of a solution of complex **40** (6 mM) with melatonin (2.5 mM) prepared in PBS/D$_2$O at pH* 7.4 in (**A**) dark and (**B**) irradiated at 463 nm for 30 min. The appearance of the N$_\alpha$ peak of complex **40** (expected at *ca.* 60 ppm) is too broad to observe under the conditions used.[77] Assignments (^{14}N, 43.3 MHz in D$_2$O): δ = 229.3 ppm, central nitrogen (N$_\beta$) of coordinated azide overlapped with the terminal nitrogen (Nγ') of free azide (N$_3^-$); 168.1, overlap between terminal nitrogen of coordinated azide (Nγ) and nitrogen from pyridine ligand (**N**); 77.3, central nitrogen (N$_\beta'$) of free azide (N$_3^-$).

Despite the detection of free azide (N_3^-) from the photo-irradiation of *trans,trans,trans*-[Pt(N$_3$)$_2$(OH)$_2$(py)$_2$] (complex **40**, 6 mM) with melatonin (2.5 mM), it was not possible to confirm if this was from the release of the azide ligand from irradiated complex **40** in the presence of melatonin or from the quenching of the azidyl radicals by melatonin. Previous quenching of the $^\bullet$N$_3$ radicals by L-Trp (**Chapter IV**) induced a photo-protective effect. Therefore, to establish the effect of melatonin on the photo-cytotoxicity of complex **40**, cell viability studies were performed in A2780 ovarian cancer cells.

5.3.10 Photo-irradiation in A2780 ovarian cancer cells with melatonin

Photo-irradiation studies were performed by Dr. Julie Woods at Ninewell's Hospital, Dundee. A2780 ovarian cancer cells were plated with complex **40** (42.4 µM) with varying doses of melatonin. Photo-irradiation at 420 nm (5 J cm^{-2}) of complex **40** (42.4 µM) in A2780 ovarian cancer cells led to ca. 2% cell viability. Interestingly, the addition of melatonin (70 µM) led to ca. 17% cell viability (Figure 5.29). A direct correlation between the successive addition of melatonin (up to 2.2 mM) and amount of viable cells can be clearly observed from Figure 5.29.
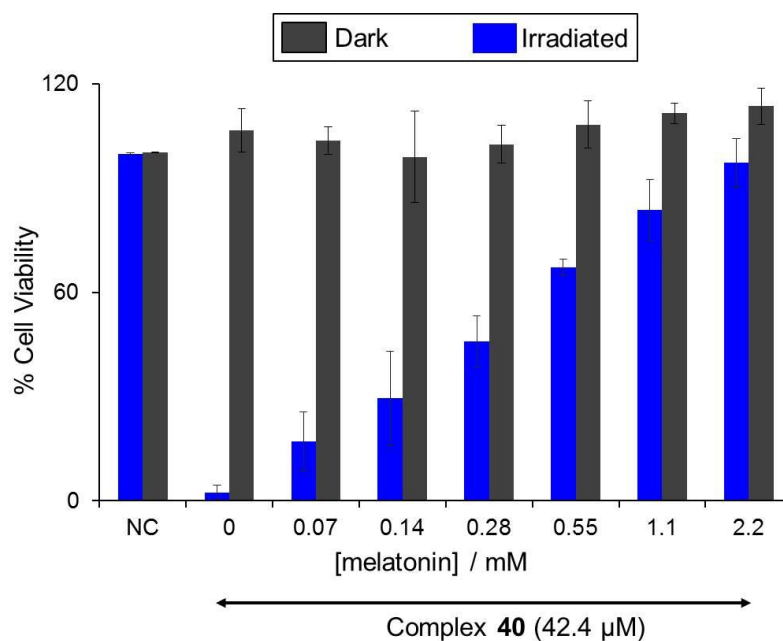
Figure 5.29 The percentage cell viability induced from the photo-irradiation of complex **40** (42.4 µM, n = 2 independent experiments) in the presence of melatonin (different concentrations) in A2780 ovarian cancer cells in the (■) dark and (■) after irradiation at λ_{max} = 420 nm (5 J cm^{-2}). NC: negative control (cells only). Data represent means ± standard errors for the mean of 6 monolayers from 2 independent experiments performed in duplicate.

ALA, precursor of the photosensitiser, protoporhyrin (PpIX) which is widely used in PDT therapy. Metabolism of ALA generates PpIX, which upon photo-activation with light of appropriate wavelength induces its photo-cytotoxic effect *via* singlet oxygen ($^1O_2$) formation.[43] Similar to the $^{\bullet}OH$ radicals, $^1O_2$ is classified as a ROS and has potential to induce a cascade of cytotoxic effects upon formation.[78] Previous studies have reported on the quenching of $^1O_2$ by melatonin.[79]

Therefore, the scavenging of ROS by melatonin was assessed by incubation of 5-aminolevulinic acid (ALA, 1 mM) in the presence of melatonin (different

concentrations) in A2780 ovarian cancer cells. No dark photo-cytotoxicity was observed (■, Figure 5.30). However, irradiation at 420 nm (5 J cm^{-2}) led to a decrease in cell viability across the range of melatonin. It appeared that under these experimental conditions, melatonin could not quench $^1O_2$ formed from PpIX generated from the precursor ALA.
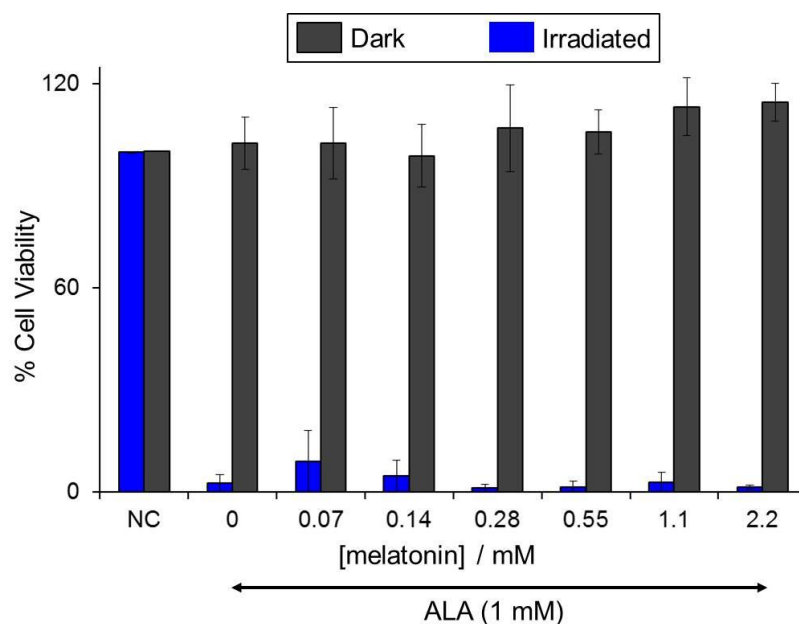
Figure 5.30 The percentage cell viability induced from 5-aminolevulinic acid (ALA, 1 mM, n = 2 independent experiments) in the presence of melatonin (different concentrations) in A2780 ovarian cancer cells in the (■) dark and (■) after irradiation at λ_{max} = 420 nm light (5 J cm^{-2}). NC: negative control (solvent only). Data represent means ± standard errors for the mean of 6 monolayers from 2 independent experiments performed in duplicate.

In the absence of melatonin, *trans,trans,trans*-[Pt(N$_3$)$_2$(OH)$_2$(py)$_2$] (complex **40**) induced a photo-cytotoxic effect. However, successive addition of melatonin, led to a photo-protective effect. Contrary to previous literature, melatonin was unable to

quench the $^1O_2$ formed from irradiated ALA, under these conditions, leading to a cytotoxic effect in A2780 ovarian cancer cells.

5.4 Discussion

5.4.1 Hydroxyl radical characterisation

Photo-irradiation of *trans,trans,trans*-[Pt(N$_3$)$_2$(OH)$_2$(py)$_2$] (complex **40**) in the absence of melatonin, led to the detection of the DMPO-N$_3$ spin adduct after 42 s irradiation at 463 nm (**Chapter III**, p 99). However, in the presence of melatonin an EPR signal was detected after irradiation for 21 min at 463 nm. The EPR signal detected after 21 min irradiation was identified as the superimposition of two DMPO nitrone spin adducts from the photo-irradiation of complex **40** and DMPO in the presence of melatonin. Using semi-continuous irradiation (irradiation for 14 min at 463 nm, after which the irradiation source is switched off), a quartet EPR spectrum in the ratio of 1:2:2:1 was identified and assigned to the hydroxyl radical DMPO-OH (**R2**) spin adduct.

However, the DMPO-OH spin adduct can be mistakenly detected from the spontaneous decay of the DMPO-OOH spin adduct (t$_½$ = 56 s).[80,81] Therefore, the method for $^•$OH radical detection, described by Finkelstein,[18] was used. This involved the addition of ethanol which led to the detection of the DMPO-α-hydroxyl-ethyl radical (**R5**), formed from the interaction of the $^•$OH radicals with ethanol. Moreover, the phosphorus spin trap, DEPMPO generates distinct EPR signals for both the DEPMPO-OH and DEPMPO-OOH spin adducts.[70] Therefore, in this work, substitution of the DMPO spin trap to DEPMPO led to the detection of an 8-lined EPR spectrum assigned to the DEPMPO-OH (**R4**) spin adduct.

Consequently, the detection of DEPMPO-OH (**R4**) and DMPO-EtOH (**R5**) spin adducts confirmed that the initial quartet EPR spectrum was due to the trapping of the $^\bullet$OH radicals by DMPO. Photo-irradiation of complex **40** alone, did not lead to the detection of the $^\bullet$OH radicals by EPR spin trapping (refer to **Chapter III).** Therefore, in this Chapter the generation of the $^\bullet$OH radicals was believed to be mediated by melatonin.

5.4.2 Photo-protective effect

Photo-irradiation of complex **40** in the presence of melatonin led to the quenching of the $^\bullet$N$_3$ radicals by melatonin and the formation of the $^\bullet$OH radicals. Reactions of $^\bullet$N$_3$ radicals with melatonin have been reported to occur with a rate constant of ca. 9.8×10^9 M^{-1} s^{-1},[37] considerably faster than $^\bullet$N$_3$ radicals trapped by DMPO (1.6×10^9 M^{-1} s^{-1}),[82] further accounting for the pronounced quenching of the DMPO-N3 spin adduct in the presence of melatonin. Moreover, melatonin possesses a reduction potential of ca. 0.73 V,[83] in contrast to the $^\bullet$N$_3$ radical possessing a reduction potential of ca. 1.33 V.[35] This suggests a one-electron donation from melatonin to the $^\bullet$N$_3$ radical occurs favourably, leading to the formation of free azide (N$_3^-$) and a melatonin radical cation (**A**, Figure 5.31). N$_3^-$ is a toxic species, however its toxicity has been reported to be dose-dependent.[84] In this work, the concentration of free azide is believed to be below the level to induce a cytotoxic effect.

Moreover, the melatonin radical cation MLT$^{\bullet+}$ radical has been previously reported by Lewis to be non-toxic to cells.[85] Similar to the L-Trp$^{\bullet+}$ species, rapid deprotonation of MLT$^{\bullet+}$ may occur at pH 7 forming the neutral MLT$^\bullet$ species.

Polymerisation of various indole radicals is a well-reported phenomenon,[86,87] and in one study polymerisation was shown to be mediated *via* the indole radical cation.[88] Therefore, in this work, the brown-coloured precipitate (refer to Figure 5.22) formed from the photo-irradiation of complex **40** in the presence of melatonin is believed to be a MLT-based polymer species.
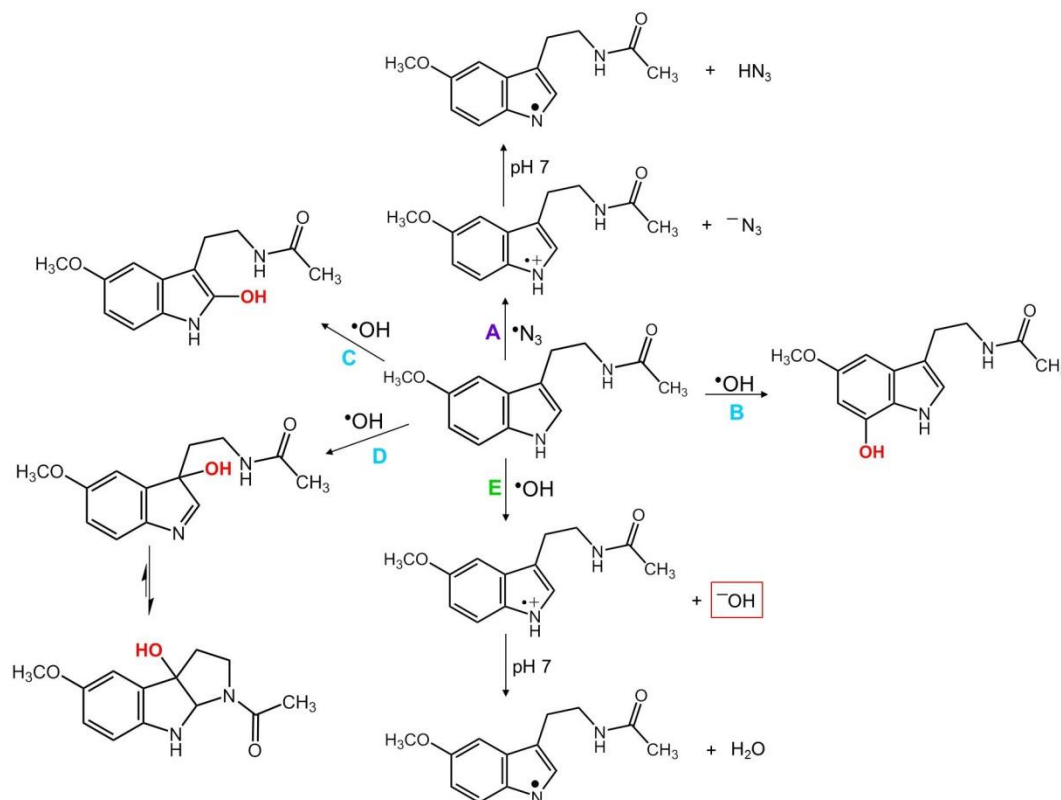
Figure 5.31 Reaction of melatonin with (**A**) the azidyl, $^\bullet N_3$; (**B-E**) the hydroxyl, $^\bullet OH$ radicals leading to the formation of various species.

Additionally, the formation of the MLT$^\bullet$ radical is suggested to account for the detection of **62**, assigned to $[Pt(OH_2)(py)_2(MLT)]^{2+}$ by HR-MS. Previous studies have reported on the binding of melatonin to various metal ions,[62,89] through absorptive stripping voltammetry. However, such studies have not, at present, identified the metal coordination site present in melatonin. Melatonin (Figure 5.3) does not illustrate any potential Pt^{II}-binding sites. However, the formation of the

MLT$^\bullet$ radical, at the nitrogen atom of the indole (**A** and **E**, Figure 5.31) has potential to react with the Pt^{II} intermediate, as shown in section **5.4.3**.

Consequently, the observation of a photo-protective, from the quenching of the azidyl radicals, was similar to that previously reported in **Chapter IV**. Interestingly, the detection of $^\bullet$OH radicals, initially proposed an enhancement in the photo-cytotoxicity of complex **40**. However, a photo-protective effect was still observed. Additional photo-products were detected by ^{1}H NMR spectroscopy (refer to Figure 5.21 and Figure 5.23), yet due to their low concentrations, complete characterisation of the formed photo-products was not feasible. HR-MS identified a mass adduct at *m/z* 271.085 (**59**), which was calculated to be 17 a.m.u higher than the parent sodium adduct of melatonin, *m/z* 255.111. Whilst, the structure of this species could not be completely determined by ^{1}H or COSY NMR, the increase in 17 a.m.u, suggested the addition of the hydroxyl radical to melatonin.

The hydroxyl radical has potential to coordinate to melatonin at the C2, C3 and C7 positions (**B-D**, Figure 5.31. Moreover, addition of the hydroxyl radical at the C7 position can induce enol-keto tautomerism leading to a thermodynamically more stable 3-cyclic-hydroxy-melatonin species (**D**, Figure 5.31). The latter species previously reported by Tan *et al.*, to a main metabolite of hydroxyl radical reaction with melatonin.[38] Furthermore, the formed hydroxyl radicals have potential to undergo a one-electron transfer reaction with melatonin (**E**, Figure 5.31), leading to the formation of the hydroxide ion ($^-$OH) and the MLT$^\bullet$. Lastly, the formed hydroxyl radicals also possess the potential to react with N$_3$$^-$ (formed from **A**, Figure 5.31), leading to the formation of both hydroxide ions and azidyl radicals, a

previously reported reaction by Neta *et al.*[90] Consequently, from this reaction, it is possible the formed hydroxide ions have potential to react with both/either melatonin and a Pt^{II} intermediate species. In summary, it appears from Figure 5.31, that both the azidyl and hydroxyl radicals can undergo numerous reactions pathways, such that neither radicals are available to induce their cytotoxic effect.

5.4.3 Mechanism of action

The detection of the mass adduct at *m/z* 430.0712, assigned to $[Pt(N_3)(OH)_2(py)_2+H]^{2+}$, suggested the loss of one coordinated azide ligand. However, the equivalent decrease in the $N_3 \rightarrow Pt^{IV}$ LMCT band of complex **40** in both the absence and presence of melatonin, as observed by UV-visible spectroscopy, confirmed that both azide ligands are lost from complex **40**. The superimposition of the azidyl and hydroxyl radical DMPO spin adducts suggested the simultaneous trapping of the azidyl and hydroxyl radical by spin trap, DMPO. From these results, the photo-decomposition pathway of complex **40** in the presence of melatonin is proposed in Figure 5.32.

Briefly, photo-irradiation of *trans,trans,trans*-$[Pt(N_3)_2(OH)_2(py)_2]$ (complex **40**) in the presence of melatonin leads to an initial loss of one azide ligand, generating a reactive Pt^{IV} mono-azide intermediate species, as detected by HR-MS (**61**) and free azide (N_3^-) as detected by ^{14}N NMR spectroscopy. This initial loss of coordinated azide, as free azide, is consistent with the lag-phase in the detection of an EPR signal. Continued irradiation of **61** gives rise to two one-electron donations from the remaining azide and one hydroxyl ligands to the Pt^{IV} metal centre, forming a Pt^{II} intermediate, azidyl and hydroxyl radicals. Then, two possible reaction

pathways are proposed for the Pt^{II} intermediate species. Firstly, the melatonin

radical ($MLT^{\bullet}$) formed from the quenching of the azidyl radicals by melatonin has

potential to react with the Pt^{II} intermediate, generating a Pt^{II}-melatonin species as

detected by HR-MS at *m/z* 603.1806, assigned to $[Pt(OH_2)(py)_2(MLT)]^{2+}$ (**62**,

where MLT represents melatonin).
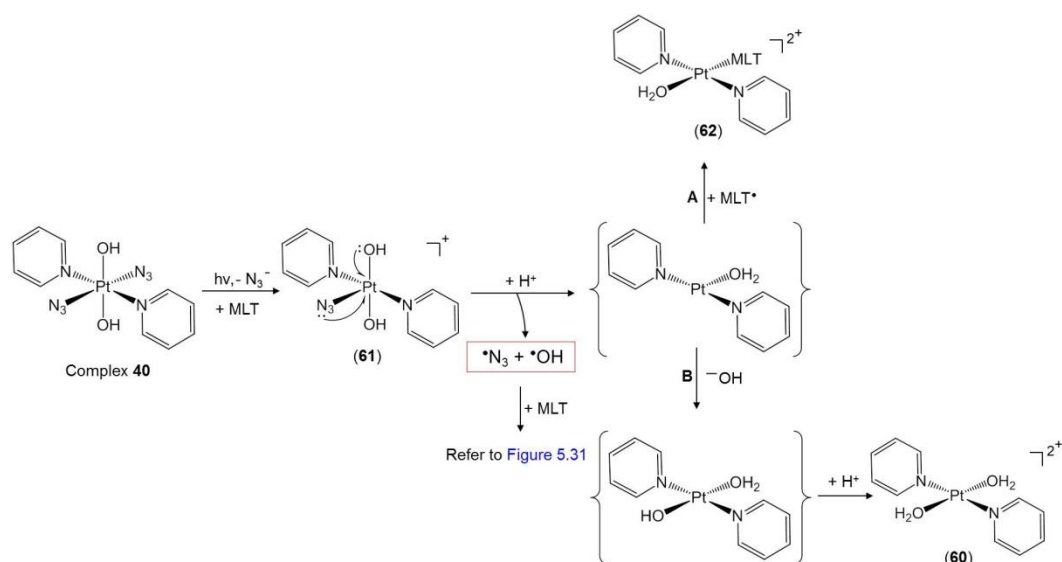
Figure 5.32 Proposed photo-decomposition pathway of complex **40** in the presence

of melatonin. Curly brackets represent non-detected species. Coordination site of

melatonin has not been explicitly determined, therefore shown as Pt-MLT bond.

The second pathway, is more complicated but also appears possible. Initially, the

hydroxyl radicals can react with melatonin (**E**, Figure 5.31) or with free azide and

generate hydroxide ions, as previously reported reaction by Neta *et al.*[90]

Consequently, from this reaction, it is possible the formed hydroxide ions react with

the Pt^{II} intermediate species and generate $[Pt(OH_2)_2(py)_2]^{2+}$ (**60**), as detected by HR-

MS. The detection of the melatonin-Pt^{II} species (**62**), suggests the amount of Pt^{II}

available to react with the N^7 atom of guanine (DNA nucleobase) is reduced in

A2780 ovarian cancer cells, leading to the observed photo-protective effect.

Interestingly, dimerisation of $^\bullet$OH radicals can also form hydrogen peroxide (H_2O_2), a well-known ROS. H_2O_2 does not damage DNA directly. However, readily diffusible across cells, H_2O_2 is a major contributor of additional ROS, far from the site of production.[91] For example, disproportionation of H_2O_2 mediated by various inorganic catalysts[92] leads to the generation of singlet oxygen ($^1O_2$),[93] the species responsible for inducing cell death in current PDT treatments.[94] The compound 5-aminolevulinic acid (ALA) is used in PDT therapy (**Chapter I**).[95] Its cytotoxic effect is induced through the formation of $^1O_2$. Previous *in vivo* studies by Princ *et al.* reported the ability of melatonin (0.5 – 2 mM) to diminish the cytotoxic effect of ALA in rat cerebellum.[79,96] In this work, photo-irradiation of ALA with blue light in the presence of melatonin led to a photo-cytotoxic effect in the A2780 ovarian cancer cells. Interestingly, it appears under conditions used here, melatonin was unable to quench $^1O_2$. Therefore, due to the observed photo-protective effect from the photo-irradiation of complex **40** in the presence of melatonin, suggests $^\bullet$OH radical dimerisation does not occur.

Melatonin regulates the circadian rhythms in humans and animals. Its maximum production is during sleep hours,[97] and the amount of melatonin produced is dependent on age,[98] as shown in Figure 5.34. In this work, it would appear that treatment of cancerous tissue(s) with complex **40** during levels of melatonin production would reduce the platinum(IV) diazido anticancer complex photo-cytotoxicity. Interestingly, this work incorporates into the new research field of Chronopharmacology.[99] This field has identified the optimum time-of-day to administer a drug to achieve sufficient metabolism and/or therapeutic efficiency. For example, the treatment of asthma has been determined to be most effective at

low plasma concentrations of dyspneas.[100,101] Furthermore, patients undergoing elective gynaecological surgery showed an increase in plasma levels of melatonin, having been anaesthetised with isoflurane in contrast to propofol.[102] Therefore, successful treatment of cancer *via* photo-chemotherapy may be achieved under non-anaesthetised conditions.
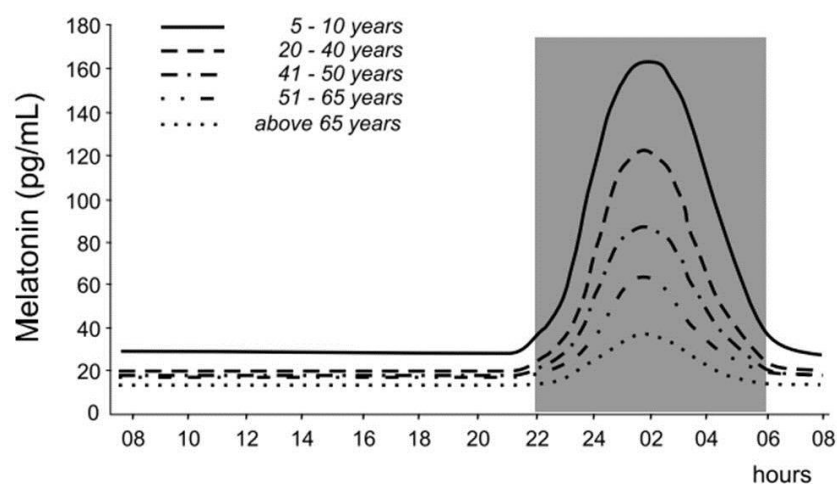
Figure 5.33 Serum concentration of melatonin in human at various age, grey area refers to darkness period (figure from ref 98).

5.5 Conclusion

This Chapter investigated the photo-irradiation of *trans,trans,trans-*[Pt(N$_3$)$_2$(OH)$_2$(py)$_2$] (complex **40**) in the presence of melatonin. Electron paramagnetic resonance (EPR) studies led to the detection and characterisation of both the azidyl ($^\bullet$N$_3$) and hydroxyl ($^\bullet$OH) radicals using both continuous and semi-continuous irradiation modes. The quartet EPR spectrum in the ratio of 1:2:2:1 was assigned to the DMPO-OH (**R1)** spin adduct. However, the quartet EPR spectrum can be easily detected from the spontaneous decay of unstable DMPO spin adducts. Therefore, the confirmation of $^\bullet$OH radical production was deduced from the

detection of the DMPO-EtOH (**R5**) spin adduct, formed from the interaction of the $^{\bullet}$OH radical with ethanol. Moreover, substitution of the spin trap DMPO by the phosphorus analogue DEPMPO, led to the observation of an eight-lined EPR spectrum. This was assigned to the DEPMPO-OH (**R4**) spin adduct in agreement with previous reported values.

^{1}H NMR spectroscopy of complex **40** in the presence of melatonin, led to the formation of new photo-products in both the aromatic and aliphatic region. MS identified mass adducts at *m/z* of 271.085, 430.0712 and 603.1806, assigned to $[C_{13}H_{16}N_2O_3+Na]^+$ (**59**), $[Pt(OH)_2(N_3)(py)_2+H]^{2+}$ (**61**) and $[Pt(OH_2)(py)_2(MLT)]^{2+}$ (**62**), respectively. The detection of the mono-azide Pt^{IV} species (**61**) suggested the loss of coordinated azide, as free azide. However, UV-visible spectroscopy identified an equivalent photo-decomposition in the $N_3{\rightarrow}Pt^{IV}$ LMCT band in both the absence and presence of melatonin, which suggested that both azide ligands were lost. The superimposition of the azidyl and hydroxyl radical DMPO spin adducts, confirmed the simultaneous release of the azide and hydroxyl ligands, in radical form. Despite the detection of the DMPO-N$_3$ spin adduct, it was ca. 21-fold lower compared to the DMPO-N$_3$ spin adduct formed in the absence of melatonin. Consequently, this suppression in the DMPO-N$_3$ spin adduct was partially attributed to the quenching of the azidyl radicals by melatonin. Quenching of the azidyl radicals by melatonin was supported by the detection of free azide, as detected by ^{14}N NMR spectroscopy. The quenching of the azidyl radicals, also proposed the formation of the melatonin radical (MLT$^{\bullet}$, undetected). Melatonin does not exhibit metal-binding sites in its structure, consequently, the detection of **62** assigned to $[Pt(OH_2)(py)_2(MLT)]^{2+}$, was suggested to form *via* the interaction of

MLT$^{\bullet}$ with the Pt^{II} intermediate. New ^{1}H NMR resonances were observed in both the aromatic and aliphatic region suggested to be related to a hydroxy-melatonin species (**59**). However, due to a low S/N of these formed photo-products complete characterisation was not possible.

Photo-irradiation of complex **40** in the presence of melatonin in A2780 ovarian cancer cells induced a photo-protective effect. The quenching of the $^{\bullet}$N$_3$ by melatonin and detection of **59**, confirmed neither of these RNS and ROS were available to induce their cytotoxic effect. The formation of the platinum(II)-melatonin species (**62**) is believed to reduce amount of Pt^{II} to bind to the guanine nucleobase of DNA to induce a cyto-toxic effect.

The concentration of melatonin varies dependent on the light-dark cycle and in accordance to age in humans. Children exhibit the highest production of melatonin in the period of darkness, in contrast to the elderly which show a slight change in melatonin production from the light-dark cycle. This study suggests treatment of antineoplastic tissue with complex **40** and possibly other structurally related platinum(IV) diazido complexes would be ineffective during the hours of melatonin production. Further, *in vivo* studies are required to confirm this effect.

5.6 References

(1)   Valko, M.; Rhodes, C. J.; Moncol, J.; Izakovic, M.; Mazur, M. *Chem. Biol. Interact.* **2006**, *160*, 1.

(2)   Reuter, S.; Gupta, S. C.; Chaturvedi, M. M.; Aggarwal, B. B. *Free Radic. Biol. Med.* **2010**, *49*, 1603.

(3)   Wiseman, H.; Kaur, H.; Halliwell, B. *Cancer Lett.* **1995**, *93*, 113.

(4)   Halliwell, B.; Gutteridge, J. M. C. *Free radicals in biology and medicine*; Oxford University Press: Oxford, **1999**.

(5)   McCord, J. M.; Day, E. D. *FEBS Lett.* **1978**, *86*, 139.

(6)   Bensasson, R. V.; Land, E. J.; Truscott, T. G. In *Excited states and free radicals in biology and medicine.*; Oxford University Press: Oxford, UK, **1993**, p 173.

(7)   Crumbliss, A. L.; Harrington, J. M. In *Advances in Inorganic Chemistry*; Rudi van Eldik, Colin D Hubbard, Eds.; Elsevier Inc USA, 2009; Vol. 61, p 179

(8)   Gutteridge, J. M.; Rowley, D. A.; Halliwell, B. *Biochem. J* **1981**, *199*, 263.

(9)   Storey, K. B. *Functional Metabolism: Regulation and Adaptation*; John Wiley & Sonds: New Jersey, **2004**, p 324.

(10)   Lloyd, R. V.; Hanna, P. M.; Mason, R. P. *Free Radic. Biol. Med.* **1997**, *22*, 885.

(11)   Bačić, G.; Spasojević, I.; Šećerov, B.; Mojović, M. *Spectrochim. Acta, Part A* **2008**, *69*, 1354.

(12)   Finkelstein, E.; Rosen, G. M.; Rauckman, E. J. *Arch. Biochem. Biophys.* **1980**, *200*, 1.

(13)   Harbour, J. R.; Chow, V.; Bolton, J. R. *Can. J. Chem.* **1974**, *52*, 3549.

(14)   Kotake, Y.; Janzen, E. G. *J. Am. Chem. Soc.* **1991**, *113*, 9503.

(15)   Buettner, G. R.; Oberley, L. W. *FEBS Lett.* **1980**, *121*, 161.

(16)   Villamena, F. A.; Merle, J. K.; Hadad, C. M.; Zweier, J. L. *J. Phys. Chem.* **2005**, *109*, 6089.

(17)   Eberhardt, M. K.; Colina, R. *J. Org. Chem.* **1988**, *53*, 1071.

(18)   Finkelstein, E.; Rosen, G. M.; Rauckman, E. J. *Mol. Pharmacol.* **1982**, *21*, 262.

(19)   JChem version:3.2.11, 2007, ChemAxon (http://www.chemaxon.com), assessed 10th-April-2013.

(20)   Cardinali, D. P.; Pévet, P. *Sleep. Med. Rev.* **1998**, *2*, 175.

(21)   Reiter, R. J. *Front. Neuroendocrinol.* **1995**, *16*, 383.

(22)   Allegra, M.; Reiter, R. J.; Tan, D. X.; Gentile, C.; Tesoriere, L.; Livrea, M. A. *J. Pineal. Res.* **2003**, *34*, 1.

(23)   Buscemi N; Vandermeer B; Pandya R; Hooton N; Tjosvold L; Hartling L; Baker G; Vohra S; T, K. *Melatonin for treatment of sleep disorders*, **2004** Nov, AHRQ Evidence Report Summaries: Agency for Healthcare Research and Quality (US). Available from: http://www.ncbi.nlm.nih.gov/books/NBK11941/.

(24)   Arendt, J.; Skene, D. J.; Middleton, B.; Lockley, S. W.; Deacon, S. *J. Biol. Rhythms* **1997**, *12*, 604.

(25)   Reiter, R. J.; Tan, D.-X. *J. Pineal. Res.* **2003**, *34*, 79.

(26)   Rodriguez, C.; Martín, V.; Herrera, F.; García-Santos, G.; Rodriguez-Blanco, J.; Casado-Zapico, S.; Sánchez-Sánchez, A.; Suárez, S.; Puente-Moncada, N.; Anítua, M.; Antolín, I. *Int. J. Mol. Sci.* **2013**, *14*, 6597.

(27)   Menaker, M. *J. Biol. Rhythms* **1997**, *12*, 532.

(28)   Matuszak, Z.; Reszka, K. J.; Chignell, C. F. *Free Radic. Biol. Med.* **1997**, *23*, 367.

(29)   Chyan, Y.-J.; Poeggeler, B.; Omar, R. A.; Chain, D. G.; Frangione, B.; Ghiso, J.; Pappolla, M. A. *J. Biol. Chem.* **1999**, *274*, 21937.

(30)   Mahal, H. S.; Sharma, H. S.; Mukherjee, T. *Free Radic. Biol. Med.* **1999**, *26*, 557.

(31)   Stasica, P.; Ulanski, P.; Rosiak, J. M. *J. Pineal. Res.* **1998**, *25*, 65.

(32)   Tan, D. X.; Reiter, R. J.; Manchester, L. C.; Yan, M. T.; El-Sawi, M.; Sainz, R. M.; Mayo, J. C.; Kohen, R.; Allegra, M. C.; Hardelan, R. *Curr. Top. Med. Chem.* **2002**, *2*, 181.

(33)   Ebelt, H.; Peschke, D.; Brömme, H. J.; Mörke, W.; Blume, R.; Peschke, E. *J. Pineal. Res.* **2000**, *28*, 65.

(34)   Scaiano, J. C. *J. Pineal. Res.* **1995**, *19*, 189.

(35)   Solar, S.; Getoff, N.; Surdhar, P. S.; Armstrong, D. A.; A., S. *J. Phys. Chem.* **1991**, *95*, 3639.

(36)   Turjanski, A. G.; Rosenstein, R. E.; Estrin, D. A. *J. Med. Chem.* **1998**, *41*, 3684.

(37)   Roberts, J. E.; Hu, D.-N.; Wishart, J. F. *J. Photchem. Photobiol. B: Biol.* **1998**, *42*, 125.

(38)   Tan, D.-X.; Manchester, L. C.; Reiter, R. J.; Plummer, B. F.; Hardies, L. J.; Weintraub, S. T.; Vijayalaxmi; Shepherd, A. M. M. *Biochem. Biophys. Res. Commun.* **1998**, *253*, 614.

(39)   Dellegar, S. M.; Murphy, S. A.; Bourne, A. E.; DiCesare, J. C.; Purser, G. H. *Biochem. Biophys. Res. Commun.* **1999**, *257*, 431.

(40)   Poeggeler, B.; Saarela, S.; Reiter, R. J.; Tan, D.-X.; Chen, L.-D.; Manchester, L. C.; Barlow-Walden, L. R. *Ann. N.Y. Acad. Sci.* **1994**, *738*, 419.

(41)   Zang, L.-Y.; Cosma, G.; Gardner, H.; Vallyathan, V. *Biochim. Biophys. Acta* **1998**, *1425*, 469.

(42)   Tomás-Zapico, C.; Martínez-Fraga, J.; Rodríguez-Colunga, M. J.; Tolivia, D.; Hardeland, R.; Coto-Montes, A. *Int. J. Biochem. Cell Biol.* **2002**, *34*, 544.

(43)   Amo, T.; Kawanishi, N.; Uchida, M.; Fujita, H.; Oyanagi, E.; Utsumi, T.; Ogino, T.; Inoue, K.; Shuin, T.; Utsumi, K.; Sasaki, J. *Cell Biochem. Funct.* **2009**, *27*, 503.

(44)   Tomás-Zapico, C.; Coto-Montes, A.; Martínez-Fraga, J.; Rodríguez-Colunga, M. J.; Hardeland, R.; Tolivia, D. *Free Radic. Biol. Med.* **2002**, *32*, 1197.

(45)   Marshall, K.; Reiter, R. J.; Poeggeler, B.; Aruoma, O. I.; Halliwell, B. *Free Radic. Biol. Med.* **1996**, *21*, 307.

(46)   Noda, Y.; Mori, A.; Liburdy, R.; Packer, L. *J. Pineal. Res.* **1999**, *27*, 159.

(47)   Zhang, H.; Squadrito, G. L.; Uppu, R.; Pryor, W. A. *Chem. Res. Toxicol.* **1999**, *12*, 526.

(48)   Perez-Reyes, E.; Mason, R. P. *J. Biol. Chem.* **1981**, *256*, 2427.

(49)   Land, E. J.; Prütz, W. A. *Int. J. Radiat Biol.* **1979**, *36*, 75.

(50)   Vijayalaxmi, T.; Charles R; Reiter, R. J.; Herman, T. S. *J. Clin. Oncol.* **2002**, *20*, 2575.

(51)   Hill, S. M.; Blask, D. E. *Cancer Res.* **1988**, *48*, 6121.

(52)   Farriol, M.; Venereo, Y.; Orta, X.; Castellanos, J. M.; Segovia-Silvestre, T. *J. Appl. Toxicol.* **2000**, *20*, 21.

(53)   Sainz, R. M.; Mayo, J. C.; Tan, D.-X.; Lopez-Burillo, S.; Natarajan, M.; Reiter, R. J. *Biochem. Biophys. Res. Commun.* **2003**, *302*, 625.

(54)   Kim, J.-H.; Jeong, S.-J.; Kim, B.; Yun, S.-M.; Choi, D. Y.; Kim, S.-H. *J. Pineal. Res.* **2012**, *52*, 244.

(55)   Casado-Zapico, S.; Rodriguez-Blanco, J.; García-Santos, G.; Martín, V.; Sánchez-Sánchez, A. M.; Antolín, I.; Rodriguez, C. *J. Pineal. Res.* **2010**, *48*, 72.

(56)   Padillo, F. J.; Ruiz-Rabelo, J. F.; Cruz, A.; Perea, M. D.; Tasset, I.; Montilla, P.; Túnez, I.; Muntané, J. *J. Pineal. Res.* **2010**, *49*, 264.

(57)   Guardiola-Lemaitre, B. *J. Biol. Rhythms* **1997**, *12*, 697.

(58)   Lissoni, P.; Paolorossi, F.; Ardizzoia, A.; Barni, S.; Chilelli, M.; Mancuso, M.; Tancini, G.; Conti, A.; Maestroni, G. J. M. *J. Pineal. Res.* **1997**, *23*, 15.

(59)   Mills, E.; Wu, P.; Seely, D.; Guyatt, G. *J. Pineal. Res.* **2005**, *39*, 360.

(60)   Hong, Y.; Won, J.; Lee, Y.; Lee, S.; Park, K.; Chang, K.-T.; Hong, Y. *J. Pineal. Res.* **2014**, *56*, 264.

(61)   Pandi-Perumal, S. R.; Trakht, I.; Srinivasan, V.; Spence, D. W.; Maestroni, G. J. M.; Zisapel, N.; Cardinali, D. P. *Prog. Neurobiol.* **2008**, *85*, 335.

(62)   Maharaj, D. S.; Glass, B. D.; Daya, S. *Biosci. Rep.* **2007**, *27*, 299.

(63)   Romero, A.; Ramos, E.; de Los Ríos, C.; Egea, J.; del Pino, J.; Reiter, R. J. *J. Pineal. Res.* **2014**, *56*, 343.

(64)   Parmar, P.; Limson, J.; Nyokong, T.; Daya, S. *J. Pineal. Res.* **2002**, *32*, 237.

(65)   Singh, G.; Abbas, J. M.; Dogra, S. D.; Sachdeva, R.; Rai, B.; Tripathi, S. K.; Prakash, S.; Sathe, V.; Saini, G. S. S. *Spectrochim. Acta. A. Mol. Biomol. Spectrosc.* **2014**, *118*, 73.

(66)   He, H.; Lin, M.; Han, Z.; Muroya, Y.; Kudo, H.; Katsumura, Y. *Org. Biomol. Chem.* **2005**, *3*, 1568.

(67)   Ronconi, L.; Sadler, P. J. *Chem. Commun.* **2008**, 235.

(68)   Harbour, J. R.; Issler, S. L. *J. Am. Chem. Soc.* **1982**, *104*, 903.

(69)   Paciolla, M. D.; Kolla, S.; Jansen, S. A. *Adv. Environ. Res.* **2002**, *7*, 169.

(70)   Frejaville, C.; Karoui, H.; Tuccio, B.; le Moigne, F.; Culcasi, M.; Pietri, S.; Lauricella, R.; Tordo, P. *J. Chem. Soc., Chem. Commun.* **1994**, 1793.

(71)   Kuchitsu, K.; Kosaka, H.; Shiga, T.; Shibuya, N. *Protoplasma* **1995**, *188*, 138.

(72)   Pou, S.; Ramos, C. L.; Gladwell, T.; Renks, E.; Centra, M.; Young, D.; Cohen, M. S.; Rosen, G. M. *Anal. Biochem.* **1994**, *217*, 76.

(73)   Ōishi, Y.; Mukai, K.; Nishiguchi, H.; Deguchi, Y.; Takaki, H. *Tetrahedron Lett.* **1968**, *9*, 4773.

(74)   Karoui, H.; Chalier, F.; Finet, J.-P.; Tordo, P. *Org. Biomol. Chem.* **2011**, *9*, 2473.

(75)   Gutteridge, J. M. C. *Ann. N.Y. Acad. Sci.* **1994**, *738*, 201.

(76)   Thorpe, T. A.; Bagh, K.; Cutler, A. J.; Dunstan, D. I.; McIntyre, D. D.; Vogel, H. J. *Plant Physiol.* **1989**, *91*, 193.

(77)   Farrer, N. J.; Gierth, P.; Sadler, P. J. *Chem. Eur. J.* **2011**, *17*, 12059.

(78)   Kanvah, S.; Joseph, J.; Schuster, G. B.; Barnett, R. N.; Cleveland, C. L.; Landman, U. *Acc. Chem. Res.* **2009**, *43*, 280.

(79)   Princ, F. G.; Maxit, A. G.; Cardalda, C.; Batlle, A.; Ana Juknat, A. *J. Pineal. Res.* **1998**, *24*, 1.

(80)   Samuni, A.; Samuni, A.; Swartz, H. M. *Free Radic. Biol. Med.* **1989**, *6*, 179.

(81)   Du, L.-B.; Wang, L.-F.; Liu, Y.-P.; Jia, H.-Y.; Liu, Y.; Liu, K.-J.; Tian, Q. *Free Radical Res.* **2010**, *44*, 751.

(82)   Ram, M. S.; Stanbury, D. M. *Inorg. Chem.* **1985**, *24*, 4233.

(83)   Kleszczyński, K.; Hardkop, L. H.; Fischer, T. W. *Dermatoendocrinol.* **2011**, *3*, 27.

(84)   Burger, E.; Bauer, H. M. *Arch. Toxikol* **1965**, *20*, 279.

(85)   Lewis, A. J.; Kerenyi, N. A.; Feuer, G. *Drug Metab. Drug Interact. Drug* **1990**, *8*, 247.

(86)   Pfluger, P.; Krounbi, M.; Street, G. B.; Weiser, G. *J. Chem. Phys.* **1983**, *78*, 3212.

(87)   Yurtsever, M.; Yurtsever, E. *Polymer* **2002**, *43*, 6019.

(88)   Choi, K. M.; Jang, J. H.; Rhee, H.-W.; Kim, K. H. *J. Appl. Polym. Sci.* **1992**, *46*, 1695.

(89)   Lack, B.; Daya, S.; Nyokong, T. *J. Pineal. Res.* **2001**, *31*, 102.

(90)   Neta, P.; Huie, R. E.; Ross, A. B. *J. Phys. Chem. Ref. Data* **1988**, *17*, 1027.

(91)   Sies, H. *Am. J. Med.* **1991**, *91*, S31.

(92)   Aubry, J. M. *J. Am. Chem. Soc.* **1985**, *107*, 5844.

(93)   Wahlen, J.; De Hertogh, S.; De Vos, D. E.; Nardello, V.; Bogaert, S.; Aubry, J.-M.; Alsters, P. L.; Jacobs, P. A. *J. Catal.* **2005**, *233*, 422.

(94)   Bown, S. G. *Phil. Trans. Soc. A.* **2013**, *371*.

(95)   Peng, Q.; Warloe, T.; Berg, K.; Moan, J.; Kongshaug, M.; Giercksky, K.-E.; Nesland, J. M. *Cancer* **1997**, *79*, 2282.

(96)   Princ, F. G.; Juknat, A. A.; Maxit, A. G.; Cardalda, C.; Batlle, A. *J. Pineal. Res.* **1997**, *23*, 40.

(97)   Claustrat, B.; Brun, J.; Chazot, G. *Sleep. Med. Rev.* **2005**, *9*, 11.

(98)   Karasek, M. *J. Physiol. Pharmacol.* **2004**, *39*, 1723.

(99)   Dallmann, R.; Brown, S. A.; Gachon, F. In *Annu. Rev. Pharmacol. Toxicol.* 2014; Vol. 54, p 339.

(100)   Smolensky, M. H.; D'Alonzo, G. E.; Kunkel, G.; Barnes, P. J. *Chronobiol. Int.* **1987**, *4*, 459.

(101)   Smolensky, M. H.; Scott, P. H.; Harrist, R. B.; Hiatt, P. H.; Wong, T. K.; Baenziger, J. C.; Klank, B. J.; Marbella, A.; Meltzer, A. *Chronobiol. Int.* **1987**, *4*, 435.

(102)   Reber, A.; Huber, P. R.; Ummenhofer, W.; Gürtler, C. M.; Zurschmiede, C.; Drewe, J.; Schneider, M. *Acta Anaesthesiol. Scand.* **1998**, *42*, 1050.

Chapter VI

Photoactivation of a Platinum(IV) Diazido Anticancer Complex in the presence of Cimetidine

Previous studies have reported on the unreactive nature of platinum(IV) diazido anticancer complexes towards sulfur containing bio-molecules in the dark.[1,2] However, there are few studies of reactions between sulfur-based biomolecules and photo-irradiated platinum(IV) diazido complexes. In this Chapter, the photo-irradiation of *trans,trans,trans*-$[Pt(N_3)_2(OH)_2(py)_2]$ (complex **40**) in the presence of a sulfur-containing drug, cimetidine, was investigated.

6.1 Introduction

Platinum-based anticancer complexes are widely used in the treatment of a variety of human cancer malignancies. However, the development of intrinsic and/or acquired resistance mechanisms limits their continued clinical efficiency.[3] Platinum resistance, a multi-factorial process, is commonly associated with the inhibition of DNA-platination or drug-induced damage mechanisms.[4] Platinum resistance has also been correlated with reduced cellular accumulation and to date, this is considered a primary marker of platinum resistance.[5] Copper transporter (CTR) proteins,[6,7] organic cation transporters (OCTs)[8] and other specific platinum influx transporters[9] have been identified as mediators of platinum accumulation. OCTs are a subgroup of the solute carrier, SLC22 family, which belong to the major facilitator superfamily. The OCTs subgroup consists of subtypes OCT1, OCT2 and OCT3, also known as SLC22A1, SLC22A2 and SLC22A3, respectively.[10] Expression in the liver (OCT1), kidneys (OCT2) and intestines (OCT3) suggests these transporters participate in the absorption, distribution and excretion of platinum anti-neoplastic agents.[11]

Early studies identified a relationship between high expression levels of OCT2 and platinum toxicity,[12] suggesting OCT2 mediated platinum accumulation. This study and others[11,12] led to the investigation into the role of OCT2-mediated uptake of platinum

anticancer complexes. To date the involvement of both SLC22A1 and SLC22A3 on platinum transport remains unclear.[13,14] However, there is compelling evidence to support the contribution of SLC22A2 in both the absorption and cyto-toxicity of numerous platinum anticancer complexes.[15,16] Expression of SLC22A2 significantly enhanced the uptake and cytotoxicity of picoplatin (**62**) and pyriplatin (**63**) (Figure 6.1).[13,17]

Picoplatin (**63**)

Pyriplatin (**64**)
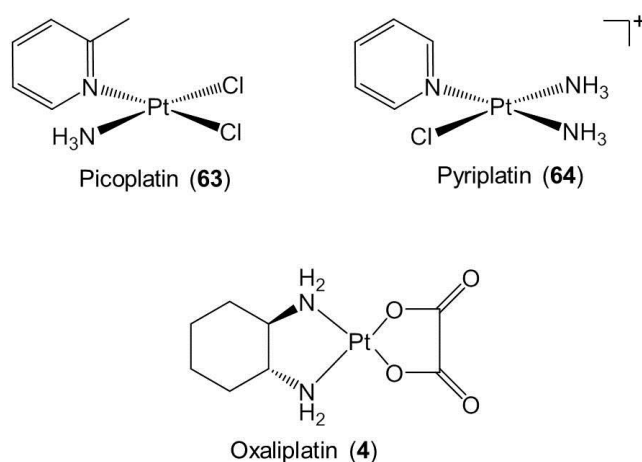
Oxaliplatin (**4**)

Figure 6.1 Platinum anticancer complexes whose absorption has been reported to be mediated by the cation transporter, SLC22A2.

Moreover, oxaliplatin (**4**) is regarded as an excellent SLC22A2 substrate. Its uptake was ca. 24-fold higher in transfected HEK293 (human embryonic kidney)-OCT2 cells compared to normal control cells.[18] The presence of SLC22A2 inhibitors such as tetraethyl ammonium (TEA, Figure 6.2**A**) and methyl-4-phenylpyridinium (MPP$^+$, Figure 6.2**B**), completely abolished the SLC22A2-mediated uptake of both oxaliplatin and picoplatin.[13,17]

Figure 6.2 Structures of (**A**) tetraethyl ammonium (TEA) and (**B**) 1-methyl-4-phenylpyridinium (MPP$^+$) inhibitors of the SLC22A2 transporter.

Cimetidine (Figure 6.3**A**) is an H2-receptor antagonist, an FDA approved drug, and is also classified as a SLC22A2 inhibitor. It is generally prescribed for the treatment of heartburn and peptic ulcers.[19] At physiological pH 7.4, ca. 20% of cimetidine exists in its cationic f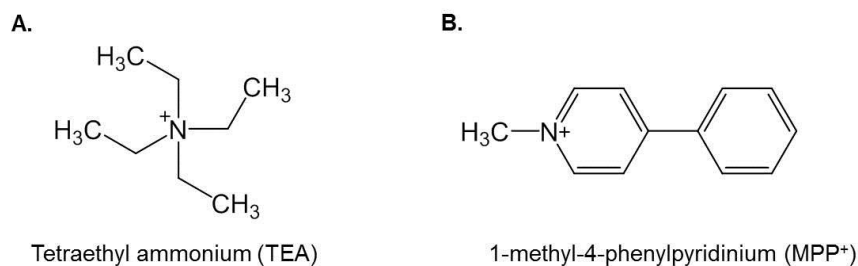orm (Figure 6.3**B**), which is essential for its transport *via* OCT2. The amount of cationic cimetidine increases with decreasing pH (ca. 67% at pH 6.5).[20] Therefore, similar to TEA and MPP$^+$, the uptake of platinum anticancer complexes mediated by SLC22A2, has potential to be inhibited in the presence of cimetidine.

Surprisingly, the pharmacological effects of cimetidine have been contradictory. Co-administration of *cis*-platin with cimetidine suppressed *cis*-platin induced nephrotoxicity, without affecting the pharmacological activity of *cis*-platin.[21,22] Dorr *et al.* found that the co-administration of CDDP with cimetidine did not affect the antitumour activity of the Pt^{II} anticancer complex in murine lymphocytic leukemia cell line. However, cimetidine increased the lethality of CDDP in normal mice cells, which was otherwise inactive.[23] Adverse side-effects of *cis*-platin therapy, such as oto- and nephro-toxicity were completely and partially supressed, respectively, in the presence of cimetidine.[24] In contrast, cimetidine completely suppressed *cis*-platin induced apoptosis in HEK293-OCT2, human embryonic kidney cells transfected with OCT2.

Moreover, the uptake of oxaliplatin was significantly reduced in the presence of cimetidine.[25] These results supported the OCT2-mediated platinum accumulation.
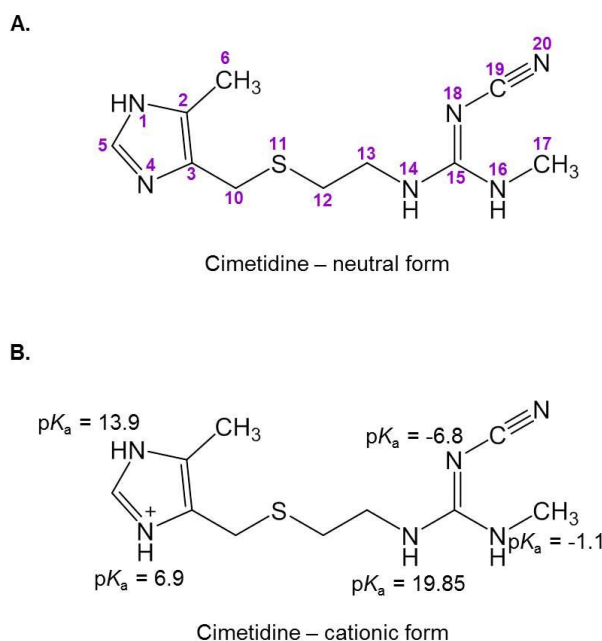
Figure 6.3 Structure of cimetidine in (**A**) neutral (ca. 80%) and (**B**) cationic (ca. 20%) form at physiological pH.

The expression of SLC22A2 was investigated in the NCI-60 panel of human cancer cells and was found to be readily expressed in OVAR-5, SKOV-3 and IGROV-1 ovarian cancer cells.[26] Despite this finding, the uptake of *cis*-platin in SKOV-3 ovarian cancer cells was not inhibited in the presence of cimetidine.[14,27] The majority of platinum compounds transported by the SLC22A2 have been noted to possess a heterocyclic aromatic ligand.[28] Therefore, is it apparent that further studies are required to determine if there is a direct correlation between the expression of SLC22A2 and accumulation of platinum.

The main pharmacological effect of cimetidine has been suggested to be mediated *via* interaction with transition metal ions.[29] Cimetidine, similar to histamine, can act like a

chelating agent. Previous studies have isolated a 1:2 polymeric Cu^{II}-cimetidine complex, with the Cu^{II} coordinated *via* the imidazole (N4) and the nitrile (N20) nitrogen atoms, as determined from its X-ray crystal structure.[30] Therefore, it appears cimetidine can compete against biological ligands such as albumin, for Cu^{II}.[31] Moreover, Kanumfre reported on the ability of cimetidine to chelate various metal ions in both the blood plasma and surrounding tissues.[32] Consequently, numerous studies have investigated the interaction of cimetidine with various metal ions, in particular those present in trace quantities *in vivo,*[33-35] such as Cu^{II}, Ni^{II} and Zn^{II}.[36,37] It was found that cimetidine coordinates to these metal ions *via* the thioether (S11) and imidazole nitrogen (N4) atoms, forming stable five-membered rings (Figure 6.4**A**), except where three ligands were coordinated to the metal ion, which led to coordination *via* the imidazole nitrogen atom only (Figure 6.4**B**).[38] Additional studies characterised the formation of $[Cr(cim)_2(Cl)_2]Cl.3H_2O$, a five-membered ring complex *via* infrared and UV-visible spectroscopy.[38] DFT calculations performed by Olea-Román identified the imidazole nitrogen (N4) and sulfur (S11) atoms, as the most reactive sites present in cimetidine. This further supported the formation of stable five-membered ring complexes.

Platinum(II) exhibits a strong binding affinity for sulfur in both L-methionine and L-cysteine residues. L-methionine (L-Met, Figure 6.5**B**) and L-cysteine (L-Cys, Figure 6.5**C**) amino acids are present in a wide variety of proteins and peptides.[39] *N*-donor atoms, such as 5'-guanosine monophosphate (5'-GMP) have the ability to displace Pt-S(thioether) bonds. Consequently, these Pt-S(thioether) bonds were termed as "drug reservoirs".[40]
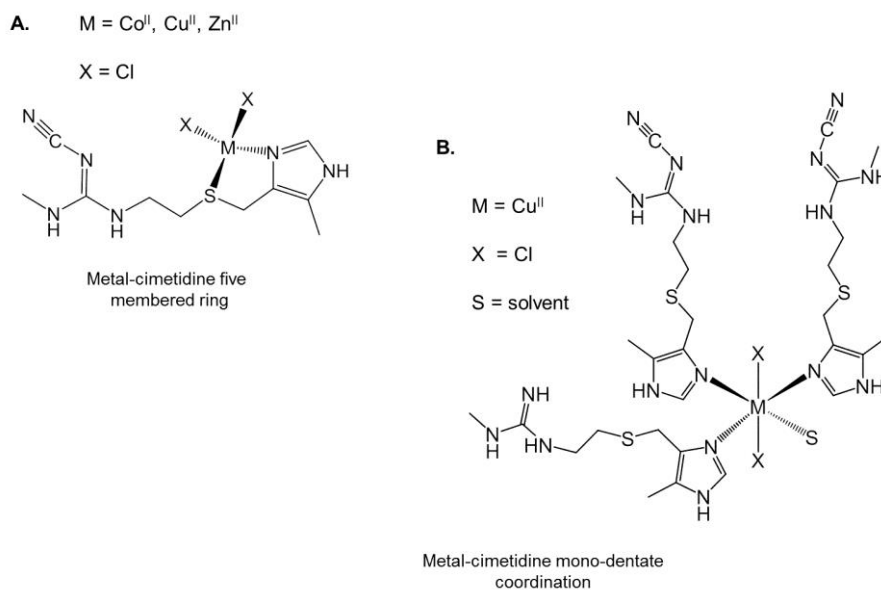
Figure 6.4 Example of transition metal-cimetidine complexes previously characterised by both UV-visible/NMR spectroscopic and DFT methods. Coordination of the transition metal to cimetidine *via* (**A**) both the sulfur (S11) and imidazole nitrogen (N4) atoms, and (**B**) imidazole nitrogen (N4) atom only (structures from ref 38).

However, displacement of the Pt-S (thioether) bond does not always occur. Chelate ring formation has been reported from the interaction of *cis*-platin with both L-methionine and the protein, ubiquitin (UBQ). A major metabolite of CDDP treatment, [Pt(L-Met)$_2$] has been identified to undergo facile *cis-trans* isomerisation in aqueous solution, characterised by ^{195}Pt and ^{1}H NMR spectroscopy (Figure 6.6**B**).[41]

Figure 6.5 Amino acids (**A**) L-methionine and (**B**) L-cysteine

A small polypeptide of ca. 8 kDa, UBQ contains seven lysines, four arginines, one histidine and one L-methionine residues,[42,43] and has been associated with an indirect role in tumour propagation. Indirect methods have identified the Met1 as the primary binding site of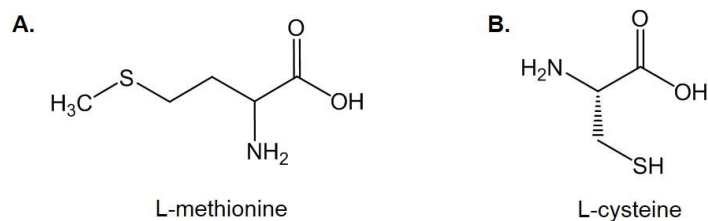 Pt[II] in UBQ.[44,45] Modification of the Met1 residue inhibited Pt[II] binding, supporting Met1 as the main binding site. A more comprehensive study, involving a travelling-wave-based ion mobility-tandem mass spectrometry approach, elucidated the formation of a stable six-membered ring (Figure 6.6**B**), formed between *cis*-platin and UBQ *via* the Met1 and His68 residues.[46]
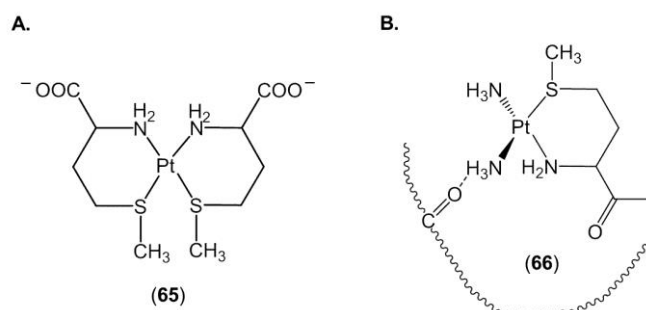
Figure 6.6 Structure of six-membered ring complexes formed by coordination of Pt[II] to the sulfur and nitrogen atoms of (**A**) L-methionine (**B**) UBQ (structures from ref 41 and 46, respectively).

Cimetidine possesses a thioether and imidazole ring functional groups. Therefore, the binding of Pt[II] appears kinetically favoured at the sulfur (S11) atom, which may undergo chelate ring formation due to the presence of the imidazolic ring. The coordination of Pt[II] to cimetidine has been primarily investigated to elucidate the pharmacological action of the FDA approved drug. Interestingly, Nurchi *et al.* first reported on a Pt[II]-cimetidine related species. Coordination of Pt[II] was reported to occur *via* the cyano-guanidine moiety of cimetidine. This was deduced from the equivalent ^{1}H NMR resonances for both free and coordinated cimetidine.[47] In contrast, Crisponi

reported on the distinct ^{1}H NMR resonances for both free and coordinated cimetidine, indicative of both Pd[II] and Pt[II] coordination *via* both the sulfur (S11) and imidazole nitrogen (N4) atoms of cimetidine.[48] Moreover, Onoa *et al.* synthesised a $[Pt(cim)_2]^{2+}$ species to investigate both its binding and anticancer properties.[49] The X-ray crystal structure of this $[Pt(cim)_2]Cl_2.12H_2O$ complex revealed two molecules of cimetidine coordinated to the Pt[II] centre *via* the thioether and imidazole nitrogen atoms (Figure 6.7).[49]
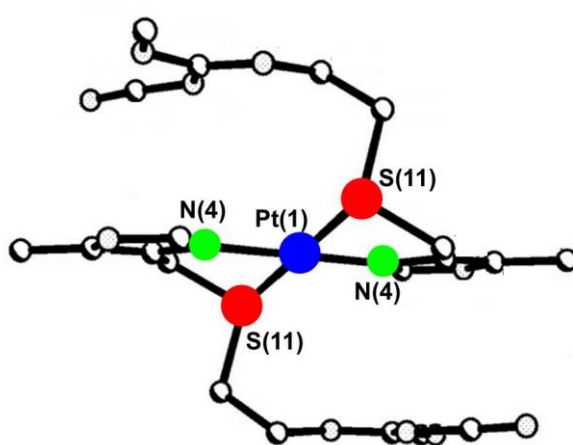
Figure 6.7 X-ray crystal structure of $[Pt(cim)_2]^{2+}$ complex, where counter ions, hydrogen atoms and solvent are not shown (structure adapted from ref 49).

These studies by Crisponi and Onoa, are in agreement with the well-known tendency of Pt[II] to preferentially coordinate *via* the sulfur atom. Unlike previous studies which led to the displacement of the Pt[II]-sulfur bond in the presence of *N*-donor complexes,[40] the presence of the competing *N*-donor atom of the imidazolic ring in cimetidine, led to chelate ring formation. Interaction of platinum(II) anti-cancer agents with L-methionine and L-cysteine, (Figure 6.5) common sulfur-containing amino acids present in an array of proteins and peptides forming Pt[II]-S based species, has been correlated with adverse toxic side-effects and platinum resistance mechanisms.[50] The biological activity of the $[Pt(cim)_2]^{2+}$ complex obtained by Onoa *et al.* (refer to Figure 6.7), was not performed

due to the lack of hydrolysable groups in the coordination sphere. Consequently, the biological activity of such Pt^{II}-cimetidine complexes, remain unknown. Instead, the anti-proliferative activity of a Pd^{II}-cimetidine derivative was investigated and the derivative was found to be non-cytotoxic towards a number of cancer cell lines.[49] This is in agreement with the facile hydrolysis of palladium complexes, ca. $10^5 \times$ faster than the corresponding platinum derivatives. This rapid dissociation generates reactive species unable to reach the target site and to induce cell death.[51]

Platinum(IV) diazido anticancer complexes **36** and **40** (Figure 6.8) have been shown to be stable in the presence of glutathione, in the dark.[2] Photo-irradiation of complex **36** with 365 nm UVA, was reported to reduce Pt^{IV} to Pt^{II} *via* two one-electron reductions from the azide ligands.[52] Therefore, the Pt^{II} photo-products have potential to interact with sulfur-containing molecules. Recently, Ronconi investigated the photo-irradiation of complex **36** in the presence of dimethyl-sulfide (DMS). Surprisingly, an alternative photo-decomposition pathway of complex **36** was observed in the presence of DMS. Initial loss of N_2 gas led to the formation of a Pt-N nitrene complex and formation of O_2 gas (detected by P_{O2} measurement).[53] This study illustrated that the photo-activation and photo-decomposition pathway(s) of platinum(IV) diazido anticancer complexes are dependent on the irradiation conditions.
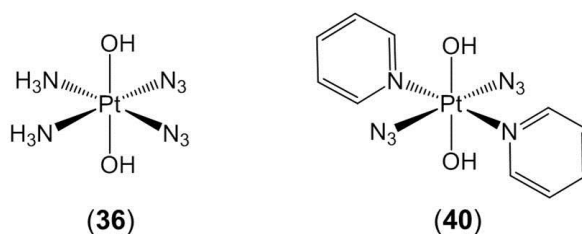

Figure 6.8 Platinum(IV) diazido complexes stable in the presence of glutathione in the dark.

In this Chapter, the photo-irradiation of *trans,trans,trans*-[Pt(N$_3$)$_2$(OH)$_2$(py)$_2$] (complex **40**) in the presence of SLC22A2 inhibitor cimetidine was performed. Primary studies focused on establishing the effect of cimetidine on photo-irradiated complex **40**, monitored by UV-visible, EPR, MS and multinuclear NMR spectroscopy. Additional cellular studies on the photo-cytotoxicity and uptake of complex **40** in HaCaT keratinocytes cells, in the presence of cimetidine, were performed.

6.2 Experimental

A brief description of sample preparation is provided below specific to this Chapter. More detailed information regarding instrumental and irradiation setup are provided in **Chapter II**.

6.2.1 Materials

Cimetidine, pyridine, L-methionine, hexamethyl-disiloxane (HMDSO, ^{1}H NMR internal reference) and histamine were purchased from Sigma Aldrich.

6.2.2 EPR spectroscopy

Samples were prepared in PBS/D$_2$O at pH* 7.4 containing *trans,trans,trans*-[Pt(N$_3$)$_2$(OH)$_2$(py)$_2$] (complex **40**, 1 mM or 450 μM) and DMPO (2 mM or 900 μM) in the absence and presence of cimetidine (2 or 4 mol equiv).

6.2.3 NMR Spectroscopy

- ^{1}H NMR

Solutions were prepared in deuterated phosphate buffer (PBS/D$_2$O) containing complex **40** (4 mM) in the absence and presence of cimetidine (8 mM) at pH* 7.4. Due to the

overlap (in some instances) between 1,4 dioxane ($\delta = 3.75$ in D_2O) with ^{1}H NMR resonances of the sample under investigation, samples were internally referenced to HMDSO ($\delta = 0.28$ in D_2O). An additional solution of complex **40** (4 mM) with DMPO (8 mM) in the presence of cimetidine (8 mM) was prepared in PBS/D_2O at pH* 7.4.

- **[14]N NMR**

Individual solutions of cimetidine (18 mM) and pyridine (10 mM) were prepared in PBS/D_2O at pH* 7.4 to record their ^{14}N NMR spectra. Solutions of complex **40** (4 mM) were prepared in PBS/D_2O at pH* 7.4 in both the absence and presence of cimetidine (8 mM). Spectra were recorded as described in **Chapter II**.

- **^{13}C-DEPT135 NMR**

Spectra were obtained on a Bruker-DRX-500 (^{13}C, 125.8 MHz) spectrometer at 298 K. Spectra were recorded with the standard ^{13}C NMR deptcp135 pulse programme and acquired with 2048 transients into 65 k data points with a spectral width of 250 ppm. Samples were irradiated in a transparent glass vial and transferred to the NMR tube to record the NMR spectrum. Spectra were processed with an exponential line-broadening of 2.0. All ^{13}C NMR spectra were internally referenced to 1,4 dioxane (67.19 ppm in D_2O).[54] The advantage of ^{13}C-DEPT135 is that it allows the distinction between signals, where CH and CH_3 are positively and CH_2 signals are negatively represented.

- **[195]Pt NMR**

Spectra were recorded on a Bruker-DRX-500 ([195]Pt, 107.5 MHz) NMR spectrometer at 298 K and externally referenced to 15 mM K_2PtCl_6 in D_2O (δ 0 ppm). [195]Pt NMR was performed on a solution containing complex **40** (4 mM) in the presence of cimetidine

(8 mM) irradiated with 463 nm light for 60 min prepared in PBS/D_2O at pH* 7.4. The [195]Pt NMR spectra were recorded in the region of -1500 – -4000 ppm for the characterisation of Pt^{II}-cimetidine species. The following parameters were used $d_1 = 0$ s, TD 2k, DE 30 μs, digmod baseopt, 256 k scans.[5a,b] However, no [195]Pt NMR resonances were detected in the region of interest.

6.2.4 UV-visible spectroscopy

Solutions of complex **40** (50 μM) were prepared in the absence and presence of cimetidine (different mol equiv) in PBS/D_2O at pH* 7.4. Samples were irradiated with 463 nm light (64 mW cm^{-2}) for 5, 15, 30 and 60 min in a 1 ml transparent glass vial. Irradiated solutions (ca. 650 μL) were transferred to a black 1 cm quartz UV-visible cuvette, where the UV-visible spectra of the irradiated solutions were recorded.

6.2.5 Mass Spectrometry

- **Electrospray Ionisation (ESI) MS**

Samples containing spin trap and/or cimetidine were run in positive mode between the range of 50-500 *m/z*, whereas samples containing complex **40**, spin trap and/or cimetidine were run in positive mode between ranges of 50-500 *m/z* and 500-1000 *m/z*. Automatic washes were pre-programmed by the computer software and spectra were acquired for ca. 3 min 21 s. Data were processed using the Bruker Daltonics software data analysis programme. The instrumentation setup was as described in **Chapter II**.

- **Inductively Coupled Plasma (ICP) MS**

Samples of HaCaT cells treated with complex **40** (42.4 μM) and cimetidine (0.5 mM) were provided by Dr. Julie Woods, Photobiology Unit, Ninewell's Hospital, Dundee,

UK for platinum determination. The samples were separated by Dr Julie Woods into cell pellets, medium and washes and analysed at Warwick University. ICP-MS was performed on both dark and irradiated (λ_{max} = 420 nm, 5 J cm^{-2}) cell samples co-incubated with complex **40** (42.4 µM) in the absence and presence of cimetidine (500 µM) in HaCaT immortal human keratinocyte cells. Sample preparation and the instrumentation setup for ^{195}Pt ICP-MS analysis were as described in **Chapter II**.

6.2.6 pK_a* Determination

The experimental pH NMR titration data were fitted to the formula below derived from the Henderson–Hasselbalch equation in which K_a, is the dissociation constant for protonated cimetidine, δ_A, and δ_B are the limiting chemical shifts of protonated cimetidine and neutral cimetidine, respectively.

$$\delta = \frac{\delta_A \cdot 10^{-pH^*} + \delta_B \cdot 10^{-pK_a}}{10^{-pH^*} + 10^{-pK_a}}$$

The pH* titration curve was fitted using the program ORIGIN version 6.0 (Microcal Software Ltd.) In this work the resultant pKa is represented as pKa* due to the value measured in D$_2$O, without correction for effects of deuterium on glass electrode. D$_2$O can decrease the acidity of acids and affect the binding affinity of protonated groups, in comparison to H$_2$O. However, it is possible to convert the pKa* determined in D$_2$O, to the pKa value (and vice versa), using the equation as previously reported by Krężel *et al.*[55]

6.3 Results

6.3.1 Stability of cimetidine

Prior to studying the effect cimetidine induced on the photo-activation of *trans,trans,trans*-[Pt(N$_3$)$_2$(OH)$_2$(py)$_2$] (complex **40**), both the photo- and solvent stability of cimetidine were investigated. As reported by Greenway, cimetidine exhibits two $\pi \rightarrow \pi^*$ transitions at 197 nm and 215 nm, attributed to the imidazole ring and guanidine moiety, respectively.[30] In this work, absorption spectra were recorded in the range of 200 – 800 nm, consequently only one $\pi \rightarrow \pi^*$ transition at ca. 216 nm was observed (Figure 6.9) for cimetidine. This absorption was unaffected after 30 min irradiation at 463 nm.
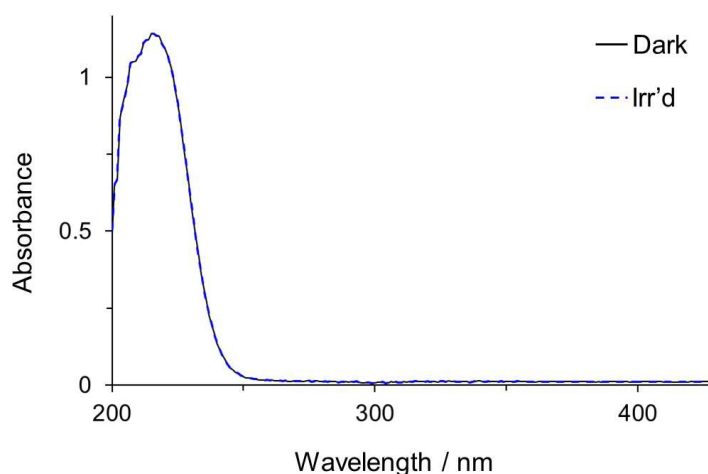
Figure 6.9 Absorbance spectra of cimetidine (50 µM) prepared in PBS/D$_2$O at pH* 7.4 both before (−) and (---) irradiation for 30 min at 463 nm.

Next, the photo-stability of cimetidine was monitored by ^{1}H NMR spectroscopy. A solution of cimetidine (8 mM) in PBS/D$_2$O was prepared at pH* 7.4. ^{1}H NMR resonances of cimetidine remained stable up to 48 h in the dark. Irradiation at 463 nm for 30 min did not induce a change in the ^{1}H NMR resonances of cimetidine (Figure

6.10), confirming the photo-stability of cimetidine both in solution and towards irradiation at 463 nm.
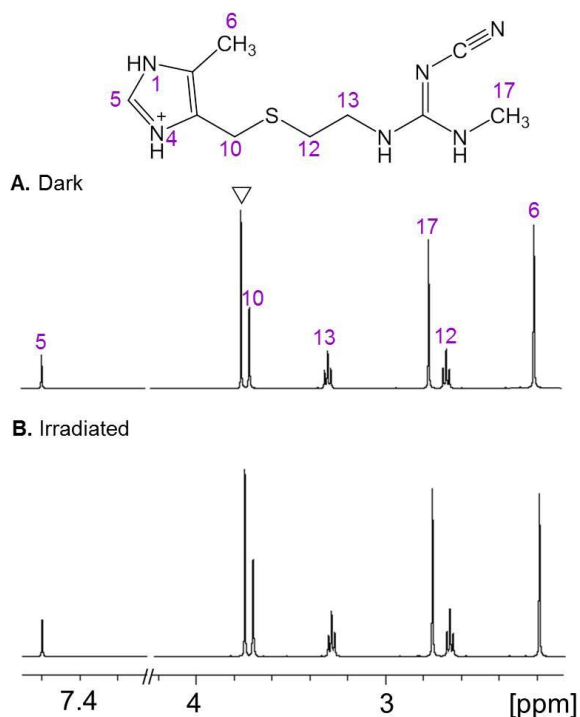
Figure 6.10 ^{1}H NMR spectra of cimetidine (8 mM) prepared in PBS/D$_2$O at pH* 7.4 in (**A**) the dark and (**B**) after 30 min irradiation at 463 nm, where ($\triangledown$) refers to internal reference, 1,4 dioxane ($\delta = 3.75$).

The stability of cimetidine both before and after irradiation was confirmed by high resolution mass spectrometry (HR-MS, Figure 6.11). The mass adducts detected at *m/z* of 253.122 and 275.105 were assigned to [Cim+H]$^+$ and [Cim+Na]$^+$ species, respectively. Both adducts remained present in solution throughout the course of monitoring the solvent and photo-stability of cimetidine.
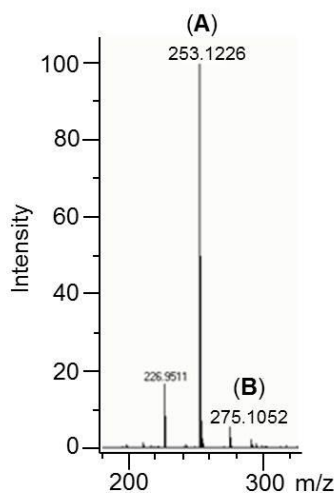
Figure 6.11 HRMS spectrum of an aqueous solution of cimetidine showing (**A**) protonated [Cim+H]$^+$ and (**B**) sodium [Cim+Na]$^+$ adducts of cimetidine, in agreement with their calculated *m/z* of 253.3480 and 275.3298, respectively.

An additional solution of cimetidine (8 mM) in the presence of spin trap DMPO (8 mM) was prepared in PBS/D$_2$O at pH* 7.4. Despite an overlap between cimetidine (H12) and DMPO (H**b**) ^{1}H NMR resonances, no reaction was observed either before or after irradiation at 463 nm for 30 min (Figure 6.12). The photo-stability of cimetidine rendered it a suitable molecule for studying its effect on the photo-irradiation of complex **40**.
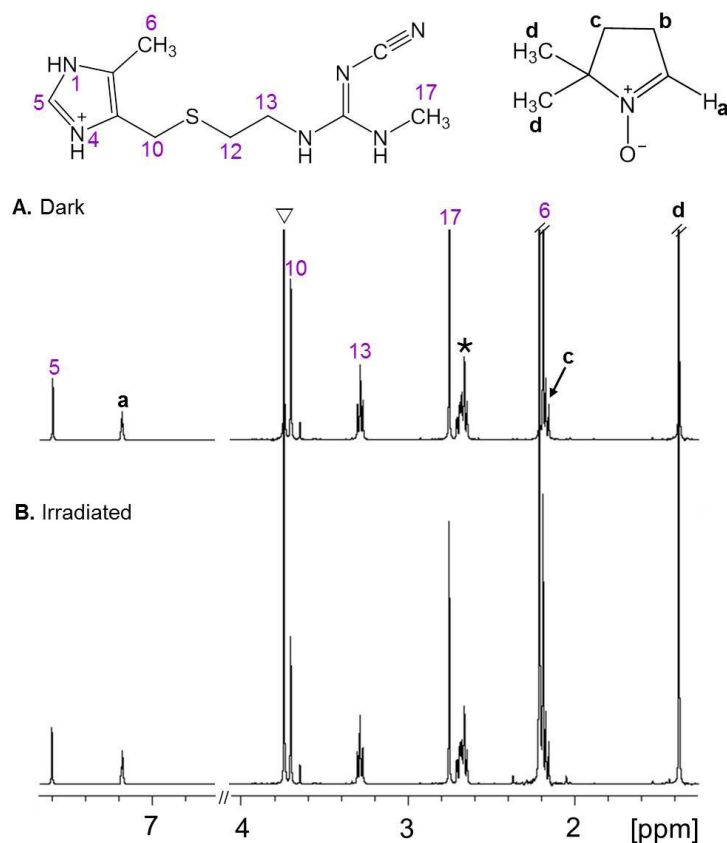
Figure 6.12 ^{1}H NMR spectra of a solution of cimetidine (8 mM) with DMPO (8 mM) prepared in PBS/D$_2$O at pH* 7.4 in (**A**) dark and (**B**) after irradiation at 463 nm for 30 min. Assignments (^{1}H, 500 MHz): Cimetidine peaks, (1-17); DMPO peaks, (**a-d**); overlap between H12 of cimetidine with H**b** of DMPO, (★); internal reference, 1,4 dioxane (δ = 3.75), (▽).

6.3.2 Irradiation of complex 40 in the presence of cimetidine

The dark UV-visible spectrum of complex **40** exhibits an absorption band at ca. 294 nm assigned as the N$_3$→Pt^{IV} LMCT band, commonly used to monitor the photo-decomposition of complex **40**. Addition of cimetidine (up to 8 mol equiv) had no effect on this LMCT band in the dark (Figure 6.13). The absorbance of cimetidine at ca. 214 nm was masked by the absorbance of complex **40**. Consequently, the rise in absorbance at ca. 245 nm is attributed to the presence of cimetidine in solution (↓, Figure 6.13).
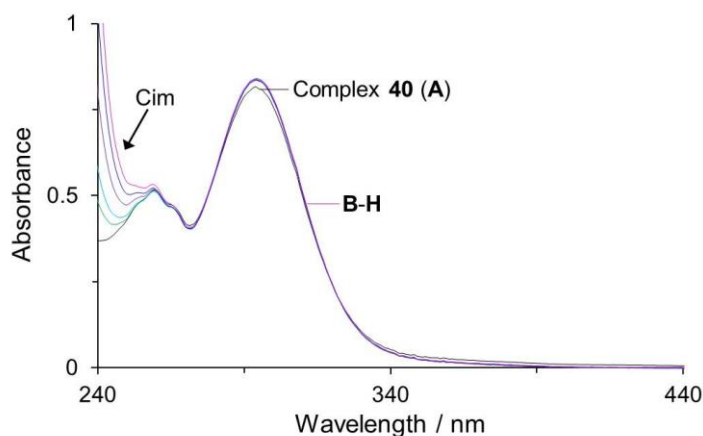
Figure 6.13 Dark UV-visible spectra of solutions containing complex **40** (50 µM) in the (**A**) absence and presence of (**B**) 10 µM; (**C**) 25 µM; (**D**) 50 µM; (**E**) 100 µM; (**F**) 200 µM; (**G**) 300 µM; (**H**) 400 µM cimetidine prepared in PBS/D$_2$O at pH* 7.4. Rise in absorbance at ca. 245 nm (↓) attributed to cimetidine absorbance.

Photo-irradiation of complex **40** (50 µM) at 463 nm for 5, 15, 30 and 60 min led to a successive decrease in the N$_3$→Pt^{IV} LMCT band, indicating the photo-release of the azide ligand, as previously reported (**A**, Figure 6.14).[1] Similar irradiations of complex **40** (50 µM) in the presence of (**B**) 10 µM; (**C**) 25 µM; (**D**) 50 µM; (**E**) 100 µM; (**F**) 200 µM; (**G**) 300 µM; (**H**) 400 µM cimetidine induced an equivalent photo-decomposition of ca. 60% (ca. 30 µM) in the LMCT band (**B-H**, Figure 6.14) of complex **40**. Interestingly, addition of 200 µM cimetidine led to the formation of an isosbestic point (**a'**, insets **F1**, Figure 6.14), together with a rise in the absorbance between 340 – 400 nm with a maximum absorbance at ca. 354 nm. This absorbance increased with successive addition of cimetidine (insets **G1** and **H1**, Figure 6.14), summarised in (Figure 6.15). Consequently, it appears that the formation of this new species with λ$_{max}$ at ca. 354 nm, is dependent on the amount of cimetidine present
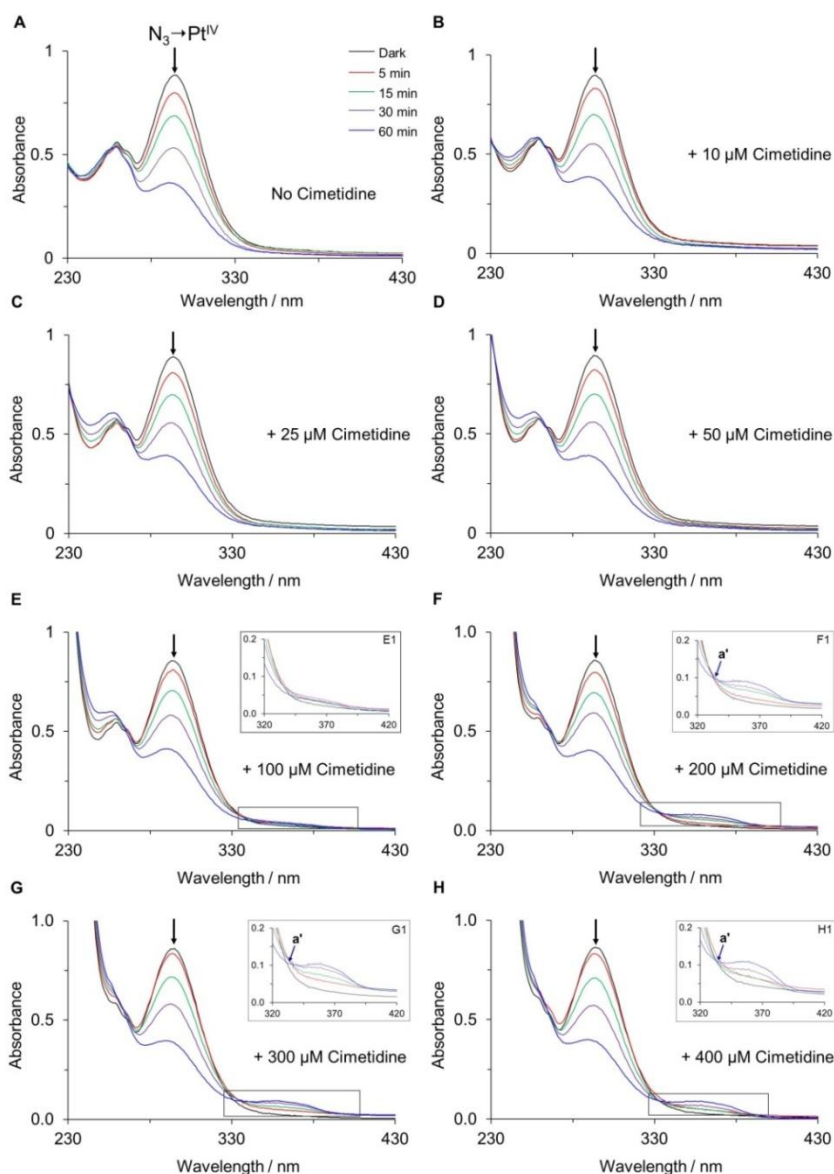
Figure 6.14 UV-visible spectra of solutions in the (–) dark and after (–) 5 min; (–) 15 min; (–) 30 min and (–) 60 min irradiation at 463 nm containing complex **40** (50 μM) in (**A**) absence and presence of (**B**) 10 μM; (**C**) 25 μM; (**D**) 50 μM; (**E**) 100 μM; (**F**) 200 μM; (**G**) 300 μM; (**H**) 400 μM cimetidine prepared in PBS/D$_2$O at pH* 7.4. Decrease (↓) observed in the N$_3$→Pt^{IV} LMCT band in all spectra (**A-H**). Insets **F1 – H1** shows isosbestic point at ca. 337 nm (**a'**). Band at ca. 354 nm attributed to LMCT transition.

.
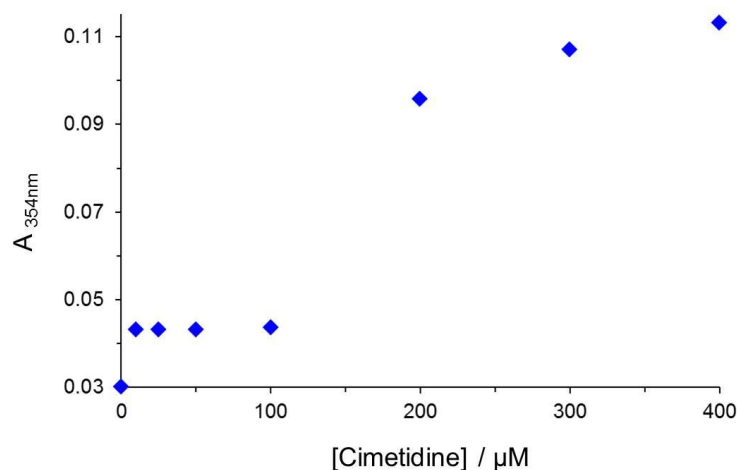
Figure 6.15 Increase in the absorbance at ca. 354 nm upon the successive addition of cimetidine (µM) to a solution containing complex **40** after 60 min irradiation at 463 nm prepared in PBS/D$_2$O at pH* 7.4.

The equivalent decrease in the N$_3$→Pt band of complex **40** in both the absence and presence of cimetidine as observed from Figure 6.14, suggested an equivalent amount of •N$_3$ radicals were generated. However, the increase in absorbance at ca. 354 nm suggested an alternative photo-decomposition pathway of complex **40** in the presence of cimetidine. This is believed to be induced from a reaction between cimetidine with the Pt^{II} intermediate formed from the photo-irradiation of complex **40**. Additionally, as discussed in **Chapter IV**, •N$_3$ radicals are known to readily undergo one-electron oxidation transfer reactions.[56] Consequently, this interaction between the formed •N$_3$ radicals with cimetidine could also contribute to the rise in absorbance. This potential interaction between the •N$_3$ radicals with cimetidine was investigated by EPR spectroscopy.

6.3.3 Azidyl radical trapping

Photo-irradiation of a solution of complex **40** (1 mM) in the presence of DMPO (2 mM) at 463 nm for 7 min and 14 min led to the formation of ca. 6.8% and 10.5% (per mol of complex **40**), respectively, of the DMPO-N_3 spin adduct (previously characterised in **Chapter III**), in the absence of cimetidine (■ Figure 6.16**A**). In the presence of cimetidine (2 and 4 mol equiv, Figure 6.16**A**), ca. 4% and 8.5% of the DMPO-N_3 spin adduct was formed after 7 min and 14 min, respectively, upon irradiation at 463 nm.
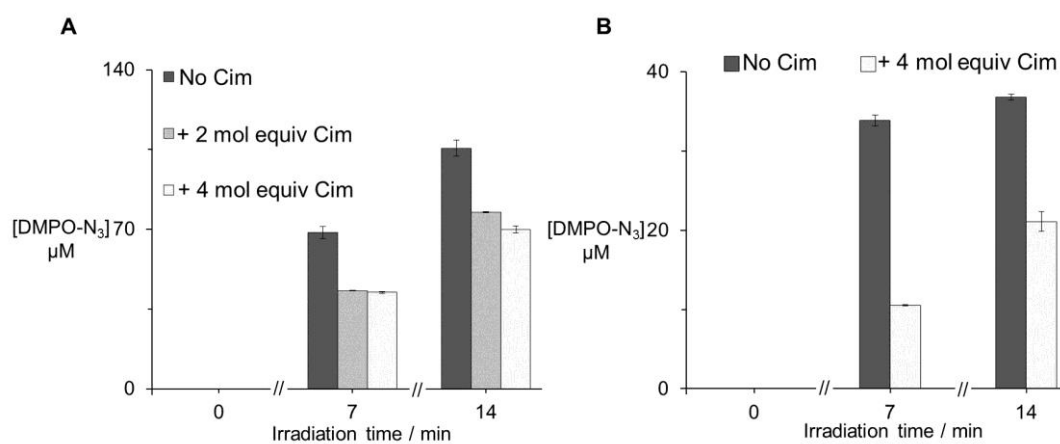
Figure 6.16 Quantification of the DMPO-N_3 spin adduct formed after 7 min and 14 min irradiation at 463 nm from a solution containing (**A**) complex **40** (1 mM) and DMPO (2 mM); (**B**) complex **40** (450 μM) and DMPO (900 μM) both in the (■) absence and presence of (■) 2 mol equiv, (□) 4 mol equiv cimetidine, prepared in PBS/D_2O at pH* 7.4. No EPR signal was observed in the dark. Error bars represent standard error of two independent experiments.

The concentration of complex **40** was reduced to more physiologically relevant conditions to observe the quenching of the $^\bullet N_3$ radicals by cimetidine. Photo-irradiation of complex **40** (450 μM) with DMPO (900 μM) in both the absence and presence of cimetidine (4 mol equiv) irradiated at 463 nm for 14 min prepared in PBS/D_2O at pH* 7.4, also led to the formation of the DMPO-N_3 spin adduct. However, in the presence

of cimetidine, the amount of the DMPO-N_3 spin adduct was ca. three-fold lower, after 7 min irradiation with 463 nm light, compared to the spin adduct formed in the absence of cimetidine, (Figure 6.16**B**). This suppression in $^{\bullet}N_3$ radical trapping became less effective with further irradiation. This reduction in $^{\bullet}N_3$ radicals trapped by DMPO suggested the possible quenching of the $^{\bullet}N_3$ radicals by cimetidine. To confirm this, NMR spectroscopy was performed.

6.3.4 ^{1}H NMR spectroscopy

6.3.4.1 Aromatic region

A solution of complex **40** (4 mM) in the presence of cimetidine (8 mM) was prepared in PBS/D_2O solution at pH* 7.4. Neither the ^{1}H NMR proton resonances of complex **40** nor cimetidine in the dark were affected (**A**, Figure 6.17). An initial 15 min irradiation with 463 nm light reduced the concentration of complex **40** to ca. 3.5 mM (12% photo-decomposition per mol of complex **40**), with sequential photo-decomposition of complex **40** observed with further (**B**-**D**, Figure 6.17) irradiation (Table 6.1). Both a decrease and a slight downfield shift of the ^{1}H NMR resonance of the imidazolic proton (H**5**, 7.6 ppm) of cimetidine were observed upon prolonged irradiation.

As can be seen from Figure 6.17, photo-irradiation of complex **40** with 463 nm light led to the generation of photo-products **e′** (8.73 ppm); **f′** (8.25 ppm); **g′** (8.0 ppm); **h′** (7.77 ppm) and **i′** (7.56 ppm). These photo-products were observed from the photo-irradiation of complex **40** only (Figure 6.17), previously characterised in **Chapter IV**. However, photo-products **j″** (8.7 ppm); **k″** (8.55 ppm); **n″** (7.88 ppm) and **q″** (7.47

ppm) were observed only from the photo-irradiation of complex **40** in the presence of cimetidine (Figure A6.1).
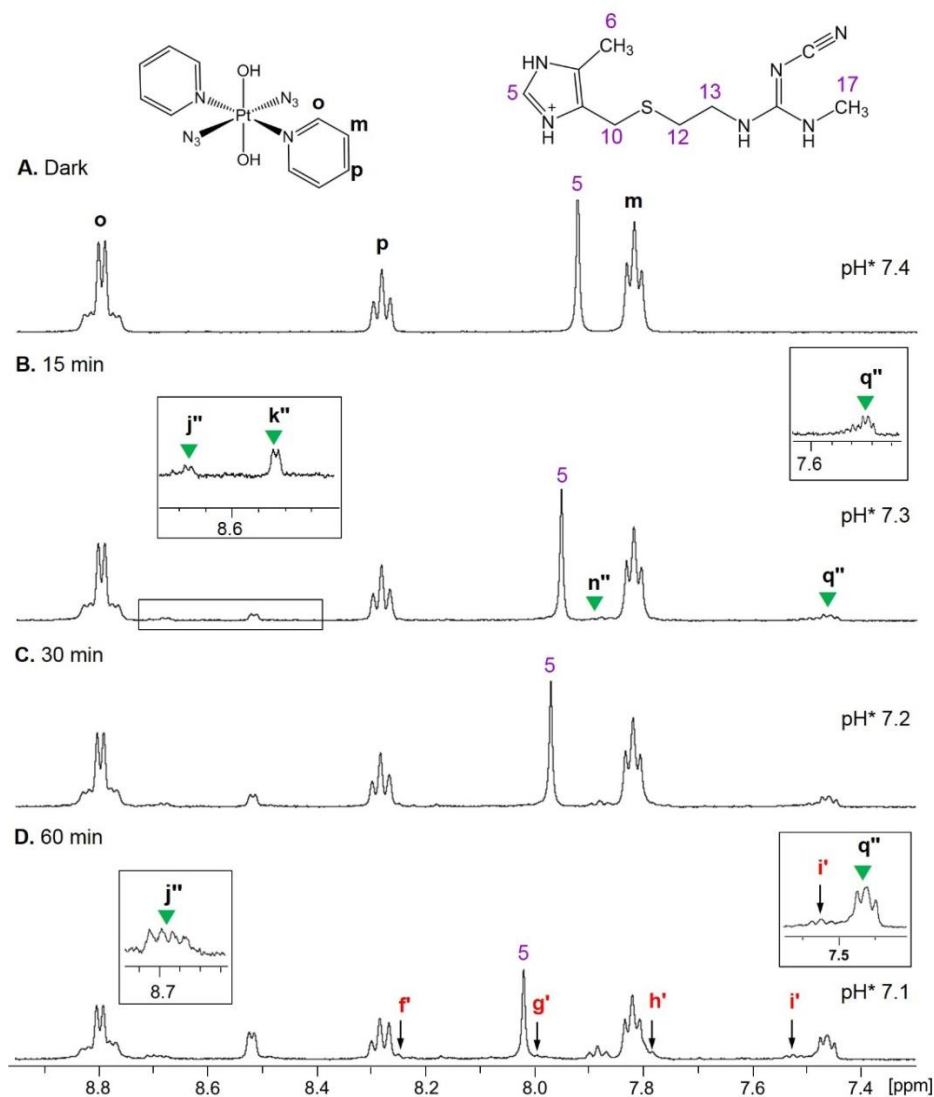
Figure 6.17 The aromatic region of the ^{1}H NMR spectra of complex **40** (4 mM) in the presence of cimetidine (8 mM) prepared in PBS/D$_2$O at pH* 7.4 in the (**A**) dark and after (**B**) 15 min; (**C**) 30 min and (**D**) 60 min irradiation at 463 nm. Assignments: Pt-py peaks, (**o/p/m**); cimetidine peak (**5**); photo-generated Pt-species in both the absence/presence of cimetidine, (**f'-i'**); photo-generated species only in the presence of cimetidine, (▼). See Figure 6.22 for aliphatic region.

Table 6.1 Quantification of complex **40** and platinum photo-products (**f'-i'**) from Figure 6.17, by ^{1}H NMR integration.

Time / (min)	[40] / (mM)	[f'-i']/ mM
0	4	-
15	3.5	0.2
30	3.3	0.5
60	1.9	0.8

The generation of these new photo-products (**j''**, **k''**, **n''** and **q''**) supports the UV-visible data that an alternative photo-decomposition pathway of photo-irradiated complex **40** occurs in the presence of cimetidine.

In an attempt to characterise the photo-products (**j''**, **k''**, **n''** and **q''**, Figure 6.17**B**), a comparison between ^{1}H NMR resonances of complex **40**, Pt^{II}-py products (intermediate species formed during the synthesis of complex **40**, previously characterised in **Chapter II**) and free pyridine were made. After 15 min irradiation at 463 nm, the ^{1}H NMR resonance **j''** at 8.7 ppm, appeared as a doublet (Figure 6.17**B**). Additional irradiation (60 min at 463 nm), changed the multiplicity of this ^{1}H NMR resonance to a pseudo-quartet (inset, Figure 6.17**D**). This change is likely to be related to the transition of mono- to bi-dentate coordination of cimetidine to the Pt^{II} photoproduct. The remaining photo-generated peaks **k''** (8.55 ppm), **n''** (7.88 ppm) and **q''** (7.47 ppm) were compared with the ^{1}H NMR resonances of pyridine (2 mM, PBS/D_2O),[54] and were in agreement (Figure 6.18).
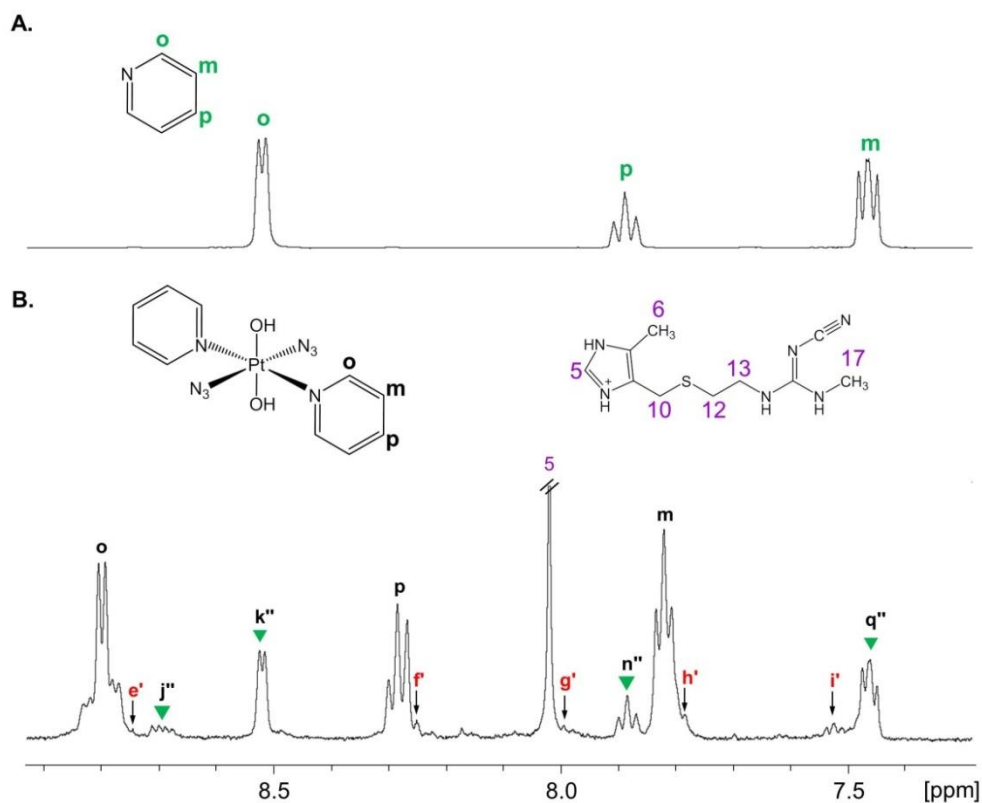
Figure 6.18 The aromatic region of the ^{1}H NMR spectra of (**A**) free pyridine and (**B**) photo-irradiation of complex **40** (4 mM) in the presence of cimetidine (8 mM) at 463 nm for 60 min prepared in PBS/D$_2$O at pH* 7.4. Assignments: pyridine peaks, (**O/P/M**); Photo-peaks **k″**, **n″** and **q″** assigned to the H$_{ortho}$, H$_{para}$ and H$_{meta}$ resonances of pyridine, respectively. Remaining peaks as assigned in Figure 6.17.

6.3.4.2 Mass Spectrometry

The formation of a Pt^{II}-cimetidine species and detection of photo-released pyridine from irradiated complex **40** was investigated, by performing mass spectrometry. MS of an irradiated solution of complex **40** (4 mM) and cimetidine (8 mM) at 463 nm for 60 min prepared in H$_2$O at pH 7.4, was recorded in the range of 500 – 1000 *m/z*. Low resolution MS led to the detection of mass adducts at *m/z* of 567.2, 622.2, 647.0 and 722.2 (Figure 6.19**A**). Performing HR-MS on the same sample led to the detection of a mass adduct at ca. *m/z* of 647.1755, assignable to [Pt(py)$_2$(OH$_2$)(cim)+Na]$^{3+}$ (**67**, Figure

287

6.19**B**), in agreement with its simulated mass spectrum. Consequently, the mass adduct at ca. *m/z* of 622.2 was assignable to *trans*-$[Pt(py)_2(OH_2)(cim)+H]^{3+}$. Furthermore, the mass adduct at ca. *m/z* of 567.2 was deduced to be *trans*-$[Pt(py)(OH_2)(cim)+Na]^{3+}$ (**68**).

The detection of a bi-dentate platinum(II)-cimetidine species may rationalise the change in the ^{1}H NMR resonance **j''**. Finally, the MS adduct at *m/z* of ca. 722.2 was assigned to $[Pt(cim)_2+Na]^{3+}$ (**69**). None of these MS adducts were detected in the absence of cimetidine. These data confirmed photo-irradiation of complex **40** in the presence of cimetidine led to an alternative photo-decomposition pathway. Furthermore, HR-MS detected a peak at ca. *m/z* 159.070, assigned to a pyridine dimer, $[2(py)+H]^+$ (Figure 6.20), a species previously reported.[57] All photo-generated MS peaks are summarised in Table 6.2.
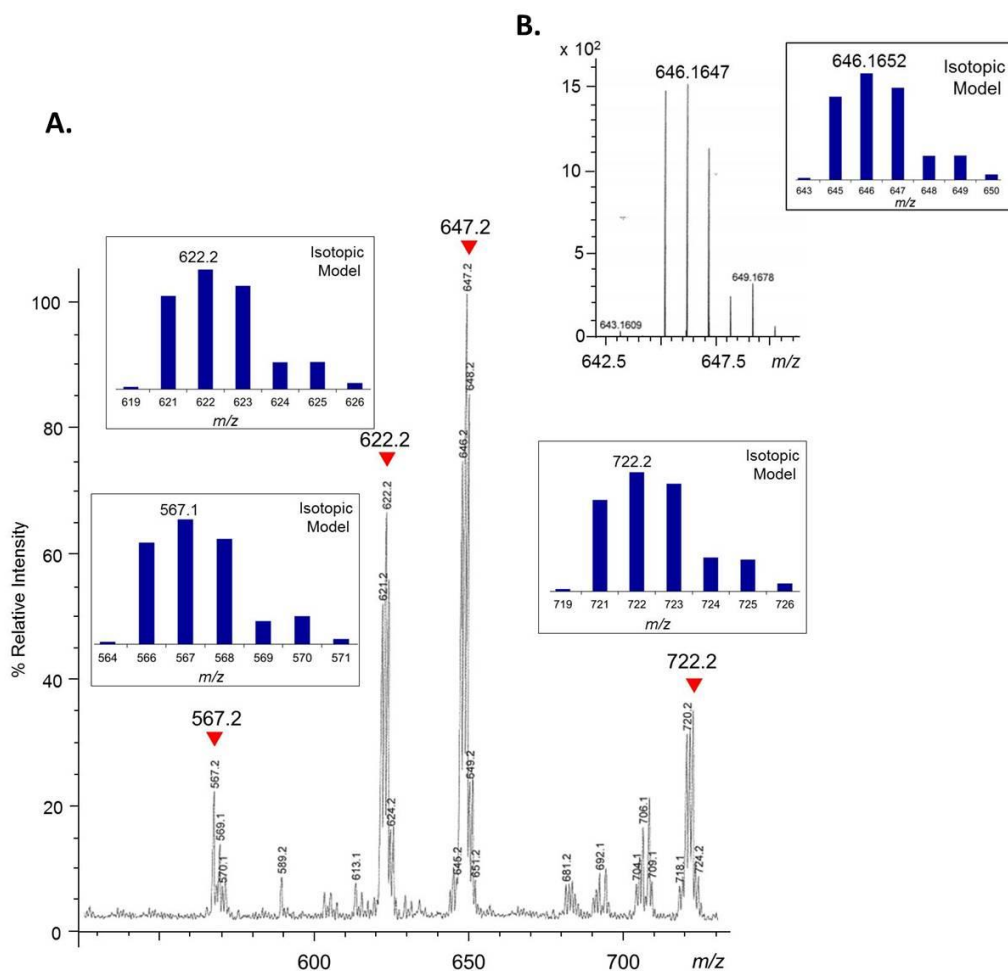
Figure 6.19 Mass spectrum from a solution containing complex **40** (4 mM) in the presence of cimetidine (8 mM) irradiated at 463 nm for 60 min prepared in H_2O at pH 7.4. Mass adducts together with simulated mass spectra detected at (**A**) low resolution and (**B**) high resolution. Mass adduct at *m/z* of ca. 646.1647 is assigned to *trans*-$[Pt(py)_2(OH_2)(cim)+Na]^{3+}$ species, **67**; 567.2 is assigned to $[Pt(py)(OH_2)(cim)+Na]^{3+}$, **68**; and 722.2 is assigned to $[Pt(cim)_2+Na]^{3+}$ (**69**), in agreement with their isotopic distribution models.
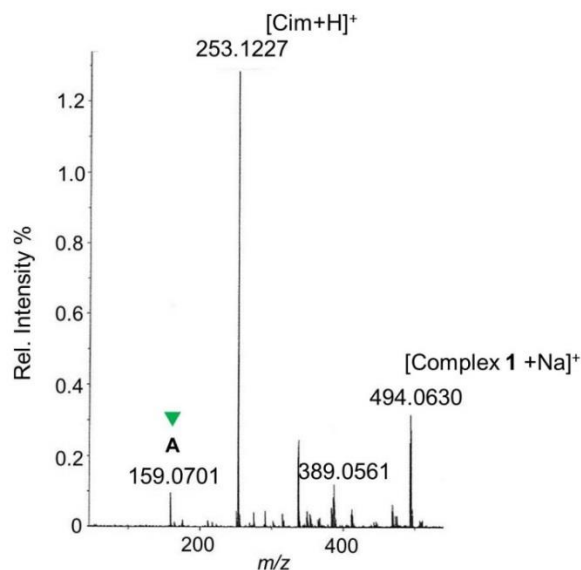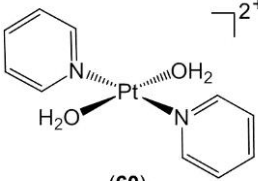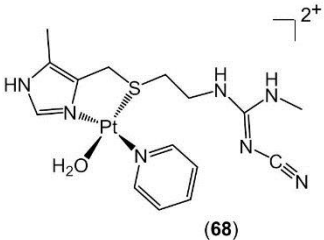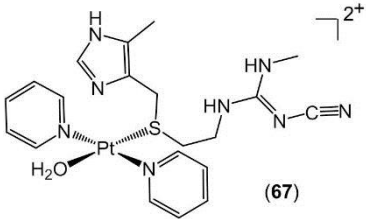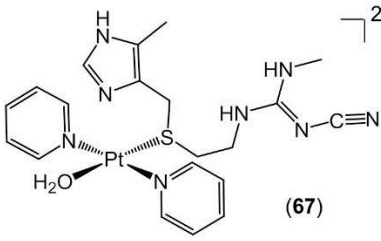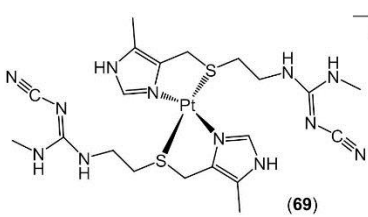
Figure 6.20 Lower *m/z* region of HR-MS spectrum from a solution containing complex **40** (4 mM) in the presence of cimetidine (8 mM) irradiated at 463 nm for 60 min**.** Release of pyridine from complex **40** gave rise to fragment at *m/z* 159.0701 (**A**) [2(py) + H]$^+$, *m/z* calc. 159.0844. Mass adducts at *m/z* 253.1227 and 494.0630 were previously assigned to [Cim+H]$^+$ and [Complex **40**+Na]$^+$, respectively, refer to section **6.3.1** and as reported by Farrer.[1]

The detection of the species [Pt(py)$_2$(OH$_2$)$_2$]$^{2+}$ (**60**, previously detected in **Chapter V**) at *m/z* of 389.056, further supported the release of the two azide ligands. Furthermore, the quantification of pyridine released from photo-irradiated complex **40** was determined *via* ^{1}H NMR integration (Table 6.3).

Table 6.2 Assignment of MS adducts found in Figures 6.19 and 6.20

Found m/z	Structure	Formula	Cal. m/z
159.0698[a]	 Pyridine	$C_{10}H_{11}N_2$ $[(py_2)+H]^+$	159.0844
389.0561[a]	 (60)	$C_{10}H_{14}N_2O_2Pt$ $[Pt(OH_2)_2(py)_2]^{2+}$	389.0703
567.2[b]	 (68)	$C_{15}H_{23}N_7OPtSNa$ $[Pt(py)(OH)_2(cim)+Na]^{3+}$	567.1
622.2[b]	 (67)	$C_{20}H_{29}N_8OPtS$ $[Pt(py)_2(OH_2)(cim) H]^{3+}$	622.2
646.1647[a]	 (67)	$C_{20}H_{28}N_8OPtSNa$ $[Pt(py)_2(OH_2)(cim)+Na]^{3+}$	646.1652
722.2[b]	 (69)	$C_{20}H_{32}N_{12}PtS_2Na$ $[Pt(cim)_2+Na]^{3+}$	722.2

[a]HR-MS; [b]low resolution MS

Table 6.3 Quantification of pyridine released from photo-irradiated complex **40** (4 mM) in the presence of cimetidine (8 mM) as depicted in Figure 6.17.

Time / min	Pyridine / mM
Dark	**-**
15	0.2
30	0.4
60	0.9

From the above data, it is apparent that cimetidine is involved in the photo-decomposition pathway of photo-irradiated complex **40**. To further confirm the involvement of cimetidine, analysis of its ^{1}H NMR resonances was performed.

6.3.4.3 pKa* of cimetidine

The down-field shift of the H5 peak in the ^{1}H NMR spectrum of cimetidine has been previously associated with metal coordination *via* the sulfur (S11) atom of cimetidine. The imidazolic nitrogen (N4) has a reported pK_a value of ca. 6.9 (Figure 6.3). As shown in the previous section, photo-irradiation of complex **40** (4 mM) in the presence of cimetidine (8 mM) led to a stepwise decrease in the pH* of the solution (refer to Figure 6.17). Therefore, a solution of cimetidine (8 mM) was prepared in PBS/D$_2$O at pH* 7.4. The pH* of this solution was adjusted using 0.1 M NaOH and 0.1 M HCl, to obtain a plot of the chemical shift of the H5 resonance of cimetidine as a function of change in pH*. From Figure 6.21, the downfield shift of the H5 peak increased with decreasing pH*, a similar effect as observed in the presence of irradiated complex **40**. Moreover, the pK_a^* value of 7.1 ± 0.07 obtained is in good agreement with previous literature,[58] slight differences can be attributed to the pK_a measured on a pH electrode without

correction effects for D_2O (refer to section **6.2.6**). Therefore, in this work, the downfield chemical shift of the H**5** NMR resonance of cimetidine, cannot be attributed to metal coordination.
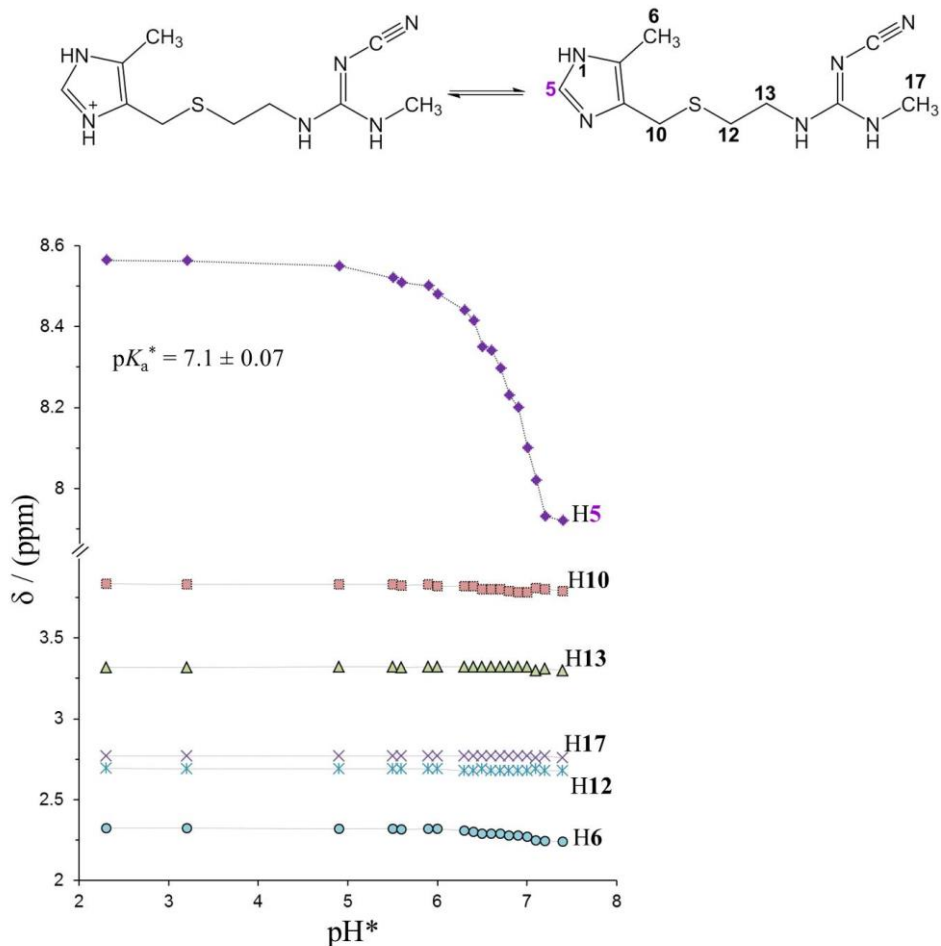
Figure 6.21 The pH* values plotted against the ^{1}H NMR chemical shifts (δ) for a solution of cimetidine (8 mM) prepared in PBS/D_2O at pH* values ranging from 7.4 - 2.3. The pK_a^* value of 7.1 ± 0.07 was determined as described in experimental section and is in agreement with previously reported value for the imidazolic NH group.[58]

6.3.4.4 Aliphatic region

Next, the ^{1}H NMR resonances of cimetidine were analysed from the solution containing complex **40** (4 mM) and cimetidine (8 mM) prepared in PBS/D_2O at pH* 7.4 in both

the dark and after 60 min irradiation at 463 nm. In the dark, cimetidine exhibited six ^{1}H

NMR resonances (Figure 6.22**A**), unaffected by the presence of complex **40**.
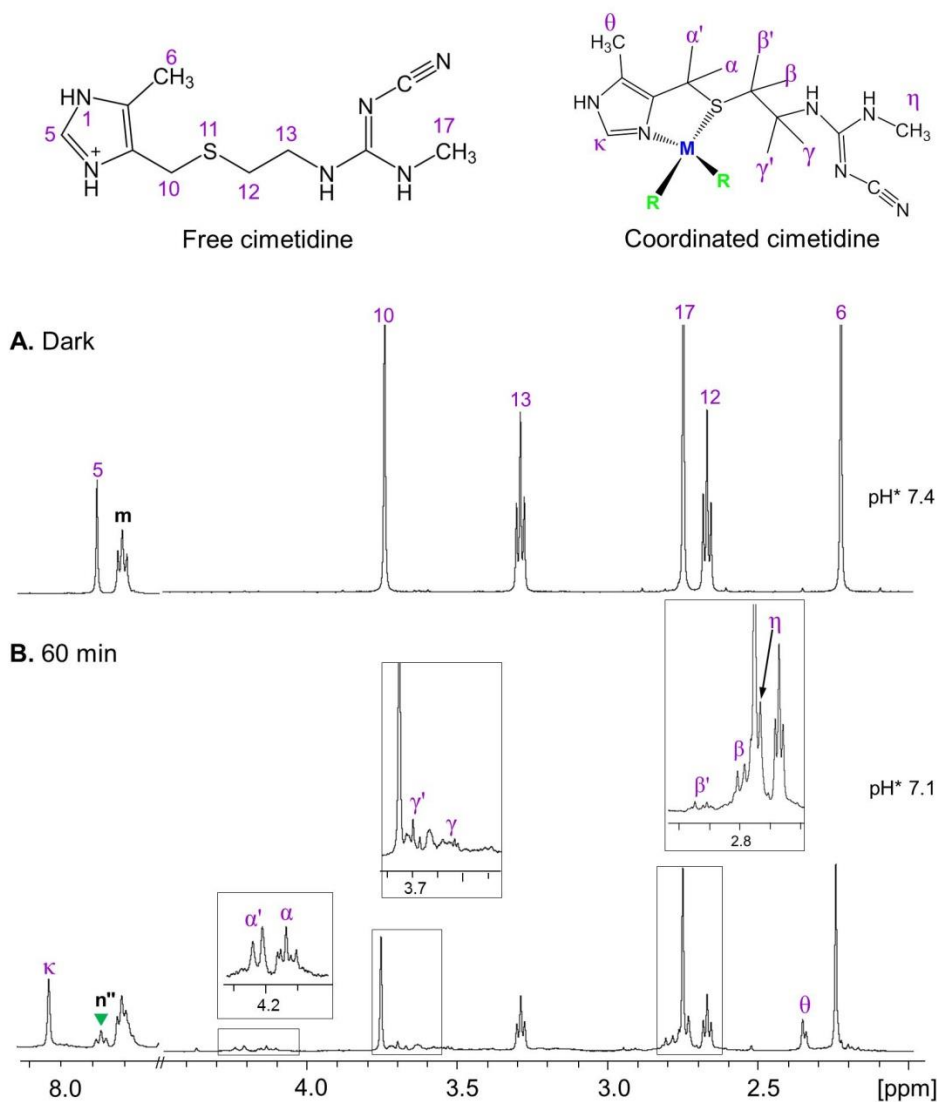
Figure 6.22 ^{1}H NMR spectra of a solution of complex **40** (4 mM) in the presence of

cimetidine (8 mM) in (**A**) the dark and (**B**) after 60 min irradiation at 463 nm.

Assignments: free cimetidine peaks (1-17); photo-generated species (α-κ). Spectra

internally referenced to HMDSO (0.28 ppm in D$_2$O) due to overlap of ^{1}H NMR

resonances of cimetidine with 1,4 dioxane. Photo-products (α-κ) assigned to a structure

as shown, where **M** = Pt^{II} metal ion and **R** refers to amine/H$_2$O ligands.

After 60 min irradiation with 463 nm light, ca. 40% (3 mM) of cimetidine photo-decomposed, as determined by ^{1}H NMR integration (Figure 6.22**B**). Additionally, new ^{1}H NMR resonances were observed (inset spectra, Figure 6.22**B**) and were distinct from ^{1}H NMR resonances of free cimetidine. The photo-products (α-κ) were compared to the ^{1}H NMR resonances of both [Pd(cim)Cl$_2$] and [Pt(cim)$_2$]Cl$_2$ species, previously characterised by Onoa.[49] The ^{1}H NMR resonances of the photo-products (α-κ) are in closer agreement with those values previously reported for the [Pd(cim)Cl$_2$] complex (Table 6.4).

Table 6.4 Comparison of the ^{1}H NMR chemical shifts (ppm) of photo-products (α-κ) as observed from Figure 6.22**B** with a previously reported [Pd(cim)Cl$_2$] species.[49]

Complex	H5	H10	H13	H17	H12	H6
[a]Pd-cim	7.93 (s)	4.13 - 4.08 (d) 3.91 – 3.86 (d)	3.52 (m)	2.69 (d)	3.08 (t)	2.18 (s)
[b]68	8.2 (κ, s)	4.25 - 4.20 (α) 4.17 – 4.11 α'	3.54 (γ, m)	2.5 (η, d)	3.12 (β, t)	2.4 (θ, s)
Δσ	0.6	-1.0	-0.24	0.3	-0.47	0.2

[a]spectra registered in DMSO-d$_6$ at RT (values from ref 49); [b]spectra registered in PBS/D$_2$O at RT from the photo-irradiation of complex **40** (4 mM) in the presence of cimetidine (8 mM) with 463 nm light after 60 min; s, singlet; b, broad; m, multiplet; Δσ refers to chemical shift (ppm) difference between free and coordinated cimetidine.

Consequently, the photo-products (α-κ) are assigned to $[Pt(py)(OH_2)(cim)]^{2+}$ (**68**) species. This further supports the MS data on the detection of the mass adduct at *m/z* of ca. 567.2, assigned to $[Pt(py)(OH_2)(cim)+Na]^{3+}$. The minor differences in the ^1H NMR resonances of **68** and $[Pd(cim)Cl_2]$ species as observed in Table 6.4, are attributed to the different solvents (PBS/D_2O vs. DMSO-d_6) used to register the species and central metal ions (Pt^{II} vs. Pd^{II}) present in both **68** and $[Pd(cim)Cl_2]$ species, respectively. Moreover, the presence of free pyridine and additional photo-products in the irradiated solution can also influence the resultant chemical shift values of **68** compared to the $[Pd(cim)Cl_2]$ species. A similar photo-irradiation of complex **40** (4 mM) and cimetidine (8 mM) was performed in the presence of spin trap, DMPO (8 mM, Figure 6.23).

Equivalent photo-products in both the aromatic and aliphatic region were observed in the presence of DMPO, as previously described in section **6.3.4.1** and **6.3.4.2**, respectively. Consequently, the presence of the spin trap, DMPO did not appear to affect the formation of **68**. New photo-products were observed in the aliphatic region (inset **iii**, Figure 6.23**B**), previously assigned to the DMPO-N_3 hydroxylamine species (**Chapter IV**). Interestingly, in the absence of cimetidine, the DMPO ^1H NMR resonances decreased by ca. 25%, in comparison to ca. 10% in the presence of cimetidine. This supports the partial quenching of the $^•N_3$ radicals by cimetidine, as observed by EPR spectroscopy. The quenching of $^•N_3$ radicals by cimetidine is investigated further by ^{14}N NMR spectroscopy, in section **6.3.5**. Additionally, ^{13}C-DEPT135 NMR spectroscopy was performed to further elucidate a distinction between free and coordinated cimetidine peaks.
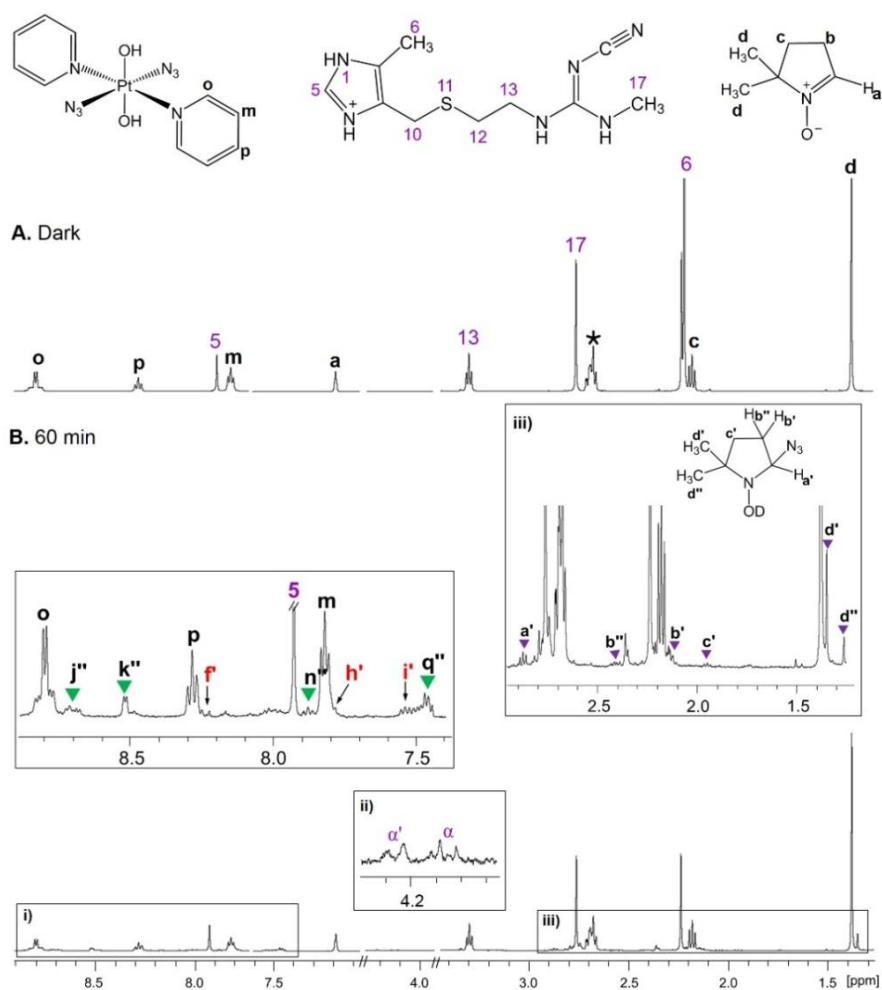
Figure 6.23 ^{1}H NMR spectra from the photo-irradiation of complex **40** (4 mM), cimetidine (8 mM) in the presence of DMPO (8 mM) prepared in PBS/D$_2$O at pH* 7.4 in (**A**) the dark and (**B**) after 60 min irradiation with 463 nm light. Additional (▼) ^{1}H NMR resonances assigned to the DMPO-N$_3$ hydroxylamine species; other resonances as labelled previously in Figures 6.17 and 6.22.

6.3.4.5 ^{13}C-DEPT135 NMR

A solution of complex **40** (9 mM) with DMPO (2 mol equiv) in the presence of cimetidine (2 mol equiv) was prepared in PBS/D$_2$O at pH* 7.4. The dark ^{13}C-DEPT135 NMR spectrum displayed resonances for all CH, CH$_3$ and CH$_2$ groups present in complex **40**, DMPO and cimetidine (Figure 6.24**A**). Carbon atoms without bound

hydrogen were not detected. Irradiation at 463 nm for 60 min led to a decrease in all

^{13}C-DEPT135 NMR resonances of complex **40**, DMPO and free cimetidine. Additional

^{13}C-DEPT135 NMR signals were observed (Figure 6.24**B**). These new peaks were

compared to ^{13}C NMR data from previously reported [Pd(cim)Cl$_2$] species (Table

6.5).[49]
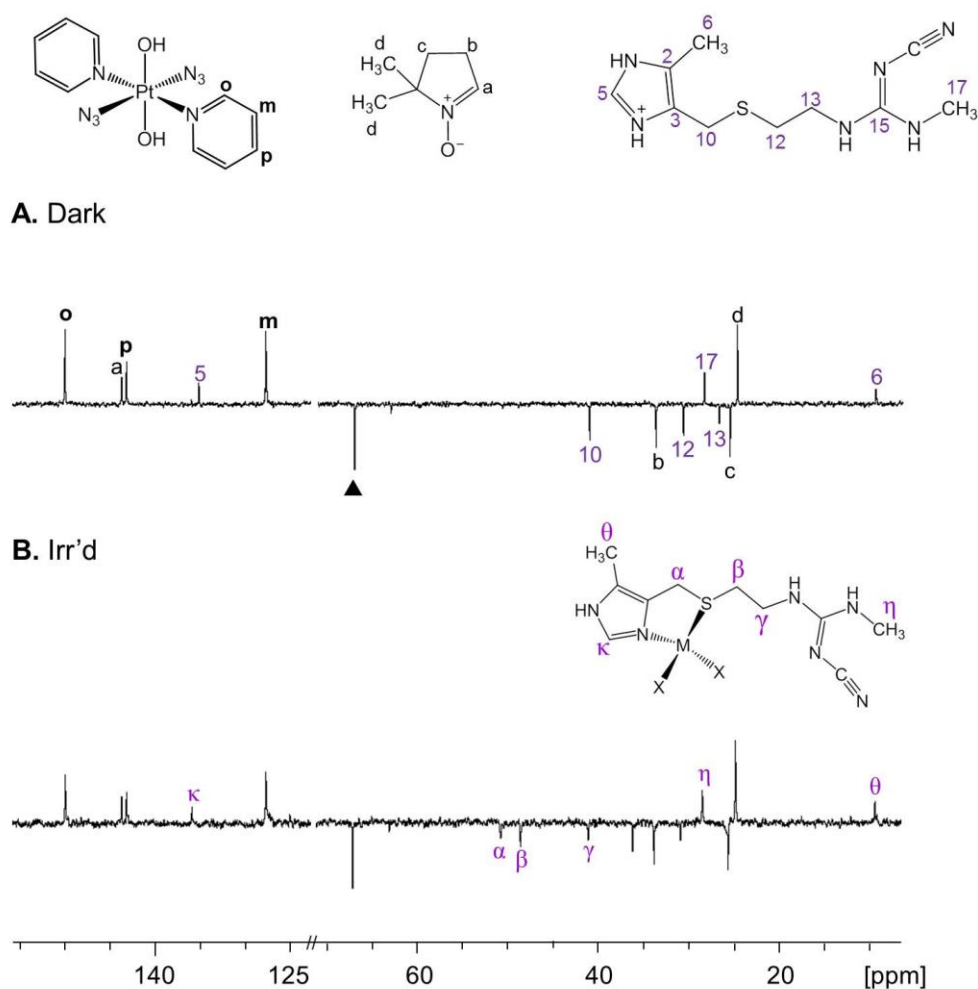
Figure 6.24 ^{13}C-DEPT135 NMR spectra of complex **40** (9 mM), DMPO (2 mol equiv)

in the presence of cimetidine (2 mol equiv) prepared in PBS/D$_2$O at pH* 7.4 in (**A**) dark

and (**B**) irradiated for 30 min at 463 nm. Assignments: pyridine carbons, (**o/p/m**);

DMPO, (a-d); free cimetidine, (5-17); coordinated cimetidine, (α-θ); internal reference

1,4-dioxane, (▲).

A downfield shift in the ^{13}C-DEPT135 NMR resonances of both C5 and C10 was observed for **68** (Table 6.5), in agreement with those reported for [Pd(cim)Cl$_2$] species. These data further support **68** as being a bidentate-cimetidine platinum(II) species, as assigned by ^{1}H NMR and mass spectrometry.

Table 6.5 Comparison of ^{13}C and ^{13}C-DEPT135 NMR chemical shifts for [Pd(cim)Cl$_2$] and **62** species, respectively.

Complex	C5	C2	C10	C13	C17	C12	C6
[a]Pd-cim	137.05	117.95	32.55	40.52	28.52	37.68	10.01
[b]68	136.0	121.0	28.55	50.9	48.6	36.2	9.4

[a]spectra registered in DMSO-d$_6$ at RT (values from ref 49); [b]spectra registered in PBS/D$_2$O at RT, refer to Figure 6.24**B**.

Moreover, Norman *et al.* reported on the ^{195}Pt NMR chemical shifts of 1:1 platinum-L-methionine complexes in the region of -2500 – 4000 ppm.[59] In this work, ^{195}Pt NMR spectra were recorded across the range of -1500 - -4000 ppm. However, no ^{195}Pt NMR peak(s) were detected. This is attributed to the amount of **68** being formed, which is below the detection limit for ^{195}Pt NMR spectroscopy.

Next, the partial quenching of the $^\bullet$N$_3$ radicals by cimetidine was investigated. Azidyl radicals are well-known to undergo one-electron oxidation reactions, leading to the formation of free azide (N$_3^-$). To confirm the reaction between the azidyl radicals with cimetidine, ^{14}N NMR was performed.

6.3.5 Quenching of the azidyl radicals by cimetidine

Prior to investigating an interaction between the formed $^{\bullet}N_3$ radicals with cimetidine various control experiments were performed. Individual solutions of pyridine (6 mM) and cimetidine (18 mM) were prepared in PBS/D$_2$O at pH* 7.4. In addition to atmospheric nitrogen gas (N$_2$), a broad peak was detected at ca. 271 ppm assigned to the nitrogen atom of free pyridine (Figure 6.25). The ^{14}N NMR spectrum of free cimetidine (25 mM) prepared in PBS/D$_2$O at pH* 7.4, displayed a resonance at ca. 168.2 ppm, assignable to the imidazole nitrogen (N1) present in cimetidine (Figure 6.25). The remaining ^{14}N resonances present in cimetidine have been reported by solid-state (SS) NMR to be outside the investigated region, N4, -155 ppm; N14, -20 ppm; N16, - 70 ppm; N18, -65 ppm; N20, -95 ppm.[60]
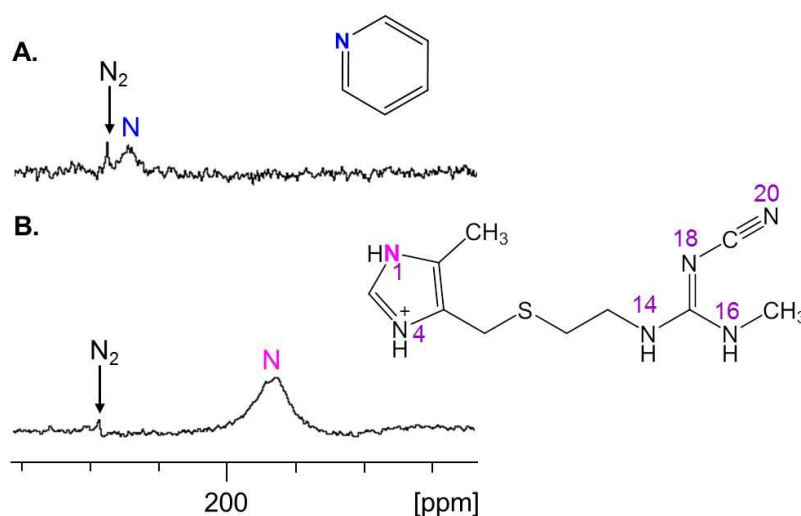
Figure 6.25 ^{14}N NMR spectra of solutions of (**A**) pyridine (6 mM) and (**B**) cimetidine (25 mM) prepared in PBS/D$_2$O at pH* 7.4. Assignments: nitrogen resonance from free pyridine, (N, 272.2 ppm); imidazolic nitrogen of cimetidine, (N1, 168.2 ppm).

The ^{14}N NMR spectrum of a solution of complex **40** (6 mM) in the presence of cimetidine (12 mM) prepared in PBS/D$_2$O at pH* 7.4 displayed resonances of coordinated azide and pyridine as well as atmospheric N$_2$ (Figure 6.25**A**) in the dark. A

decrease in both coordinated azide and pyridine ^{14}N NMR resonances were observed, after 60 min irradiation with 463 nm light. An additional peak at ca. 78.1 ppm was assigned to the central (N_β) nitrogen of free azide (Figure 6.26**B**), as previously observed in **Chapter IV**.
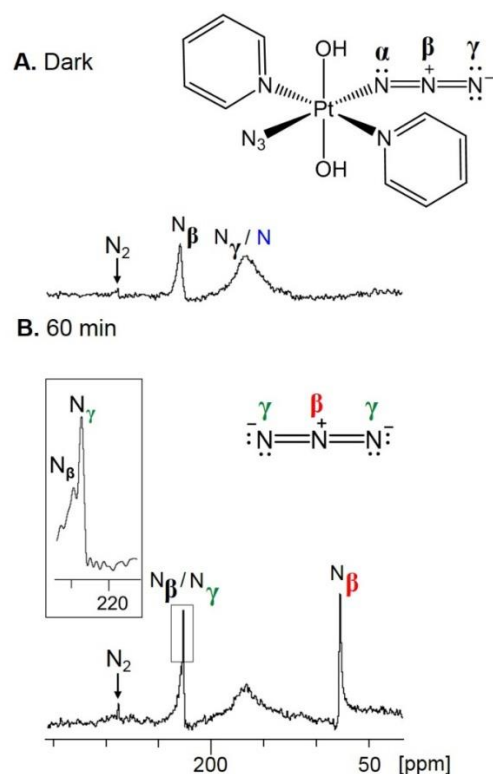
Figure 6.26 ^{14}N NMR spectra of complex **40** (6 mM) in the presence of cimetidine (12 mM) prepared in PBS/D$_2$O at pH* 7.4 in (**A**) the dark and (**B**) after irradiation with 463 nm light for 60 min. Assignments: atmospheric nitrogen gas, (N$_2$, 289.2 ppm); inset illustrating distinction between central nitrogen (N$_\beta$) of coordinated azide with terminal nitrogen (N$_\gamma$) of free azide (N$_3^-$), (N$_\beta$/N$_\gamma$, 229.1 ppm); overlap between terminal nitrogen of coordinated azide with nitrogen of coordinated pyridine (N), (N$_\gamma$/N, 166.5 ppm); central nitrogen of free azide, (N$_\beta$, 77.3 ppm).

Interestingly, an increase in the ^{14}N NMR resonance of N$_2$ (289.2 ppm) was observed suggesting azidyl radical decomposition to form molecular nitrogen (Figure 6.26**B**).

The resonance at 166.5 ppm, appeared to exhibit a broadening after irradiation, thought to be due to the coordination of the imidazolic nitrogen (N4) of cimetidine to the Pt^{II} metal centre. This is in agreement with previous reports of Pt^{II} coordination to 1-methylimidazole *via* the imidazolic NH atom.[61] The broadening in the ^{14}N NMR resonance at 166.5 ppm, further supports the ^{13}C-dept135 downfield shifts of both C5 and C10, attributed to Pt^{II} coordination to both the sulfur (S11) and imidazolic nitrogen (N4) atoms of cimetidine. Free azide (N_3^-) has not been reported from the photo-irradiation of complex **40** alone (see **Chapter IV**). Consequently, detection of N_3^- in this work confirms the interaction between the formed azidyl radicals with cimetidine. However, from these data the site at which the $^\bullet N_3$ radical abstracts an electron was not apparent.

Therefore, in an attempt to elucidate the site of $^\bullet N_3$ radical reactivity, two molecules, L-methionine and histamine were chosen to represent the thioether (Figure 6.27**A**) and imidazole (Figure 6.27**B**) moieties present in cimetidine.
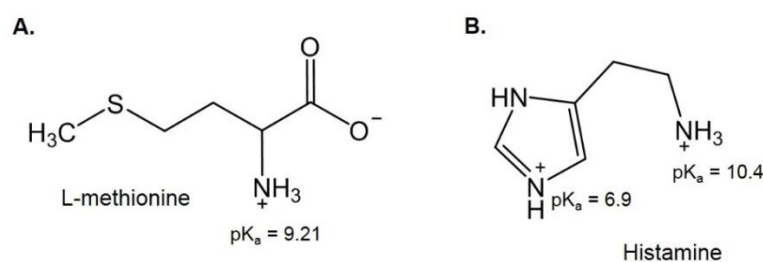
Figure 6.27 Structure of (**A**) L-methionine and (**B**) histamine at physiological pH 7.0

6.3.5.1 Thioether or imidazole radical formation

Individual solutions of complex **40** (4 mM), DMPO (8 mM) in the absence and presence of L-methionine (2 mol equiv) and histamine (2 mol equiv) were irradiated with 463 nm light for 14 min prepared in PBS/D_2O at pH* 7.4 (Figure 6.28).
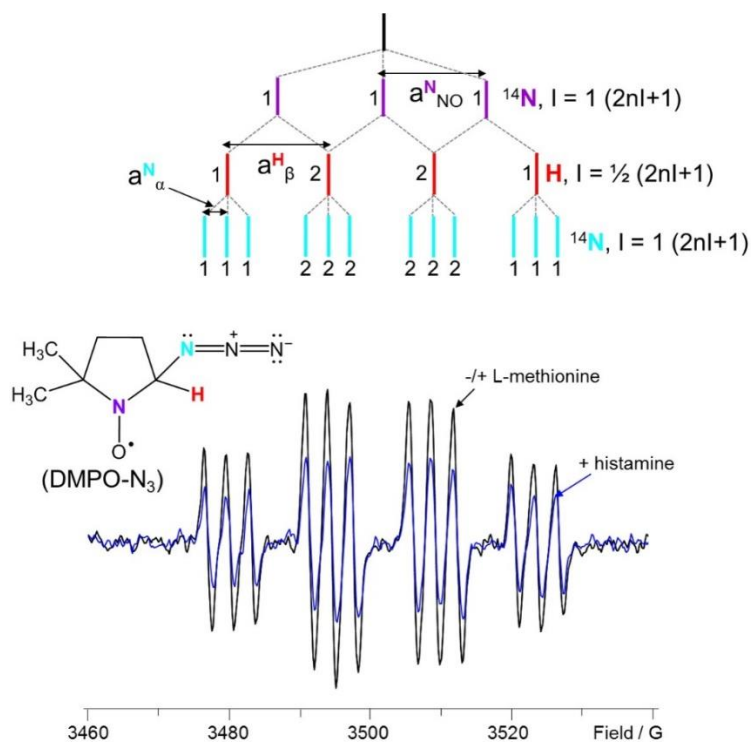
Figure 6.28 EPR spectra of the DMPO-N$_3$ spin adduct formed from the photo-irradiation of complex **40** (4 mM), DMPO (8 mM) with 463 nm light after 7 min prepared in PBS/D$_2$O at pH* 7.4 in the absence and presence of L-methionine (8 mM, 2 mol equiv) and presence of histamine (8 mM, 2 mol equiv). Decrease (ca. 20%) in the DMPO-N$_3$ spin adduct determined in the presence of histamine.

An equivalent formation in the DMPO-N$_3$ spin adduct (previously characterised in **Chapter III**), was observed in both the absence and presence of L-methionine. This suggests that neither the thioether nor the amino (-NH$_2$) groups, are the site of $^\bullet$N$_3$ radical reaction. In contrast, a ca. 20% reduction in the DMPO-N$_3$ spin adduct was observed in the presence of histamine (blue line, Figure 6.28). This decrease supports the suggestion that the imidazole ring is the site of one-electron transfer. Moreover, one-electron transfer of cimetidine to the $^\bullet$N$_3$ radicals suggests formation of a cimetidine radical cation), which has potential to deprotonate at neutral pH 7 and form the neutral cimetidine radical.

Interestingly, no precipitate was observed from the photo-irradiation of complex **40** in the presence of cimetidine. This suggests that the formed cimetidine neutral radical did not undergo polymerisation, in contrast to L-tryptophan and melatonin radicals (refer to **Chapter IV** and **Chapter V**).

To conclude this section, EPR, ^{1}H/^{13}C-dept135 NMR spectroscopy and mass spectrometry detected and characterised various photo-products, including azidyl radicals, free azide, Pt^{II}-cimetidine species and free pyridine. Formation of Pt-S(thioether) species have been associated with adverse toxic effects and resistance mechanisms.[50] Therefore, cellular studies were performed to determine the photo-cytotoxicity of complex **40** in the presence of cimetidine in HaCaT immortal human keratinocyte cells.

6.3.7 Cell studies

6.3.7.1 Cell viability in HaCaT keratinocytes cells

To assess the photo-cytotoxicity of complex **40** in the presence of cimetidine, cell viability in both the dark and after irradiation with 420 nm (5 J cm^{-2}) light was determined for the co-incubation of cimetidine (0.15 and 1.5 mM) in the presence of complex **40** (different concentrations) in HaCaT keratinocytes cells. None of the solutions exhibited dark toxicity (filled markers, Figure 6.29). Increasing the concentration of complex **40** from ca. 1.7 µM to ca. 107 µM, efficiently demonstrated its potent anti-proliferative activity in HaCaT cells (open squares, □; Figure 6.29). Photo-irradiation of complex **40** (3.3 µM) with 420 nm light reduced the viability of HaCaT cells by ca. 7%, in contrast to ca. 4% viable cells remaining after photo-irradiation of 53 µM complex **40**. Interestingly, photo-irradiation of complex **40** (53

μM) but in the presence of cimetidine (0.15 mM) led to ca. 91% of viable cells (○, Figure 6.29). The photo-cytotoxicity of complex **40** (different concentrations) was completely suppressed in the presence of 1.5 mM cimetidine.
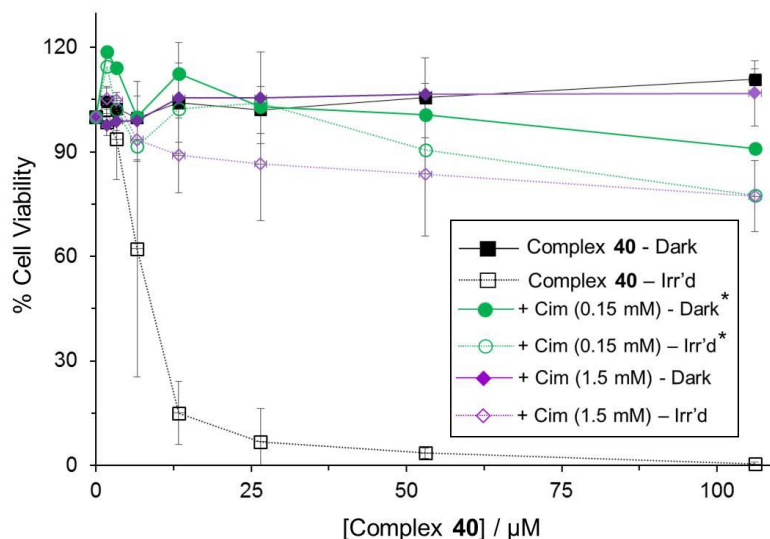
Figure 6.29 The percentage cell viability induced by the photo-irradiation of complex **40** (various concentrations) in the presence of cimetidine (0.15 mM and 1.5 mM) in HaCaT keratinocytes cells in the (filled markers) dark and (open markers) after irradiation with $\lambda_{max} = 420$ nm light (5 J cm^{-2}). Error bars represent ± standard errors for the mean of two experiments performed in triplicate, where * refers to one experiment performed in triplicate.

To assess the dose-dependent nature of this protective effect, the cell viability in both the dark and after irradiation with 420 nm (5 J cm^{-2}) was determined from the co-incubation of complex **40** (42.4 μM) in the presence of cimetidine (various concentrations) in HaCaT keratinocytes cells. As before no dark toxicity was observed. Interestingly, irradiation of complex **40** (42.4 μM) with 420 nm light led to an equivalent photo-protective effect in the presence of both the lowest (46.9 μM) and

highest (1.5 mM) concentrations of cimetidine (Figure 6.30). These data confirmed that

the photo-protective effect induced by cimetidine was dose independent.
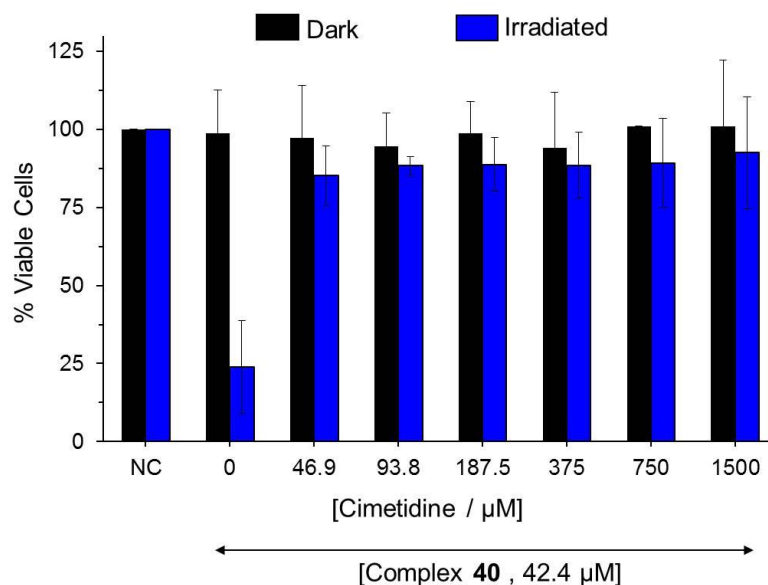
Figure 6.30 The percentage cell viability induced by the photo-irradiation of complex

40 (42.4 µM) in the presence of cimetidine (various concentrations) in HaCaT

keratinocytes cells in the (■) dark and (■) after irradiation with $\lambda_{max} = 420$ nm light (5

J cm^{-2}). Error bars represent $\pm$ standard deviation for the mean of two independent

experiments performed.

The induction of this photo-protective effect had potential to be due to a reduced

platinum accumulation in the presence of cimetidine. Therefore, ICP-MS was

performed to determine the Pt accumulation in HaCaT keratinocyte cells, in both the

absence and presence of cimetidine.

6.3.7.2 Platinum accumulation in the presence of cimetidine

ICP-MS was performed on both dark and irradiated cell samples provided by Dr. Julie

Woods. Cell samples contained complex **40** (20 µg/ml) in both the absence and

presence of cimetidine (0.5 mM) and were prepared for ICP-MS as described in

Chapter II. In the dark, an equivalent accumulation of [195]Pt was observed for both samples (ca. 0.0010 ± 0.002 ppb/10^6 cells, **A** and **B**, Figure 6.31). However, irradiation of complex **40** at $\lambda_{max} = 420$ nm (5 J cm^{-2}) in the presence of cimetidine led to reduction of ca. 20% in platinum uptake in HaCaT cells (Figure 6.31**D**).
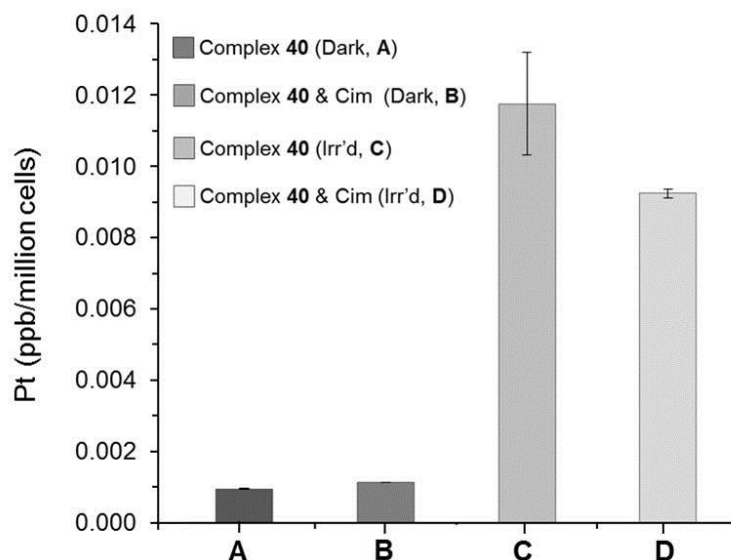
Figure 6.31 Platinum accumulation determined by ICP-MS for HaCaT cells co-incubated with complex **40** (50 µM) in both the absence and presence of cimetidine (0.5 mM) in both the dark (**A** and **B**) and after irradiation (**C** and **D**) with 420 nm light (5 J cm^{-2}). Error bars represent ± standard error of the mean for two independent experiments performed in duplicate.

These results indicated the ability of cimetidine to suppress the photo-cytotoxicity of complex **40**. Interestingly, previous photo-irradiation studies of **36** (Figure 6.8) in the presence of DMS, led to an alternative photo-decomposition pathway, as reported by Ronconi.[53] Consequently, it appears that sulfur-containing complexes have the ability to induce alternative photo-decomposition pathways of platinum(IV) diazido anticancer complexes.

6.4 Discussion

6.4.1 Bi-dentate cimetidine-platinum(II) complex

A decrease in the $N_3{\rightarrow}Pt^{IV}$ LMCT band at ca. 294 nm of photo-irradiated complex **40**, has been previously attributed to the loss of the coordinated azide ligands, in azidyl ($^{\bullet}N_3$) radical form. Photo-irradiation of complex **40** in the presence of cimetidine led to the successive and equivalent decrease in the $N_3{\rightarrow}Pt^{IV}$ LMCT band, as previously observed. Therefore, the initial photo-decomposition pathway of complex **40** appeared to be unaffected by the presence of cimetidine. The release of the azide ligands was confirmed by detection of the DMPO-N_3 spin adduct, by EPR spectroscopy.

Photo-irradiation of complex **40** in the presence of cimetidine (0.2 – 8 mol equiv) led to the formation of an isosbestic point at ca. 337 nm and an increase in absorbance at ca. 354 nm. The rise in absorbance at ca. 354 nm was determined to be directly dependent on the amount of photo-decomposed cimetidine. Deducing ca. 15 µM (50% of the photo-decomposed complex **40**) reacts with cimetidine (**H1**, Figure 6.14), an extinction coefficient of ca. 7334 M^{-1} cm^{-1} is obtained. This high ε value suggests this band at ca. 354 nm is due to a ligand-metal-charge transfer (LMCT) transition.

Previous studies of M^{II} transition metals (e.g. Cu^{II}, Pd^{II} and Pt^{II}) bound to sulfur ligands have reported on the occurrence of $S{\rightarrow}M^{2+}$, ligand-to-metal-charge-transfer transitions. These have been attributed to the presence of the lone pair on the sulfur atom residing at a lower energy than the $d_x{}^2$-$_y{}^2$ orbital[62] of the M^{II} (refer to **Chapter I**, p. 10 for d-orbital splitting in square planar complexes). Consequently, the absorbance observed at ca. 354 nm is in agreement with a $S{\rightarrow}Pt^{II}$, LMCT transition. The observation of this absorbance suggested the formation of a Pt^{II}-cimetidine related species. Consequently,

this rationalised the presence of the isosbestic point at ca. 337 nm. This is in agreement with previous characterisation of transition metal-cimetidine complexes where various absorption bands in the visible region of the absorption spectrum were attributed to LMCT transitions.[63]

^{1}H NMR spectroscopy revealed that photo-irradiation of *trans,trans,trans*-$[Pt(N_3)_2(OH)_2(py)_2]$ (**40**) in the presence of cimetidine led to the release of coordinated pyridine from complex **40**, which increased with prolonged irradiation. Moreover, additional ^{1}H NMR resonances in the aromatic region were attributed to a Pt^{II}-cimetidine related species. A change in the ^{1}H NMR resonance **j''** from a doublet to a multiplet may be due to a transition from a mono- to a bi-dentate coordination of cimetidine to platinum(II). Pt^{II} is a soft metal ion and exhibits a strong affinity for sulfur, a soft ligand. Therefore, an initial reaction between the platinum(II) photo-product, *trans*-$[Pt(py)_2(OH)_2]^{2+}$, as detected by MS is believed to undergo mono-dentate coordination of cimetidine, through substitution of a water ligand. This was confirmed by the detection of the mass adduct at 646.1647 (Figure 6.19) assigned to $[Pt(OH_2)(py)_2(cim)+Na]^{3+}$ (**67**).

Previous studies by Chen reported that the imidazole ring of L-histidine can displace the Pt-S(thioether) bond, at pH > 6.[64] However, additional reactions of *cis*-platin performed with L-methionine and/or UBQ, identified six-membered *S,N* ring species as products. In this work, cimetidine contains an imidazole ring. The observation of free pyridine from the photo-irradiation of complex **40** in the presence of cimetidine, suggests ring closure occurs opposed to transformation of Pt^{II}-S(thioether) to Pt^{II}-N(imidazole ring). The distinct change in the H10 ^{1}H NMR resonance from an "A$_2$" to

an "AB" type system was indicative of the formation of a stereogenic centre at the sulfur (S11) atom of cimetidine (refer to Figure 6.22). This supported the formation of a mono-cimetidine platinum(II) species. Additionally, the downfield shifts of C5 and C10 ^{13}C-DEPT135 NMR resonances were indicative of Pt^{II} coordination *via* both the sulfur and imidazole nitrogen atoms, in agreement with the MS data from the detection of [Pt(py)(OH$_2$)(cim)+Na]$^{3+}$ (**68**). Additionally, these NMR spectroscopic results were in agreement with a previous characterisation of a mono-cimetidine palladium complex, [Pd(cim)Cl$_2$]. These results were in contrast to the high ^{1}H NMR multiplicity and pronounced downfield ^{13}C chemical shifts for both C5 and C10 resonances, from a previously characterised Pt(cim)$_2$]Cl$_2$ species. This further supported the formation of a mono-cimetidine platinum(II) species. Finally, the formation of **68** is consistent with the detection of coordinated pyridine release.

6.4.2 Mechanism of action

The proposed formation of **68** is depicted in Figure 6.32. Firstly, reduction of the Pt^{IV} centre of complex **40** to Pt^{II} occurs *via* the loss of two azide ligands, in azidyl radical form. The OH groups become protonated, assigned to [Pt(OH$_2$)$_2$(py)$_2$]$^{2+}$ (**60**) by HR-MS as species **60**. Then, two possible pathways can occur. Firstly, one water ligand can be substituted for cimetidine and binds to Pt^{II} *via* coordination through the sulfur (S11) atom of cimetidine. This generates species **67**, [Pt(py)$_2$(OH$_2$)(cim)+Na]$^{3+}$, as detected by mass spectrometry. However, once formed this species is believed to undergo additional reaction, rationalising the detection of free pyridine. Within this pathway, there are two possible routes for pyridine release. As shown by pathway **A** (Figure 6.32), ring closure followed by pyridine release can occur due to the imidazolic ring present in cimetidine, forming a stable five-membered ring species [Pt(py)(OH$_2$)(*S*,*N*-

cim)]$^{2+}$. This process can be repeated, ultimately forming a [Pt(cim)$_2$]$^{2+}$ (**69**), minor species, as detected by MS.

Alternatively, the presence of the Pt^{II}-S(thioether) bond can lead to the release of the H$_2$O ligand due to the large *trans* effect of the sulfur thioether, which upon release induces coordination of second cimetidine molecule (**B**, Figure 6.32). Then, ring closure of both coordinated cimetidine molecules would occur, followed by loss of coordinated pyridine and the final step leading to the equivalent formation of the [Pt(cim)$_2$]$^{2+}$ (**69**).

The quenching of the $^{\bullet}$N$_3$ radicals and the reaction of the Pt^{II} intermediate with cimetidine, is believed to be a simultaneous reaction occurring on the same molecule of cimetidine. Consequently, the Pt^{II} atom in **67** has potential to coordinate to either the imidazolic nitrogen or the NH (**14**, inset Figure 6.32) both of which can lead to the formation of stable five-membered ring species. However, the bidentate coordination of Pt^{II} to the imidazolic nitrogen of cimetidine is believed to be favoured to the presence of unpaired electron at that nitrogen atom, formed from the one-electron transfer of cimetidine to the $^{\bullet}$N$_3$ radicals (Figure 6.33). Consequently, the formed cimetidine radical is not available to undergo a polymerisation reaction, forming a cimetidine polymer-type species. Therefore, this also accounts for the lack of observed precipitate in this work. In this work, the NMR spectroscopic data, ^{1}H NMR signals were in closer agreement to that of a [Pt(cim)$_2$Cl$_2$] (1:1) species, compared to a [Pt(cim)$_2$]Cl$_2$ (1:2) species. This suggested the major species after 60 min irradiation with 463 nm light is assignable to [Pt(py)(OH$_2$)(cim)]$^{2+}$ (**68**), formed *via* **67**.
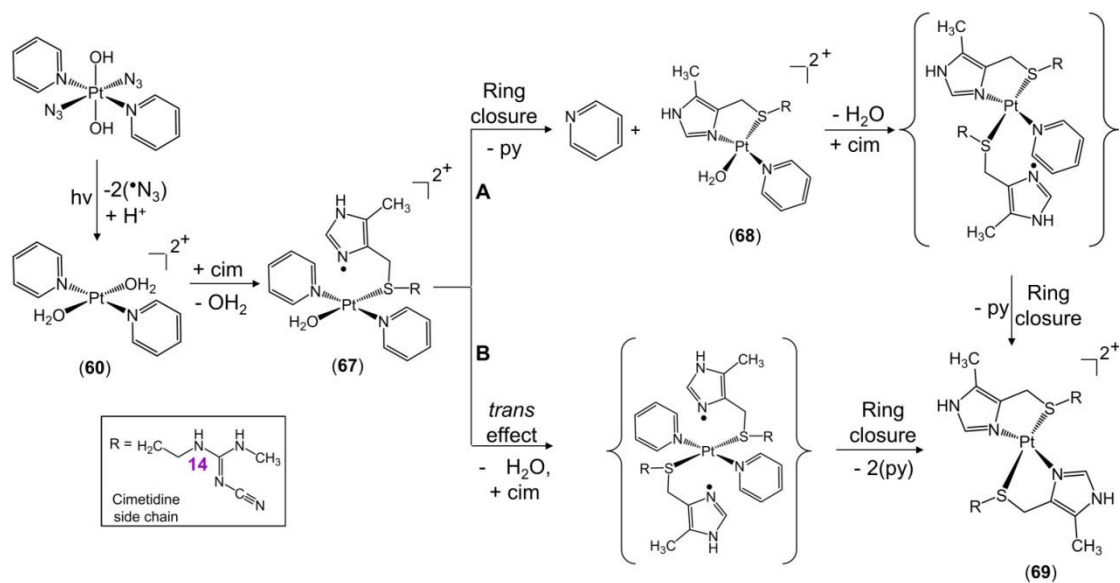
Figure 6.32 Proposed photo-decomposition pathway of irradiated complex **40** in the presence of cimetidine forming Pt^{II}-cimetidine species through (**A**) stepwise and (**B**) simultaneous loss of coordinated pyridine from complex **40**. Curly brackets refer to species not detected in this work, remaining species characterised by EPR, MS and ^{1}H NMR spectroscopic methods.

Therefore, the MS detected at *m/z* of ca. 722.2, assigned to $[Pt(cim)_2+Na]^{3+}$ appears to be the minor species, under these experimental conditions. This work was performed with therapeutically relevant irradiation doses, whereby irradiation >60 min at 463 nm is beyond the region of interest. Consequently, the formation of the $[Pt(cim)_2]^{2+}$ is not believed to induce the observed photo-protective effect.
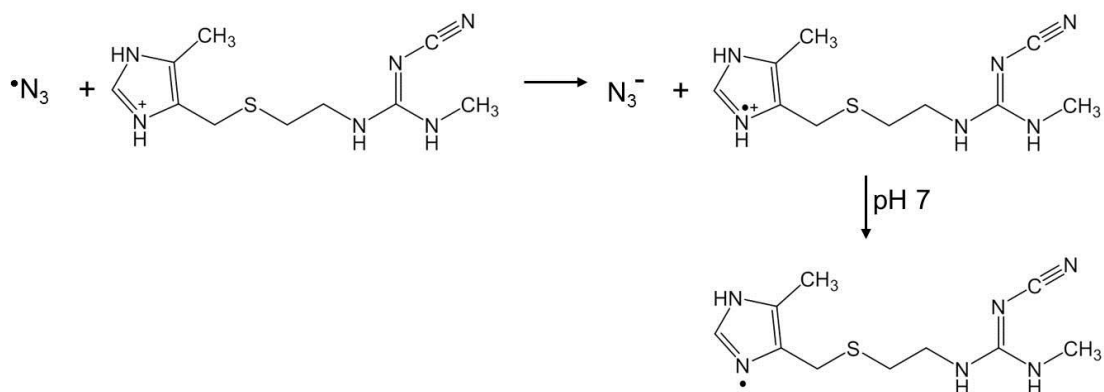
Figure 6.33 One-electron transfer of cimetidine to the $^{\bullet}N_3$ radicals forming free azide and a cimetidine radical cation, the latter which can deprotonate at pH 7 to the neutral cimetidine radical.

6.4.3 Azidyl radical quenching

Previous studies have reported the abstraction of an electron from the NH moiety of an indole ring present in L-Trp (**Chapter IV**). At pH 7.4, ca. 20% of cimetidine exists in protonated form (refer to Figure 6.3), this suggests $^{\bullet}N_3$ radicals may undergo one-electron transfer reaction at the imidazolic NH(1) or NH(4) atoms present in cimetidine. Additionally, $^{\bullet}N_3$ radicals have been reported to undergo one-electron transfer with thioether compounds, generating a thioether radical cation ($R_2S^{\bullet+}$) and free azide (N_3^-).[65] Cimetidine exhibited a partial quenching of the azidyl radicals. The imidazolic ring of cimetidine was attributed to the target moiety at which the one-electron transfer between the $^{\bullet}N_3$ radicals and cimetidine occurred. The redox couple ($Met^{\bullet+}/Met$) has a reduction potential of ca. 1.65 V.[66] However, the $^{\bullet}N_3$ radicals with a reduction potential of ca. 1.33 V $[E^{\circ}(^{\bullet}N_3/ N_3^-)]$,[67] suggests a one-electron transfer between the $^{\bullet}N_3$ radicals and methionine to be unfavourable. Consequently, this accounts for the equivalent formation of the DMPO-N_3 spin adduct in both the absence and presence of L-Met. In this work, the reduction in the DMPO-N_3 spin adduct was attributed to the quenching

of the $^\bullet N_3$ radicals by histamine. However, a reduction potential of ca. 1.40 V was reported for the redox couple (His$^{\bullet+}$/His).[68] However, as reported by Solar *et al.* reduction potentials are known to be dependent on experimental conditions.[56] Consequently, in this work, histamine must possess a lower reduction potential to that as previously reported, to account for the decrease in $^\bullet N_3$ radicals trapped by DMPO in the presence of histamine. Webber *et al.* reported on a the reduction potential of the cimetidine couple (Cim$^{\bullet+}$/Cim)[69] in the range of -0.8 − -1.0 V[70] which supports the quenching of the $^\bullet N_3$ radicals by cimetidine. However, unlike the quenching of the $^\bullet N_3$ radicals by L-Trp (**Chapter IV**) and melatonin (**Chapter V**), the quenching by cimetidine is less effective. Consequently, the reaction of the $^\bullet N_3$ radicals with indole related compounds appears to be more favourable, under the conditions used in this work.

6.4.4 Photo-protective effect

As mentioned in **Chapter IV**, N_3^- is a well-known cytotoxic species. However, its cytotoxicity is concentration dependent.[71] Partial suppression of the $^\bullet N_3$ radicals by cimetidine suggests the concentration of N_3^- formed would be below the level required to induce a cytotoxic effect. The quenching of the $^\bullet N_3$ radicals reduced their ability to induce a photo-cytotoxic effect. Moreover, the detection of N_3^- also suggests the formation of a cimetidine radical cation (undetected). Previous gamma-ray irradiation studies have reported the detection of a ring-based radical from a crystal of cimetidine by EPR spectroscopy.[72] The cytotoxic effect(s) of the cimetidine radical is currently unknown. Since the cimetidine radical possesses an unpaired electron it is envisaged that it would react rapidly either through radical dimerisation of two cimetidine radicals or with a biological target.

Inhalation or ingestion of pyridine can induce nausea, dizziness and severe abdominal pain. Pyridine has also been associated with minor genotoxic, neurotoxic and clastogenic effects.[73] However, pyridine is not classified as a cytotoxic species. Moreover, Gadberry *et al.* reported on the morphology of liver present in mice treated with pyridine which were determined to be equivalent to the control liver without any treatment with pyridine.[74] Therefore, pyridine is not expected to induce a cytotoxic effect.

The accumulation of platinum was also investigated to rationalise the observed photo-protective effect. A reduction of ca. 20% in platinum uptake in HaCaT cells supports a minor deactivation in the photo-cytotoxic activity of complex **40** in the presence of cimetidine. However, in this work, ca. 90% of HaCaT cells remained viable. This suggested the observed photo-protective effect was due to the formation of the Pt^{II}-cimetidine species, $[Pt(py)(OH_2)(cim]^{2+}$ (**68**). Previous literature has reported on the association of "non-leaving ligands" also referred as carrier ligands, with the level of antitumour activity.[75] The presence of carrier ligands has the ability to distort the DNA molecule and prevent enzyme recognition pathways, thereby, inducing cell death. Moreover, the loss of the ammine ligand from *cis*-platin has been associated with reduced anticancer activity and subsequent resistance mechanisms.[76,77] Additionally, substitution of ammine ligands by amine ligands in platinum(IV) diazido anticancer complexes enhanced their photo-cytotoxic activity.[78] Previous photo-irradiation studies of complex **40** in the presence of 5'-GMP have reported on formation of both mono-$[Pt(py)_2(N_3)(GMP)]^+$ and bis-$[Pt(py)_2(GMP)_2]^{2+}$ species.[1] The formation of these adducts correlates with the potent photo-cytotoxic activity of complex **40**.

Consequently, it appears that thioether molecules affect the photo-decomposition of platinum(IV) anticancer diazido complexes. An array of intracellular molecules possess thioether moieties, such that further investigations of photo-activatable platinum(IV) diazido anticancer complexes in the presence of these biomolecules are warranted, to provide a greater understanding of the *in cellulo* mechanism of action of platinum(IV) diazido anticancer complexes.

6.5 Conclusion

In vivo platinum accumulation has been reported to be mediated by a variety of transporters including copper transporter proteins (CTRs) and organic cation transporters (OCTs). Previous literature has correlated the expression of OCT2 (subgroup of the OCT family) in cells with both the uptake and cytotoxicity of platinum anticancer complexes. This was confirmed in the presence of OCT2 inhibitors such as TEA and cimetidine, which reduced the uptake of the platinum anticancer complexes.

Therefore, in this Chapter the effect on the photo-activation and photo-decomposition of *trans,trans,trans*-[Pt(N$_3$)$_2$(OH)$_2$(py)$_2$] (complex **40**) in the presence of the OCT2 inhibitor, cimetidine, was investigated. It was determined photo-irradiation of **40** in the presence of cimetidine induced an alternative photo-decomposition pathway.. Reduction of the Pt^{IV} to Pt^{II} of complex **40** occurred *via* two successive one-electron donations from the azide ligands. This was later confirmed by the detection of the DMPO-N$_3$ spin adduct by EPR spectroscopy.

Photo-irradiation of complex **40** in the presence of cimetidine led to an increase in the amount of photo-decomposed cimetidine, whilst the percentage photo-decomposition

of cimetidine remained consistent. From these data, it was deduced that the rise in absorbance at ca. 354 nm was dependent on the amount of photo-decomposed cimetidine. An extinction coefficient of ca. 7,300 M^{-1} cm^{-1} was deduced for this transition, consequently, it was attributed to a $S \rightarrow Pt^{II}$ ligand-to-metal-charge-transfer (LMCT) band. This suggested the formation of a Pt^{II}-cimetidine species.

^{1}H NMR studies revealed the release of coordinated pyridine from complex **40**. Additionally, new ^{1}H NMR resonances in both the aromatic and aliphatic region were consistent with Pt^{II} coordination *via* the sulfur atom of cimetidine forming a sterogenic centre. This was in agreement with the mass spectrometry data from the detection of a mass adduct assignable to $[Pt(py)_2(OH_2)(cim)+Na]^{3+}$ (**67**). Complex **67** was suggested to undergo *S,N* chelate ring formation leading to the release of pyridine, generating $[Pt(py)(OH_2)(cim)]^{2+}$ (**68**). This was confirmed by MS upon the detection of a mass adduct assignable to $[Pt(py)(OH_2)(cim)+Na]^{3+}$. The formation of the bidentate coordination of Pt^{II} to cimetidine, believed to be mediated by the cimetidine radical, formed from the one-electron transfer reaction between the cimetidine to the azidyl radicals. Moreover, ^{13}C-DEPT135 NMR observed downfield chemical shifts for both C5 and C10, supported the bi-dentate coordination of cimetidine to Pt^{II} *via* the thioether and imidazole nitrogen atoms. These results were in agreement with previous reports of a mono-cimetidine palladium(II), $[Pt(cim)Cl_2]$ complex.

The quenching of the $^\bullet N_3$ radicals by cimetidine was confirmed from the detection of N_3^-, by ^{14}N NMR spectroscopy. Photo-irradiation of complex **40** with L-methionine and histamine, identified a reduction in the DMPO-N_3 spin adduct, only in the presence of histamine. Consequently, the imidazole ring was the suggested site of one-electron

transfer of the $^\bullet$N$_3$ radicals. The –NH groups in the imidazole ring of cimetidine present a more favourable site of one-electron donation, due to their lower reduction potential relative to the $^\bullet$N$_3$ radicals, in contrast to the thioether moiety. The presence of a Pt-S(thioether) complex was believed to enhance the photo-cytotoxicity of complex **40** in the presence of cimetidine.

However, cell studies of co-incubated complex **40** with cimetidine irradiated at 420 nm light led to an observed photo-protective effect. At constant concentrations of photo-irradiated complex **40** (42.4 μM), ca. 90% of HaCaT cells remained viable across a range of cimetidine concentrations. This established the photo-protective effect induced by cimetidine was dose independent. Consequently, the amount of N$_3^-$ formed was believed to be below the level needed to induce a cyto-toxic effect. The formation of [Pt(py)(OH$_2$)(cim)]$^{2+}$ (**68**), through the loss of a carrier (pyridine) ligand, is attributed for the reduced photo-cytotoxic nature of complex **40**. An array of biological substrates possess thioether moieties, consequently this observed effect has potential to occur *in cellulo*.

This work was undertaken to assess the photo-irradiation of *trans,trans,trans*-[Pt(N$_3$)$_2$(OH)$_2$(py)$_2$] (complex **40**) in the presence of an OCT2 inhibitor molecule, cimetidine. To date, the expression of OCT2 in HaCaT keratinocytes cells remains unknown.[26] Photo-activation of complex **40** in the presence of cimetidine led to the formation of Pt^{II}-cimetidine species, due to the strong affinity for Pt^{II} for sulfur. The observed photo-protective effect was attributed to the formation of [Pt(py)(OH$_2$)(cim]$^{2+}$ (**68**). Therefore, from this reaction it was not feasible to deduce if complex **40** was mediated by OCT2. Further investigations of photo-irradiated complex **40** in the

presence of other OCT2 mediated molecules, such as TEA and MPP$^+$, compounds lacking a sulfur atom, have potential to deduce the involvement of OCT2 in platinum(IV) diazido anticancer complexes accumulation/photo-cytotoxicity.

6.6 References

(1)   Farrer, N. J.; Woods, J. A.; Salassa, L.; Zhao, Y.; Robinson, K. S.; Clarkson, G.; Mackay, F. S.; Sadler, P. J. *Angew. Chem. Int. Ed.* **2010**, *49*, 8905.

(2)   Mackay, F. S.; Woods, J. A.; Heringová, P.; Kašpárková, J.; Pizarro, A. M.; Moggach, S. A.; Parsons, S.; Brabec, V.; Sadler, P. J. *Proc. Natl. Acad. Sci. USA.* **2007**, *104*, 20743.

(3)   Zwielly, A.; Mordechai, S.; Brkic, G.; Bogomolny, E.; Pelly, I. Z.; Moreh, R.; Gopas, J. *Eur Biophys J* **2011**, *40*, 795.

(4)   Brabec, V.; Kasparkova, J. *Drug Resis. Update* **2005**, *8*, 131.

(5)   Gately, P. D.; Howell, B. S. *Br. J. Cancer* **1993**, *67*, 1171.

(6)   Blair, B. G.; Larson, C. A.; Adams, P. L.; Abada, P. B.; Safaei, R.; Howell, S. B. *Mol. Pharmacol.* **2010**, *77*, 912.

(7)   Kuo, M.; Chen, H. W.; Song, I.-S.; Savaraj, N.; Ishikawa, T. *Cancer Metast. Rev.* **2007**, *26*, 71.

(8)   Koepsell, H.; Endou, H. *Eur. J. Physiol.* **2004**, *447*, 666.

(9)   Helleman, J.; Burger, K.; Hamelers, I. H. L.; Boersma, A. W. M.; de Kroon, A. I. P. M.; Stoter, G.; Nooter, K. *Cancer Biol. Ther.* **2006**, *5*, 943.

(10)   Koepsell, H. *Trends Pharmacol. Sci.* **2004**, *25*, 375.

(11)   Koepsell, H. *Mol. Aspects Med.* **2013**, *34*, 413.

(12)   Yokoo, S.; Yonezawa, A.; Masuda, S.; Fukatsu, A.; Katsura, T.; Inui, K. I. *Biochem. Pharmacol.* **2007**, *74*, 477.

(13)   Lovejoy, K. S.; Todd, R. C.; Zhang, S.; McCormick, M. S.; D'Aquino, J. A.; Reardon, J. T.; Sancar, A.; Giacomini, K. M.; Lippard, S. J. *Proc. Natl. Acad. Sci. USA.* **2008**, *105*, 8902.

(14)   Zhang, S.; Lovejoy, K. S.; Shima, J. E.; Lagpacan, L. L.; Shu, Y.; Lapuk, A.; Chen, Y.; Komori, T.; Gray, J. W.; Chen, X.; Lippard, S. J.; Giacomini, K. M. *Cancer Res.* **2006**, *66*, 8847.

(15)   Burger, H.; Zoumaro-Djayoon, A.; Boersma, A. W. M.; Helleman, J.; Berns, E.; Mathijssen, R. H. J.; Loos, W. J.; Wiemer, E. A. C. *Br. J. Pharmacol.* **2010**, *159*, 898.

(16)   Filipski, K. K.; Loos, W. J.; Verweij, J.; Sparreboom, A. *Clin. Cancer. Res.* **2008**, *14*, 3875.

(17)   More, S. S.; Li, S.; Yee, S. W.; Chen, L.; Xu, Z.; Jablons, D. M.; Giacomini, K. M. *Mol. Cancer Ther.* **2010**, *9*, 1058.

(18)   Yonezawa, A.; Masuda, S.; Yokoo, S.; Katsura, T.; Inui, K.-i. *J. Pharmacol. Exp. Ther.* **2006**, *319*, 879.

(19)   Kubecova, M.; Kolostova, K.; Pinterova, D.; Kacprzak, G.; Bobek, V. *Eur. J. Pharma. Sci* **2011**, *42*, 439.

(20)   Barendt, W. M.; Wright, S. H. *J. Biol. Chem.* **2002**, *277*, 22491.

(21)   Sleijfer, T. D.; Offerman, J. J. G.; Mulder, N. H.; Verweij, M.; van der Hem, G. K.; Koops, H. S.; Meijer, S. *Cancer* **1987**, *60*, 2823.

(22)   Katsuda, H.; Yamashita, M.; Katsura, H.; Yu, J.; Waki, Y.; Nagata, N.; Sai, Y.; Miyamoto, K.-i. *Biol. Pharm. Bull.* **2010**, *33*, 1867.

(23)   Dorr, R. T.; Soble, M. J. *J. Cancer Res. Clin. Oncol.* **1988**, *114*, 1.

(24)   Ciarimboli, G.; Deuster, D.; Knief, A.; Sperling, M.; Holtkamp, M.; Edemir, B.; Pavenstädt, H.; Lanvers-Kaminsky, C.; Zehnhoff-Dinnesen, A. A.; Schinkel, A. H.; Koepsell, H.; Jürgens, H.; Schlatter, E. *Am. J. Pathol.* **2010**, *176*, 1169.

(25)   Ciarimboli, G.; Ludwig, T.; Lang, D.; Pavenstädt, H.; Koepsell, H.; Piechota, H. J.; Haier, J.; Jaehde, U.; Zisowsky, J.; Schlatter, E. *Am. J. Pathol.* **2005**, *167*, 1477.

(26)   Burger, H.; Loos, W. J.; Eechoute, K.; Verweij, J.; Mathijssen, R. H. J.; Wiemer, E. A. C. *Drug Resis. Update* **2011**, *14*, 22.

(27)   Ludwig, T.; Riethmuller, C.; Gekle, M.; Schwerdt, G.; Oberleithner, H. *Kidney Int.* **2004**, *66*, 196.

(28)   Zolk, O.; Solbach, T.; König, J.; Fromm, M. *Naunyn-Schmied. Arch. Pharmacol.* **2009**, *379*, 337.

(29)   Bonora, S.; Foggia, M. D.; Tugnoli, V.; Righi, V.; Benassi, E.; Maris, A. *J. Raman Spectrosc.* **2011**, *42*, 612.

(30)   Greenaway, F. T.; Brown, L. M.; Dabrowiak, J. C.; Thompson, M. R.; Day, V. W. *J. Am. Chem. Soc.* **1980**, *102*, 7782.

(31)   Kimura, E.; Koike, T.; Shimizu, Y.; Kodama, M. *Inorg. Chem.* **1986**, *25*, 2242.

(32)   Kanumfre, F.; Lima, E. M. d.; Scheidt, G.; Carneiro, P. I. B.; Rosso, N. D. *J. Braz. Chem. Soc.* **2010**, *21*, 800.

(33)   Sorenson, J. R. J. In *Copper and Zinc in Inflammation*; Milanino, R., Rainsford, K. D., Velo, G. P., Eds.; Springer Netherlands: 1989; Vol. 4, p 69.

(34)   Freijanes, E.; Berthon, G. *Inorg. Chim. Acta.* **1986**, *124*, 141.

(35)   Zbaida, S.; Kariv, R.; Fischer, P.; Silman-Greenspan, J.; Tashma, Z. *Eur. J. Biochem.* **1986**, *154*, 603.

(36)   Soto, L.; Legros, J. P.; Sancho, A. *Polyhedron* **1988**, *7*, 307.

(37)   Sancho, A.; Soto, L.; Borrás, J. *Transition Met. Chem.* **1985**, *10*, 214.

(38)   Olea-Román, D.; Villeda-García, J. C.; Colorado-Peralta, R.; Solano-Peralta, A.; Sanchez, M.; Hernández-Ahuactzi, I. F.; Castillo-Blum, S. E. *J. Mex. Chem. Soc.* **2013**, *57*, 230.

(39)   Wang, X.; Guo, Z. *Anti-cancer Agents Med. Chem.* **2007**, *7*, 19.

(40)   Bogojeski, J.; Petrović, B.; Bugarčić, Z. D. In *Chronic Lymphocytic Leukemia*; Oppezzo, P., Ed. 2012, p 339.

(41)   Murdoch, S. d. P.; Ranford, J. D.; Sadler, P. J.; Berners-Price, S. J. *Inorg. Chem.* **1993**, *32*, 2249.

(42)   Gibson, D.; Costello, C. *Eur. J. Mass Spectrom.* **1999**, *5*, 501.

(43)   Hoeller, D.; Hecker, C. M.; Dikic, I. *Nat. Rev. Cancer* **2006**, *6*, 776.

(44)   Hartinger, C. G.; Tsybin, Y. O.; Fuchser, J.; Dyson, P. J. *Inorg. Chem.* **2007**, *47*, 17.

(45)   Peleg-Shulman, T.; Najajreh, Y.; Gibson, D. *J. Inorg. Biochem.* **2002**, *91*, 306.

(46)   Williams, J. P.; Phillips, H. I. A.; Campuzano, I.; Sadler, P. J. *J. Am. Soc. Mass. Spectrom.* **2010**, *21*, 1097.

(47)   Nurchi, V.; Cristiani, F.; Crisponi, G.; Ganadu, M. L.; Lubinu, G.; Panzanelli, A.; Naldini, L. *Polyhedron* **1992**, *11*, 2723.

(48)   Crisponi, G.; Cristiani, F.; Nurchi, V. M.; Silvagni, R.; Ganadu, M. L.; Lubinu, G.; Naldini, L.; Panzanelli, A. *Polyhedron* **1995**, *14*, 1517.

(49)   Onoa, G. B.; Moreno, V.; Freisinger, E.; Lippert, B. *J. Inorg. Biochem.* **2002**, *89*, 237.

(50)   Hall, M. D.; Okabe, M.; Shen, D.-W.; Liang, X.-J.; Gottesman, M. M. *Annu. Rev. Pharmacol. Toxicol.* **2008**, *48*, 495.

(51)   Abu-Surrah, A. S.; Al-Sa'doni, H. H.; Abdalla, M. Y. *Cancer Ther.* **2008**, *6*, 1.

(52)   Müller, P.; Schröder, B.; Parkinson, J. A.; Kratochwil, N. A.; Coxall, R. A.; Parkin, A.; Parsons, S.; Sadler, P. J. *Angew. Chem. Int. Ed.* **2003**, *42*, 335.

(53)   Ronconi, L.; Sadler, P. J. *Chem. Commun.* **2008**, 235.

(54)   Gottlieb, H. E.; Kotlyar, V.; Nudelman, A. *J. Org. Chem.* **1997**, *62*, 7512.

(55)   Krężel, A.; Bal, W. *J. Inorg. Biochem.* **2004**, *98*, 161.

(56)   Solar, S.; Getoff, N.; Surdhar, P. S.; Armstrong, D. A.; A., S. *J. Phys. Chem.* **1991**, *95*, 3639.

(57)   Vitaliy, K.; Gregory, K. K.; Voislav, B.; Diethard, K. B. *J. Breath. Res.* **2013**, *7*, 026005.

(58)   Tomlinson, E.; Haffkenscheid, T. L. In *Partition Coefficient, Determination and Estimation*; Dunn, W., Block, J., Pearlman, J. H., Eds.; Pergamon Pres: New York, 1986.

(59)   Norman, R. E.; Ranford, J. D.; Sadler, P. J. *Inorg. Chem.* **1992**, *31*, 877.

(60)   Tatton, A. S.; Pham, T. N.; Vogt, F. G.; Iuga, D.; Edwards, A. J.; Brown, S. P. *Cryst. Eng. Comm.* **2012**, *14*, 2654.

(61)   Phillips, H. I. A.; Ronconi, L.; Sadler, P. J. *Chem. Eur. J.* **2009**, *15*, 1588.

(62)   Levers, A. B. P. In *Inorganic Electronic Spectroscopy, Studies in Physical and Theoretical Chemistry*; Lappert, M. F., Ed.; Elsevier: New York, 1968.

(63)   Kahn, E.; Rheingold, A.; Shupack, S. *J. Crystallogr. Spectrosc. Res.* **1993**, *23*, 697.

(64)   Chen, Y.; Guo, Z.; del Socorro Murdoch, P.; Zang, E.; J. Sadler, P. *J. Chem. Soc., Dalton Trans.* **1998**, 1503.

(65)   Lanzalunga, O.; Lapi, A. *J. Sulfur Chem.* **2011**, *33*, 101.

(66)   Bergès, J.; de Oliveira, P.; Fourré, I.; Houée-Levin, C. *J. Phys. Chem. B* **2012**, *116*, 9352.

(67)   Harriman, A. *J. Phys. Chem.* **1987**, *91*, 6102

(68)   Sarada, B. V.; Rao, T. N.; Tryk, D. A.; Fujishima, A. *Anal. Chem.* **2000**, *72*, 1632.

(69)   Webber, A.; Shah, M.; Osteryoung, J. *Anal. Chim. Acta* **1983**, *154*, 105.

(70)   Scott, R. A.; Lukehart, C. M. *Applications of Physical Methods to Inorganic and Bioinorganic Chemistry*; Wiley and sons: Sussex, UK., 2007.

(71)   Suzuki, O.; Watanabe, K. *Drugs and Poisons in Humans: A Handbook of practical analysis*; 1st ed.; Springer: Berlin, Heidelberg., 2005; p 633.

(72)   Sayin, U. *J. Mol. Struct.* **2013**, *1031*, 132.

(73)   *IARC Monographs on the Evaluation of Carcinogenic Risks to Humans*; IARC Press: Lyon, 2000; Vol. 77, pp 504-528.

(74)   Gadberry, M. G.; DeNicola, D. B.; Carlson, G. P. *J. Toxicol. Environ. Health* **1996**, *48*, 273.

(75)   Coluccia, M.; Natile, G. *Anti-cancer Agents Med. Chem.* **2007**, *7*, 111.

(76)   Lau, J. K.-C.; Deubel, D. V. *Chem. Eur. J.* **2005**, *11*, 2849.

(77)   Li, H.; Zhao, Y.; Phillips, H. I. A.; Qi, Y.; Lin, T.-Y.; Sadler, P. J.; O'Connor, P. B. *Anal. Chem.* **2011**, *83*, 5369.

(78)   Bednarski, P. J.; Korpis, K.; Westendorf, A. F.; Perfahl, S.; Grünert, R. *Phil. Trans. Soc. A.* **2013**, *371*.

Chapter VII

Conclusions and Future Work

This thesis is concerned with investigating the photo-decomposition pathways of photo-activatable platinum(IV) diazido anticancer complexes. Previous studies suggested photo-activation of such complexes have potential to lead to the generation of various reactive oxygen and nitrogen species (ROS/RNS).[1-3] Prior to this thesis direct detection of radical species produced from the photo-activation of platinum(IV) diazido complexes has not been performed.

7.1 Conclusions

Chapter III focused on the photo-irradiation of various platinum(IV) diazido complexes using spin trapping EPR spectroscopy. Photo-irradiation of complexes **40** and **44** with blue light (λ = 450 nm and 463 nm), in addition to the photo-irradiation of complexes **56-58** with both blue (463 nm) and green (517 nm) light sources led to a quartet of triplets[4] EPR spectrum assigned to the DMPO-$^{14}N_3$ spin adduct. Confirmation that the azidyl radicals arose from the platinum(IV) diazido complex was established from the photo-irradiation of ^{15}N-complex **40** (50% ^{15}N at N_α). This led to a quartet of doublets[5] EPR spectrum assigned to the DMPO-$^{15}N_3$ spin adduct. The trapping of the $^\bullet N_3$ radicals was also observed for spin traps, 4-POBN generating a triplet of quartets[6] EPR spectrum and phosphorus spin trap DEPMPO leading to the formation of an octet of triplets[7] EPR spectrum, assigned to the DEPMPO-N_3 spin adduct. Quantification of the spin adducts, determined the DEPMPO-N_3 spin adduct trapped a greater quantity of the $^\bullet N_3$ radicals compared to both 4-POBN-N_3 and DMPO-N_3 spin adducts. This was attributed to DEPMPO possessing a faster rate constant for the trapping of the $^\bullet N_3$ radicals.

Solvent and wavelength of irradiation were both varied to explore the optimum condition of azidyl radical release from the photo-irradiation of **40**. A higher yield of the DMPO-N$_3$ spin adduct was formed in PBS/D$_2$O, which was attributed to the Brownian motion[8] of the $^\bullet$N$_3$ radicals. In contrast, EPR spin trapping in RPMI-1640 led to a reduction in the amount of DMPO-N$_3$ spin adduct formation. This lower yield in spin adduct formation was assigned to the numerous constituents present in the cell culture medium which possess the potential to behave as $^\bullet$N$_3$ radical quenchers. Irradiation of complex **40** at 517 nm light led to the observation of the DMPO-^{14}N$_3$ spin adduct only in the cell culture medium. This was attributed to the minor absorption transitions present in complex **40**, as determined from previous DFT calculations.[1]

Chapter IV focused on the reactivity of the formed azidyl radicals generated from irradiated complex **40** in the presence of various amino acids. EPR spectroscopy established the unreactive nature of the $^\bullet$N$_3$ radicals towards the amino acids glycine and L-tyrosine, under the conditions used in this work. However, in the presence of L-tryptophan, the DMPO-N$_3$ spin adduct was supressed. This was attributed to the quenching of the $^\bullet$N$_3$ radicals by L-Trp. The detection of free azide *via* ^{14}N NMR spectroscopy, determined this quenching mechanism proceeded through a one-electron transfer pathway. Furthermore, photo-irradiation of complex **40** co-incubated with L-Trp in A2780 ovarian cancer cells led to an observed photo-protective effect. This photo-protective effect was attributed to the quenching of the $^\bullet$N$_3$ radicals by L-Trp. Consequently, it was deduced the photo-cytotoxicity of **40** is comprised of both an acute (radical) and chronic (DNA platination)-based mechanisms.

Chapter V investigated the photo-decomposition pathway of **40** in the presence of melatonin. Melatonin, an analogue of L-Trp has been reported to enhance the cytotoxic activity of chemotherapeutic drugs.[9-11] Both the anti-oxidant and metal-chelation ability of melatonin have been previously reported.[12-15] EPR spectroscopy established the superimposition of two radical spin adducts assigned to both the DMPO-N_3 (**R1**) and DMPO-OH (**R2**) spin adducts, although the DMPO-N_3 spin adduct was present at a reduced intensity. Irradiation conditions were varied to confirm $^\bullet$OH radical formation *via* the addition of ethanol forming the DMPO-EtOH (**R5**) spin adduct and the substitution of the spin trap DMPO for the phosphorus analogue, DEPMPO generating the DEPMPO-OH (**R4**) spin adduct.[7] The detection of hydroxyl ($^\bullet$OH) radicals suggested the possible enhancement in the photo-cytotoxicity complex **40** in the presence of melatonin. However, detection by HR-MS of a mass adduct 17 a.m.u higher than that of the sodium adduct of melatonin, suggested the addition of the hydroxyl radical to melatonin. However, due to the low S/N of the formed photo-products, complete structural assignment was not feasible. Photo-irradiation of complex **40** co-incubated with melatonin in A2780 ovarian cancer cells induced a photo-protective effect. This photo-protective effect was attributed to the one-electron transfer reaction between the $^\bullet$$N_3$ radicals and melatonin and the addition reaction of the $^\bullet$OH radicals to melatonin. Consequently, both the RNS/ROS were not available to induce their cytotoxic effect. Furthermore, the detection of $[Pt(py)_2(OH_2)(MLT)]^{2+}$ (**62**), was suggested to reduce the amount of Pt^{II} available to bind to the N^7 of guanine nucleobase of DNA and thereby inhibit cell death.

Numerous studies have identified various transporters which mediate the accumulation of platinum anticancer complexes[16-19] In particular, the expression of the organic cation transporter OCT2 has been correlated with high platinum toxicity.[20] Therefore, **Chapter VI** focused on the photo-irradiation of complex **40** in the presence of cimetidine, an OCT2 inhibitor.[21] UV-visible spectroscopy led to the observation of an isosbestic point, becoming more pronounced with increasing concentrations of cimetidine. ^{1}H NMR spectroscopy identified the formation of free pyridine, new platinum-photo products and evidence of coordinated cimetidine peaks. HR-MS identified a mass adduct at a *m/z* of 646.1647, assigned to $[Pt(OH_2)(py)_2(cim)+Na]^{3+}$. The loss of coordinated pyridine was attributed to either ring closure or due to the *trans effect*, mediated by cimetidine radical, formed from the one-electron transfer of cimetidine to the azidyl radicals. Finally, photo-irradiation of **40** co-incubated with cimetidine in HaCaT keratinocytes cells demonstrated a potent photo-protective effect at low concentrations (μM) of cimetidine. The extent of the photo-protective effect was attributed to both azidyl radical quenching and formation of the platinum(II)-cimetidine complex.

Overall, this thesis identified the release of azidyl radicals from photo-activated platinum(IV) diazido anticancer complexes. Varying the experimental conditions led to alternative photo-decomposition pathways which induced a direct effect on the photo-cytotoxicity of complex **40**. Therefore, the studies presented in this thesis offer the potential to contribute to the overall understanding on the reactivity of photo-irradiated platinum(IV) diazido complexes and their generated photo-products.

7.2 Future Work

This work was concerned with the primary identification and characterisation of azidyl radicals from the photo-irradiation of platinum(IV) diazido anticancer complexes *in vitro*. Performing *in cellulo* spin trapping EPR has the ability to elucidate a more comprehensive understanding of azidyl radical reactivity under biologically relevant conditions. *In cellulo* spin trapping EPR has been reported for both the superoxide ($O_2^{-\bullet}$) and hydroxyl ($^\bullet OH$) radicals.[22,23] Additionally, due to their non-toxic nature both DMPO and DEPMPO spin traps are commonly used for *in cellulo* and *in vivo* spin trapping EPR.[24,25] The cell contains a variety of constituents, such that monitoring the photo-decomposition of platinum(IV) diazido anti-tumour complexes has potential to further contribute to the understanding of their induced photo-cytotoxicity.

Interestingly, previous reports have documented Gly as a cyto-protective agent[26] against a number of injurious agents.[27-29] Zhong *et al.* reported on the protective ability of Gly in both liver and renal tissues caused by hepatic/renal toxins and/or drugs. Platinum chemotherapeutic agents are commonly excreted through the kidneys, inducing renal damage as reported from treatment with *cis*-platin. Consequently, assuming complex **40** is excreted through the kidneys similar to *cis*-platin, the unreactive nature of the $^\bullet N_3$ radicals towards Gly postulates the induction of a photo-cytotoxic effect whilst protecting against renal toxicity from the photo-irradiation of complex **40** in the presence of Gly. Although prior studies to assess the accumulation of complex **40** in the kidneys would have to be performed.

Secondly, L-tryptophan, melatonin and cimetidine radicals were suggested to form during this work. The tryptophanyl radical could be detected *via* spin trapping EPR spectroscopy using spin trap, 3,5-dibromo-4-nitrobenzene-sulfonic acid (DBNBS),[30,31] however the availability of this spin trap is difficult to source. Therefore, a more reliable method for trapping of amino acid radicals and derivatives is rapid freeze quench (RFQ) EPR spectroscopy. RFQ-EPR freezes the sample and slows down the molecular tumbling rates of the radical under investigation. The L-Trp radical present in proteins/peptides has been previously detected by RFQ-EPR at both X-and W-band.[32] The melatonin radical has been identified by other spectroscopic techniques[14,33,34] but not directly *via* EPR spectroscopy. Gamma ray radiation of a crystal of cimetidine identified a ring-based radical by X-band EPR spectroscopy.[35] These radical species have potential to be involved in the observed photo-protective effect, such that detection of these radical species is paramount for the complete understanding of induced photo-protective effect.

Thirdly, investigating the expression levels of the autophagic proteins LC3-I and LC3-II *via* various cell assays as described by Tanida *et al.*,[36] has potential to determine if the suggested L-Trp radical interacts with the LC3-I autophagic protein, providing a deeper understanding of the induced photo-protective effect in the presence of L-Trp.

Fourthly, the detection of a platinum(II)-cimetidine complex highlights the necessity to investigate the photo-irradiation of platinum(IV) diazido complexes in the presence of various sulfur-containing compounds. Earlier studies by

Ronconi also reported on the ability of DMS (another sulfur-containing complex) to alter the photo-decomposition of complex **36**.[37] The displacement of the pyridine ligand from complex **40** was attributed to the observed photo-protective effect. However, this may be avoided in the presence of platinum(IV) diazido complexes possessing alternative equatorial ligands than that of pyridine. Consequently, this preliminary study suggests additional photo-cytotoxicity studies of platinum(IV) diazido complexes in the presence of sulfur-containing species is a prerequisite for more in-depth knowledge about their *in vivo* mechanism of action.

Fifthly, photo-irradiation of **40** in the presence of melatonin led to the detection of the hydroxyl ($^\bullet$OH) radical. An additional method of $^\bullet$OH radical detection could be observed from the synthesis of ^{17}O-labelled[38] complex **40**. Therefore, the trapping of the $^{17\bullet}$OH would be expected to exhibit an alternative EPR spectrum upon trapping with spin trap, DMPO. This could also provide information on the release of the hydroxyl ligands from the platinum(IV) diazido complexes. This could also be expanded to NMR spectroscopy.

Numerous photo-products were detected in this thesis. Complete characterisation of these photo-products by NMR spectroscopy alone, was not feasible. Therefore, performing detailed High Performance Liquid Chromatography (HPLC)[39] analysis on all irradiated solutions has the ability to elucidate all formed photo-products and their time of evolution. Consequently, the photo-cytotoxicity/photo-protective effect could then be directly correlated to the formed photo-products.

Finally, various insoluble precipitates were observed in this work, consequently, solution phase experiments were not possible. Although their formation is believed to be triggered at millimolar (mM) concentrations and not believed to contribute to the photo-cytotoxicity of complex **40**, identification of these precipitates is still of interest for future NMR spectroscopic studies. Primarily solid state NMR spectroscopy has the potential to identify the species present in the formed precipitates. Although ^{1}H SSNMR is not proposed due to the broad spectra obtained owning to the strong homonuclear dipole couplings, as reported by Lucier,[40] analysis of ^{195}Pt and ^{14}N nuclei appear to be more suitable by SSNMR spectroscopy.[41] The development of a new pulsing sequence referred to as wideband uniform rate smooth truncation-Carr-Purcell Meiboom-Gill (WURST-CPMG)[42] offers the ability of rapid acquisition for ^{195}Pt SSNMR. Both ^{195}Pt and ^{15}N SSNMR spectroscopy have been previously reported for various platinum(IV) and platinum(II)-anticancer complexes.[43] Alternatively, X-ray fluorescence (XRF),[44] synchrotron-radiation induced X-ray emission (SRIXE),[45,46] and X-ray absorption near-edge structure (XANES)[47] have been performed on platinum anti-cancer complexes. These X-ray based techniques can provide insight into the various oxidation states of the species providing additional information of the formed species.

7.3 References

(1)   Farrer, N. J.; Woods, J. A.; Salassa, L.; Zhao, Y.; Robinson, K. S.; Clarkson, G.; Mackay, F. S.; Sadler, P. J. *Angew. Chem. Int. Ed.* **2010**, *49*, 8905.

(2)   Mackay, F. S.; Woods, J. A.; Heringová, P.; Kašpárková, J.; Pizarro, A. M.; Moggach, S. A.; Parsons, S.; Brabec, V.; Sadler, P. J. *Proc. Natl. Acad. Sci. USA.* **2007**, *104*, 20743.

(3)   Mackay, F. S.; Woods, J. A.; Moseley, H.; Ferguson, J.; Dawson, A.; Parsons, S.; Sadler, P. J. *Chem. Eur. J.* **2006**, *12*, 3155.

(4)   Buettner, G. R. *Free Radic. Biol. Med.* **1987**, *3*, 259

(5)   Kalyanaraman, B.; Janzen, E. G.; Mason, R. P. *J. Biol. Chem.* **1985**, *260*, 4003.

(6)   Walter, T. H.; Bancroft, E. E.; McIntire, G. L.; Davis, E. R.; Gierasch, L. M.; Blount, H. N. *Can. J. Chem.* **1982**, *60*, 1621.

(7)   Paciolla, M. D.; Kolla, S.; Jansen, S. A. *Adv. Environ. Res.* **2002**, *7*, 169.

(8)   Saffman, P. G.; Delbrück, M. *Proc. Natl. Acad. Sci. USA.* **1975**, *72*, 3111.

(9)   Kim, J.-H.; Jeong, S.-J.; Kim, B.; Yun, S.-M.; Choi, D. Y.; Kim, S.-H. *J. Pineal. Res.* **2012**, *52*, 244.

(10)   Casado-Zapico, S.; Rodriguez-Blanco, J.; García-Santos, G.; Martín, V.; Sánchez-Sánchez, A. M.; Antolín, I.; Rodriguez, C. *J. Pineal. Res.* **2010**, *48*, 72.

(11)   Padillo, F. J.; Ruiz-Rabelo, J. F.; Cruz, A.; Perea, M. D.; Tasset, I.; Montilla, P.; Túnez, I.; Muntané, J. *J. Pineal. Res.* **2010**, *49*, 264.

(12)   Gulcin, İ.; Buyukokuroglu, M. E.; Kufrevioglu, O. I. *J. Pineal. Res.* **2003**, *34*, 278.

(13)   Limson, J.; Nyokong, T.; Oaya, S. *J. Pineal. Res.* **1998**, *24*, 15.

(14)   Mahal, H. S.; Sharma, H. S.; Mukherjee, T. *Free Radic. Biol. Med.* **1999**, *26*, 557.

(15)   Maharaj, D. S.; Glass, B. D.; Daya, S. *Biosci. Rep.* **2007**, *27*, 299.

(16)   Blair, B. G.; Larson, C. A.; Adams, P. L.; Abada, P. B.; Safaei, R.; Howell, S. B. *Mol. Pharmacol.* **2010**, *77*, 912.

(17)   Kuo, M.; Chen, H. W.; Song, I.-S.; Savaraj, N.; Ishikawa, T. *Cancer Metast. Rev.* **2007**, *26*, 71.

(18)   Koepsell, H.; Endou, H. *Eur. J. Physiol.* **2004**, *447*, 666.

(19)   Helleman, J.; Burger, K.; Hamelers, I. H. L.; Boersma, A. W. M.; de Kroon, A. I. P. M.; Stoter, G.; Nooter, K. *Cancer Biol. Ther.* **2006**, *5*, 943.

(20)   Yokoo, S.; Yonezawa, A.; Masuda, S.; Fukatsu, A.; Katsura, T.; Inui, K. I. *Biochem. Pharmacol.* **2007**, *74*, 477.

(21)   Ciarimboli, G.; Deuster, D.; Knief, A.; Sperling, M.; Holtkamp, M.; Edemir, B.; Pavenstädt, H.; Lanvers-Kaminsky, C.; Zehnhoff-Dinnesen, A. A.; Schinkel, A. H.; Koepsell, H.; Jürgens, H.; Schlatter, E. *Am. J. Pathol.* **2010**, *176*, 1169.

(22)   Davies, M. J. In *Electron Paramagnetic Resoance: A Practitioner's Toolkit*; Brustolon, M., Giamello, E., Eds.; John Wiley & Sons: New Jersey, 2009, p 427.

(23)   Khan, N.; Wilmot, C. M.; Rosen, G. M.; Demidenko, E.; Sun, J.; Joseph, J.; O'Hara, J.; Kalyanaraman, B.; Swartz, H. M. *Free Radic. Biol. Med.* **2003**, *34*, 1473.

(24)   Liu, K. J.; Miyake, M.; Panz, T.; Swartz, H. *Free Radic. Biol. Med.* **1999**, *26*, 714.

(25)   Berliner, L. J.; Khramtsov, V.; Fujii, H.; Clanton, T. L. *Free Radic. Biol. Med.* **2001**, *30*, 489.

(26)   Howard, A.; Tahir, I.; Javed, S.; Waring, S. M.; Ford, D.; Hirst, B. H. *J. Physiol.* **2010**, *588*, 995.

(27)   Frink, R. J. In *Inflammatory Atherosclerosis: Characteristics of the Injurious Agent.*; Heart Research Foundation: Sacramento, California, 2002.

(28)   Silva, P.; Rosen, S.; Spokes, K.; Epstein, F. H. *Kidney Int.* **1991**, *39*, 653.

(29)   Wang, Y.; Yan, Y.; Zou, X. *Chin. Med. J.* **2010**, *123*, 1931.

(30)   Gunther, M. R.; Kelman, D. J.; Corbett, J. T.; Mason, R. P. *J. Biol. Chem.* **1995**, *270*, 16075.

(31)   Gunther, M. R.; Tschirret-Guth, R. A.; Lardinois, O. M.; Ortiz de Montellano, P. R. *Chem. Res. Toxicol.* **2003**, *16*, 652.

(32)   Bleifuss, G.; Kolberg, M.; Pötsch, S.; Hofbauer, W.; Bittl, R.; Lubitz, W.; Gräslund, A.; Lassmann, G.; Lendzian, F. *Biochemistry.* **2001**, *40*, 15362.

(33)   Stasica, P.; Ulanski, P.; Rosiak, J. M. *J. Pineal. Res.* **1998**, *25*, 65.

(34)   Scaiano, J. C. *J. Pineal. Res.* **1995**, *19*, 189.

(35)   Sayin, U. *J. Mol. Struct.* **2013**, *1031*, 132.

(36)   Tanida, I.; Ueno, T.; Kominami, E. In *Autophagosome and Phagosome*; Deretic, V., Ed.; Humana Press: 2008; Vol. 445, p 77.

(37)   Ronconi, L.; Sadler, P. J. *Chem. Commun.* **2008**, 235.

(38)   Gatti, R. M.; Alvarez, B.; Vasquez-Vivar, J.; Radi, R.; Augusto, O. *Arch. Biochem. Biophys.* **1998**, *349*, 36.

(39)   Malviya, R.; Bansal, V.; Pal, O. P.; Sharma, P. K. *J. Global Pharama Technol.* **2010**, *2*, 22.

(40)   Lucier, B. E. G.; Reidel, A. R.; Schurko, R. W. *Can. J. Chem.* **2011**, *89*, 919.

(41)   O'Dell, L. A.; Schurko, R. W. *Phys. Chem. Chem. Phys.* **2009**, *11*, 7069.

(42)   O'Dell, L. A.; Schurko, R. W. *Chem. Phys. Lett.* **2008**, *464*, 97.

(43)   Austin, E. J. W.; Barrie, P. J.; Clark, R. J. H. *Inorg. Chem.* **1992**, *31*, 4281.

(44)   Waern, J.; Harris, H.; Lai, B.; Cai, Z.; Harding, M.; Dillon, C. *JBIC Journal of Biological Inorganic Chemistry* **2005**, *10*, 443.

(45)   Jones, K. W.; Berry, W. J.; Borsay, D. J.; Cline, H. T.; Conner, W. C.; Fullmer, C. S. *X-Ray Spectrom.* **1997**, *26*, 350.

(46)   Kwiatek, W. M.; Hanson, A. L.; Paluszkiewicz, C.; Gałka, M.; Gajda, M.; Cichocki, T. *J. Alloys Compd.* **2004**, *362*, 83.

(47)   Hall, M. D.; Foran, G. J.; Zhang, M.; Beale, P. J.; Hambley, T. W. *J. Am. Chem. Soc.* **2003**, *125*, 7524.
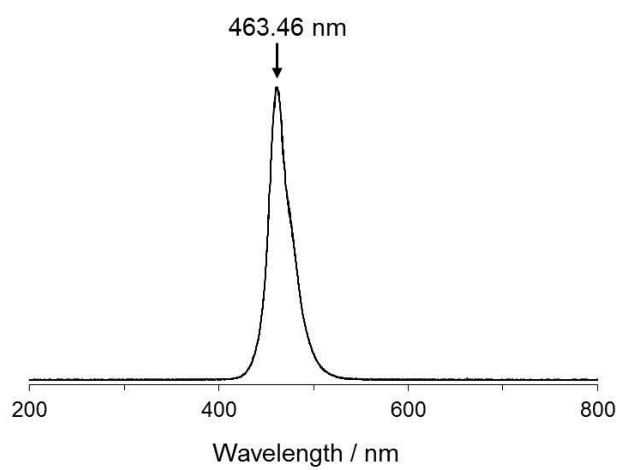
<u>Appendices</u>

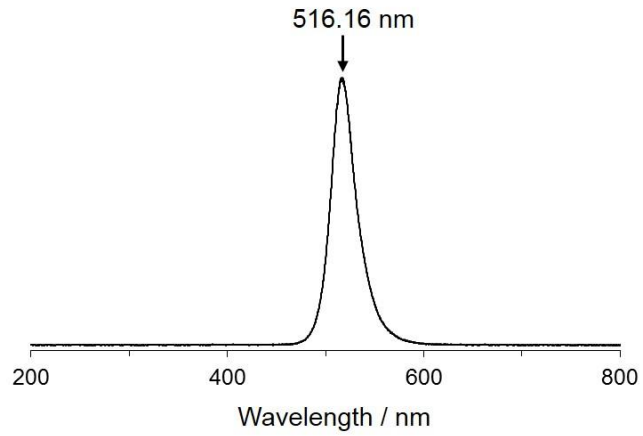**Figure A2.1** Spectral output of blue LED light source (463 nm, 64 mW cm^{-2}).

Figure A3.1 Spectral output of 517 nm green (33 mW cm^{-2}) light source.
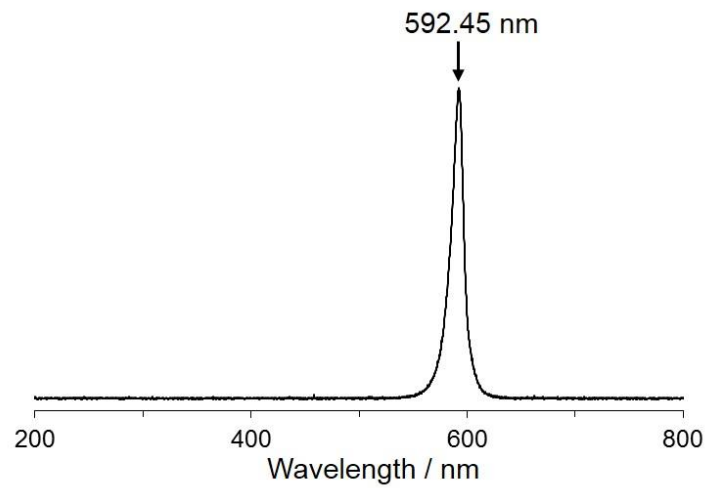

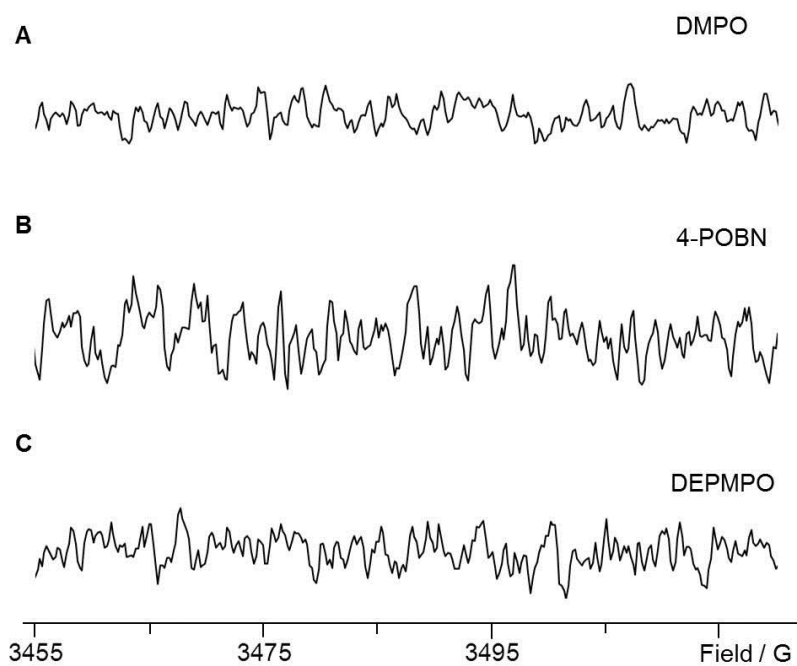**Figure A3.2** 593 nm (17 mW cm^{-2}) yellow LED light source.

Figure A3.3 Dark EPR spectra of the different spin traps used in this work. Aqueous solutions of (**A**) DMPO; (**B**) POBN and (**C**) DEPMPO prepared at 8 mM at pH 7.4. No background EPR signals from either of the spin traps.
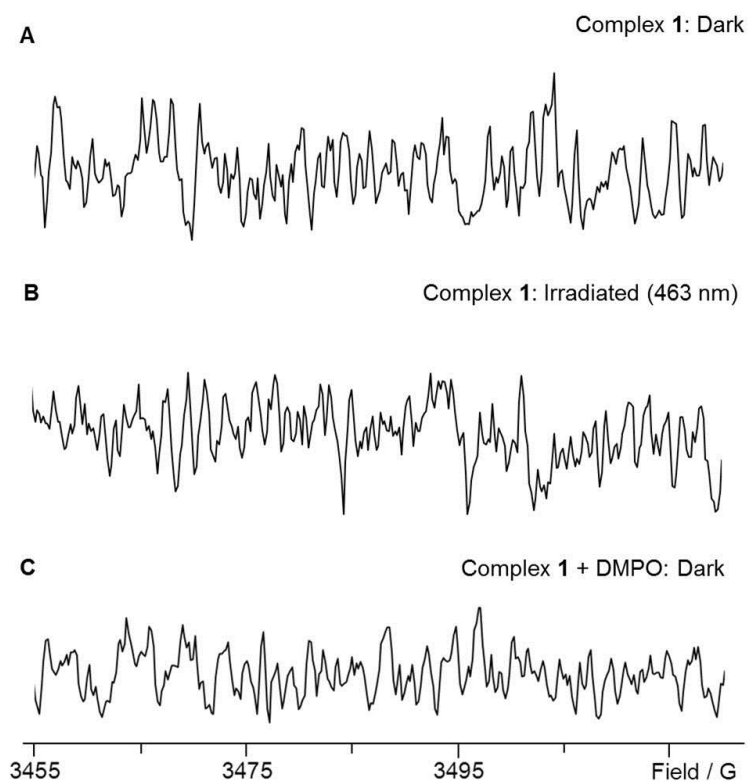
Figure A3.4 EPR spectra of (**A**) dark aqueous solution complex **1**; (**B**) irradiated for 7 min with 463 nm light; (**C**) dark aqueous solution of complex **1** in the presence of DMPO. Substituting spin trap DMPO with 4-POBN and DEPMPO generated EPR spectrum equivalent to **C**.
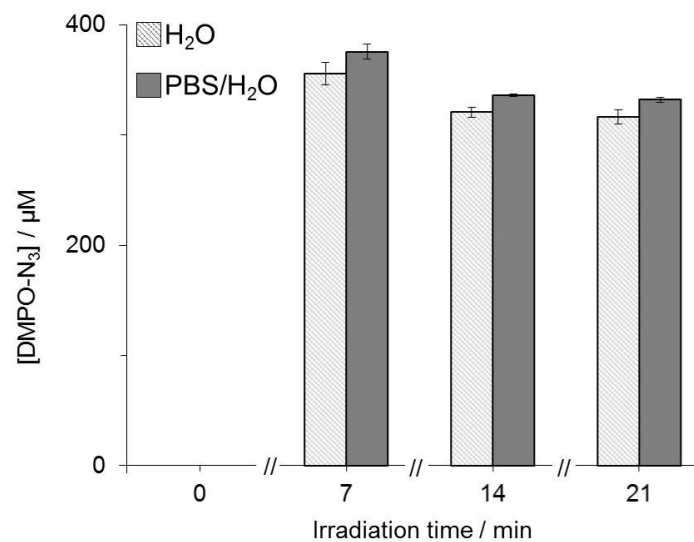
Figure A3.5 Quantification of the DMPO-N$_3$ spin adduct formed from the photo-irradiation at 463 nm after 7 min, 14 min and 21 min intervals from a solution containing complex **40** (5 mM) in the presence of DMPO (2 mol equiv relative to complex **40**) prepared in H$_2$O (□) and PBS/H$_2$O (■) at pH 7.4. No spin adduct was observed in the dark (0 min). Error bars represent standard error of three independent experiments.

RMPI-1640: R7755			
Component	g/L	Component	g/L
Inorganic Salts		**Vitamins**	
Calcium Nitrate • 4H$_2$O	0.1	D-Biotin	0.0002
Magnesium Sulfate (anhydrous)	0.04884	Choline Bitartrate	0.00544
Potassium Chloride	0.4	Folic Acid	0.001
Sodium Chloride	6	myo-Inositol	0.035
Sodium Phosphate Dibasic (anhydrous)	0.8	Niacinamide	0.001
Succinic Acid • 6H$_2$O • Na	0.1	p-Aminobenzoic Acid	0.001
Succinic Acid (free acid)	0.075	D-Pantothenic Acid (hemicalcium)	0.00025
Amino Acids		Pyridoxine • HCl	0.001
L-Arginine	0.2	Riboflavin	0.0002
L-Asparagine (anhydrous)	0.05	Thiamine • HCl	0.001
L-Aspartic Acid	0.02	Vitamin B$_{12}$	0.000005
L-Cystine • 2HCl	0.0652	**Other**	
L-Glutamic Acid	0.02	D-Glucose	2
Glycine	0.01	Glutathione (reduced)	0.001
L-Histidine	0.015	Phenol Red • Na	0.00318
Hydroxy-L-Proline	0.02	**Add**	
L-Isoleucine	0.05	L-Glutamine	0.3
L-Leucine	0.05	Sodium Bicarbonate	2
L-Lysine • HCl	0.04		
L-Methionine	0.015		
L-Phenylalanine	0.015		
L-Proline	0.02		
L-Serine	0.03		
L-Threonine	0.02		
L-Tryptophan	0.005		
L-Tyrosine	0.02		
L-Valine	0.02		

Figure A3.6 Components of cell culture medium RMPI-1640 without L-glutamine*, *information adapted from Sigma Aldrich.
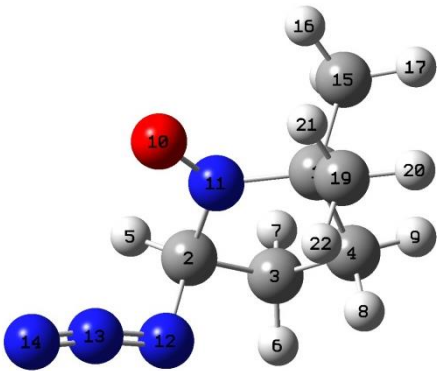
DMPO-N$_3$	Spin Density	Structure
1 C	-0.021989	
2 C	-0.015911	
3 C	0.000796	
4 C	0.001167	
5 H	0.012612	
6 H	0.000895	
7 H	0.000651	
8 H	-0.000343	
9 H	0.000339	
10 O	0.528840	
11 N	0.411518	
12 N	0.013552	
13 N	0.007677	
14 N	0.038469	
15 C	0.021260	
16 H	0.001813	
17 H	0.002161	
18 H	-0.000309	
19 C	0.017718	
20 H	-0.000209	
21 H	-0.001319	
22 H	-0.000408	

Figure 3A.7 Spin density values for all atoms present in the DMPO-N$_3$ spin adducts, as determined from DFT calculations.

DEPMPO-N₃	Spin Density	Structure
1 C	-0.028644	
2 C	-0.018967	
3 C	0.000356	
4 C	0.002835	
5 H	0.000602	
6 H	0.000595	
7 H	0.000519	
8 H	-0.000377	
9 O	0.515280	
10 N	0.422550	
11 C	0.017319	
12 H	0.001265	
13 H	0.000582	
14 H	0.000127	
15 P	0.026697	
16 O	0.001884	
17 C	0.002083	
18 C	0.000126	
19 H	-0.000094	
20 H	-0.000103	
21 H	0.000195	
22 H	0.000003	
23 H	-0.000003	
24 C	0.001997	
25 C	-0.000298	
26 H	0.001471	
27 H	-0.000058	
28 H	0.000176	
29 H	0.000157	
30 H	0.000003	
31 O	0.001099	
32 O	0.002096	
33 N	0.012383	
34 N	-0.006576	
35 N	0.031643	
36 H	0.014771	

Figure 3A.8 Spin density values for all atoms present in the DMPO-N₃ spin adducts, as determined from DFT calculations.

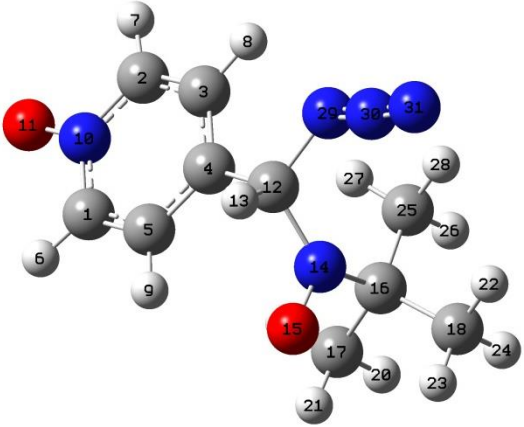| 4-POBN-N₃	Spin Density	Structure
1 C	-0.004927	
2 C	-0.003988	
3 C	0.007854	
4 C	0.012194	
5 C	0.003748	
6 H	0.000211	
7 H	0.000468	
8 H	-0.000305	
9 H	-0.001045	
10 N	0.003864	
11 O	0.008436	
12 C	-0.027121	
13 H	0.001697	
14 N	0.442148	
15 O	0.533465	
16 C	-0.022259	
17 C	0.023610	
18 C	0.014544	
19 H	-0.000707	
20 H	0.000208	
21 H	-0.001513	
22 H	0.000249	
23 H	-0.001405	
24 H	-0.000430	
25 C	0.000571	
26 H	-0.001006	
27 H	-0.000220	
28 H	0.000401	
29 N	0.011496	
30 N	0.000550	
31 N	-0.000785	

Figure 3A.9 Spin density values for all atoms present in the 4-POBN-N₃ spin adducts, as determined from DFT calculations.
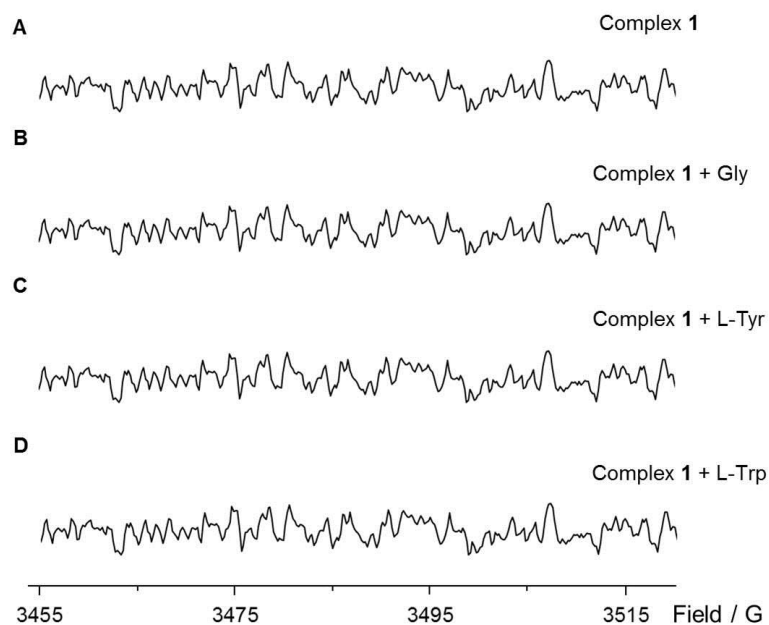
Figure A4.1 Dark EPR spectra of deuterated phosphate buffered solutions all containing complex **1** (4 mM); (**A**) complex **1** only; addition of (**B**) Gly; (**C**) L-Tyr and (**D**) L-Trp. No EPR signals formed in the dark.
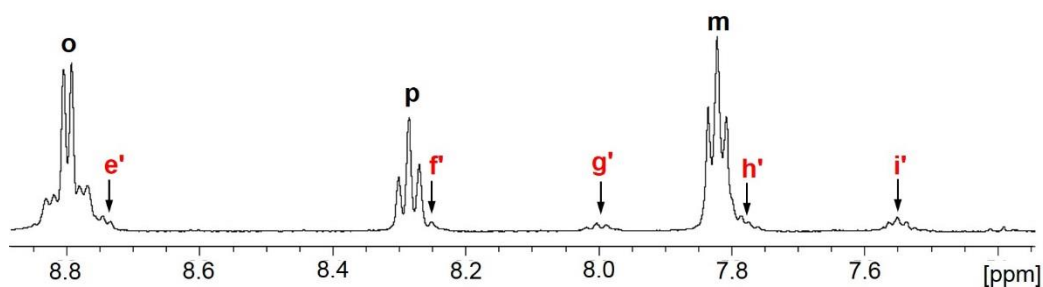

Figure A4.2 The aromatic region of the ^{1}H NMR spectra from a solution of complex **40** (4 mM) and DMPO (8 mM) prepared in D_2O buffer at pH* 7.4 in (**A**) dark and (**B**) after 30 min irradiation with 463 nm light. Assignments: Pt-py peaks, (**o/p/m**); platinum photoproducts, (**e'-i'**).
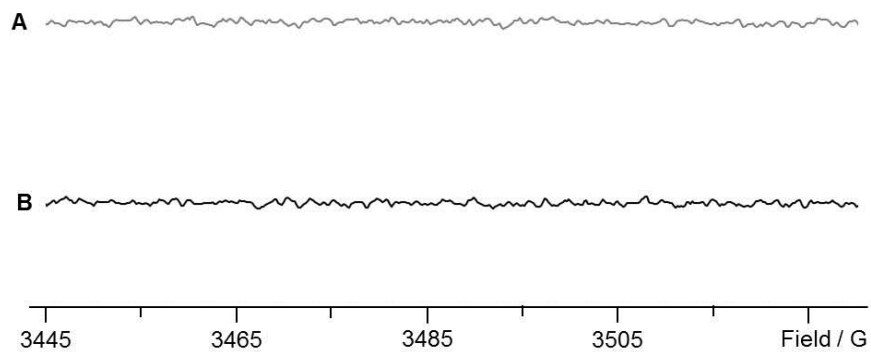
Figure A5.1 Dark EPR spectra of solutions containing (**A**) melatonin with DMPO and (**B**) complex **1**, DMPO and melatonin prepared in PBS/D$_2$O at pH* 7.4.
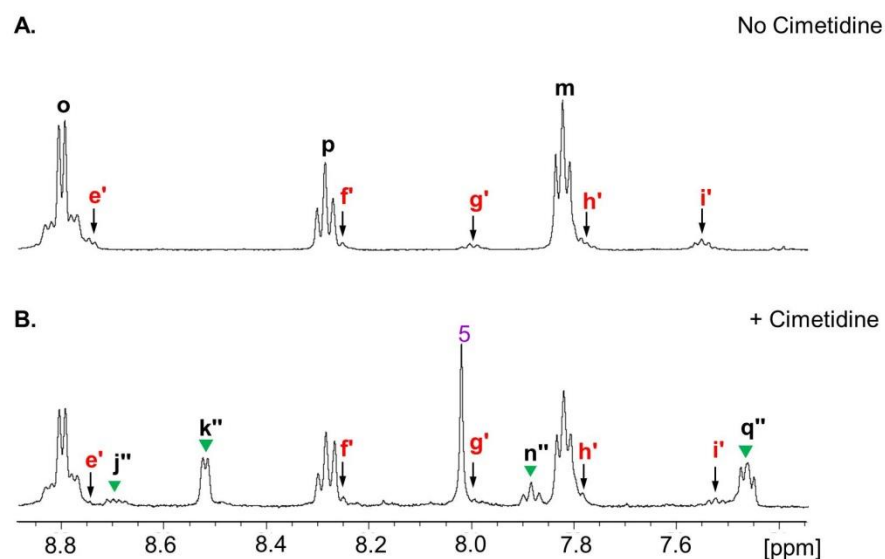
Figure A6.1 Comparison of ^{1}H NMR spectra of photo-products formed from a solution containing complex **40** (4 mM) prepared in PBS/D$_2$O in the (**A**) absence and (**B**) presence of cimetidine irradiated at 463 nm for 60 min. Assignments: Pt-py peaks, (**o**/**p**/**m**); cimetidine peak, (5); photo-generated Pt-species in both the absence/presence of cimetidine, (**e'-i'**); photo-generated species only in the presence of cimetidine, (▼).